NASA CR-168215
RI/RD83-150

NASA

FINAL REPORT

SSME MAIN COMBUSTION CHAMBER LIFE PREDICTION

by

R. T. Cook
E. E. Fryk
J. F. Newell

Rockwell International
Rocketdyne Division

prepared for

NATIONAL AERONAUTICS AND SPACE ADMINISTRATION

May 1983

NASA-Lewis Research Center

Contract NAS3-23256

H. J. Kasper, Project Manager

28 1 1 RN/NASA-CR-168215
DISPLAY 28/2/1
83N36101*# ISSUE 24 PAGE 3920 CATEGORY 20 RPT#: NASA-CR-168215 NAS 1.26:168215 RI/RD83-150 CNT#: NAS3-23256 83/05/00 294 PAGES
UNCLASSIFIED DOCUMENT
UTTL: SSME main combustion chamber life prediction TLSP: Final Report, Jan. 1982 - May 1983
AUTH: A/COOK, R. T.; B/FRYK, E. E.; C/NEWELL, J. F.
CORP: Rocketdyne, Canoga Park, Calif. AVAIL.NTIS SAP: HC A13/MF A01
MAJS: /*COMBUSTION CHAMBERS/*CREEP PROPERTIES/*CYCLIC LOADS/*SERVICE LIFE/*SPACE SHUTTLE MAIN ENGINE
MINS: / FATIGUE LIFE/ HEAT FLUX/ STRUCTURAL ANALYSIS
ABA: S.L.
ABS: Typically, low cycle fatigue life is a function of the cyclic strain range, the material properties, and the operating temperature. The reusable life is normally defined by the number of strain cycles that can be accrued before severe material degradation occurs. Reusable life is normally signified by the initiation or propagation of surface cracks. Hot-fire testing of channel wall combustors has shown significant mid-channel wall thinning or deformation during accrued cyclic testing. This phenomenon is termed cyclic-creep and appears to be significantly accelerated at elevated surface temperatures. This failure mode was analytically modelled. The cyclic life of the baseline SSME-MCC based on measured calorimeter heat transfer data, and the life sensitivity of local
ENTER:

1. Report No. NASA CR-168215	2. Government Accession No.	3. Recipient's Catalog No.

4. Title and Subtitle	5. Report Date
Space Shuttle Main Engine Main Combustion Chamber Life Prediction	May 1983
	6. Performing Organization Code
7. Author(s)	8. Performing Organization Report No.
R.T. Cook, E.E. Fryk, and J.F. Newell	RI/RD83-150
	10. Work Unit No.
9. Performing Organization Name and Address	11. Contract or Grant No.
Rocketdyne Division Rockwell International 6633 Canoga Avenue Canoga Park, CA 91304	NAS3-23256
	13. Type of Report and Period Covered
12. Sponsoring Agency Name and Address	(January 1982 - May 1983)
National Aeronautics and Space Administration NASA-Lewis Research Center Cleveland, OH	14. Sponsoring Agency Code

15. Supplementary Notes

16. Abstract

The reusable life of the Space Shuttle Main Engine (SSME) and future engines is greatly influenced by the cyclic life of several major components that are exposed to a high temperature combustion gas environment. The main combustion chamber (MCC) liner is typically exposed to the most severe environment. The SSME and future engines operate in excess of 3000 psia chamber pressure at approximately 6500 R combustion gas temperature. These conditions produce a heat flux of approximately 100 Btu/in.^{2}-sec in the life-limited throat region. The thrust chamber reusable life is attained by regenerative cooling a copper base MCC liner configured of rectangular cooling channels. During an operational duty cycle (mission) the MCC liner is subjected to a large transient thermal gradient which imparts a high thermal cyclic strain to the MCC liner hot gas wall.

Typically, low cycle fatigue life is a function of the cyclic strain range, the material properties, and the operating temperature. The reusable life is normally defined by the number of strain cycles that can be accrued before severe material degradation occurs. Reusable life is normally signified by the initiation or propagation of surface cracks. Hot-fire testing of channel wall combustors at Rocketdyne and NASA LeRC has shown significant mid-channel wall thinning or deformation during accrued cyclic testing. This phenomenon is termed cyclic-creep and appears to be significantly accelerated at elevated surface temperatures.

A study was conducted to analytically model this failure mode. This study consisted of (1) determining the cyclic life of the baseline SSME-MCC based on measured calorimeter heat transfer data, (2) determining the life sensitivity of local hot spots caused by injector effects, and (3) assessing four life enhanced designs. These analyses utilized an upgraded analytical model which accounted for cyclic creep. Cyclic channel deformation and wall thinning geometry were updated for each analysis to account for the accrued distortions. The cyclic life results of these analyses were then compared to the typically used low-cyclic-fatigue (LCF) analyses that do not address the cyclic creep phenomenon.

The results of this study show that cyclic creep is the dominating factor in defining the reusable life of a combustion chamber. It is typically shown that the usable cyclic-creep life is approximately 30 to 50% of the commonly used low-cycle-fatigue life. This reduction in usable life is basically attributed to the accrued channel wall thinning as a result of cyclic creep.

17. Key Words (Suggested by Author(s))	18. Distribution Statement
SSME Main Combustion Chamber Fatigue Life Cyclic-Creep, Life enhanced designs	

19. Security Classif. (of this report)	20. Security Classif. (of this page)	21. No. of Pages	22. Price*
Unclassified	Unclassified	294	

* For sale by the National Technical Information Service, Springfield, Virginia 22151

FOREWORD

This program was conducted by the Rocketdyne Division of Rockwell International for the NASA-Lewis Research Center under Contract NAS3-23256. The program was directed by Mr. Harold Kasper at NASA, and Messrs. Frank Kirby, Program Manager, and Ronald Cook, Project Engineer, at Rocketdyne.

The major efforts of this program were conducted by the Rocketdyne Engineering Structural, Aerothermal, and Materials Departments. The responsible Engineers in these areas were:

Edward Fryk	Structures
James Newell	Structures and Dynamics
Dennis Lim	Heat Transfer
Lillian Ng	Materials and Processes
Glenn Coffey	Combustion Devices (SSME Test History)

Special thanks go to Margaret Haven for her efforts in the computer modeling of the various configurations, summary of results and associated inputs to the final report, and to Robert Cooper, fatigue specialist, who furnished valuable comments and technical assistance.

CONTENTS

ILLUSTRATIONS

TABLES

SUMMARY

The primary objective of this study was to establish an accurate method to predict the cyclic-life of high chamber pressure regeneratively cooled rocket engine main combustion chambers constructed of a channel configuration. This objective was to be accomplished by a refined analytical model that accommodated the experimentally observed cyclic-creep phenomenon as an additional life limiting factor. This cyclic-creep phenomenon is characterized by mid-channel wall thinning and hot wall deformation which is cyclic dependent but independent of engine mainstage duration. The basis for this study was the channel deformation and wall thinning observed during hot-fire cyclic-testing of the Space Shuttle Main Engine-Main Combustion Chamber (SSME-MCC) and other combustion chambers tested at NASA-LeRC and NASA-MSFC; as typically noted in Fig. 1.

This study consisted of (1) determining the cyclic life of the baseline SSME-MCC based on measured calorimeter heat transfer data, (2) determining the life sensitivity of local hot spots caused by injector effects, and (3) assessing life enhanced redesigns. The overall program methodology applied for this study is presented in Fig. 2. These analyses utilized an upgraded analytical model which accounted for cyclic creep. Cyclic channel deformation and wall thinning geometry were updated for each analysis to account for the accrued distortions. The cyclic life results of these analyses were then compared to the typically used low-cyclic-fatigue (LCF) analyses that do not address the cyclic creep phenomenon.

The analytical model was characterized with the basic SSME-MCC channel geometry. First-order sensitivity studies were performed between a nominal full-power-level heat transfer condition (100% hg) and a condition of 135% hg that may be related to an extreme local hot spot condition over a width of five or more channels. The analytical model was further sensitized with artificial pressure gradients and artificial temperature gradients across the channel wall.

The results of this study show that cyclic creep is the dominating factor in defining the reusable life of a combustion chamber. It is typically shown that the usable cyclic-creep life is approximately 30 to 50% of the commonly used low-cycle-fatigue life. This reduction in usable life is basically attributed to (1) the accrued channel wall thinning as a result of cyclic creep and (2) the ultimate strain or tensile instability criterion. The range of biaxial tensile instability was determined to be between 5 and 8% wall thinning, which is approximately equivalent to the average effective strain.

The analytical model depicts the mid-channel hot wall being deformed slightly inward toward the combustor centerline as the channel wall is thinned due to cyclic creep. The degree of channel wall thinning relative to hot wall deformation is characterized by the channel geometry and surface temperature. The lower wall temperature condition reflects less wall thinning for a given channel wall deformation or number of duty cycles. These analytical results are supported by experimental combustion chamber data which have indicated varying degrees of wall thinning for similar hot wall deformation. The analyses also

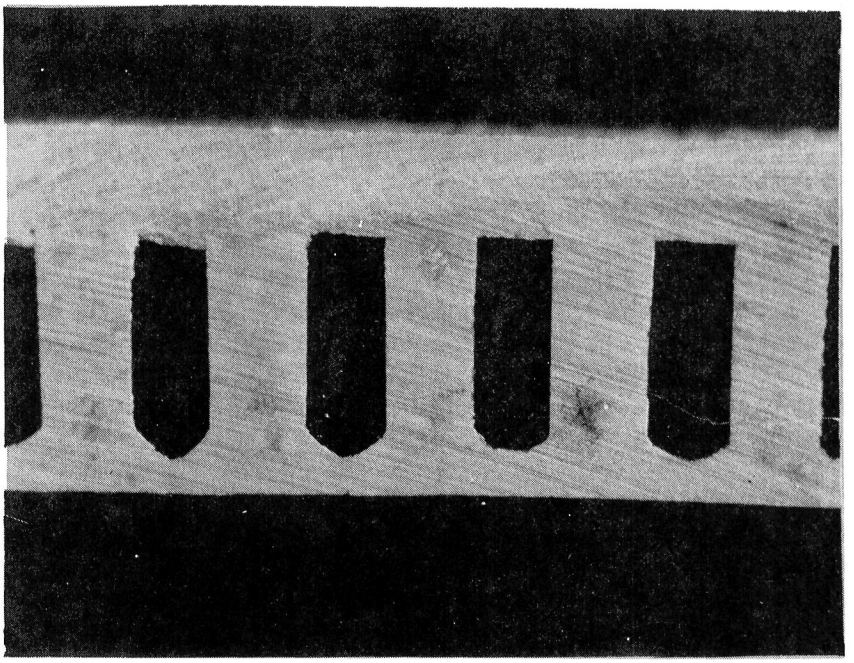

Figure 1. Throat Section of SSME-MCC Showing Thinned Hot-Gas Wall

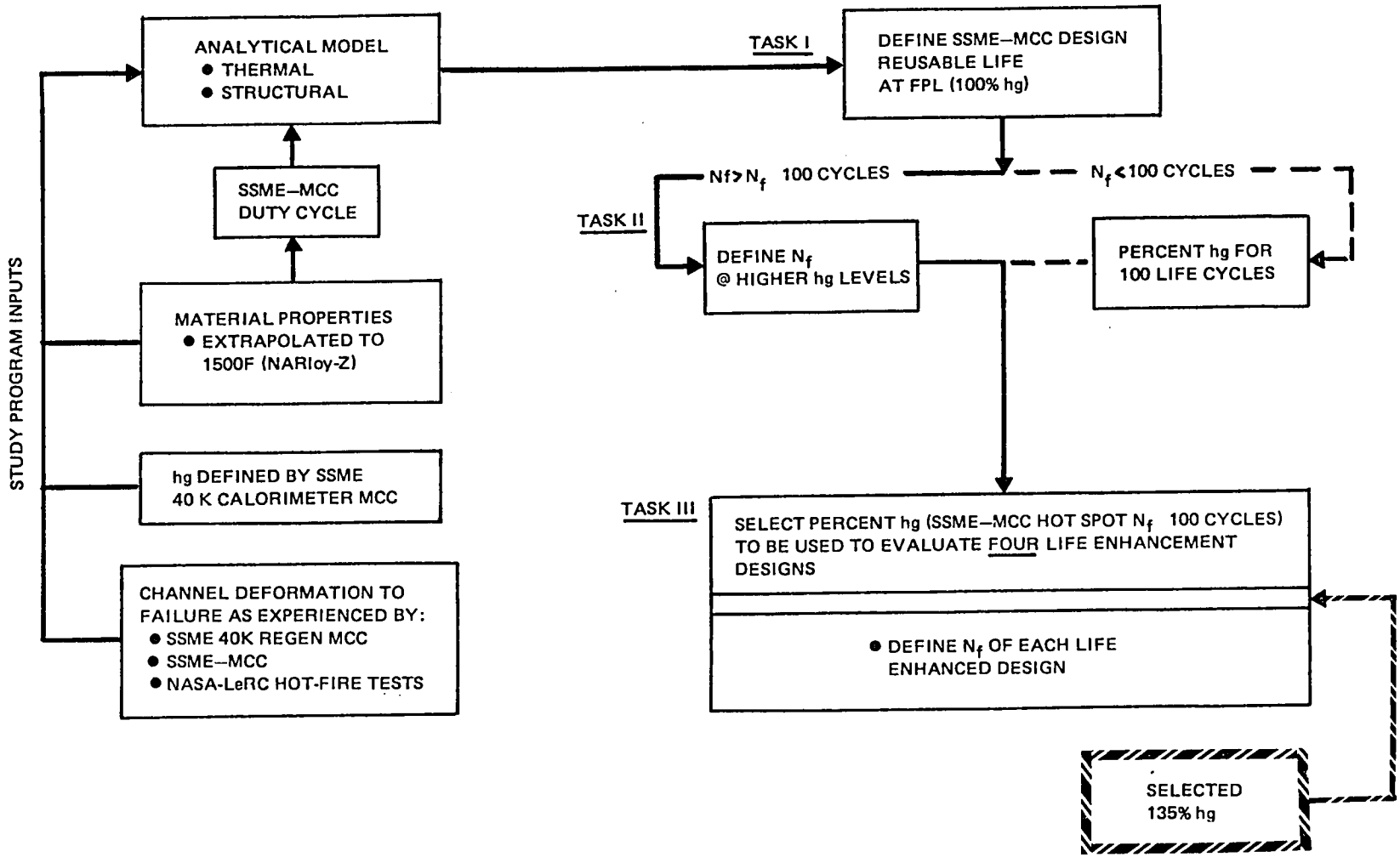

Figure 2. Overall Program Methodology

show that continued wall thinning persists after hot wall deformation is curtailed. This appears to occur in the projected range where tensile instability is initiated. This characteristic has also been experimentally evidenced on hot-fired combustion chambers.

Four potential life-enhanced designs were analytically assessed at the extreme 135% hg thermal condition. These designs stemmed from the cyclic-creep sensitivity analyses of the baseline SSME-MCC channel geometry. These designs spanned a wide spectrum of channel geometry and manufacturing feasibility. A maximum usable life benefit of a factor of three was shown for the maximum risk design which incorporated two life enhancement features. The next best design is considered currently feasible with moderate risk and reflected twice the usable life. The other two designs did not provide any usable life benefits and consisted of a moderate risk design and a minimum risk design with a minimum SSME-MCC design change.

The primary technology gained from this study is the establishment of a cyclic creep life prediction methodology along with a working analytical model capable of evaluating innumerable channel wall design concepts in a cost effective manner.

INTRODUCTION

The reusable life of the Space Shuttle Main Engine (SSME) and future engines are greatly influenced by the cyclic life of several major components that are exposed to a high temperature combustion gas environment. The main combustion chamber (MCC) liner is typically exposed to the most severe environment. The SSME and future engines operate in excessof 3000 psia chamber pressure at approximately 6500 R combustion gas temperature. These conditions produce a heat flux of approximately 100 Btu/in.^{2}-sec in the life limited throat region. The thrust chamber reusable life is attained by regenerative cooling a copper base MCC liner configured of rectangular cooling channels. During an operational duty cycle (mission) the MCC liner is subjected to a large transient thermal gradient which imparts a high thermal cyclic strain to the MCC liner hot gas wall.

Typically, low cycle fatigue life is a function of the cyclic strain range, the material properties, and the operating temperature. The reusable life is normally defined by the number of strain cycles that can be accrued before severe material degradation occurs. Reusable life is normally signified by the initiation or propagation of surface cracks. Hot-fire testing of channel wall combustors at Rocketdyne and NASA-LeRC has shown significant mid-channel wall thinning or deformation during accrued cyclic testing. This phenomenon is termed cyclic-creep and appears to be significantly accelerated at elevated surface temperatures. The sensitivity of this phenomenon to surface temperature is evidenced by the non-uniformity of channel wall deformation around the circumference of the combustors. History has shown the non-uniformity is first evidenced by local discoloration (blanching) of the copper base alloy hot gas wall signifying higher surface temperature hot spots. Hot-fire test history also shows that minor changes in operational level significantly degrade the cycle life in these hot-spot regions.

The purpose of this study was to provide an analytical model that accounted for cyclic creep channel deformation and establish the methodology necessary to upgrade the SSME-MCC design and future engine designs. The analytical model was to provide the capability of accounting for the coolant channel wall deformation cyclic history.

The approach taken to accomplish the study objectives consisted of three technical tasks as follows:

Task I: SSME Main Combustion Chamber Life Analysis consisted of performing an SSME MCC life analysis at standard operating conditions that considered cyclic-creep damage as an additional life-limiting factor. Analyses included thermal, structural, and failure mode analysis. Two-dimensional thermal and structural analyses were performed in the critical throat region. The structural analysis was to include elastic-plastic behavior of structures subjected to constant and variable amplitude cyclic mechanical and thermal loads, nonlinear material properties variation as a function of temperature, and nonlinear geometric updating. The combined analysis was to identify the failure mode and predict the combustion chamber life.

Task II: Effect of Localized Temperature Extremes on SSME Main Combustion Chamber Life was investigated to define the impact of local hot-gas-wall temperature extremes due to injector anomalies on reusable life. The analysis was similar to that performed in Task I. The duty cycle was identical to that of the SSME with the exception of the varying local thermal conditions. Parametric analyses were conducted to define the cyclic life sensitivity to local heat flux and material temperature variations.

Task III: SSME MCC Life Enhanced Redesign consisted of identifying a minimum of four viable life-enhancing main combustion chamber designs based on the results of Tasks I and II. Two of the selected designs analyzed utilized minimum changes to the existing SSME main combustion chamber. One of the four designs represented a best concept (maximum life), and deviated extensively from the current design. The remaining design was a combination of the other proposed designs. The use of hot gas wall coatings was excluded from the study.

DISCUSSION

THERMAL ANALYSIS

The reusable life of the Space Shuttle Main Engine (SSME) is greatly influenced by the cyclic life of several major components that are exposed to a high temperature combustion gas environment. The SSME main combustion chamber (MCC) liner is exposed to the most severe environment. It operates in excess of 3000 psia chamber pressure and 6500 R combustion gas temperature. These conditions produce a nominal heat flux of 100 Btu/in.^{2}-sec in the throat region.

The SSME-MCC reusable life is attained by regenerative hydrogen cooling the copper base (NARloy-Z) MCC liner configured of rectangular cooling channels. During an operational duty cycle (mission) the MCC liner is subjected to a transient thermal gradient approaching 860 K (1500 R). The peak SSME MCC heat flux region, located 3.1 cm (1.22 inch) upstream of the geometric throat, was selected for this study. A two-dimensional thermal model was used to define the life cycle transient temperature history as a function of time. The MCC average axial thermal conditions were determined from hot-fire calorimeter chamber measured heat transfer rates. These type of measurements cannot distinguish circumferential heat transfer variations commonly associated with injection/combustion abnormalities. SSME-MCC regenerative cooled cyclic life testing has shown that failures occur in local hot spot regions. These hot spot regions are identified by hot gas wall surface discoloration (blanching) and typically exist over a width of 5 to 10 channels.

This section presents the thermal analyses for:

1. The baseline SSME-MCC sensitivity study between 100% FPL hg level and 140% FPL hg level.

2. The baseline SSME-MCC channel wall thinning sensitivity study between the nominal channel wall thickness of 0.071 cm (0.028 inch) and deformed mid-channel wall thickness of 0.010 cm (0.004 inch).

3. Four life-enhanced channel redesigns, evaluated at 135% FPL hg level.

SSME-MCC BASELINE DESIGN

The baseline design for this study was the SSME-MCC. The SSME Main Combustion Chamber is shown in Fig. 3. The selected baseline operating level was Full Power Level (FPL) with the heat transfer rates noted as 100% hg. This power level is 9% above the SSME Rated Power Level (RPL). The FPL chamber pressure is 3250 psia and the MCC mixture ratio is 6.0 (oxygen/hydrogen). The SSME duty cycle, including the start and cutoff transient conditions, were used for all analyses. The SSME-MCC chamber pressure and mixture ratio duty cycle are depicted in Fig. 4 and 5.

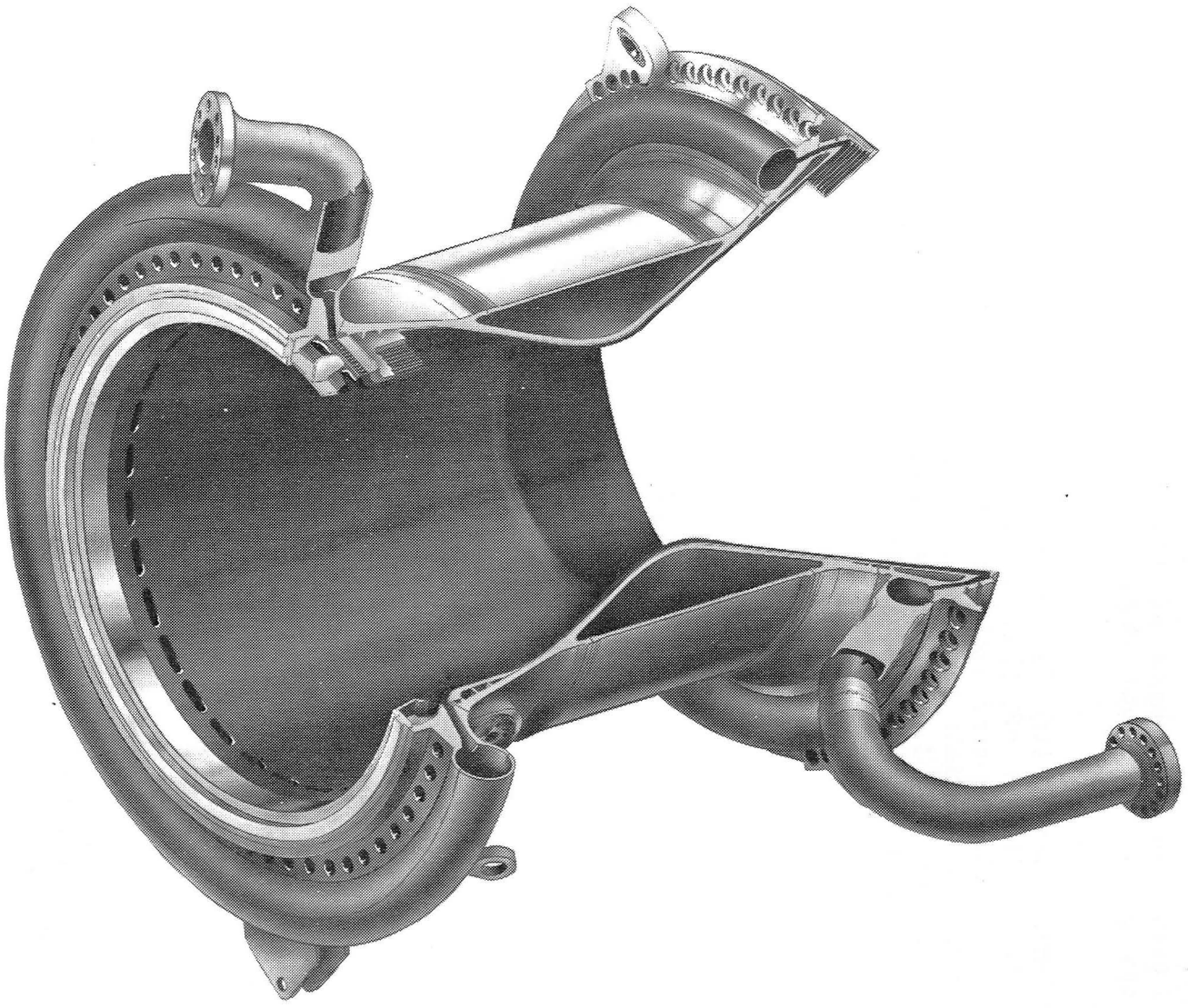

Figure 3. SSME Main Combustion Chamber (MCC)

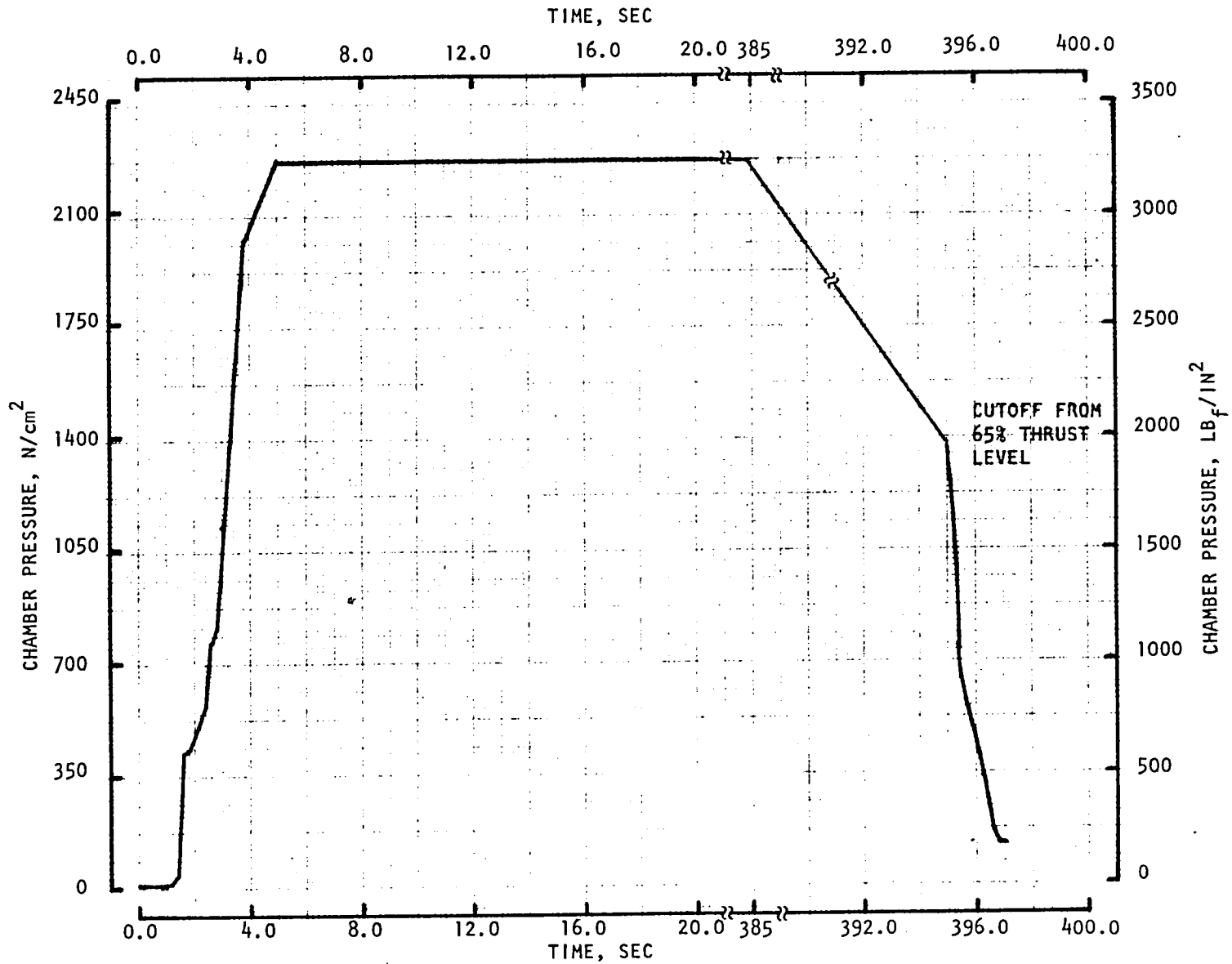

Figure 4. SSME MCC Chamber Pressure Profile to FPL Operation (100% hg)

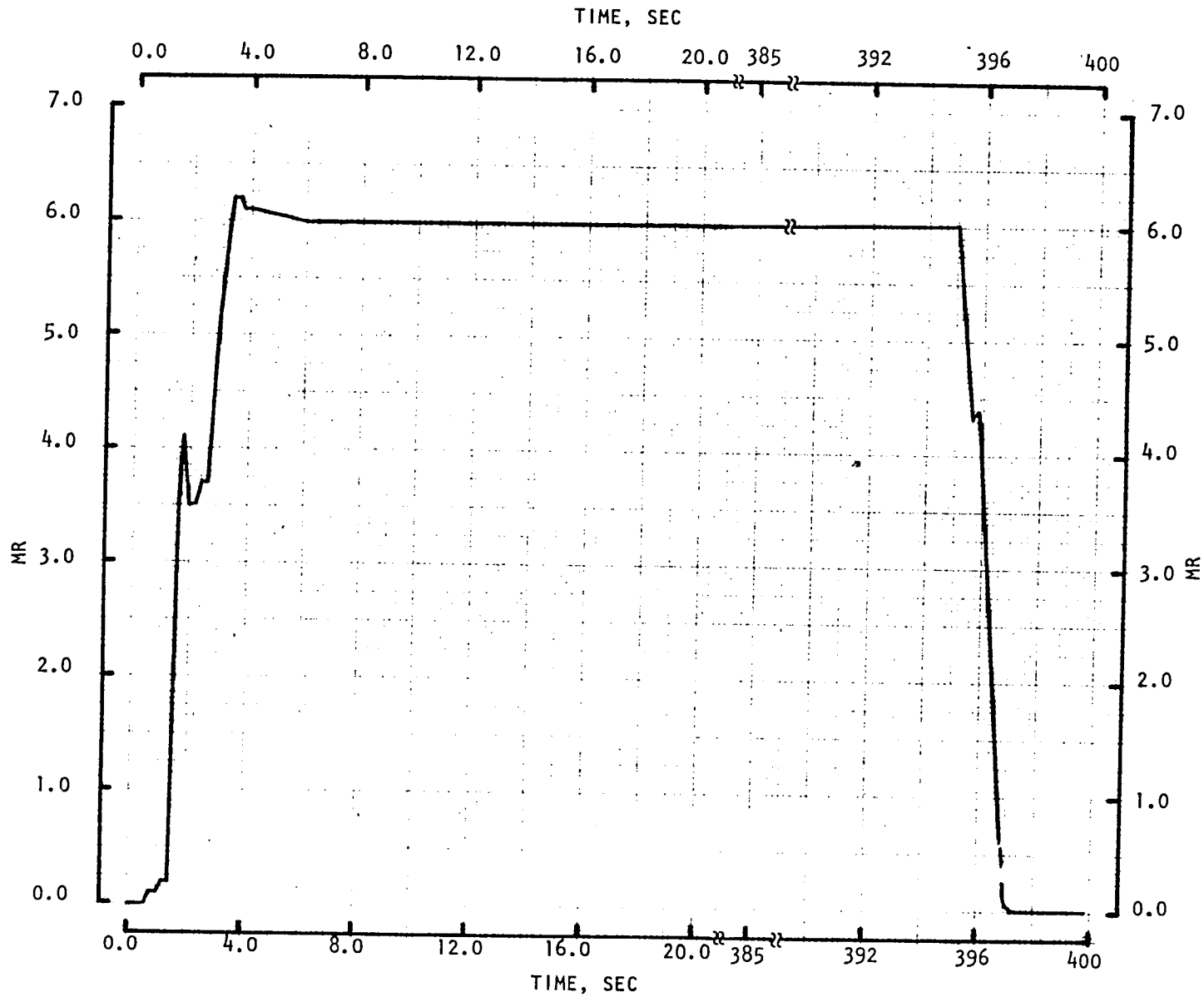

Figure 5. SSME MCC LOX/H_2 Mixture Ratio Profile to FPL Operation (100% hg)

The minimum life region is located slightly upstream of the geometric throat. The peak heat flux and maximum thermal gradient across the MCC NARloy-Z liner occurs at -3.1 cm (-1.22 inch). The two-dimensional thermal conditions at this location were used for all analyses in this study.

Gas Side Heat Transfer

The SSME-MCC heat transfer rates were based on subscale 40K thrust calorimeter chamber testing. The subscale test article is shown in Fig. 6. It employed a staged combustion system and utilized main injector elements identical to the SSME. The combustor length (injector to throat) was identical to the SSME-MCC. This water-cooled calorimeter chamber provided local axial heat flux measurements over a range of chamber pressure up to 1750 psia. Chamber pressure scaling criteria were attained from the 40K calorimeter MCC and subsequent testing on two 40K hydrogen cooled chambers up to 3000 psia chamber pressure. These hydrogen cooled chambers were configured of the SSME-MCC channel geometry. Comparison of local heat flux measurements and total heat load data provided local heat transfer scaling to 3000 psia chamber pressure, which adhered to the classical scaling relationship of

$$hg \propto (Pc)^{0.8}$$

Since the purpose of the two 40K hydrogen cooled chambers was a life demonstration, these combustion chambers utilized the identical SSME-MCC throat region channel geometry and hot gas wall contour. The local gas-side heat transfer conditions of the full-size SSME-MCC were obtained by correcting for local hot gas wall mass velocity ($hg \propto (\rho V)^{0.8}$) where the SSME-MCC axisymmetric geometry differend from the 40K-MCC. This correction is effectively attained by integrating the measured 40K calorimeter-MCC heat transfer data with the Rocketdyne analytical boundary layer computer program. This allows evaluation of any chamber and nozzle-geometry on an empirical basis. The injector end heat transfer conditions are based on experimental data. This empirical approach was subsequently verified by measured SSME-MCC heat load measurements.

Coolant Heat Transfer

The hydrogen convective coolant coefficient was based on the Rocketdyne hydrogen coolant correlation as noted below:

$$hc = C_H \, G \, C_P \, \left(\frac{T_B}{T_W}\right) \, \phi_c$$

where

T_B = bulk temperature
T_W = wall temperature
C_P = heat capacity
G = mass flux

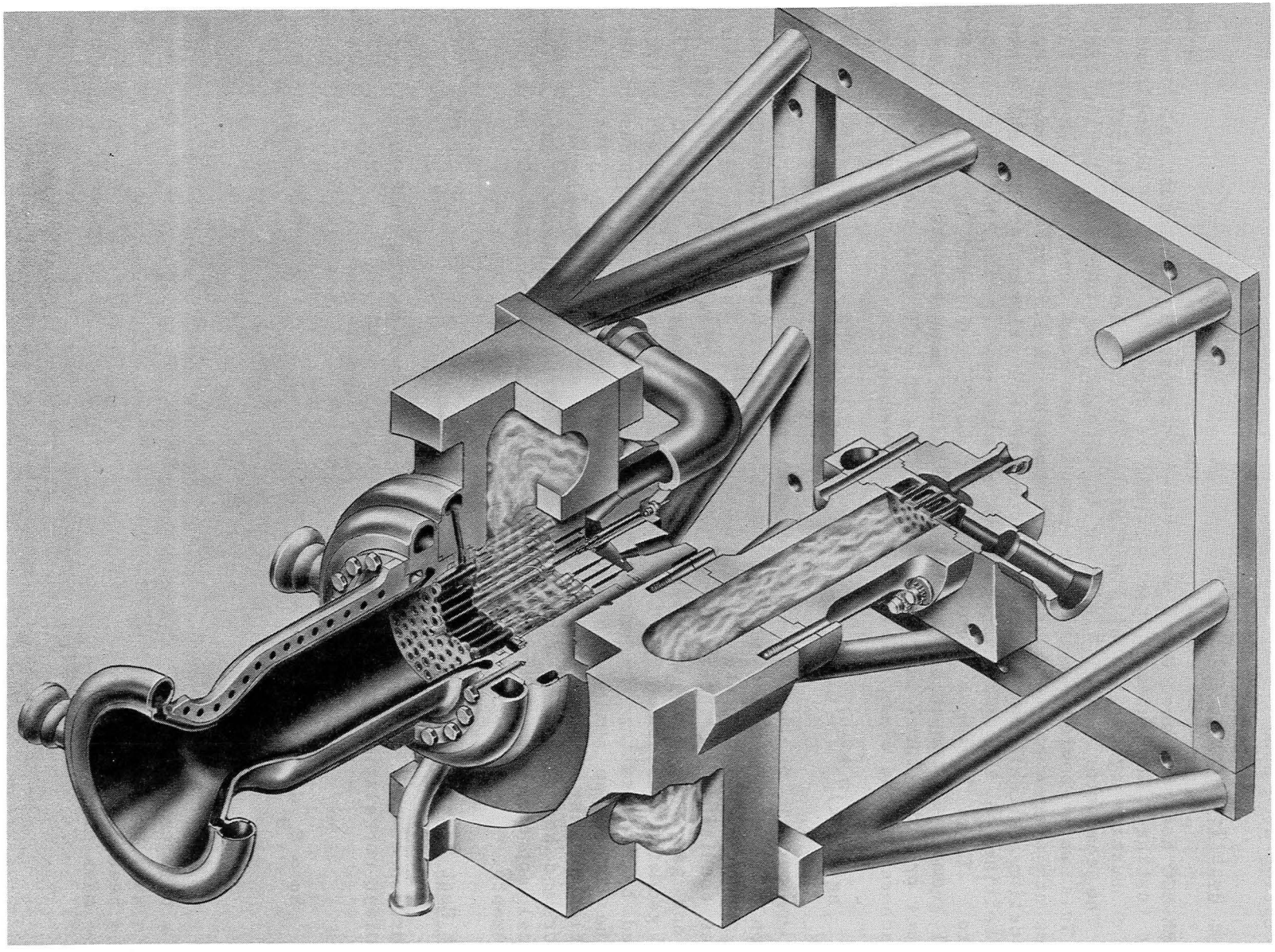

LC302-735

Figure 6. SSME 40K Subscale Combustion System

ϕ_c = curvature enhancement

$$C_H = \frac{f/8}{0.92 + \sqrt{f/8}\,[g(\epsilon^*) - 8.48]}$$

where

$$g(\epsilon^*) = 4.7\ \epsilon^{*0.2} \text{ for } \epsilon^* \geq 7.0$$

$$g(\epsilon^*) = 4.5 + 0.57\ \epsilon^{*0.75} \text{ for } \epsilon^* < 7.0$$

A coolant curvature enhancement (ϕ_c) of 1.4 was used in the life-limited throat region at X = -3.1 cm (-1.22 inch). This enhancement was expreimentally evaluated by laboratory tests for the SSME-MCC geometry.

The thermal computer-program logic diagram used in this study is shown in Fig. 7. The temperature distribution of the coolant channel is determined by a sophisticated 277 node dimensional grid model as shown in Fig. 8. The model uses a finite difference technique. The nodal temperature distribution is stored on tape and subsequently used with the structural/stress analysis computer code. The same nodal network was used for the thermal and structural analyses. The coolant channel thermal distribution is shown in Fig. 9 at 3.1 cm (1.22 inch) upstream of the geometric throat. The maximum hot-gas wall temperature is 866 K (1100 F) at steady-state FPL (100% hg) conditions. The coolant bulk temperature and combustion gas temperature profiles are shown in Fig. 10. Noteworthy transient and steady-state thermal conditions of indicated analytical model nodes (Fig. 11) are shown in Fig. 12 over midchannel and Fig. 13 over midland.

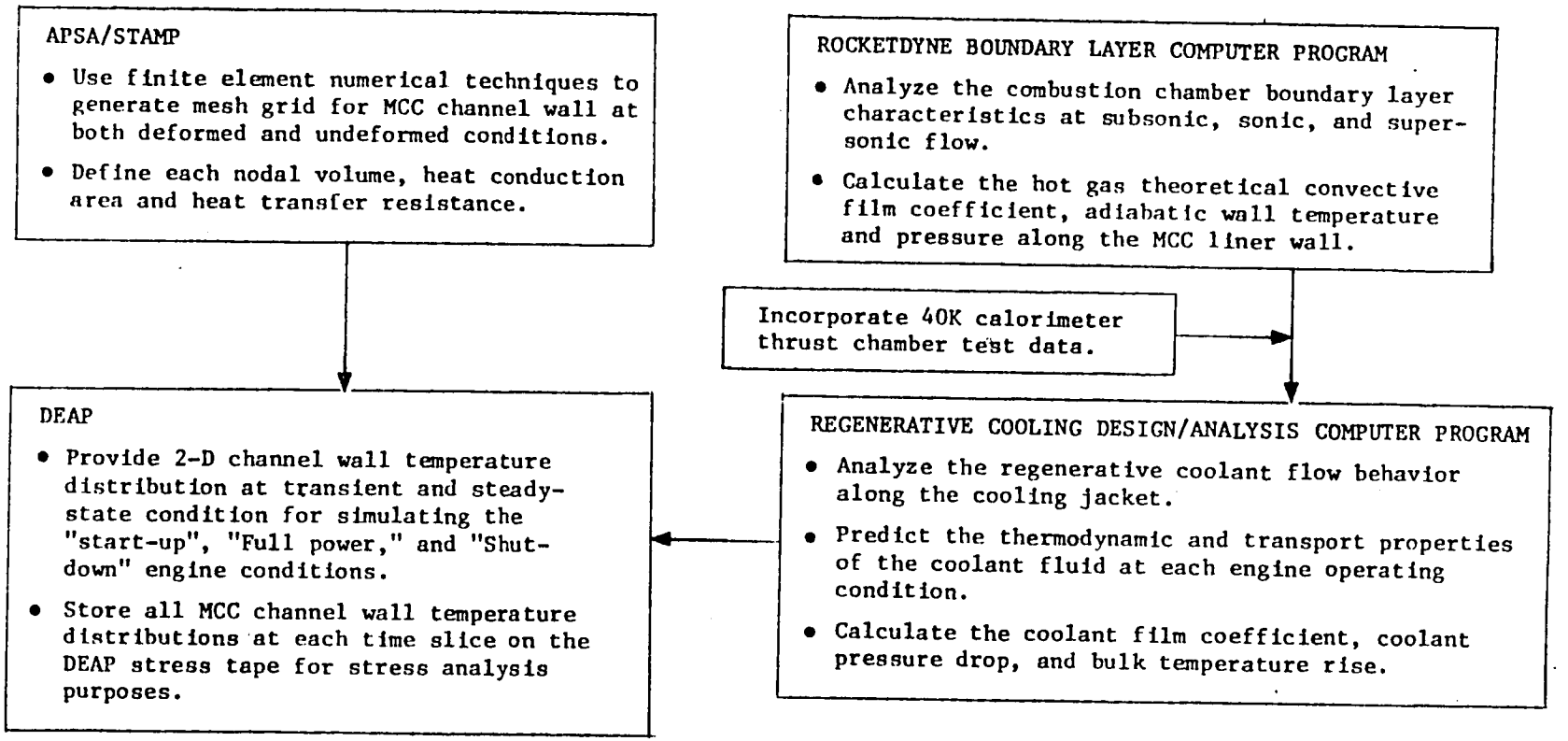

Figure 7. Thermal Computer Programs Flow Chart

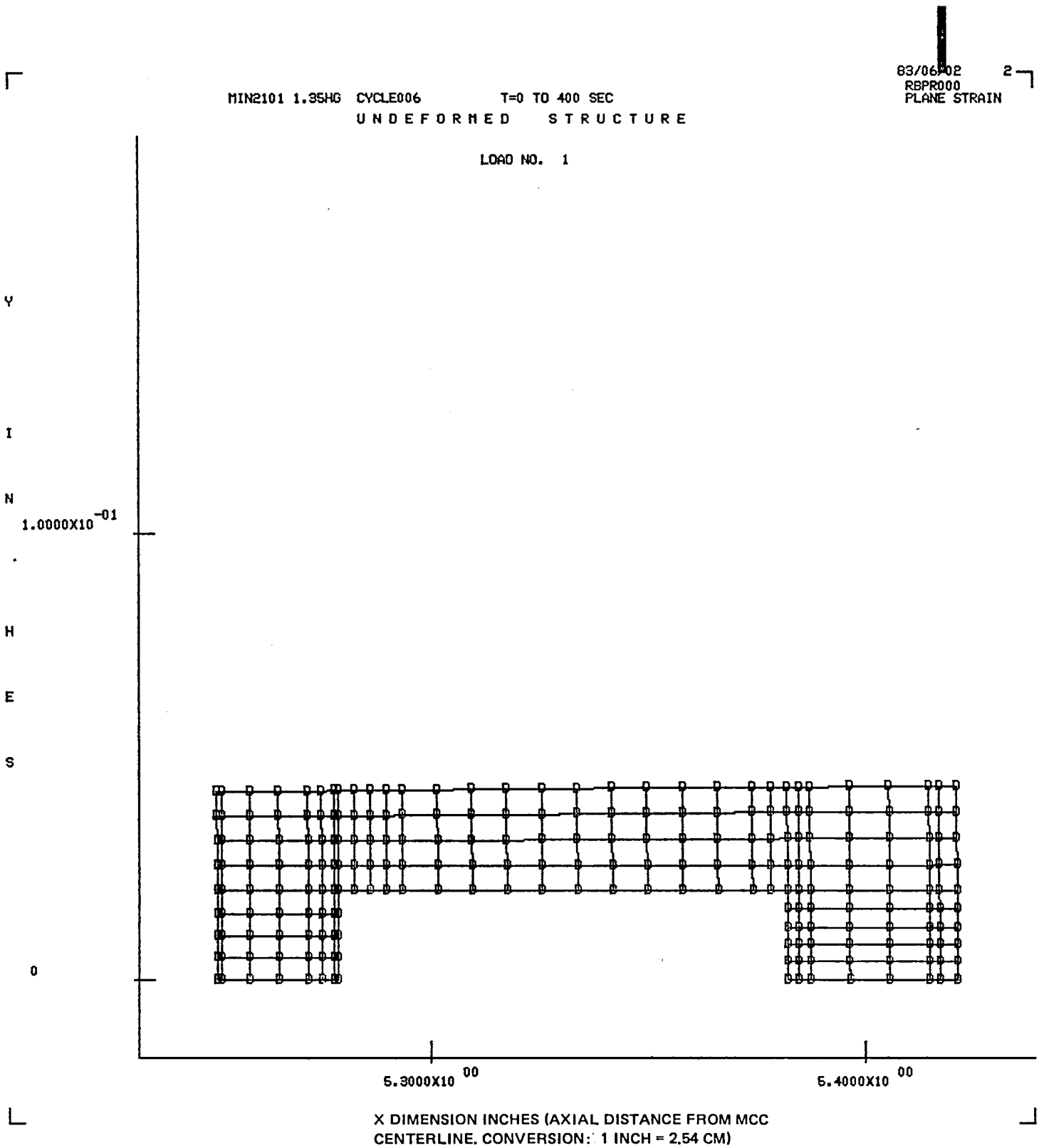

Figure 8. SSME MCC Cooling Channel Geometry and Nodal Structure

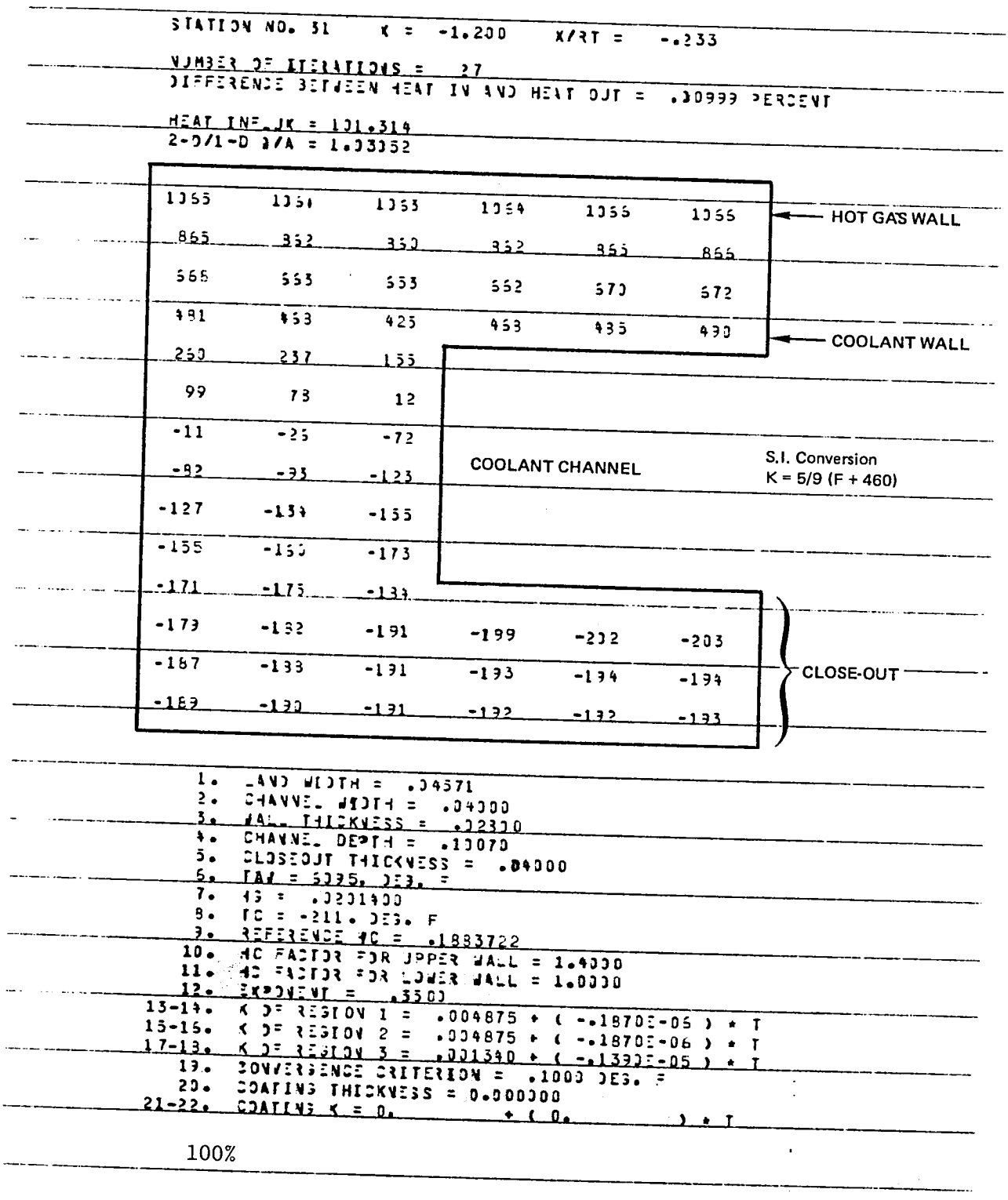

Figure 9. Coolant Channel Thermal Distribution at 100% FPL hg

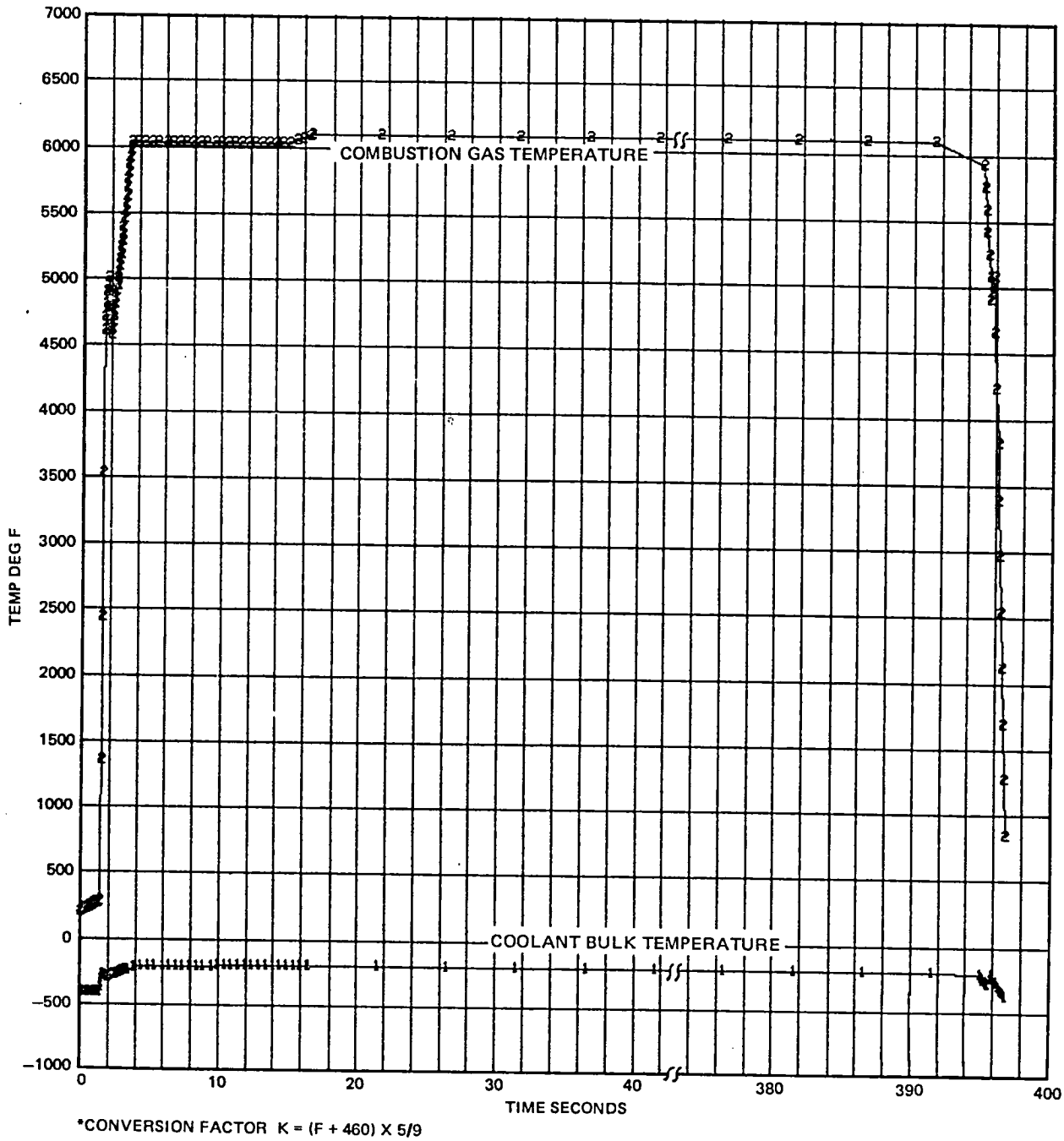

Figure 10. Combustion Gas Temperature and Hydrogen Coolant Temperature Duty Cycle Profiles for SSME at X=-3.1 cm (X=-1.22 Inch)

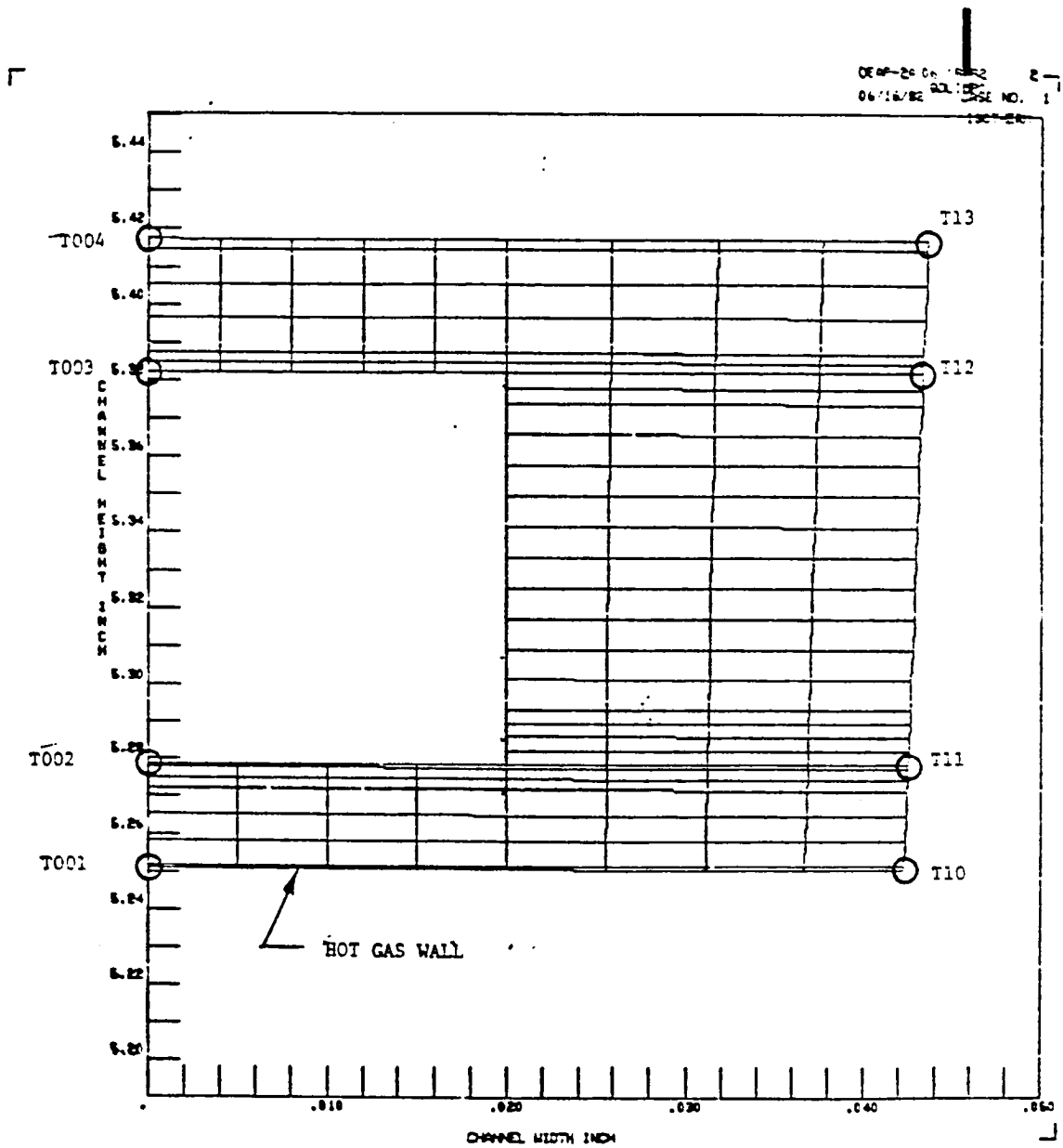

Figure 11. SSME MCC Coolant Channel Geometry at X=-3.1 cm (X=-1.22 Inch)

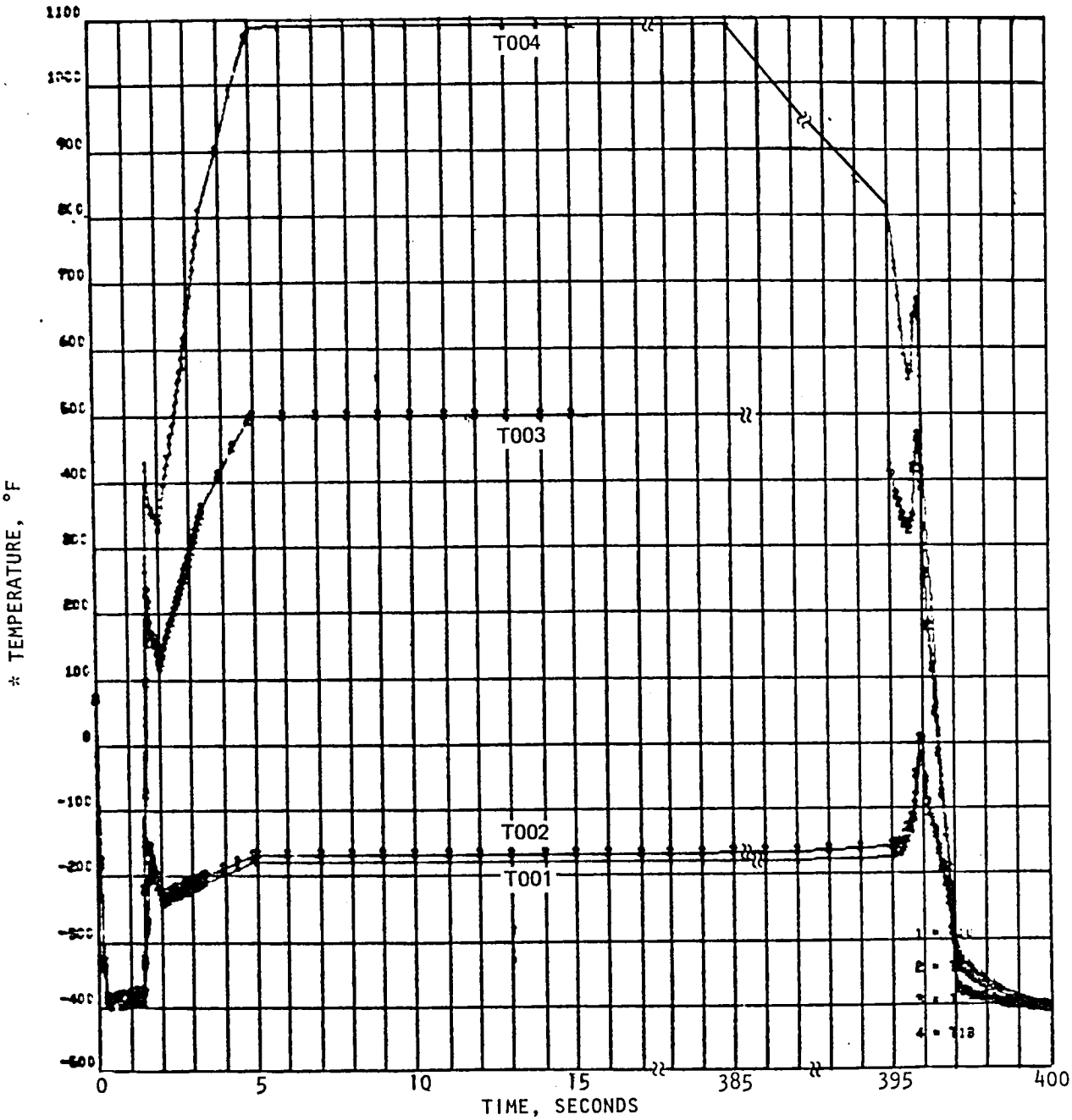

* CONVERSION FACTOR $^{o}K = (^{o}F + 460) \times 5/9$

Figure 12. SSME MCC Liner Midchannel Temperature Response at X=-3.1 cm (X=-1.22 Inch) at FPL Operation (100% FPL hg)

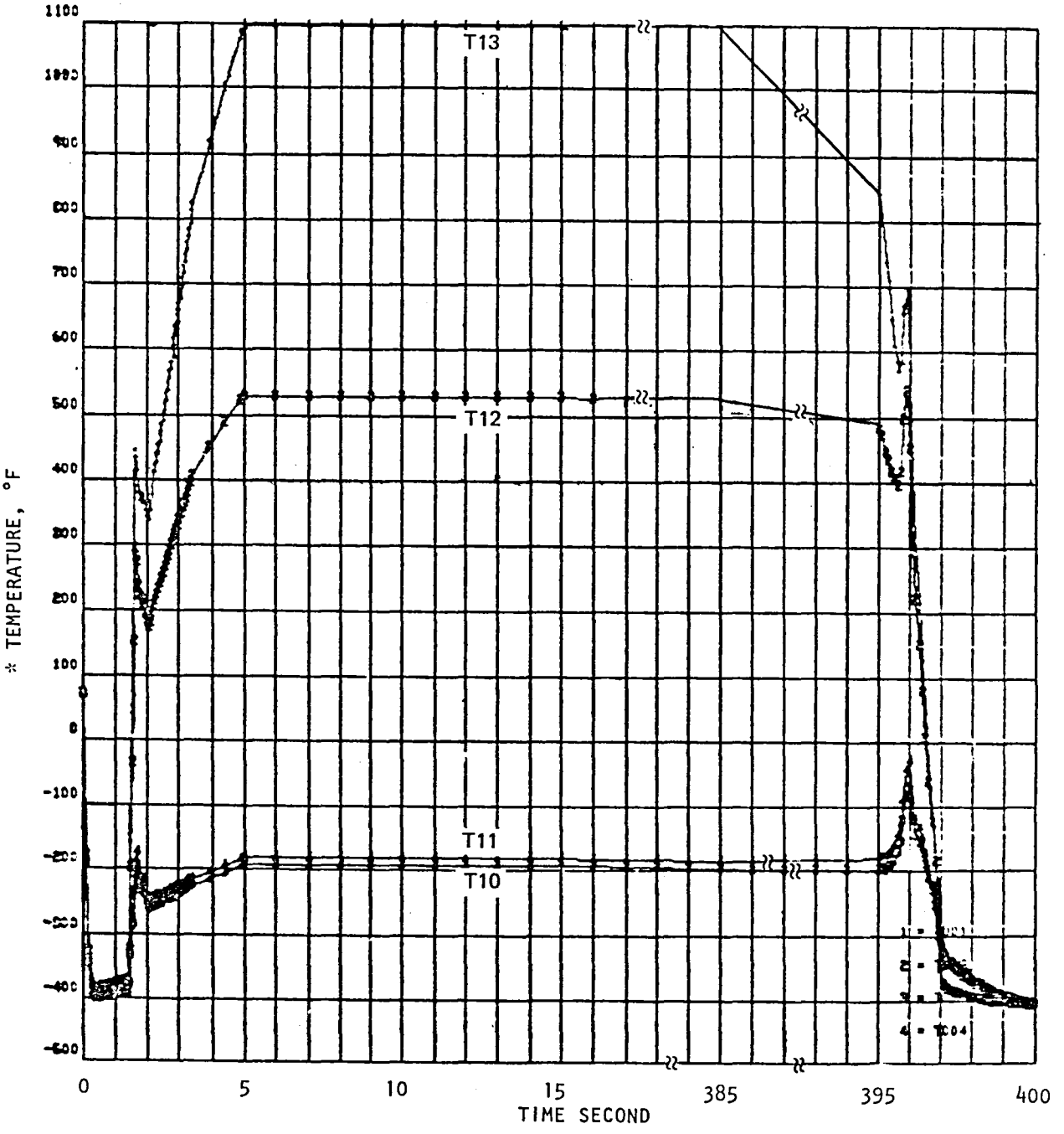

* CONVERSION FACTOR $^{o}K = (^{o}F + 460) \times 5/9$

Figure 13. SSME MCC Liner Midland Temperature Response at X=-3.1 cm (X=-1.22 Inch) at FPL Operation (100% FPL hg)

HEAT FLUX (HOT SPOT) SENSITIVITY

Hot-fire testing of channel wall combustors at Rocketdyne and NASA-LeRC has shown significant midchannel wall thinning or deformation during accrued cyclic testing of regeneratively cooled combustors. This phenomenon is termed cyclic-creep and appears to be significantly enhanced at elevated surface temperatures. The sensitivity of this phenomenon to surface temperature is evidenced by the nonuniformity of channel wall deformation around the circumference of the combustors. History has shown the nonuniformity is attributed to injector effects which may not necessarily be detectable by laboratory flow checks or physical measurements. This nonuniformity is first evidenced by local discoloration (blanching) of the copper base alloy hot-gas wall, signifying higher surface temperature hot spots. MCC regenerative cooled life hot-fire testing has shown that failurs occur in these circumferentially located hot-spot regions. The SSME-MCC axial thermal conditions were determined from measured 40K subscale hot-fire calorimeter chamber heat transfer rates. However, these type of measurements cannot distinguish circumferential heat transfer variations commonly associated with injection/combustion abnormalities.

Two hot spot thermal sensitivity studies were conducted at the life limited axial location -3.1 cm (-1.22 inch) to provide insight to the subsequent life sensitivity evaluation. These consisted of:

1. Heat Transfer (hg) Sensitivity

   Thermal (hg) assessment of nondeformed channels between an hg level of 100% FPL and 140% FPL was conducted. The influence of the gas side heat transfer (hg) level on the MCC hot-gas wall temperature over midchannel is shown in Fig. 14. The coolant channel thermal distribution is shown in Fig. 15 through 18 for hg levels of 110%, 120%, 130%, and 140%. The hot-gas wall temperature sensitivity to hg level is about 65 K (120 F) per 10% variation in the heat transfer rate.

2. Midchannel Wall Cyclic Creep Distention

   Thermal assessment of midchannel wall thinning sensitivity was conducted at the 120% hg level. These results are summarized in Fig. 19 which depicts midland and midchannel hot-gas wall temperature and mid-channel coolant wall temperature as a function of midchannel wall thickness. The channel wall geometry utilized for this preliminary assessment and the resultant thermal distributions are shown in Fig. 20 through 23 for four cyclic-creep distention levels.

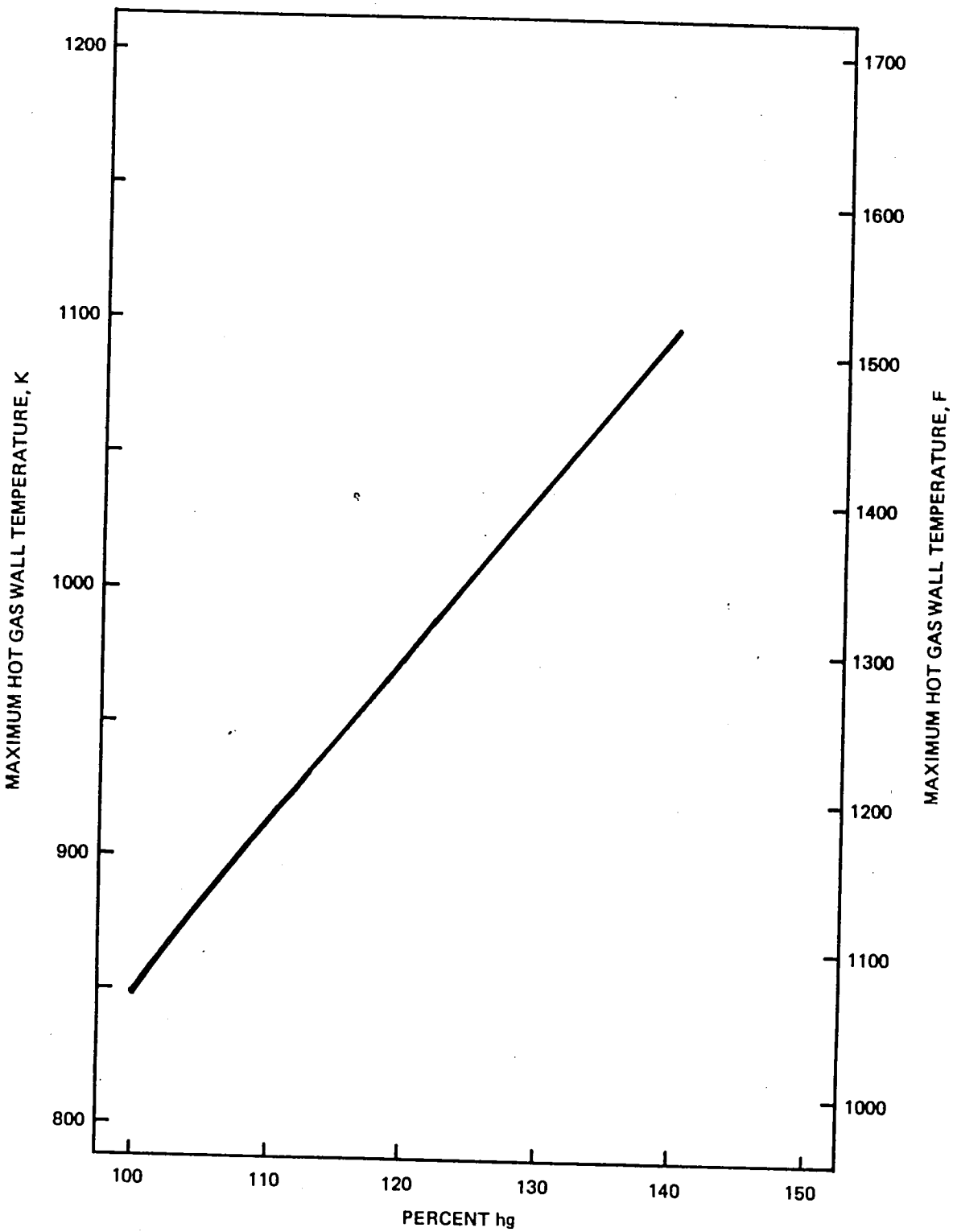

Figure 14. Impact of Hot-Gas Film Coefficient on Hot-Gas Wall Over Midchannel for Basic SSME-MCC Design

STATION NO. 31 ξ = -1.200 X/RT = -.233

NUMBER OF ITERATIONS = 35
DIFFERENCE BETWEEN HEAT IN AND HEAT OUT = .00422 PERCENT

HEAT INFLUX = 103.365
Z-D/L-D B/A = 1.03733

1161	1160	1179	1181	1183	1184
964	962	960	964	967	968
752	746	737	743	757	760
550	535	491	539	559	564
309	283	135			
132	109	33			
12	-5	-35			
-67	-79	-113			
-117	-125	-143			
-143	-154	-159			
-166	-170	-131			
-175	-178	-139	-198	-201	-202
-184	-186	-139	-191	-192	-193
-186	-187	-139	-190	-190	-191

HOT GAS WALL

COOLANT WALL

COOLANT CHANNEL

S.I. Conversion
K = 5/9 (F + 460)

CLOSE-OUT

1. LAND WIDTH = .04571
2. CHANNEL WIDTH = .04000
3. WALL THICKNESS = .02330
4. CHANNEL DEPTH = .10070
5. CLOSEOUT THICKNESS = .04000
6. TAW = 5295. DEG. F
7. HG = .0221540
8. TC = -211. DEG. F
9. REFERENCE HC = .1383856
10. HC FACTOR FOR UPPER WALL = 1.4000
11. HC FACTOR FOR LOWER WALL = 1.0000
12. EXPONENT = .5500
13-14. K OF REGION 1 = .004875 + (-.1870E-06) * T
15-16. K OF REGION 2 = .004875 + (-.1870E-06) * T
17-18. K OF REGION 3 = .001340 + (-.1390E-05) * T
19. CONVERGENCE CRITERION = .1000 DEG. F
20. COATING THICKNESS = 0.000000
21-22. COATING K = 0. + (0.) * T

Figure 15. Coolant Channel Thermal Distribution (110% FPL hg)

STATION NO. 31 X = -1.200 X/RT = -.235

NUMBER OF ITERATIONS = 42
DIFFERENCE BETWEEN HEAT IN AND HEAT OUT = .00778 PERCENT

HEAT INF IN = 115.113
2-D/1-D A/A = 1.04427

1293	1293	1293	1295	1297	1293
1351	1352	1353	1352	1355	1353
834	828	819	832	842	845
516	501	557	510	532	538
357	329	236			
165	140	64			
34	15	-39			
-52	-65	-112			
-107	-115	-141			
-141	-147	-154			
-161	-165	-175			
-171	-174	-185	-195	-200	-201
-181	-185	-185	-188	-190	-190
-184	-183	-185	-187	-183	-183

HOT GAS WALL

COOLANT WALL

COOLANT CHANNEL

S.I. Conversion
K = 5/9 (F + 460)

CLOSE-OUT

1. LAND WIDTH = .04571
2. CHANNEL WIDTH = .04000
3. WALL THICKNESS = .02310
4. CHANNEL DEPTH = .10070
5. CLOSEOUT THICKNESS = .04000
6. TAW = 5035. DEG. F
7. HG = .0241580
8. TC = -211. DEG. F
9. REFERENCE HC = .1333930
10. HC FACTOR FOR UPPER WALL = 1.4000
11. HC FACTOR FOR LOWER WALL = 1.0000
12. EXPONENT = .5500
13-14. K OF REGION 1 = .004875 + (-.1870E-06) * T
15-16. K OF REGION 2 = .004875 + (-.1870E-06) * T
17-18. K OF REGION 3 = .001340 + (-.1390E-05) * T
19. CONVERGENCE CRITERION = .1000 DEG. F
20. COATING THICKNESS = 0.000000
21-22. COATING K = 1. + (0.) * T

Figure 16. Coolant Channel Thermal Distribution (120% FPL hg)

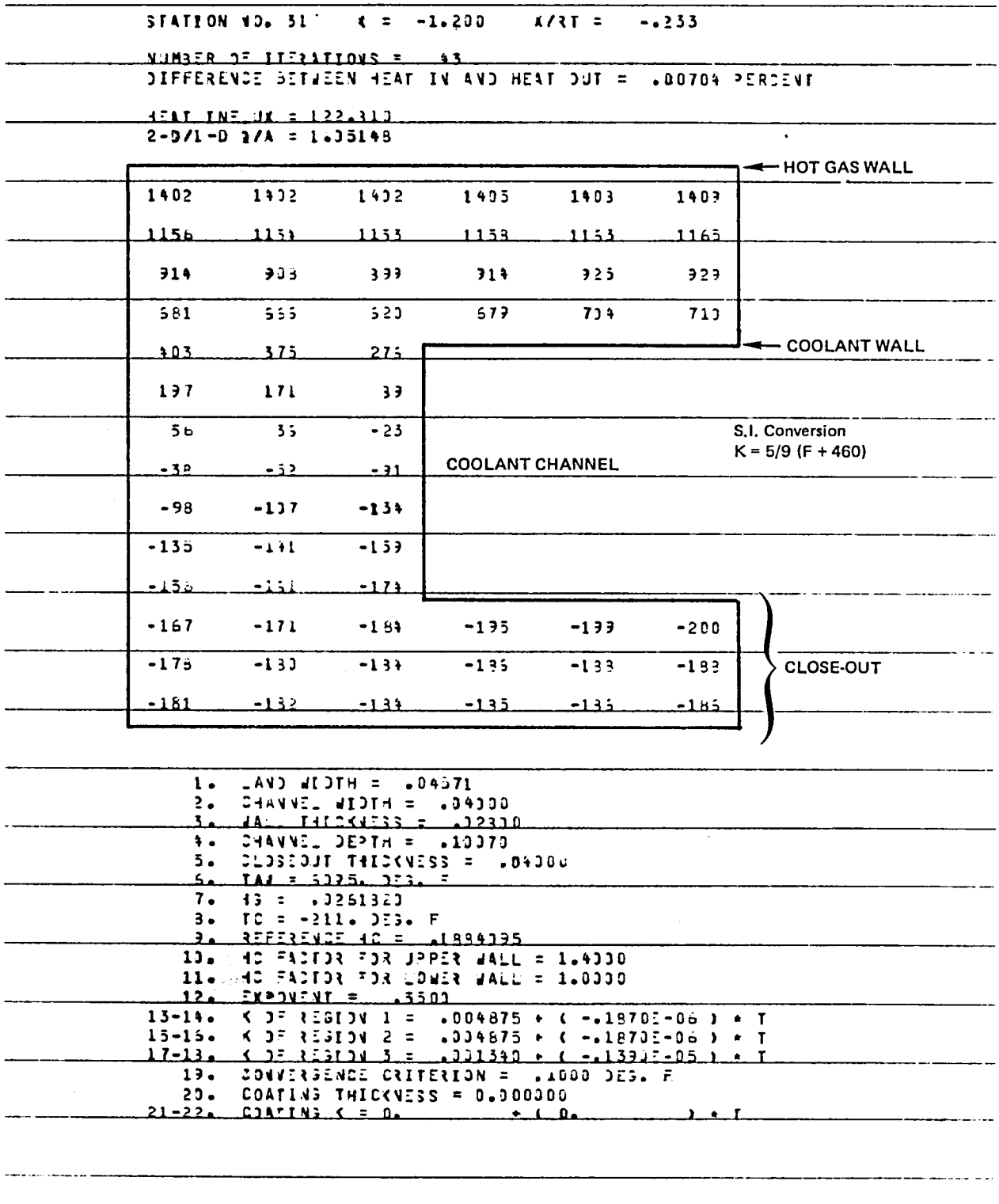

Figure 17. Coolant Channel Thermal Distribution (133% FPL hg)

STATION NO. 51 X = -1.200 X/RT = -.233

NUMBER OF ITERATIONS = 16
DIFFERENCE BETWEEN HEAT IN AND HEAT OUT = .00034 PERCENT

HEAT IN, BTU = 123.253
2-D/1-D B/A = 1.05374

1508	1503	1509	1512	1515	1517
1247	1245	1245	1251	1255	1253
991	985	978	994	1006	1010
745	729	535	747	774	781
342	319	315			
229	231	115			
77	55	-5			
-23	-33	-31			
-86	-93	-127			
-128	-135	-155			
-152	-157	-171			
-163	-157	-131	-193	-193	-199
-175	-177	-131	-134	-135	-186
-178	-173	-181	-182	-133	-184

HOT GAS WALL

COOLANT WALL

COOLANT CHANNEL

CLOSE-OUT

S.I. Conversion
K = 5/9 (F + 460)

1. LAND WIDTH = .04571
2. CHANNEL WIDTH = .04000
3. RIB THICKNESS = .02800
4. CHANNEL DEPTH = .13070
5. CLOSEOUT THICKNESS = .04000
6. TAW = 5035. DEG. F
7. HG = .0281950
8. TC = -211. DEG. F
9. REFERENCE HC = .1934212
10. HC FACTOR FOR UPPER WALL = 1.4000
11. HC FACTOR FOR LOWER WALL = 1.0000
12. EXPONENT = .5500
13-14. K OF REGION 1 = .004875 + (-.137JE-05) * T
15-16. K OF REGION 2 = .004875 + (-.187JE-06) * T
17-18. K OF REGION 3 = .001340 + (-.139JE-05) * T
19. CONVERGENCE CRITERION = .1000 DEG. F
20. COATING THICKNESS = 0.000000
21-22. COATING K = 0. + (0.) * T

Figure 18. Coolant Channel Thermal Distribution (140% FPL hg)

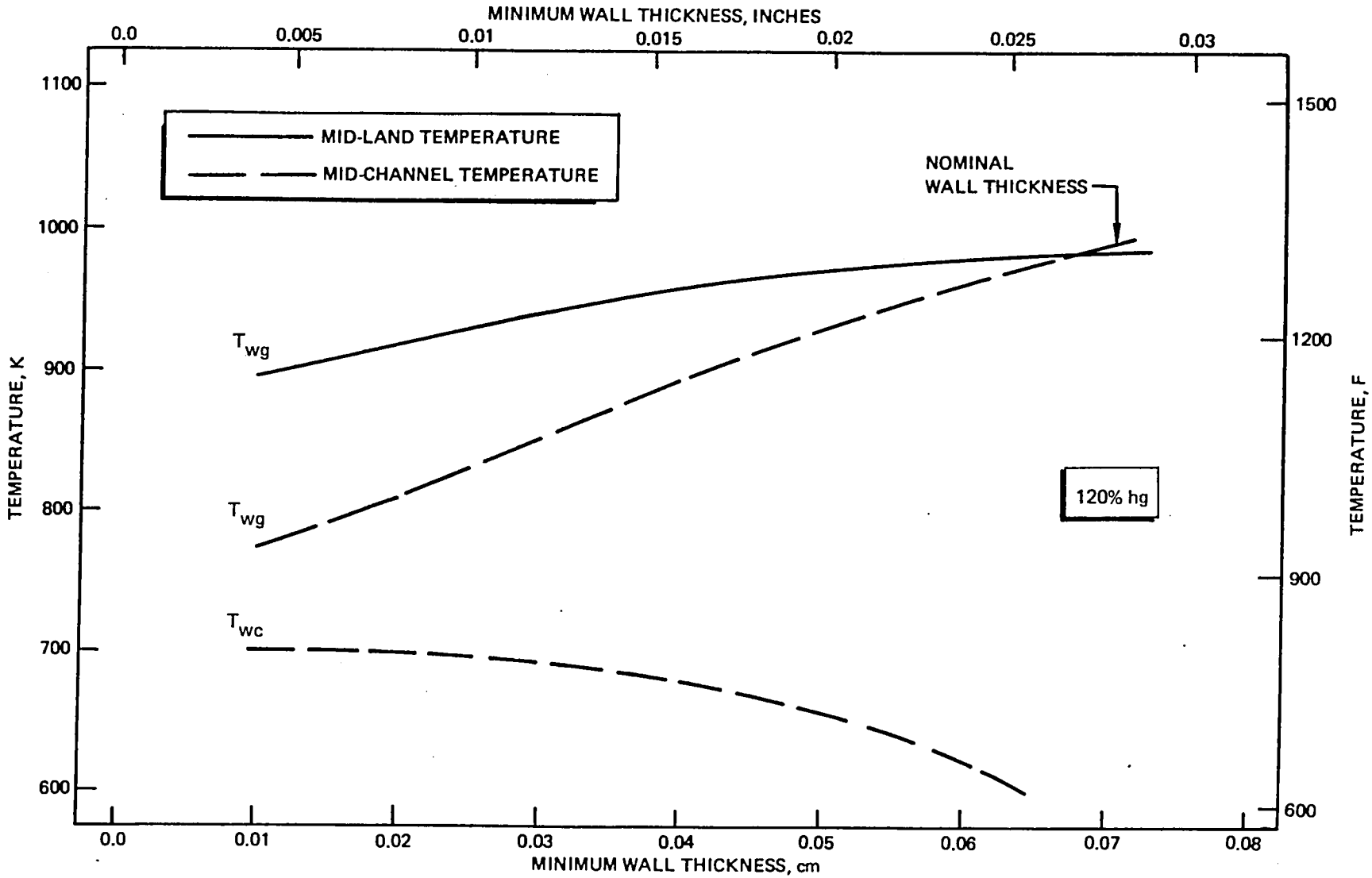

Figure 19. Influence of Midland and Midchannel Hot-Gas Wall and Coolant Wall Temperature as a Function of Midchannel Wall Thinning for 120% FPL hg

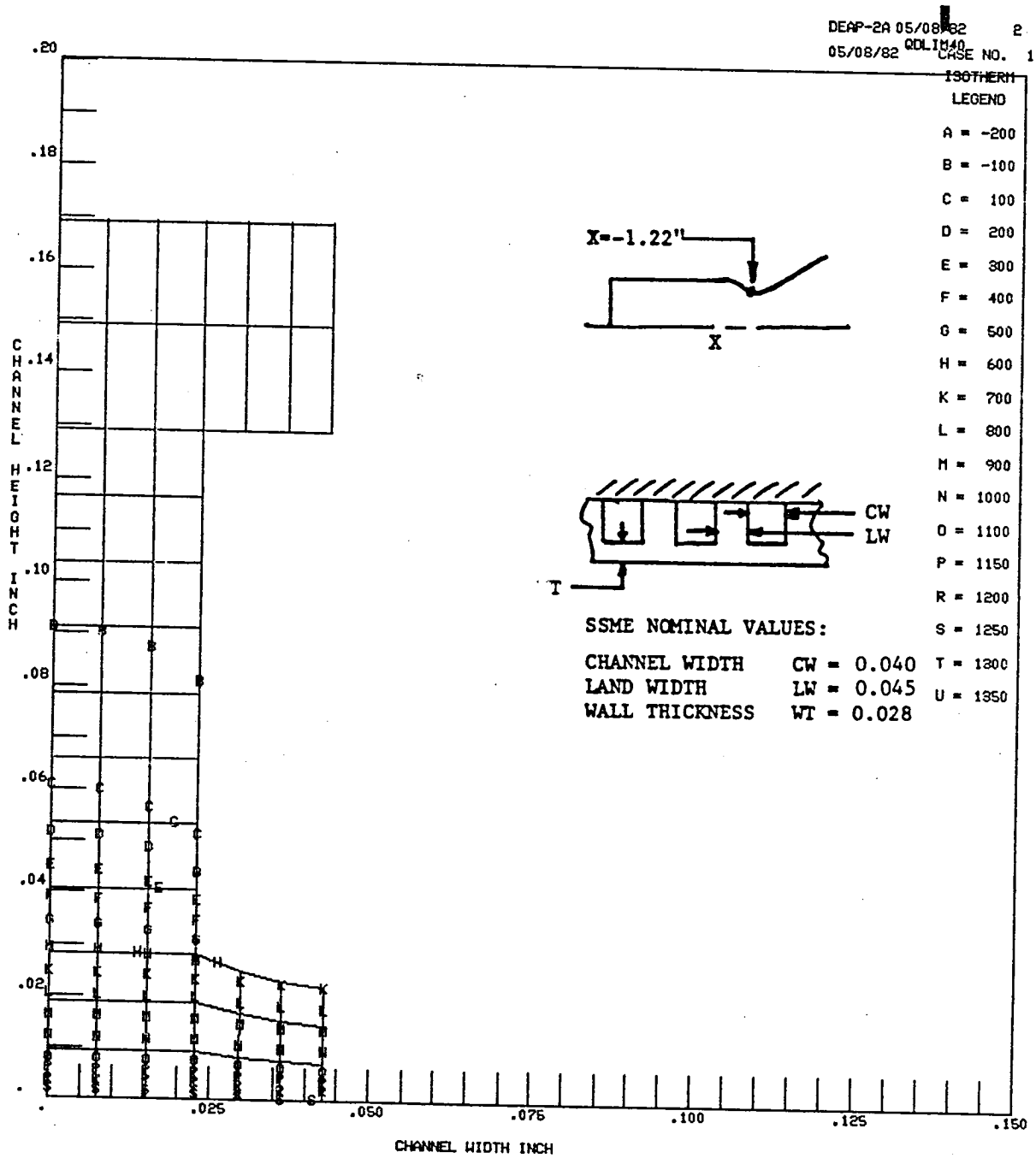

Figure 20. First Channel Geometry Cyclic-Creep Distention Isotherms at Minimum Wall Thickness = 0.056 cm (0.022 Inch) for 120% FPL hg

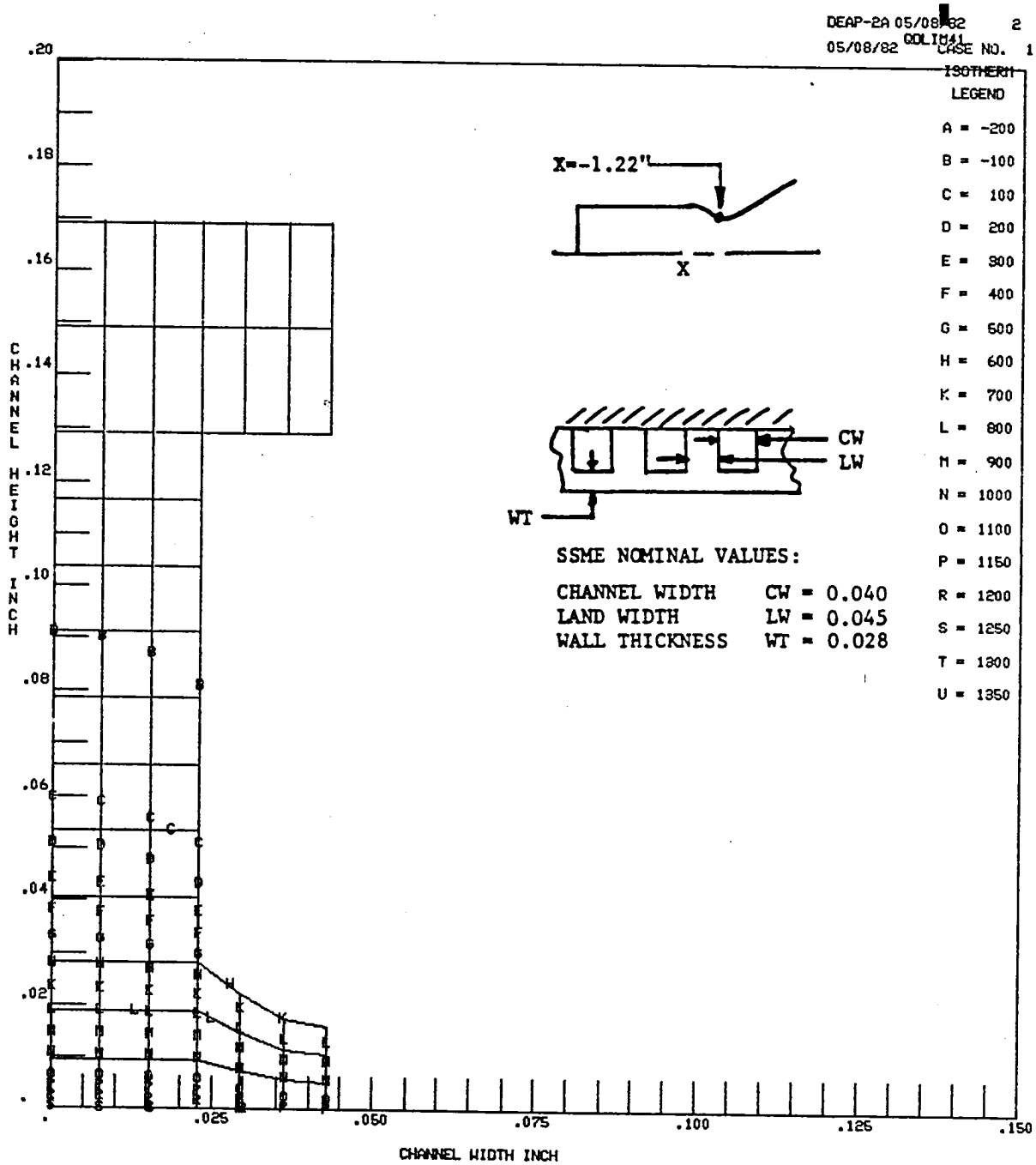

Figure 21. Second Channel Geometry Cyclic-Creep Distention Isotherms at Minimum Wall Thickness = 0.041 cm (0.016 Inch) for 120% FPL hg

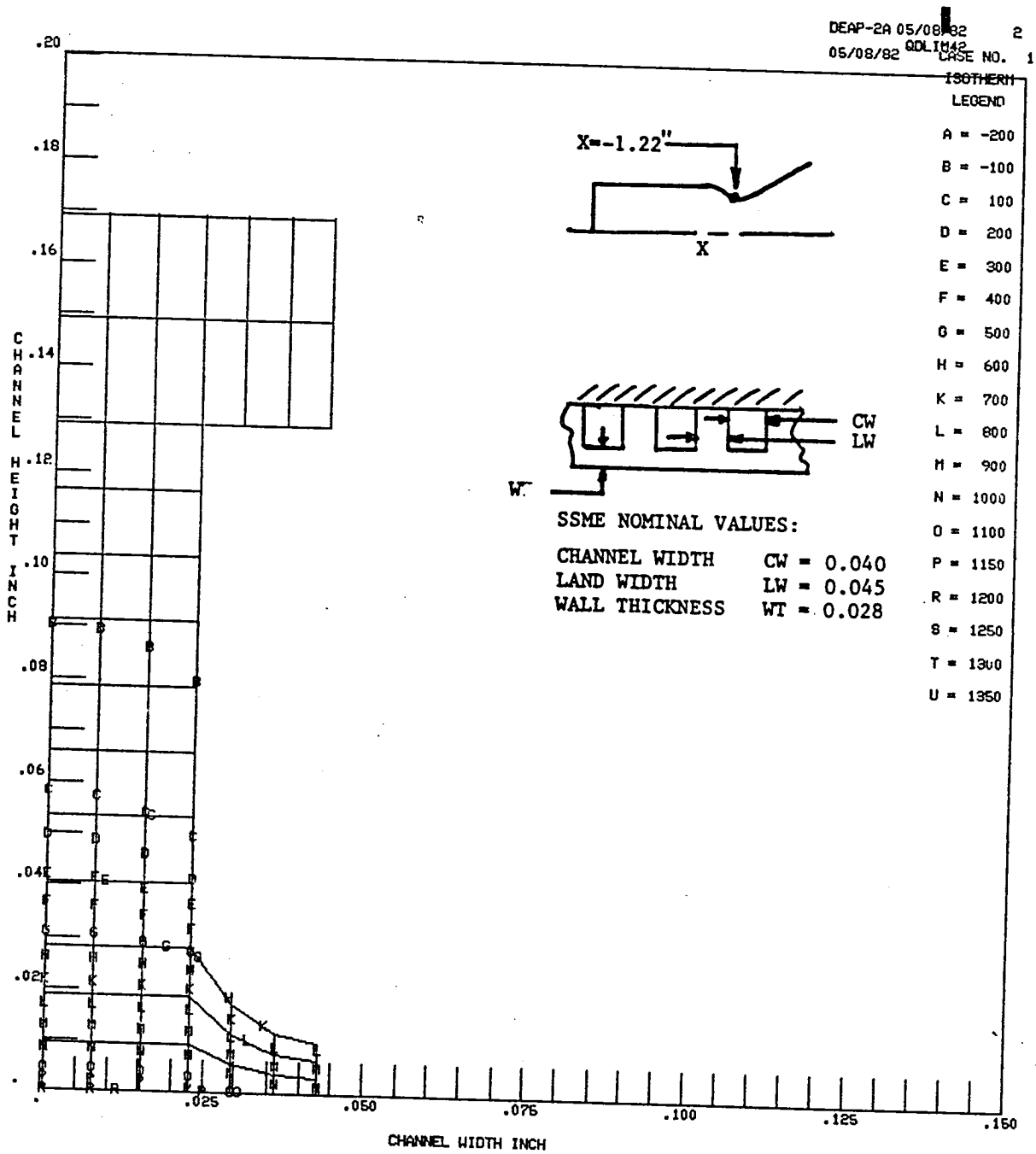

Figure 22. Third Channel Geometry Cyclic-Creep Distention Isotherms at Minimum Wall Thickness = 0.025 cm (0.010 Inch) for 120% FPL hg

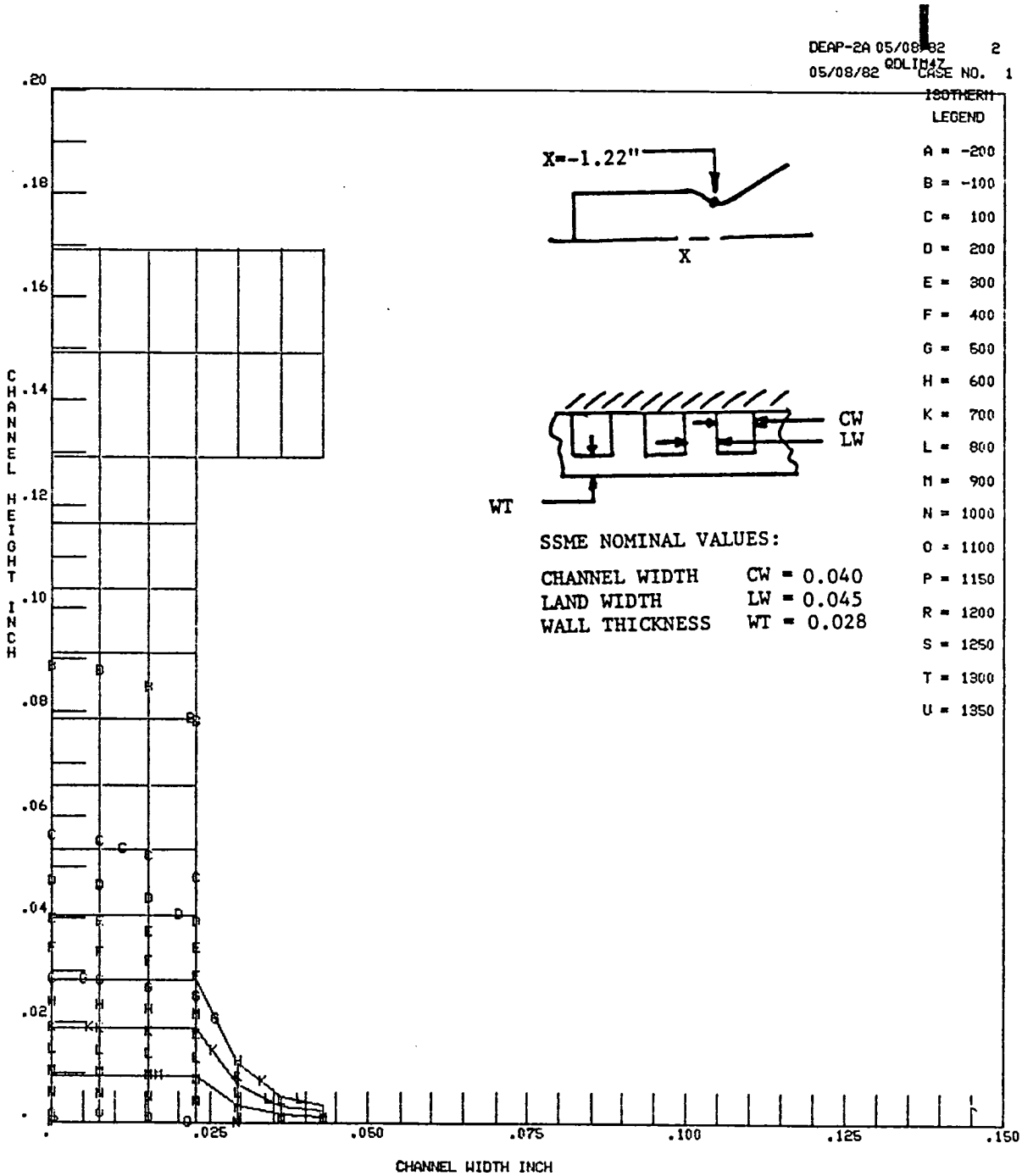

Figure 23. Fourth Channel Geometry Cyclic-Creep Distention Isotherms at Minimum Wall Thickness = 0.010 cm (0.004 Inch) for 120% FPL hg

LIFE ENHANCED DESIGNS

Four potential life-enhanced designs were assessed at the 135% hg level. This 135% gh level represents an extreme injector effected hot spot condition. This elevated thermal level may be related to the SSME-MCC liner thermal conditions near the time of incipient cyclic life channel failure and probably possesses some degree of hot gas wall surface roughening. These designs stemmed from the thermal sensitivity analyses and the cyclic-creep channel distention sensitivity analyses of the baseline SSME-MCC as related to hg level and strain level.

The selected designs, noted below, span a wide spectrum of channel geometry and manufacturing feasibility. The first two MCC liner designs can accommodate the current SSME-MCC without any changes to the inner mold-line (same hot gas wall contour) and outer mold-line (same structural jacket with the same Cu/Ni closeout thickness). These two designs require minimum to moderate technology advancements. The third and fourth designs require changing either the inner or outer MCC liner mold-lines. Either change would be costly, requiring new combustion chamber tooling plus a new structural jacket (outer mold-line change) or accepting a smaller throat diameter with a slightly modified hot gas wall contour. The third design requires moderate technology advancement while the fourth design requires entensive technology advancement.

1. Contoured Midchannel Coolant Wall
2. Increased Number of Channels
3. Keel-Rib (Midchannel Fin)
4. Combined Slotted Hot Gas Wall Midland with increased number of channels

These four life-enhanced designs are pictorially depicted in Fig. 24 and compared to the baseline SSME-MCC design at the life limited region located 3.1 cm (1.22 inch) upstream of the geometric throat. Pertinent dimensions, number of channels, and thermal operating conditions are noted for comparison. The thermal conditions represent a constant coolant ΔP equivalent to the SSME-MCC baseline design. The design considerations, guidelines, and constraints are discussed separately for each design as follow:

GUIDELINES

• Minimum Channel Width	0.076 cm	0.030 in.
• Minimum Land Width	0.076 cm	0.030 in.
• Minimum Wall Thickness	0.063 cm	0.025 in.
• Maximum Channel Height/Width	5:1	
• Coolant Liner Material	NARloy-Z	
• Hot Gas Wall Contour	Same as SSME	
• Coolant Pressure Drop	Same as SSME	

● THERMAL CONDITIONS ARE FOR 135% OF FPL hg EXCEPT AS NOTED FOR THE 100% FPL hg SSME DESIGN CONDITION

BASELINE SSME–MCC

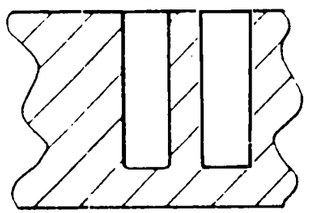

WALL THICKNESS	0.071 CM (0.028 IN.)
CHANNEL WIDTH	0.102 CM (0.04 IN.)
LAND WIDTH	0.102 CM (0.04 IN.)
CHANNEL HEIGHT	0.257 CM (0.101 IN.)
NO. OF CHANNELS	390

	100% FPL	135% FPL
Twg (MID CHANNEL)	848 K (1066 F)	1069 K (1464 F)
Twg (MID LAND)	847 K (1065 F)	1066 K (1458 F)
Twc (CHANNEL BASE)	528 K (490 F)	669 K (74[illegible] F)

(1) CONTOURED MID-CHANNEL WALL

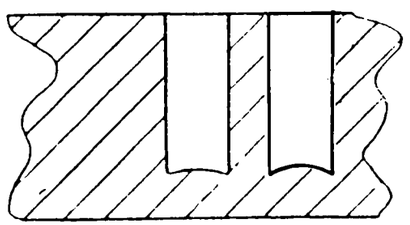

WALL THICKNESS	0.071/0.079 (0.028/0.031 IN.)
CHANNEL WIDTH	0.102 CM (0.04 IN.)
LAND WIDTH	0.102 CM (0.04 IN.)
CHANNEL HEIGHT	0.257 CM (0.101 IN.)
NO. OF CHANNELS	390
Twg (MID CHANNEL 1081 K	(1486 F)
Twg (MID LAND)	1066 K (1458 F)
Twc (CHANNEL BASE) 670 K	(745 F)

(2) INCREASED NUMBER OF CHANNELS

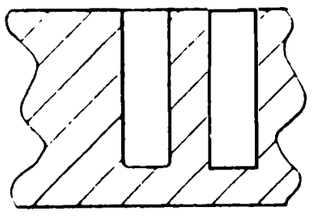

WALL THICKNESS	0.064 CM (0.025 IN.)
CHANNEL WIDTH	0.076 CM (0.03 IN.)
LAND WIDTH	0.076 CM (0.03 IN.)
CHANNEL HEIGHT	0.257 CM (0.101 IN.)
NO. OF CHANNELS	540
Twg (MID CHANNEL) 977 K	(1298 F)
Twg (MID LAND) 971 K	(1288 F)
Twc (CHANNEL BASE) 616 K	(649 F)

(3) KEEL RIB DESIGN

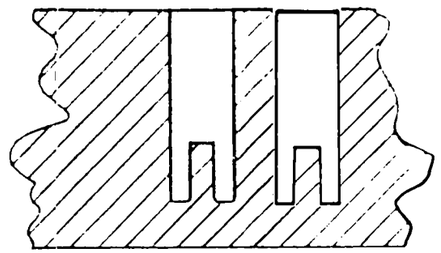

WALL THICKNESS	0.071 CM (0.028 IN.)
CHANNEL WIDTH	0.102 CM (0.04 IN.)
LAND WIDTH	0.102 CM (0.04 IN.)
CHANNEL HEIGHT	0.312 CM (0.123 IN.)
NO. OF CHANNELS	390
Twg (MID CHANNEL	963 K (1273 F)
Twg (MID LAND)	984 K (1311 F)
Twc (CHANNEL BASE)	520 K (475 F)

(4) SLOTTED HOT GAS MID-LAND WITH INCREASED NUMBER OF CHANNELS

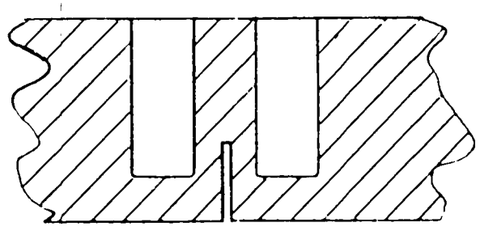

WALL THICKNESS	0.071 CM (0.028 IN.)
CHANNEL WIDTH	0.076 CM (0.03 IN.)
LAND WIDTH	0.102 CM (0.04 IN.)
CHANNEL HEIGHT	0.3 CM (0.118 IN.)
NO. OF CHANNELS	460
Twg (MID CHANNEL)	1006 K (1351 F)
Twg (MID LAND)	1006 K (1350 F)
Twc (CHANNEL BASE)	643 K (698 F)

MID-LAND SLOT = 0.010 WIDTH X 0.040 DEPTH

Figure 24. Comparison of Baseline SSME MCC Design and Life Enhanced Designs at 3.1 cm (1.22 Inches) Upstream of the Geometric Throat

CONTOURED MID CHANNEL WALL DESIGN

The contoured channel wall represents the minimum change life enhanced redesign. The same coolant channel geometry is utilized with the exception of increasing the wall thickness ($\leq$10%) at midchannel in an attempt to counteract the structural life phenomenon of midchannel thinning. The only design change to the current SSME-MCC is contouring the milling cutter to provide a slightly convex coolant channel inner wall. This change can be accommodated without an engine system rebalance and without any changes to the MCC coolant liner or structural jacket mold lines.

The thermal model and impact on the two-dimensional hot gas wall temperature of the MCC coolant channel as a function of wall thickness is shown in Fig. 25. The midchannel wall thickness was varied from a nominal value of 0.071 to 0.079 cm (0.028 to 0.031 inch). A hot gas film coefficient of 135% of FPL was used in this study to be consistent with other life enhanced design analyses. The results show that the maximum channel wall temperature increases 17 K (22 F) when compared to the nominal channel configuration for the maximum wall thickness considered.

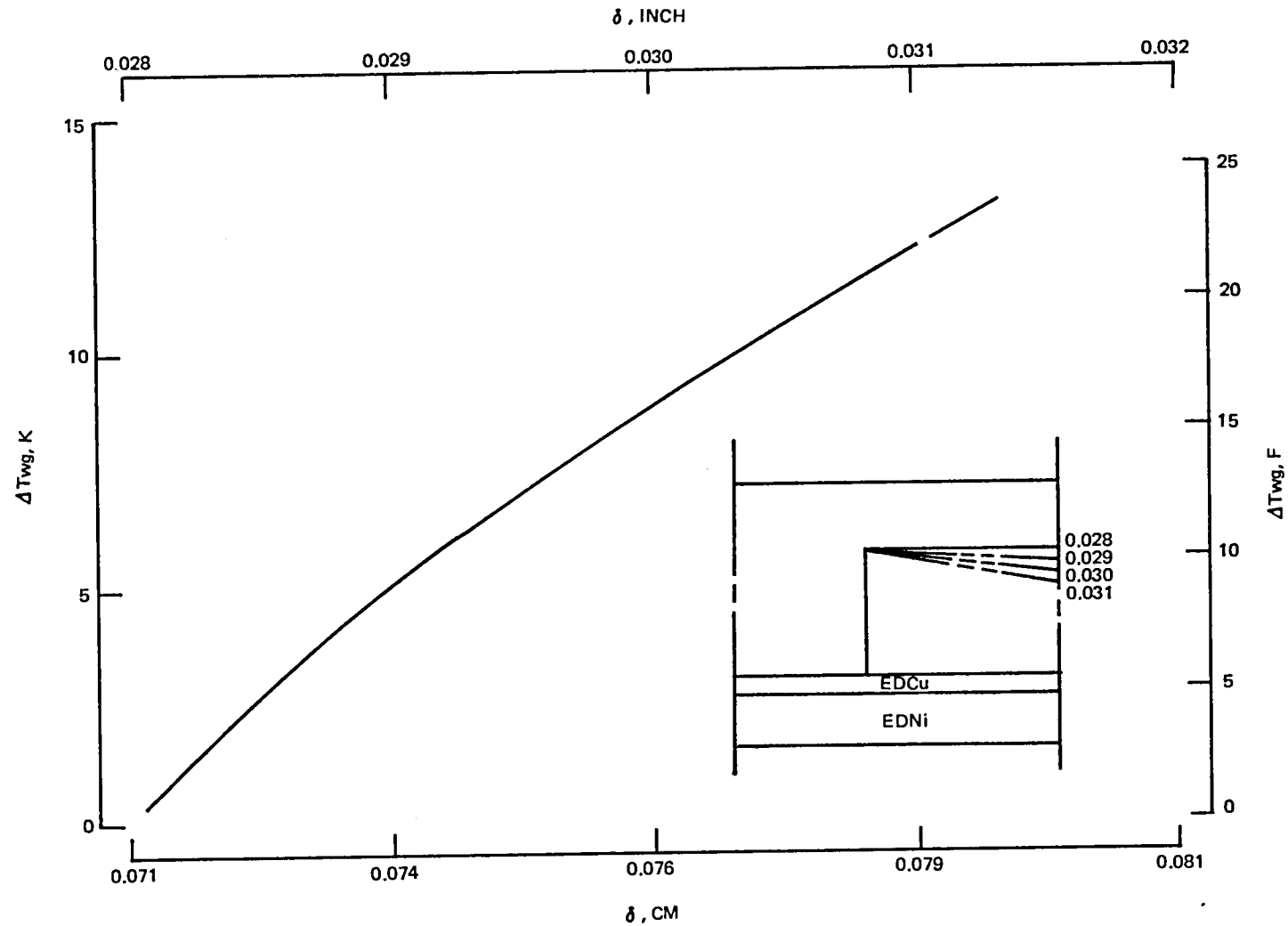

Figure 25. SSME MCC Hot-Gas Wall Temperature Increase at X = -3.1 cm (-1.22 inch) as a Function of Increased Midchannel Wall Thickness

INCREASED NUMBER OF COOLANT CHANNELS DESIGN

This life enhanced redesign utilizes a typical approach to increase life by reducing hot gas wall temperature while maintaining the same coolant delta pressure (ΔP) and therefore the same pump discharge pressure. This is accomplished by reducing the coolant channel width, wall thickness, and land width which results in increasing the number of channels from 390 to 540. This approach provides a larger surface area exposed to the coolant for the same hot gas wall surface area.

This redesign is the logical life enhanced approach that has been used over the past several years for future high pressure MCC design studies. The design constraints used for this redesign are shown in Table 1 and compared to the current SSME-MCC design parameters. The redesign constraints are typical of those used for previous NASA and Air Force studies.

TABLE 1. COMPARISON OF THE DESIGN PARAMETERS CONSTRAINTS OF THE LIFE ENHANCED INCREASED NUMBER OF CHANNELS REDESIGN AND THE SSME-MCC DESIGN IN THE LIFE-LIMITED THROAT REGION

PARAMETERS	SSME MCC DESIGN	INCREASED NUMBER OF CHANNELS REDESIGN
NUMBER OF CHANNELS	390	540
MINIMUM CHANNEL WIDTH	0.1016 cm (0.040 in.)	0.0762 cm (0.030 in.)
MINIMUM LAND WIDTH	0.10922 cm (0.043 in.)	0.762 cm (0.030 in.)
MAXIMUM CHANNEL HEIGHT/ WIDTH RATIO	5:1	5:1
MINIMUM HOT GAS WALL THICKNESS	0.07112 cm (0.028 in.)	0.0635 cm (0.025 in.)

This life enhanced design is considered to be currently feasible from a manufacturing viewpoint, but does require some fabrication verification. Areas requiring fabrication verification are:

1. Reduction of the minimum land width from the current 0.10922 cm (0.043 inch) on the SSME-MCC to 0.762 cm (0.030 inch). Fabrication verification is required to demonstrate adequate exposed surface area of the land for bonding the electrodeposited copper strike (to prevent hydrogen embrittlement) and the electrodeposited nickel closeout structure.

2. Reduction of the hot gas wall thickness from 0.0.07112 cm (0.028 inch) to 0.0635 cm (0.025 inch). The bending stress of this redesign is more favorable than the current SSME-MCC as reflected by the ratio of wall thickness to channel width. However, fabrication verification is required to assure that coining or bulging of the hot gas channel wall does not occur from the pressure of the milling cutter.

The life enhanced 540 channel design axial hot gas wall temperature profile is compared to the SSME-MCC design at 135% FPL hg in Fig. 26. The life limited throat region temperature distribution is shown in Fig. 26 for the 540 channel design and Fig. 27 for the SSME-MCC design at 135% FPL hg. This 540 channel design realizes a reduction of 92 K (165 F) in hot gas wall temperature.

The life enhanced redesign can accommodate the current SSME-MCC or any uprated version structural jacket and hot gas wall mold lines without any changes. The 540 channel design is optimized by increasing the channel height in the combustion zone which allows a more normalized hot gas wall temperature axial profile (see Fig. 28) and provides a ΔP tradeoff to allow the channel height reduction at the aerodynamic throat required to meet the SSME-MCC hot gas wall mold line.

STATION NO. 31 X = -1.200 X/RT = -.233

NUMBER OF ITERATIONS = 45
DIFFERENCE BETWEEN HEAT IN AND HEAT OUT = .00844 PERCENT

HEAT INFLUX = 136.563
2-D/1-D Q/A = 1.07859

1288	1289	1292	1295	1297	1298
1054	1054	1057	1062	1066	1068
820	818	819	833	844	847
591	582	556	615	641	649
284	283	197			
80	64	16			
-44	-54	-84			
-115	-122	-139			
-156	-160	-170			
-178	-180	-187			
-190	-192	-195			
-195	-197	-200	-203	-205	-205
-199	-200	-200	-201	-201	-201
-200	-200	-200	-200	-200	-201

HOT GAS WALL

COOLANT WALL

CLOSEOUT

S.I. Conversion
K = 5/9 (F + 460)

1. LAND WIDTH = .03186
2. CHANNEL WIDTH = .03000
3. WALL THICKNESS = .02500
4. CHANNEL DEPTH = .10100
5. CLOSEOUT THICKNESS = .04000
6. TAW = 6095. DEG. F
7. HG = .0271890
8. TC = -210. DEG. F
9. REFERENCE HC = .1896745
10. HC FACTOR FOR UPPER WALL = 1.4000
11. HC FACTOR FOR LOWER WALL = 1.0000
12. EXPONENT = .5500
13-14. K OF REGION 1 = .004875 + (-.1870E-06) * T
15-16. K OF REGION 2 = .004875 + (-.1870E-06) * T
17-18. K OF REGION 3 = .001340 + (-.1396E-05) * T
19. CONVERGENCE CRITERION = .1000 DEG. F
20. COATING THICKNESS = 0.000000
21-22. COATING K = 0. + (0.) * T

540

Figure 26. 540 Channel Design Thermal Distribution for 135% FPL hg

STATION NO. 31 Y = -1.200 X/RT = -.235

NUMBER OF ITERATIONS = 45
DIFFERENCE BETWEEN HEAT IN AND HEAT OUT = .00089 PERCENT

HEAT INFLUX = 125.273
2-D/1-D RATIO = 1.05510

1456	1455	1456	1459	1462	1464
1202	1200	1200	1205	1211	1212
953	947	939	954	965	970
713	693	652	713	739	746
426	337	235			
213	185	102			
56	46	-14			
-31	-45	-55			
-93	-102	-110			
-131	-138	-137			
-154	-159	-173			
-165	-169	-182	-194	-199	-200
-177	-179	-183	-185	-187	-187
-180	-180	-182	-184	-184	-185

HOT GAS WALL

COOLANT WALL

COOLANT CHANNEL

S.I. Conversion
K = 5/9 (F + 460)

CLOSE-OUT

1. LAND WIDTH = .04571
2. CHANNEL WIDTH = .04000
3. RIB THICKNESS = .02300
4. CHANNEL DEPTH = .10070
5. CLOSEOUT THICKNESS = .04000
6. TAW = 5035. DEG. F
7. HG = .0271890
8. TG = -211. DEG. F
9. REFERENCE HC = .1384150
10. HC FACTOR FOR UPPER WALL = 1.4000
11. HC FACTOR FOR LOWER WALL = 1.0000
12. EXPONENT = .5500
13-14. K OF REGION 1 = .004875 + (-.1870E-06) * T
15-16. K OF REGION 2 = .004875 + (-.1870E-06) * T
17-18. K OF REGION 3 = .001340 + (-.1390E-05) * T
19. CONVERGENCE CRITERION = .1000 DEG. F
20. COATING THICKNESS = 0.000000
21-22. COATING K = 0. + (0.) * T

Baseline 135

Figure 27. SSME-MCC Baseline 390 Channel Thermal Distribution for 135% FPL hg

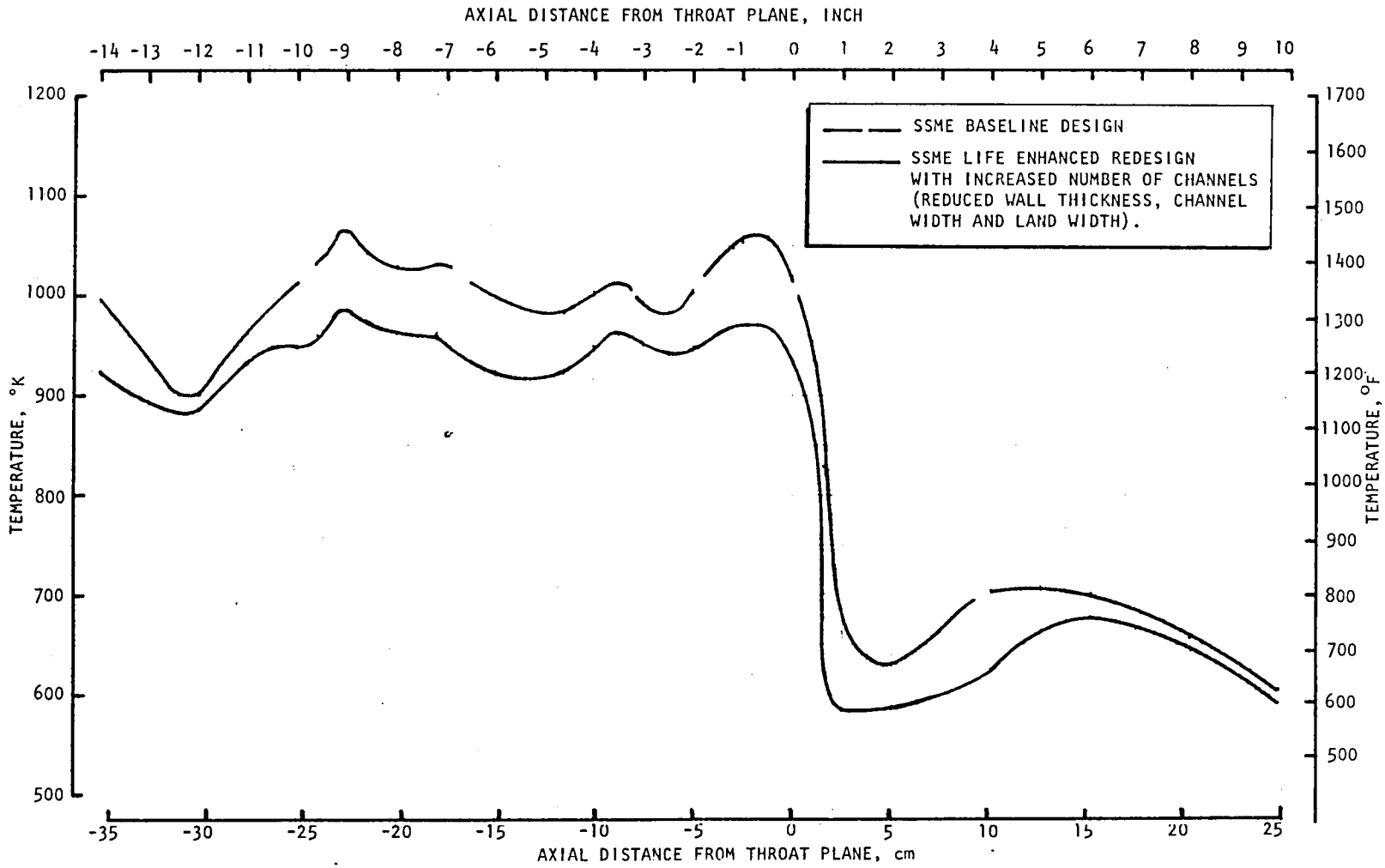

Figure 28. MCC Hot-Gas Wall Temperature Profile at 135% FPL for SSME Baseline Design and Life Enhanced Redesign With Increased Number of Channels

KEEL RIB (MID-CHANNEL FIN) DESIGN

This life enhanced design employs finned channels from the MCC throat plane to 3 inches downstream of the injector (11 inches upstream of the throat) as depicted in Fig. 29 to realize the maximum available reduction in the throat region hot-gas wall temperature.

The finned channel configuration is a straight uniform rectangular shape placed at mid-channel. The channel has a bi-width design typical of the SSME-MCC as shown in Fig. 30. The channel width is 0.062 inch in the combustion zone and narrows down to 0.040 inch in the throat region. The finned channel height and fin height are determined by the design constraints shown in Table 2. The logic diagram for determining the channel height is shown in Fig. 31 for a given fin height to channel ratio. For a constant coolant pressure drop, the ratio of wetted perimeter to the flow area is determined by

$$\left(\frac{WP_1}{WP_2}\right)\left(\frac{A_2}{A_1}\right)^3 = \left(\frac{\rho_1}{\rho_2}\right)$$

where WP, A, and ρ are the wetted perimeter, flow area, and coolant density, respectively. Subscripts 1 and 2 denote finned and nonfinned channel configuration respectively. Since the total heat input for the finned channel is usually 1 to 5% more, the density ratio effect is approximated by 0.978.

The cooling effectiveness of the fin was parametrically defined. Figure 32 shows the mid-channel and mid-land temperature as a function of fin height to channel height ratio. As noted in Fig. 32, the mid-channel is cooled more efficiently due to the fin effect. The maximum thermal efficiency is obtained for a fin height to channel height ratio of 30% for the SSME channel geometry. This is the keel-rib design used for life enhancement structural evaluation as shown in Fig. 33. Typical 2-D temperatures are shown in Fig. 34 for the fin height configuration selected in Fig. 34. The life enhanced redesign provides a 83 K (150 F) decrease in mid-channel hot-gas wall temperature as compared to the current SSME-MCC design.

COMBINED LIFE ENHANCEMENT DESIGN

(HOT-GAS WALL MID-LAND SLOTS WITH INCREASED NUMBER OF CHANNELS)

This life enhanced design consists of cutting axial slots in the liner hot gas surface over mid-land. The slots reduce the total effective strain in the liner by minimizing the compressive tangential strain. The effectiveness of this life enhanced design depends on the impact the slots have on the liner temperature and total heat load. A selected slot geometry was analyzed in detail and a parametric analysis was made to determine the effects of significant variables.

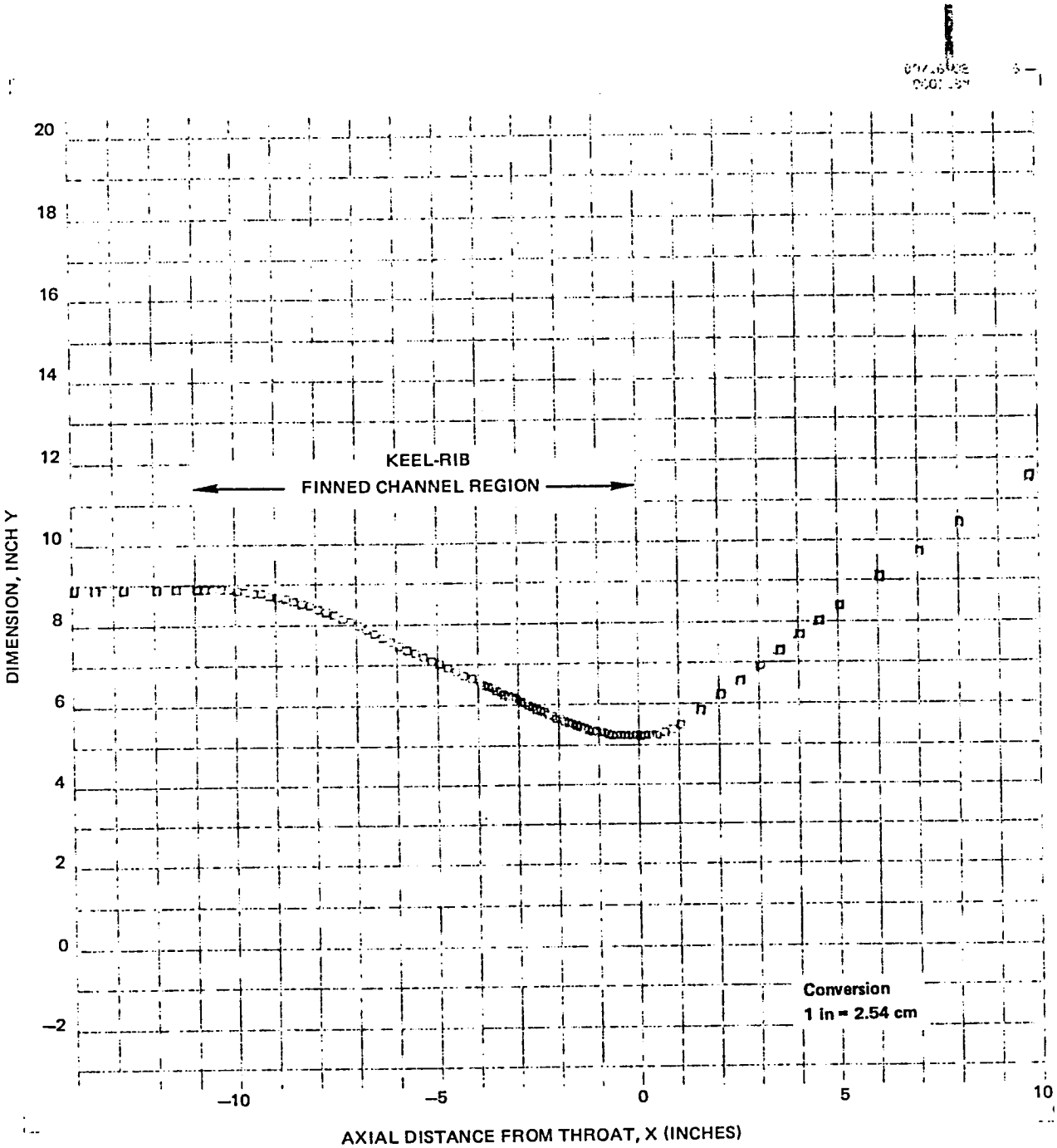

Figure 29. SSME MCC Contour Plot Noting Region of Finned Channels (Keel-Rib Design)

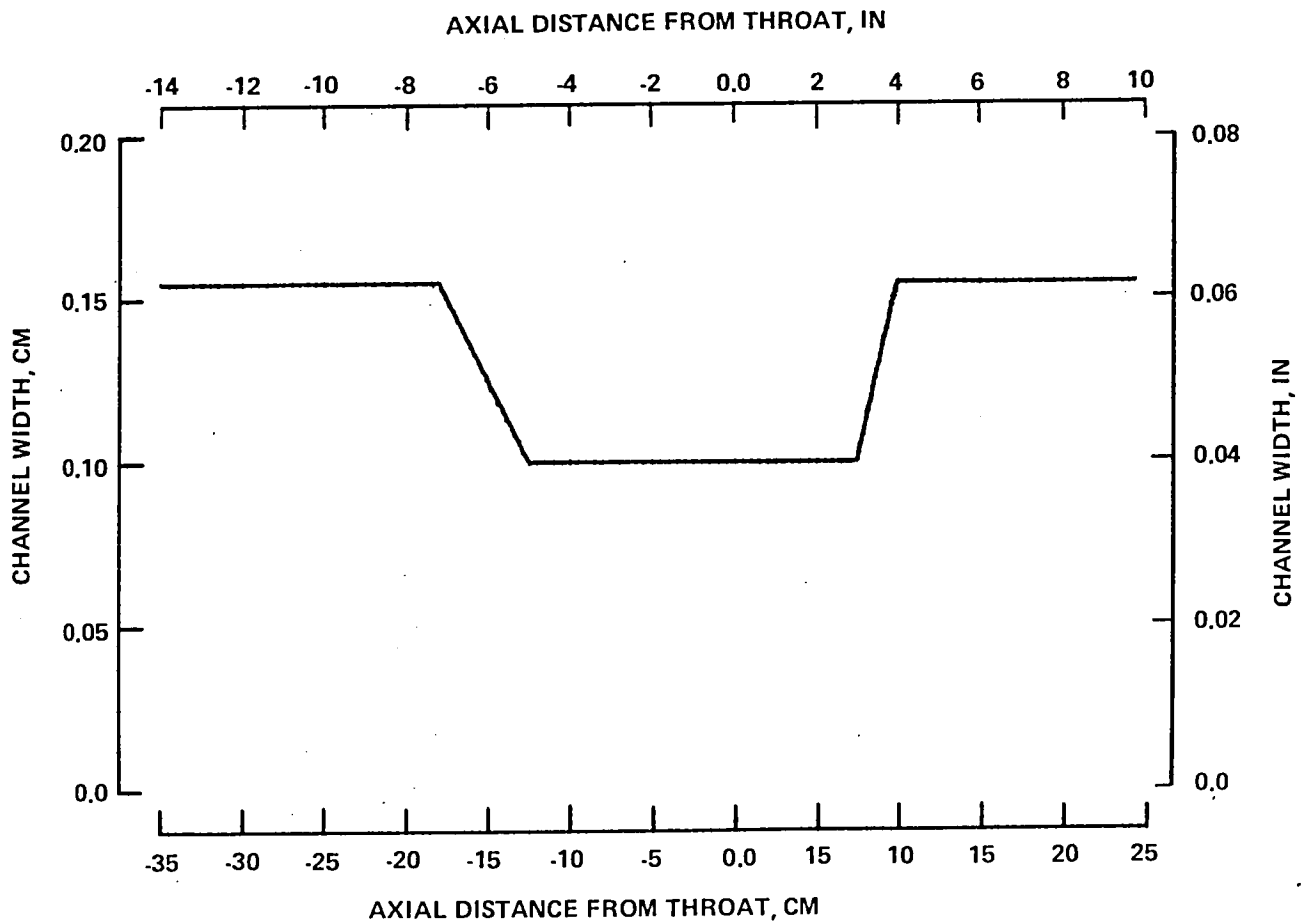

Figure 30. SSME MCC Coolant Channel Width Profile

TABLE 2. SSME MCC FINNED CHANNEL (KEEL-RIB) DESIGN CONSTRAINTS

PARAMETERS	CONSTRAINTS
NUMBER OF CHANNELS	390 (SAME AS SSME)
CHANNEL WIDTH, BI-WIDTH	0.157/0.102/0.157 CM 0.062/0.04/0.062 IN. (SAME AS SSME)
LAND WIDTH, MINIMUM	0.109 CM 0.043 IN. (SAME AS SSME)
HOT-GAS WALL THICKNESS (INCH)	0.084/0.066/0.084 CM 0.035/0.028/0.035 IN. (SAME AS SSME)
MAXIMUM CHANNEL HEIGHT/WIDTH	5:1

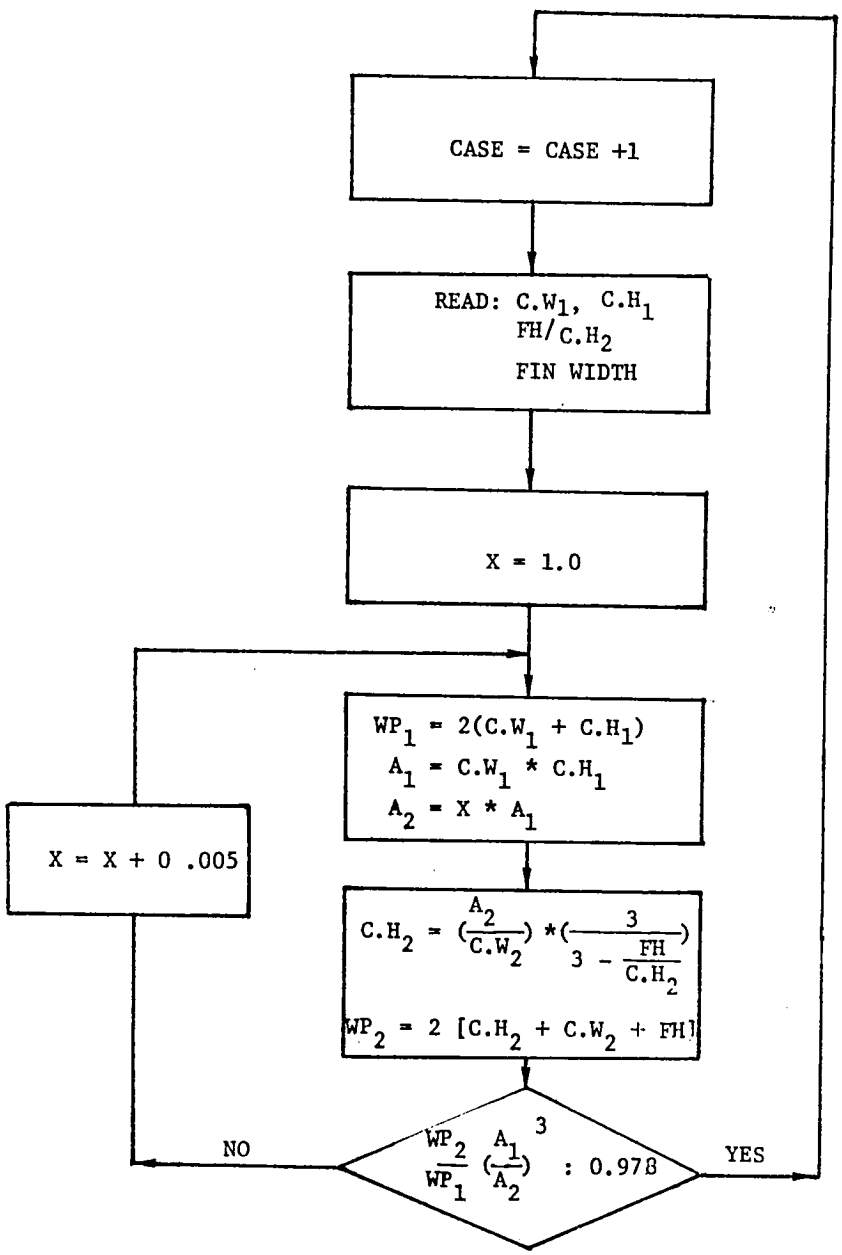

NOMENCLATURE:

X = MULTIPLIER
FH = FIN HEIGHT
C.W = CHANNEL WIDTH
C.H = CHANNEL HEIGHT
A = FLOW AREA
WP = CHANNEL WETTED PERIMETER

SUBSCRIPT:

1 = NON-FINNED
2 = FINNED

Figure 31. Procedure for Determining Finned Channel Parameters

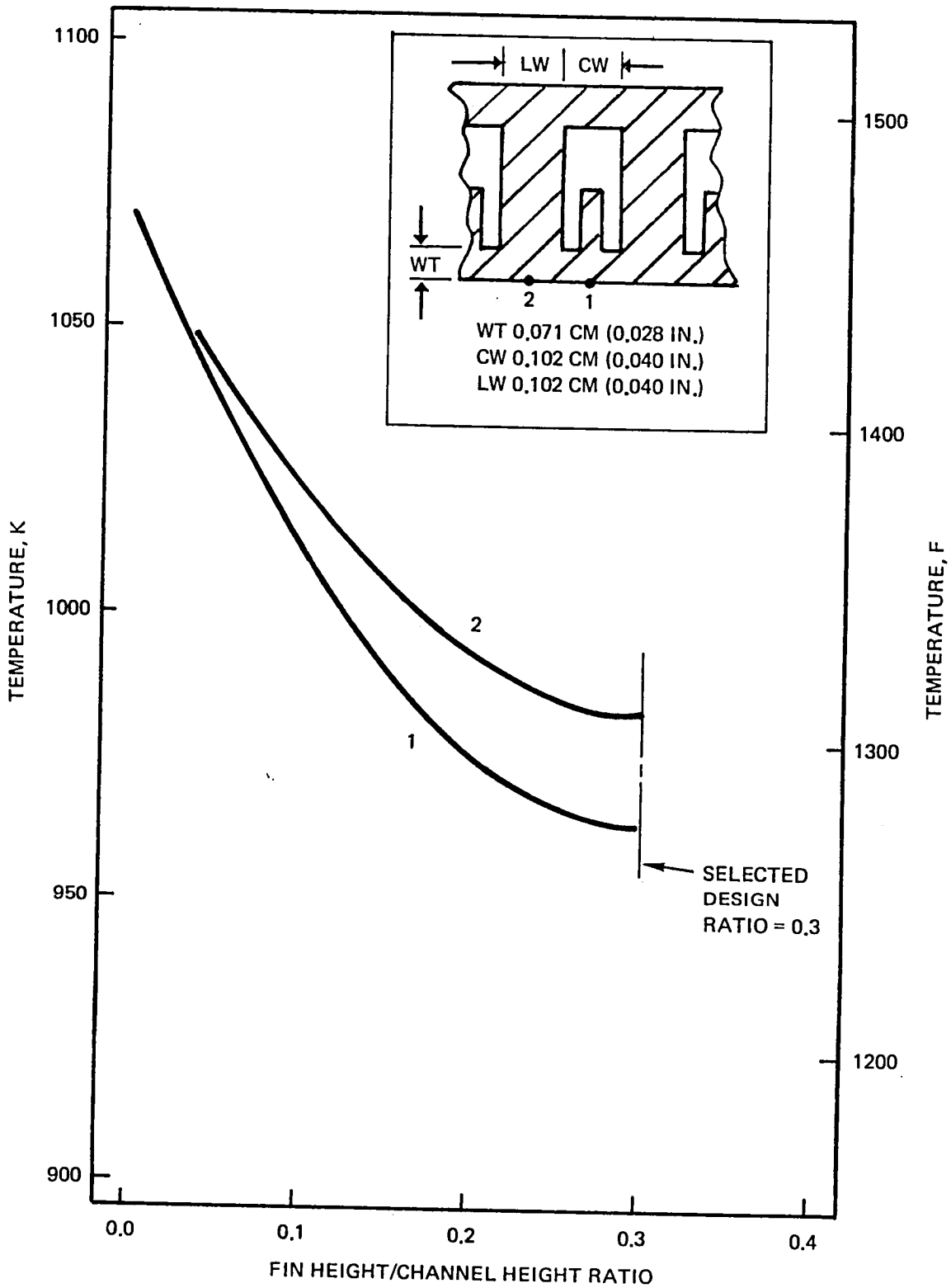

Figure 32. SSME MCC Finned Cooling Channel at X = -3.1 cm (-1.2 inch) Mainstage Temperature Profile for a Constant Coolant Pressure Drop at 135% FPL hg

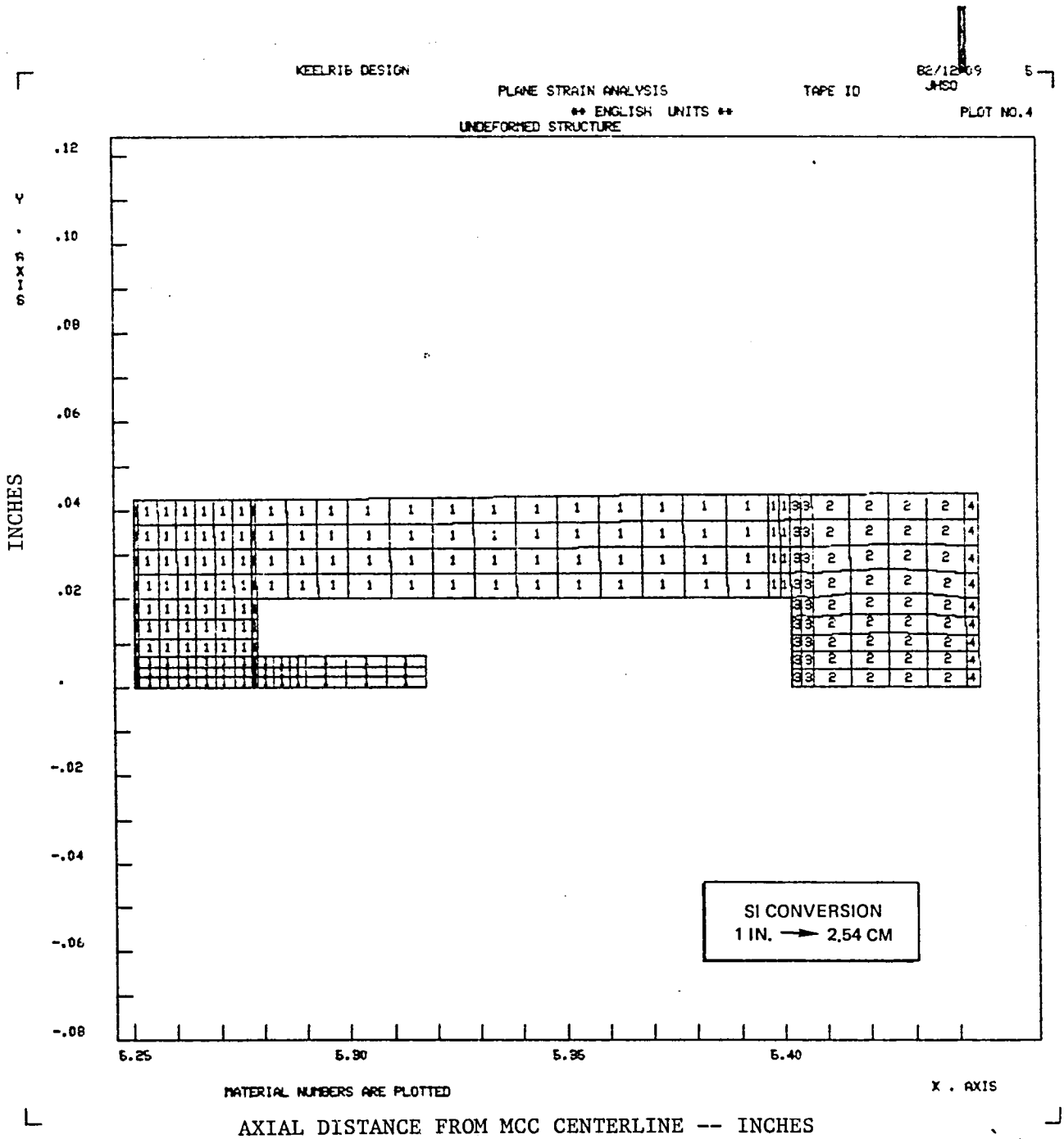

Figure 33. Keel Rib Geometry and Nodal Structure

STATION NO. 31 ℄ = -1.200 X/RT = -.233

NUMBER OF ITERATIONS = 54
DIFFERENCE BETWEEN IN AND HEAT OUT = .00642 PERCENT

HEAT INFLUX = 130.531

1273	1273	1275	1279	1284	1290	1300	1308	1311
1006	1006	1009	1014	1020	1027	1041	1051	1054
730	731	734	745	757	766	789	805	811
440	439	454	476	503	496	549	578	588
258	254	245			168	233	277	289
100	94	72			5	53	82	92
-6	-11	-27			-83	-53	-34	-28
-75	-78	-83			-132	-114	-103	-99
-117	-119	-126			-160	-149	-143	-140
-141	-143	-148			-175	-169	-165	-163
					-183	-179	-177	-176
-194	-193	-192	-192	-190	-187	-184	-182	-181
-189	-189	-189	-188	-188	-187	-185	-186	-185
-188	-188	-188	-188	-188	-187	-187	-186	-186

HOT GAS WALL

FIN

S.I. Conversion
K = 5/9 (F + 460)

CLOSE-OUT

4. FIN HEIGHT = .03850
3. FIN BASE = .01333
1. LAND WIDTH = .04537 FIN TIP WIDTH = .01333
2. CHANNEL WIDTH = .04000 HG FACTOR = 1.00000
3. WALL THICKNESS = .02800
4. CHANNEL DEPTH = .12270
5. CLOSEOUT THICKNESS = .04000
6. TAW = 5095. DEG. F
7. HG = .0271890
8. TC = -199. DEG. F
9. REFERENCE HC = .26359
10. HC FACTOR FOR UPPER WALL = 1.4000
11. HC FACTOR FOR LOWER WALL = 1.0000
12. EXPONENT = .55000
13-14. K OF REGION 1 = .004875 + (-.1870E-06) * T
15-16. K OF REGION 2 = .004875 + (-.1870E-06) * T
17-18. K OF REGION 3 = .001340 + (-.1390E-05) * T
19. CONVERGENCE CRITERION = .1000 DEG. F

Keel Rib

Figure 34. Keel Rib Thermal Distribution at 135% FPL hg

The heat transfer within the hot-gas wall slot is a function of

1. The radial mass transfer between the combusiton gas and the slot gas
2. The axial flow of the gas within the slot
3. The heat flow to the slot walls

The mass transferred to the slot is from the boundary layer that has developed on the chamber liner wall. The boundary layer gas is at a lower temperature than the mainstream combustion gas. The transfer of this gas into the slot represents a complex flow condition which may result in a very thin boundary layer at the slot corners, causing high local heat transfer rates. This analysis considers only axial gas flow and does not attempt to account for these boundary layer corner effects.

Analytical Approach

The slot configuration at any axial position was shown schematically in Fig. 24. A one-dimensional compressible gas flow analysis is used to determine the mass flowrate within the slot. The slot mass velocity is adjusted through mass exchange between the slot and undisturbed hot-gas wall static pressure. Once the slot flowrate profile is determined, the heat transfer between the slot gas and the liner can be determined and, hence, the liner temperature can be calculated. The equations used for arriving at the solution at each axial position are described below.

1. Slot Gas Mach Number

   The slot gas Mach number is calculated from the following compressible gas flow relationship.

$$\frac{W}{A} = \sqrt{\frac{\gamma}{R}}\,\frac{P}{T_o}\sqrt{1 + \frac{\gamma-1}{2} M^2}$$

where

- W = slot gas flow rate
- A = slot cross-sectional area
- γ = ratio of slot gas specific heats
- R = gas constant of slot gas
- P = slot gas static pressure
- T_o = slot gas stagnation temperature
- M = slot gas Mach number

2. Friction Factor

   The friction factor for the slot gas is calculated from the Darcey-Weisbach equation, given below. (This relationship is typical of that used for tube and channel flow.)

$$\frac{1}{\sqrt{f}} = 1.74 - 2 \log \left(\frac{2\epsilon}{D_h} + \frac{18.7}{Re\sqrt{f}}\right)$$

where

f = Darcey-Weisbach friction factor
c = slot surface roughness
D_h = slot hydraulic diameter
Re = Reynolds number of slot gas

The Fanning friction factor (which is used in a subsequent calculation) has a value one-fourth the Darcey-Weisbach friction factor.

3. Heat Transfer

The heat transfer from the slot gas to the liner wall is determined as follows. The slot gas convective heat transfer coefficient is calculated using a empirical equation for flow within passages.

$$hg = 0.023 \frac{k}{D_h} Re^{0.8} Pr^{0.4}$$

where

hg = convective heat transfer coefficient
k = thermal conductivity of slot gas
Pr = Prandtl number of slot gas

Then the heat transfer per unit mass of slot gas is calculated from

$$Q = hg\ A\ (T_{wg} - T_o)/w$$

where

Q = heat transfer per unit mass of slot gas
A = slot wall heat transfer area
T_{wg} = slot wall surface temperature

4. Enthalpy Charge of Slot Gas

The change in enthalpy of the slot gas depends on whether there is mass transfer from the mainstream to the slot ($\Delta w > 0$) or mass transfer from the slot to the mainstream ($\Delta w > 0$). The change in slot gas enthalpy per unit mass of slot gas can be written as

$$\Delta H = C_p [T - T_o)_{slot}] \frac{\Delta w}{w}$$

where

ΔH = enthalpy change of slot gas per unit mass of slot gas
C_p = specific heat of slot gas
T = T_o of mainstream gas for $\Delta w > 0$
T = T_o of slot gas for $\Delta w > 0$

5. Equation for Change in Stagnation Temperature

Once the heat transfer (ΔQ) and enthalpy change (ΔH) of the slot gas are known, an equation for the charge: in stagnation temperature can be written

$$\Delta T_o = (\Delta Q + \Delta H)/C_p$$

By substituting for ΔH and dividing by $C_p T_o$, this equation becomes

$$\frac{\Delta T_o}{T_o} = \frac{\Delta Q}{C_p T_o} + \frac{T - T_o}{T_o} \frac{\Delta w}{w}$$

6. Equation for Change in Flowrate

Using the table of influence coefficients for constant specific heat and molecular weight, the equation for the change in flow rate as a function of pressure gradient, area change, stagnation temperature change, friction factor, and Mach number can be written as

$$\frac{\Delta w}{w} = \frac{\left[-\frac{\Delta P}{P}\right] + \left[\frac{-\gamma M^2 (1 + \frac{\gamma-1}{2} M^2)}{1 - M^2}\right] \frac{\Delta T_o}{T_o} + \left[\frac{-\gamma M^2 \; 1 + (\gamma-1)M^2}{2\,(1-M^2)}\right] 4f \frac{\Delta x}{D_h} + \frac{\gamma M^2}{(1-M^2)} \frac{\Delta A}{A}}{\frac{2\gamma M^2 (1 + \frac{\gamma-1}{2} M^2)}{1 - M^2}}$$

The equations for the change in stagnation temperature and flowrate were solved simultaneously for ΔT_o and Δw. By marching axially along the slot in small increments (Δx), the flowrate and stagnation temperature profiles for the slot gas flow were determined for a particular slot geometry.

The stagnation temperature of the free stream gas is assumed to be 6500 R throughout the length of the combustor. The liner wall temperature to which the slot gas transfers heat is assumed to be 1000 F. For the major portion of the liner (injector to throat), this is a reasonable average temperature of the surface of the slot periphery (as verified by subsequent two-dimensional results).

The free stream static pressure profile corresponds to the local wall operating condition. This should be the most severe operating condition relative to heat transfer in the slot. The surfaces of the slot are assumed to be at a finish of 40 microinches rms for calculation of the friction factor.

At the beginning of the slot, the stagnation temperature of the gas in the slot is set equal to the mainstream gas. An initial value is assumed for the flow rate in the slot. This is not at all critical since the initial flow rate value was found to affect the flow solution for only a short distance at which time the solution becomes independent of the initial flow rate estimate.

Parametric Analysis

Parametric analyses were made to provide insight to acceptable slot dimensions. For these analyses, it was assumed the slots were initiated 1 inch downstream of the injector, since it is possible the slots will be cut throughout the combustion zone. The slots are terminated 2 inches downstream of the throat since the liner strains in the nozzle portion of the chamber are much lower than the combustion zone and throat. For 1 inch at the beginning and end of each slot, the slot depth is tapered linearly to its maximum value. Therefore, from 12 inches upstream of the throat (2 inches from the injector) to 1 inch downstream of the throat, the slot depth is maintained constant. A constant width is used for the entire length of each slot. The axial location of the slots in the combustion zone could be tayloreed to the amount of strain or strain relief desired to extend the chamber life. Thus, while this study investigates slots that extend through most of the combustion zone, shorter length slots that are cut only in the throat region may provide all of the cycle life extension that is desired. However, the reduction of slot adiabatic wall temperature with slot length must be considered.

The mass flux profile in the slots along the axial position of the chamber is shown in Fig. 35. For comparison, the main chamber hot gas mass flux profiel is also shown. An increase in mass flux means that gas is being added to the slot from the mainstream gas while the opposite is true when the mass flux is decreased (supersonic region). Since the heat transfer coefficient is directly related to the mass flux, the heat transfer in the slot will be highest where the mass flux is highest (throat region) for a given gas temperature.

The calculated stagnation temperature profile of the gas in the slots is given in Fig. 36. It should be noted that this is an averazge stagnation temperature.

Using the two-dimensional thermal model, the liner wall temperature distribution is calculated. Since the flow conditions in the slot are assumed to possess one-dimensional effects, the gas temperature is constant around the periphery of the slot. Therefore, as shown in Fig. 35, the temperature increase over the mid-land is higher than over the mid-channel region.

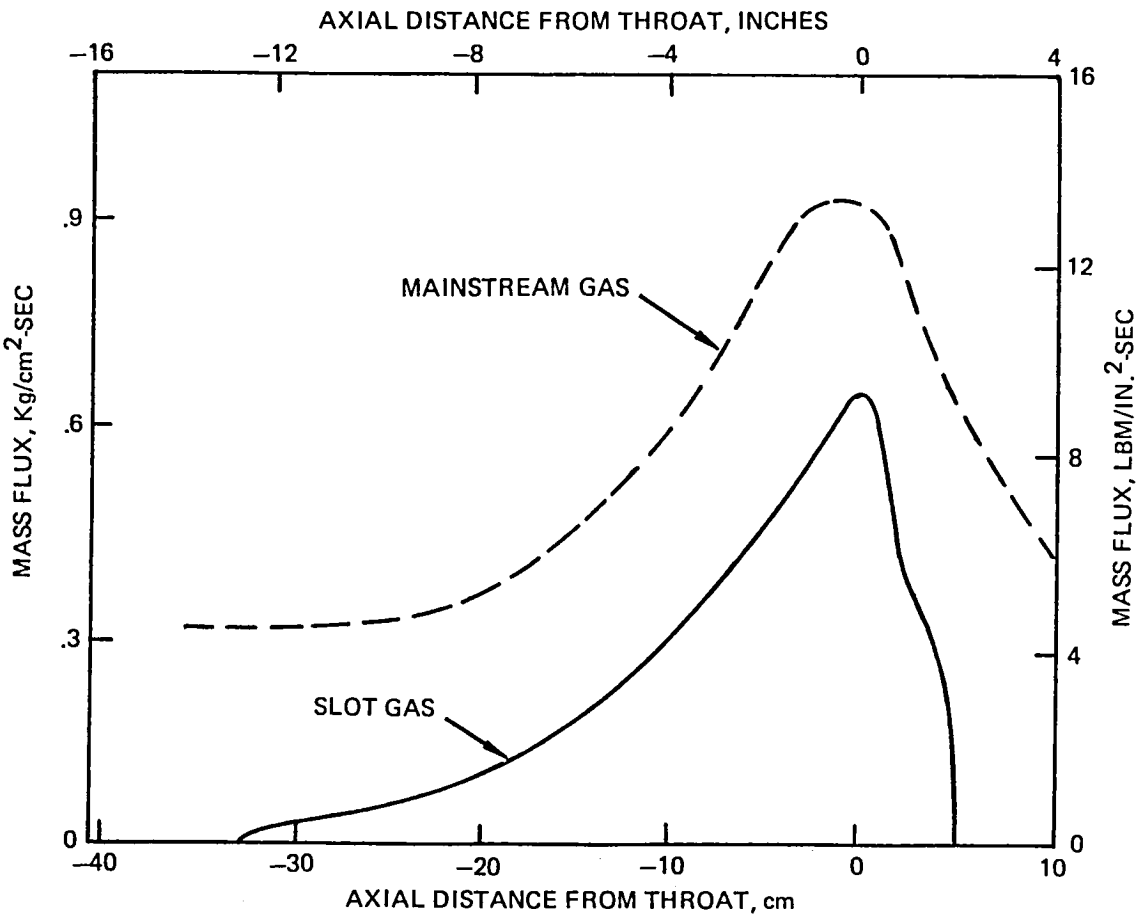

Figure 35. Hot Gas Mass Flux Profile for Slotted Main Chamber Liner

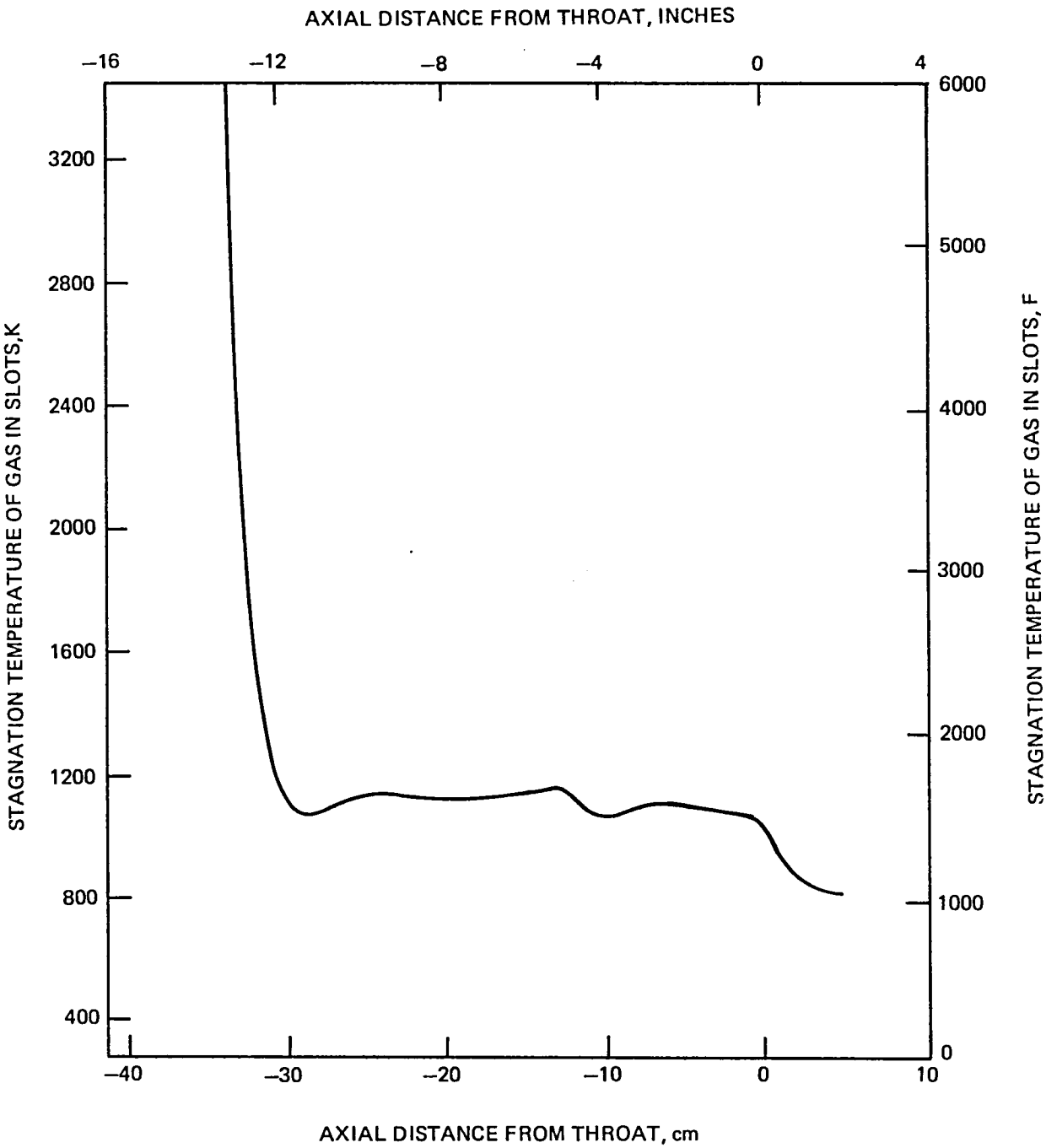

Figure 36. Stagnation Temperature Profile for Gas in Slots in Main Chamber Liner

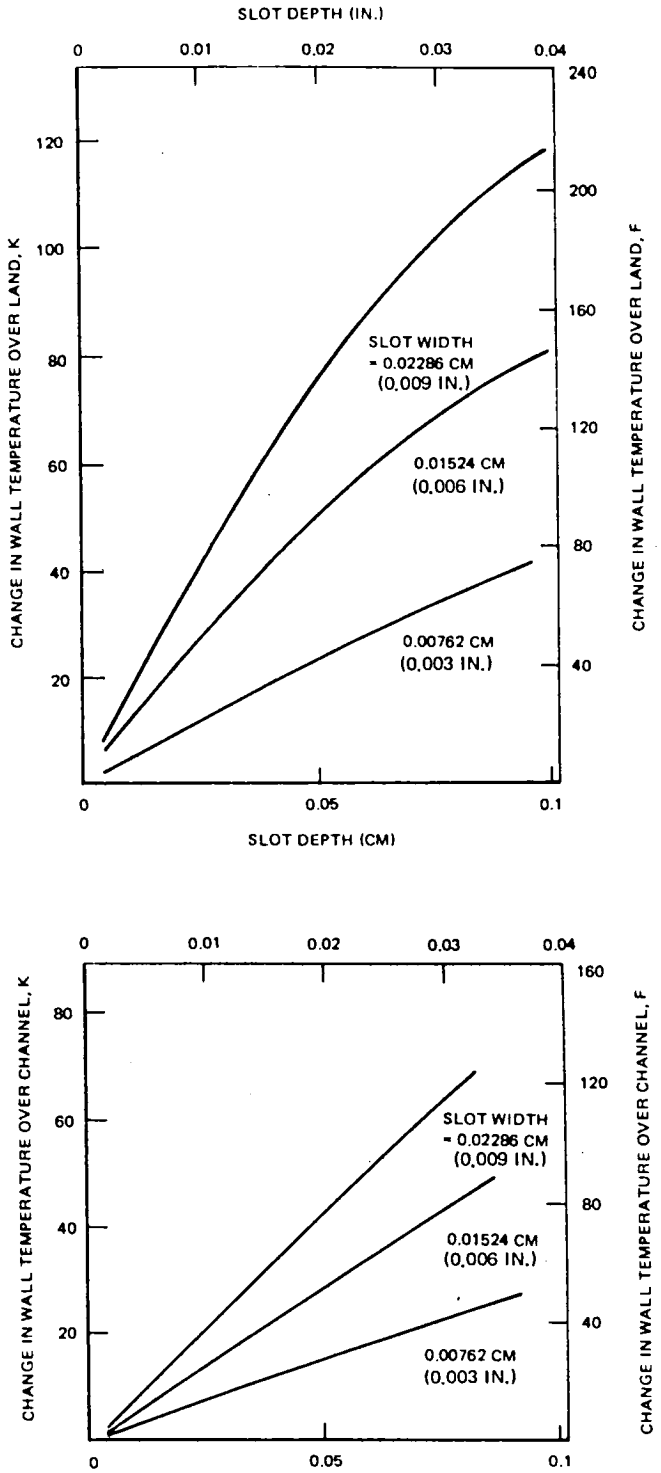

Figure 37. Effect of Slot Dimensions on MCC Hot Gas Wall Temperature at -0.48 cm (-1.2 inch) Upstream of Throat

Manufacturing and Structural Life Considerations

A maximum usable life design would consist of a very narrow slot that would basically close up within a few ten-thousandths of an inch during mainstage hot-fire testing, negating the aerothermal activity. This would also provide the minimum tangential strain. The depth of the slot should be between 1.5 to 2.0 times the thickness of the channel wall so any resultant geometrically oriented strain concentrations at the slot base would be located in a region of nearly zero strain. Therefore, the most desirable slot dimensions would be approximately 0.102 cm (0.040 inch) deep with a 0.025 cm (0.001 to 0.002 inch) width. However, from a manufacturing viewpoint, these slot dimensions are not attainable. Manufacturing experts contend that a minimum attainable slot width for a 0.102 cm (0.040 inch) depth is 0.025 cm (0.010 inch).

Selected Mid-Land Slot Design

The point design selected for this study is an advanced dual-enhanced design representing combined thermal and structural life enhancement benefits. The slotted mid-land life enhanced design is shown in Fig. 38. It utilizes a minimum channel width of 0.030 inch and a minimum wall-thickness of 0.025 inch, identical to the increased number of channels (540) design for enhanced life. However, a basic land-width of 0.040 inch is used to accommodate a mid-land manufacturing limited minimum slot width of 0.010 inch. This combination results in 460 channels.

The parametric thermal analyses show that a slot with 0.102 cm (0.040 inch) depth and 0.023 cm (0.009 inch) width during mainstage would increase the mid-channel wall temperature approximately 89 K (160 F) with a mid-land temperature increase of over 111 K (200 F). This temperature level is considered intolerable, even with a reduced biaxial strain level. Therefore, the selected design assumes that either a physical or fluid barrier exists within the mid-land-slot to negate any adverse thermal effects. This can be attained by either film cooling at the upstream entrance or bonding a high temperature non-structural composite material at the slot base. A physical barrier gap of 0.00127 cm (0.0005 inch) would allow transverse strain relaxation and negate any thermal effects. Adequate cooling of the physical barrier filler material would be provided by a braze interface at the slot base. The coolant channel geometry to accommodate this design and the 135% FPL hg thermal conditions are depicted in Fig. 39.

This life enhanced design is considered to be an extremely advanced design requiring a high degree of technology. It is also combined with the most beneficial life enhancement design (increased number of channels design) and possesses the majority of the benefits of the 540 channel design. Considerable life enhancement can be obtained with this combined design, but much advanced technology is required.

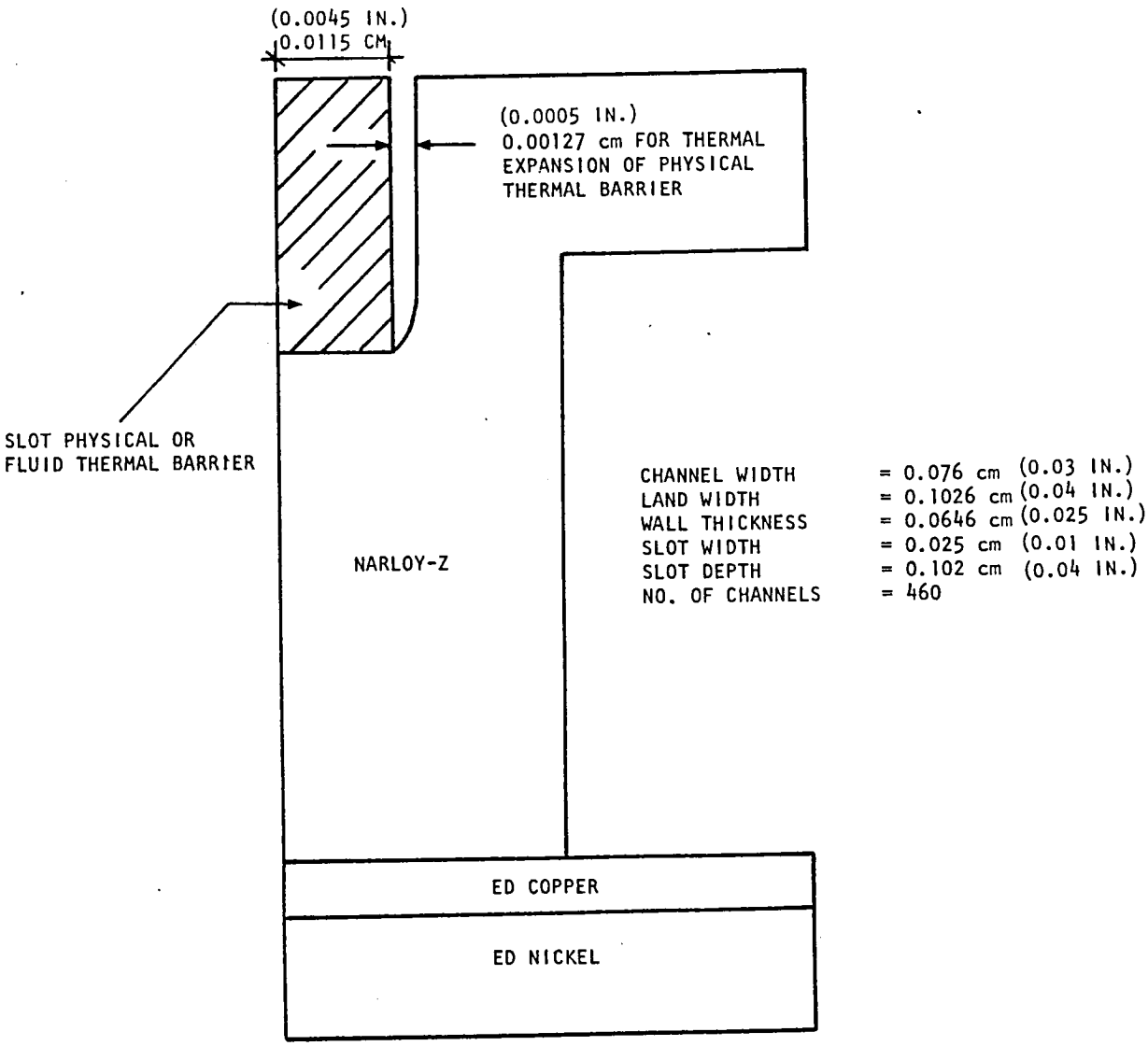

Figure 38. SSME MCC Slotted Cooling Channel Configuration

STATION NO. 31 X = -1.200 X/RT = -.233

NUMBER OF ITERATIONS = 43
DIFFERENCE BETWEEN HEAT IN AND HEAT OUT = .01198 PERCENT

HEAT INFLUX = 123.028
2-D/1-D B/A = 1.06507

1350	1349	1348	1349	1351	1351
1119	1117	1115	1118	1120	1122
894	887	877	888	897	900
5.8	662	614	657	691	698
346	318	226			
122	100	33			
-15	-30	-73			
-96	-105	-131			
-143	-148	-154			
-169	-172	-131			
-183	-185	-191			
-189	-191	-195	-199	-201	-202
-193	-194	-195	-195	-195	-195
-194	-195	-195	-195	-195	-196

HOT GAS WALL

COOLANT WALL

COOLANT CHANNEL

S.I. Conversion
K = 5/9 (F + 460)

CLOSE-OUT

1. LAND WIDTH = .04262
2. CHANNEL WIDTH = .03000
3. WALL THICKNESS = .02500
4. CHANNEL DEPTH = .11900
5. CLOSEOUT THICKNESS = .04000
6. TAW = 5035. DEG. F
7. HG = .0271890
8. TC = -203. DEG. F
9. REFERENCE HC = .1895480
10. HC FACTOR FOR UPPER WALL = 1.4000
11. HC FACTOR FOR LOWER WALL = 1.0000
12. EXPONENT = .5500
13-14. K OF REGION 1 = .004875 + (-.1870E-06) * T
15-16. K OF REGION 2 = .004875 + (-.1870E-06) * T
17-18. K OF REGION 3 = .001340 + (-.1330E-05) * T
19. CONVERGENCE CRITERION = .1000 DEG. F
20. COATING THICKNESS = 0.000000
21-22. COATING K = 0. + (0.) * T

Slotted

Figure 39. Slotted Mid-Land Design Thermal Distribution for a Thermally Isolated Slot at 135% FPL hg

DISCUSSION

STRUCTURAL ANALYSIS

HISTORY AND DESIGN ANALYSIS APPROACH

History of Channel Wall Combustors

Rocketdyne has designed and tested several channel wall thrust chamber configurations. Typically, the structural analysis calculates the maximum strain range and minimum LCF life to occur in the hot gas wall over the center of the land. Hot fire testing of chambers shows a different mode of failure. The hot gas wall material at the center of the channel progressively thins from the inside of the channel and the material moves and thickens the adjacent material (Fig. 40). This phenomenon is a thermal ratchet condition termed "cyclic creep." In some cases the center of the channel thins sufficiently such that the wall fractures with an attendant local loss of coolant through the wall. Small cracks have occurred mid-land on the SSME as predicted by analysis, but they have not grown large enough to cause a problem. The cyclic creep mode of local channel cracking has usually been associated with local hot spots from injector effects, and has not been predictable by analysis.

SSME History and Status

Main combustion chambers (MCC) for the SSME have been hot-fired nearly 800 times in static ground tests. The 25 MCCs used have accumulated approximately 140,000 seconds of hot fire testing. Durations of these tests have ranged from less than 1.0 second to 832.0 seconds. Present operating range of the SSME is 65 to 109% of rated power level (RPL), which encompases a combustion chamber pressure range of 13.4 MPa (1950 psia) to 22.5 MPa (3270 psia) P_c. For certain test objec- tives, SSMEs have been tested up to 111% of RPL, and as low as 50% of RPL.

The current SSME MCC meets all design and operational requirements even though local injector effects may cause small areas of channel wall cracking. Techniques have been developed to meet those requirements with minor loss in performance.

The initial main injector design had no provisions for film cooling of the MCC. After inception of hot-fire development testing, it was discovered that local circumferential areas of the combustion chamber had experienced over-heating. The overheating resulted in conditions ranging from blanching to surface roughening to surface erosion. Surface erosion was generally resolved by the addition of film coolant holes and larger face nuts in the outer region of the main injector faceplate. These modifications increased the fuel flow along the walls of the combustion chamber, resulting in reduction of the hot gas wall temperature. In extreme cases, film coolant holes are locally enlarged to provide an extra measure of protection for the combustion chamber hot gas wall.

Note cold wall cracks at corners of channels with hot-gas wall through cracks.

Also, note deformation of EDNi aligned with cracked channels.

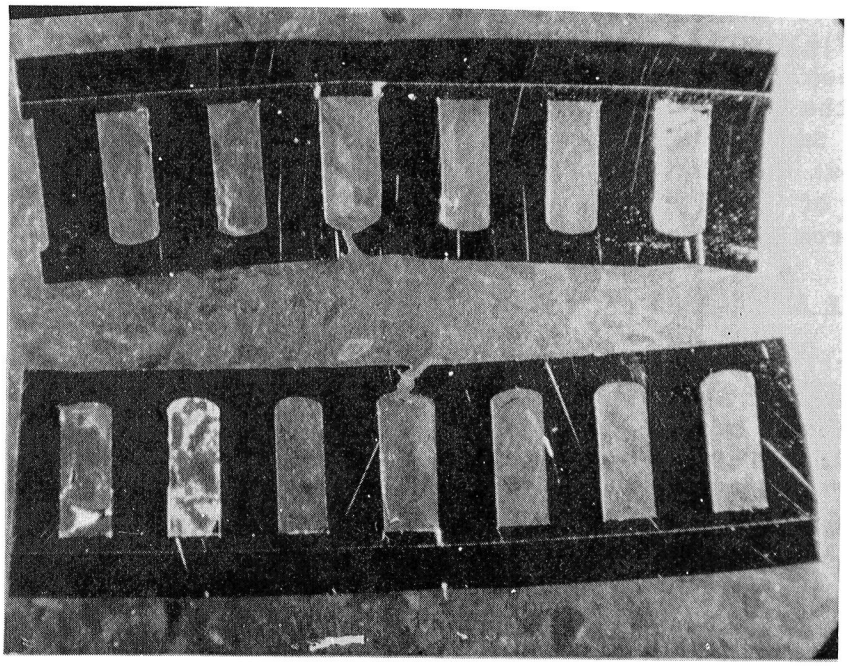

Figure 40. Two Sections from MCC 9002 Approximately 3.175×10^{-2} m (1.25 in.) Forward of the Throat

During the early stages of SSME testing, MCC hot gas wall roughening due to hot fire operation was not considered detrimental to engine operation. As testing progressed, it was discovered that roughening contributed to escalating heat loads and further roughening and degradation of the hot gas wall. Polishing of the MCC liner between tests with fine grit sandpaper was chosen as the method for reducing the deterioration of the hot gas wall. The smoother hot gas wall surface is credited with reducing local distress, especially on long duration tests. Certification testing of the MCC, up to and including full power level (FPL--109% RPL), has shown the component to have the capability of meeting a certification cycle without deterioration of the hot gas wall. This is accomplished with minor maintenance between tests; by polishing the hot gas wall if necessary and selectively increasing the film coolant flow over local hot spots that indicate signs of duress. Even with these modifications, the MCC has encountered minor cracking. This damage occurs only in local hot spots and is attributed to injector effects (anomalies) rather than a general deficiency in the cooling capability or design of the chamber.

No performance degradation has been observed in the SSME engine with as many as 20 thermal cracks or thermal pin holes in the hot gas wall. These cracks tend to close during mainstage when the material is hot and result in little or no leakage. Based on extrapolation of observed degradation of the MCC liner and resulting performance effects, the MCC will meet minimum performance requirements for the required cycle life.

The degradation of the SSME combustion chambers with operating cycles and time is very consistent among components. Cyclic creep damage can be observed from initiation to development of a crack in the coolant channel. The consistency of data makes the MCC an excellent tool to develop improved analysis procedures. When this analysis is correlated to laboratory and subscale testing to verify improved design concepts for demonstrating the capability for fabricating more efficient coolant channels, and as a tool for developing thermal barriers, the result will be new MCC technology. This technology could be applied to improved performance of future engines or uprated SSME configurations.

Existing Analysis Methodology

Channel wall combustion chambers are sized by hand solutions followed by local detailed finite element analysis of a channel cross section. The finite element analysis utilizes a duty cycle considering the prechill, start, mainstage and cutoff conditions for temperature , pressure and movement of any support jacket. The conditions that maximize the strain range are utilized in defining the computerized duty cycle. Detailed temperatures and pressures are applied to the model and a maximum strain range calculated. In the 1970 to 1975 time period when the SSME chamber was designed, the available finite element codes were limited to small deflection theory. Rocketdyne now uses codes that can account for geometric deformations as part of the incremental duty cycle analysis.

The chamber channel hot wall analysis is based on predicted maximum engine conditions. The environment is assumed axisymmetric and therefore local injector effects are not analyzed from either the heat transfer or structural analysis standpoint. It should be noted that for the SSME chamber design, temperatures are below the creep initiation temperature so creep relaxation or creep rupture are not a significant problem.

Current Study Effort

Rocketdyne's current effort in this study has been to analyze the SSME MCC using the methodology previously developed under LeRC sponsorship. This methodology consists of analyzing the chamber considering more increments in the duty cycle and geometric deformation effects. The geometric deformation formulation allows the analysis to adjust to the small geometry changes that occur during each duty cycle that are cumulative in nature. At higher than nominal temperatures, creep relaxation effects are also considered. In order to minimize computer time, an extrapolation procedure obtained from LeRC was utilized. To perform the analysis, five duty cycles are sequentially analyzed and the change in geometric shape is extrapolated to the deformation conditions 15 cycles further on, e.g., 5 cycles + 15 cycles = 20 cycle condition. Using the new geometry, additional duty cycles are analyzed and another extrapolated shape projection made. This technique is continued until failure occurs. A second part of this study was to evaluate temperature effects and design modifications to improve the life of the chamber.

Once this analysis technique is calibrated to the SSME engine database, it can be utilized to analytically determine whether new designs are sensitive to the cyclic creep phenomena. These designs may have significant geometric differences from the current channel configurations. At this point, the whole analysis technique would be only partially validated in that it is calibrated only to an SSME MCC and no test demonstration would have been made of its suitability for geometrically different configurations.

SSME CONFIGURATION AND OPERATION

The SSME MCC configuration and cross-section shown in Fig. 41 and 42 depict the basic geometry and component details. The design consists of an outer structural jacket forming the shape of the combustion chamber liner and carrying the internal pressure and external loads from interfacing components. The liner is attached to the jacket at the ends of the structure. It ducts hydrogen coolant along axial channels and acts as a thermal barrier between the jacket and the combustion gases, as well as a heat exchanger for heating the hydrogen used to drive the low pressure fuel pump. The regeneratively cooled liner forms the desired combustion chamber profile. The slotted liner is closed out with EDCu and EDNi to form channels for the hydrogen coolant. The liner is supported by a high strength structural jacket, and is attached only at the ends of the jacket. Structurally, the liner is required to strain out to contact the structural jacket, to react the differential pressure load between the coolant and the combustion gases, and to accommodate the cyclic and racheting strain ranges from the extreme thermal operating environment. The structural jacket is required to provide external support for the liner, plus react the internal combustion pressure loads and the resulting thrust and gimbaling loads generated during hot-fire operation. Even though the liner is not attached all along the MCC, the liner motion is restricted during operation by the motion of the external jacket. During steady-state operation, the liner hot-gas surface is nominally 867 K (1100 F), and the back wall on the jacket side is typically 172 K (-150 F). During start and cutoff, the complete liner temperature reaches approximately 33 K (-400 F). This total cycle is a severe thermal cycle for the liner to accomodate. At the analysis location near the throat, the internal pressure of the coolant hydrogen is 43.4 MPa (6300 psi), which is 30.0 MPa (4200 psi) greater than the hot wall chamber pressure of 14.5 MPa (2100 psi).

Hot-Spot Cracking

After a series of duty cycles, the geometry of the channel cross-section gradually distorts, thins along the channel hot wall, and cracks. Figure 40 shows typical cross-sections of SSME MCC hardware-through hot spots like the ones shown in Fig. 43.

The geometric changes of the channels that result in cracks are a small portion of the total surface area of the MCC. The cracked channels are located typically in the center of the elliptical-shaped hot spots that occur just forward of the throat. The two cross-sections show that the deformation pattern occurs over a 5 to 10 channel width and each channel has its own geometric change. The liner consistently shows a thinning of the center of the coolant channel's hot wall, plus a thickening and rounding of the corner forming the intersection of the channel and land. Detail measurement of channel geometries indicate that material volume has essentially been conserved; the thinned section is balanced by the thickened shape at the channel corner.

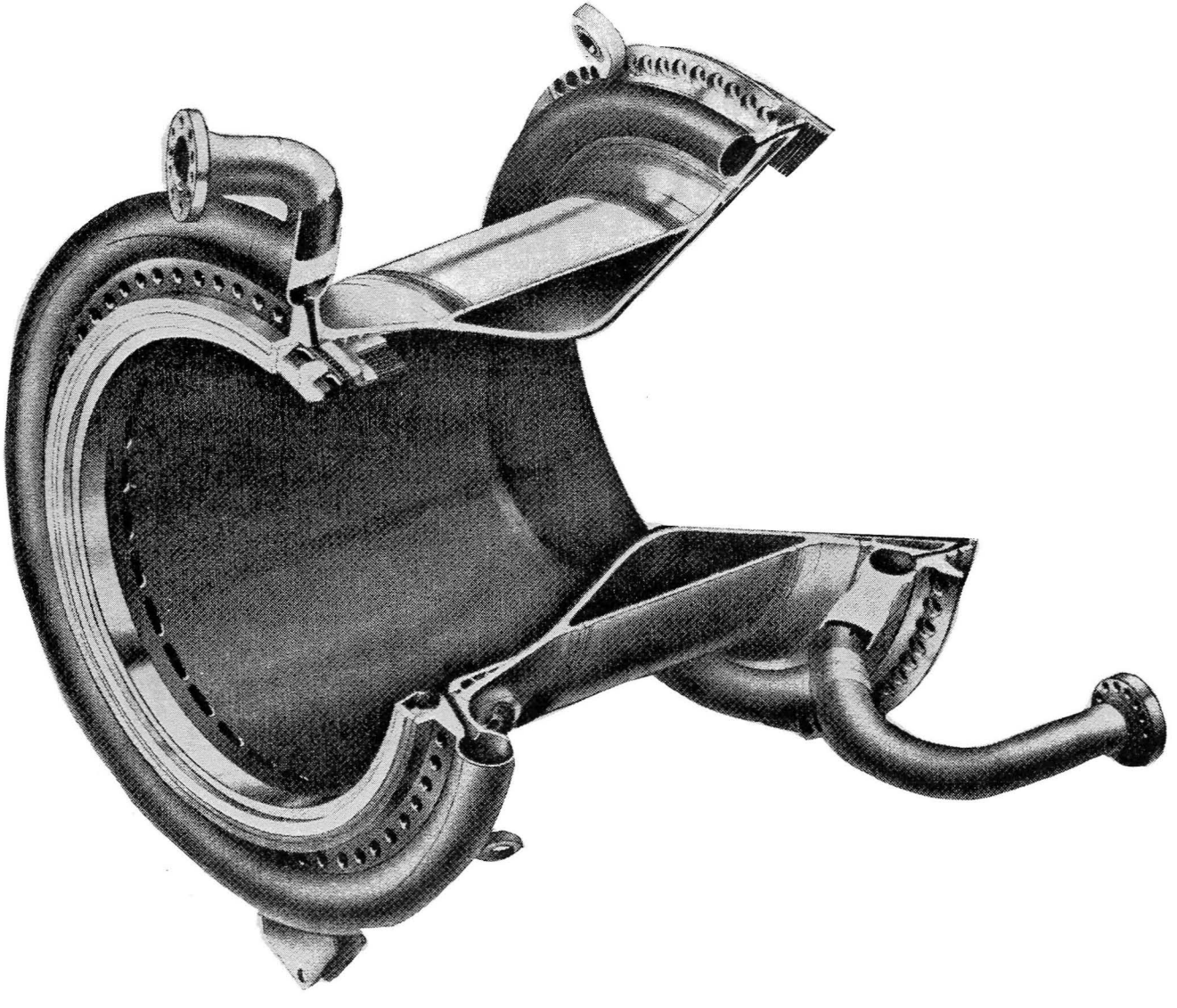

LC301-381B

Figure 41. Main Combustion Chamber

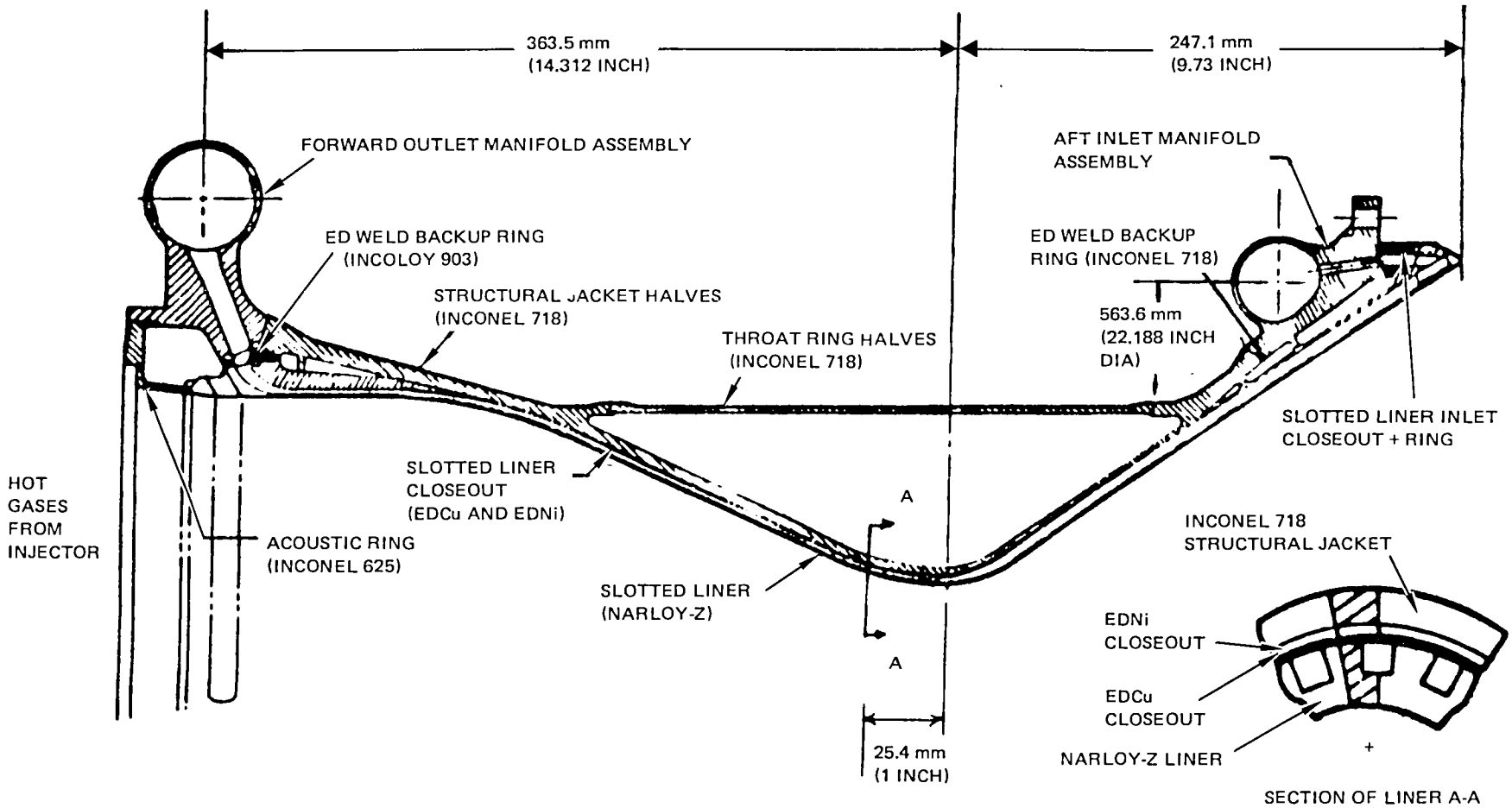

Figure 42. Main Combustion Chamber Liner Materials and Part Name

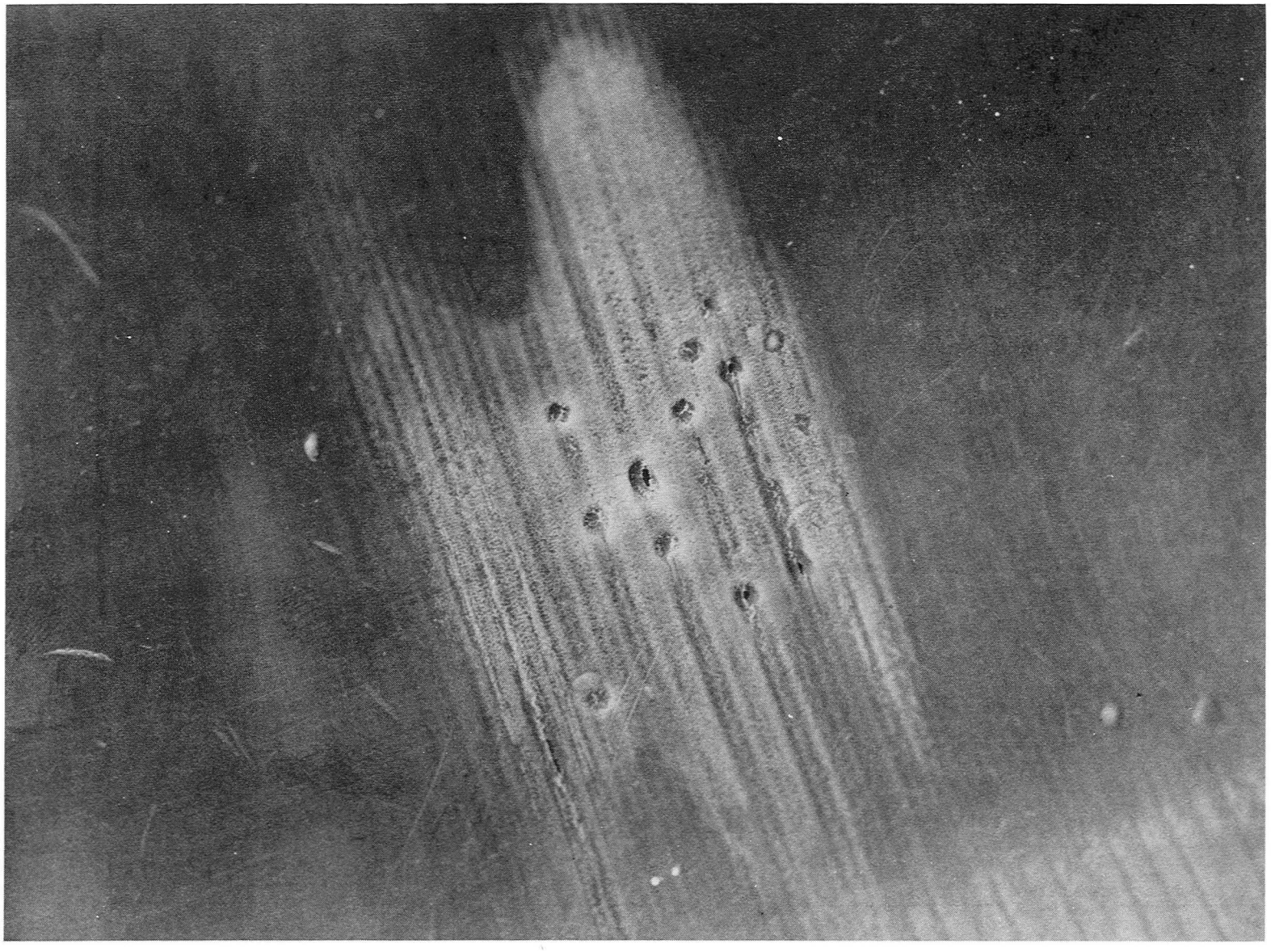

1SM35-1/21/82-S1B*

Figure 43. Typical SSME MCC Hardware-through Hot Spots

This means that material has not been significantly removed from the surface by the hot gas environment. Other observations are that the channel thinning at the point of cracking is 5 to 10 % and that there is only small radial distortion at the inner wall. This thinning varies from hot spot to hot spot, and liner to liner. Each combustion chamber has similar deformation patterns with large variations in the thinning and radial distortions (Ref. 1 and 2). In order to adequately analyze this type of structure, the standard structural considerations of strength, creep, and low cycle fatigue must be supplemented by a cyclic thermal ratchet analysis termed cyclic creep.

Cyclic Creep Influence

The cyclic creep phenomenon requires a biased load-structural duty cycle to cause an increase to the average maximum hoop strain in the mid channel for each duty cycle. Figure 44 summarizes the significant biased conditions that occur during the SSME duty cycle. The observed thinning and distortion of the channels show that the mid-channel thinning is a result of a local biased negative radial strain and a compatible increase in a local hoop strain. The reshaping of the corner is dominantly a large shear strain which resolves into plus and minus principal strains that thicken the corner zone.

The dominant load is thermally induced, but the other biased conditions accentuate the cyclic creep. For the SSME MCC, significant biased conditions include pressure, creep or relaxation effects, material strength effects, and the liner support. The differential pressure loading from the coolant varies throughout the duty cycle, and is significant only over a portion of the duty cycle. This variation in pressure may be part of the difference between the small radial distortion mid-channel and the thinning rate for this MCC vs results from smaller test chambers at Rocketdyne and NASA that maintain significant differential pressures throughout the test duty cycle.

The maximum average liner channel wall temperature in a hot spot is approximately 867 K (1100 F). The maximum liner temperature of 1089 K (1500 F) in a local hot spot is well above the creep activation temperature for NARloy-Z. However, the temperature gradient through the hot wall is approximately 672 K (750 F), which results in half of the hot wall being at temperatures below the creep activation temperature. The primary load-differential coolant pressure in the MCC can be easily supported by this low temperature portion of the wall. This essentially changes the load condition from a potential load-dependent creep problem to a local relaxation phenomenon. The stress state on the hotter portion of the wall reduces to a displacement-limited steady-state condition. The primary load is essentially shifted to the cooler half of the channel wall. Therefore, the creep/relaxation effects are a minor addition to the biased loading in this hardware, whereas it could be a more significant parameter if the total hot wall was above the creep activation temperature. This can occur in a plugged channel versus a hot-spot condition.

- BIASED CYCLIC STRAIN
  - MID CHANNEL
  - ϵ_R CAUSING THINNING
  - ϵ_H CAUSING EXTENSION
  - LAND
  - ϵ_R, γ INCREASING
- BIASED LOADING/CONDITIONS
  - PRESSURE
  - CREEP/RELAXATION AT SS
  - THERMAL CYCLING
    - YIELD STRENGTH
    - ULTIMATE STRENGTH
    - LIMITED CYCLIC STRAIN HARDENING
  - LINER SUPPORT
    - STIFF DURING FIRING
    - RELEASED DURING START/CUTOFF
- LIFE LIMITS
  - STRAIN RANGE – LOW CYCLE FATIGUE CURVE
  - ULTIMATE STRAIN (TENSILE INSTABILITY)
    - BIAXIAL 5 TO 8%
    - UNIAXIAL 10 TO 16%

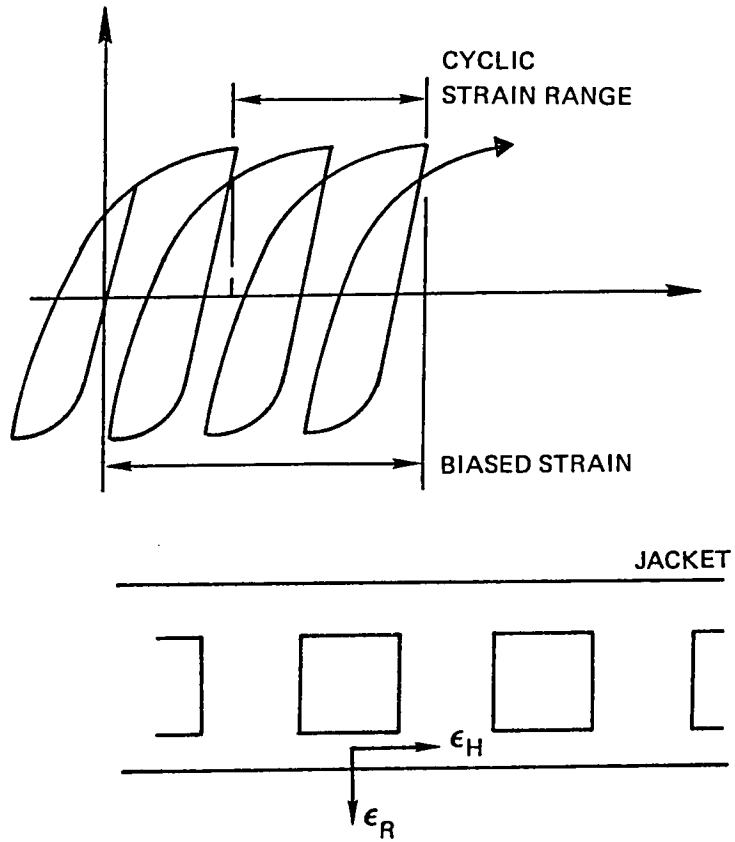

Figure 44. What's Needed to Demonstrate Cyclic Creep

Plugged channels crack earlier than a typical hot-spot condition. Figure 45 shows creep relaxation results for NARloy-Z from standard materials test specimens. It is evident that relaxation effects occur rapidly within less than 1 second of hold time and achieves an approximate steady-state condition within 10 to 20 seconds. For the SSME engine duty cycle, this means that steady-state creep relaxation occurs during every typical test firing of 50 to 800 seconds. The creep effects are basically test-cycle dependent, not test-time dependent.

Another parameter for the biased loading is the temperature-dependent cyclic strength of the NARloy-Z material. The hot-cold duty cycle causes a bias in the strain cycle because the elastic vs plastic strain distribution is different in the overall channel cross-section between steady state and the remaining portion of the duty cycle.

The cyclic stability of the material can also be a significant parameter for some of the materials used for coolant liners. In this case, the NARloy-Z material used for the MCC is cyclic stable, i.e., it has a relatively small increase in load at constant cyclic strain range (Fig. 46). Therefore, cyclic strain hardening effects are not a significant consideration, and uniaxial stress-strain data were used in the analysis.

The design concepts used for the MCC also bias the cyclic strain. The liner and jacket are similar in operation to a tube in a tire where the outer jacket limits the motion both radially and axially during the pressurized portion of the duty cycle. During the portion of the duty cycle where the liner is cold, the liner separates and pulls away from the jacket, which reduces the strain range, but biases the strain cycle.

The other primary contributor to the cyclic creep mode is the geometric distortion of the liner cross-sections. Previous SSME MCC analyses performed in 1970 to 1975 were limited to small displacement analyses that utilize only the original geometry. This means that geometry distortions are not accounted for in developing the cyclic straining of the liner. The maximum strain or tensile instability-type failure mode typically requires the displacements and distortions of the structure to be considered as part of the stiffness-load-stress and strain conditions. The current analysis methodology incorporates those geometric changes that occur throughout the operating duty cycle. Analysis results show that this is a significant parameter in changing the rate of distortion as the analysis progresses through the total duty-cycle analysis.

The life analysis, therefore, consists of evaluation of the liner through a series of duty cycles to a point of liner cracking. From a low cycle failure evaluation standpoint, this reduces to a low cycle fatigue (LCF) failure mode that is related to the cyclic strain range vs a cyclic creep failure mode that is related to the total strain. The LCF is evaluated from an individual assessment of the cyclic strain range of local zones of the liner channel cross-section. The cyclic creep failure mode is evaluated as an average strain condition in the channel hot wall that is conveniently related to the channel wall thinning in the analysis methodology used.

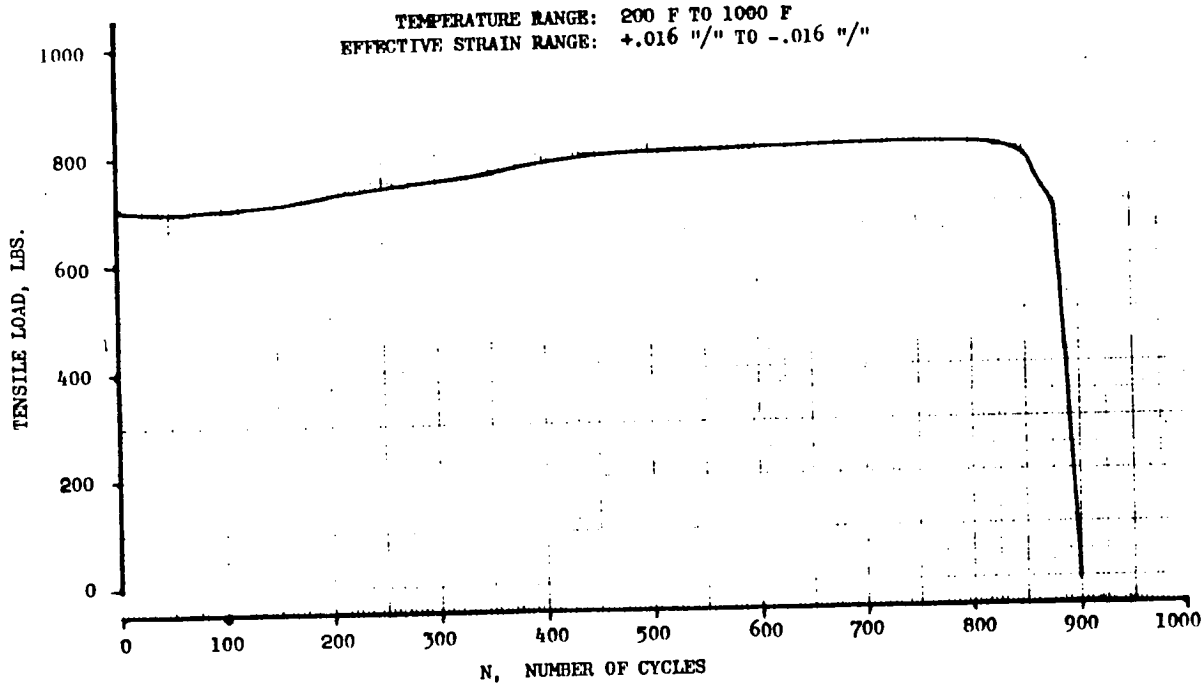

Figure 45. NARloy-Z Thermal Fatigue Test - Load vs Cycles

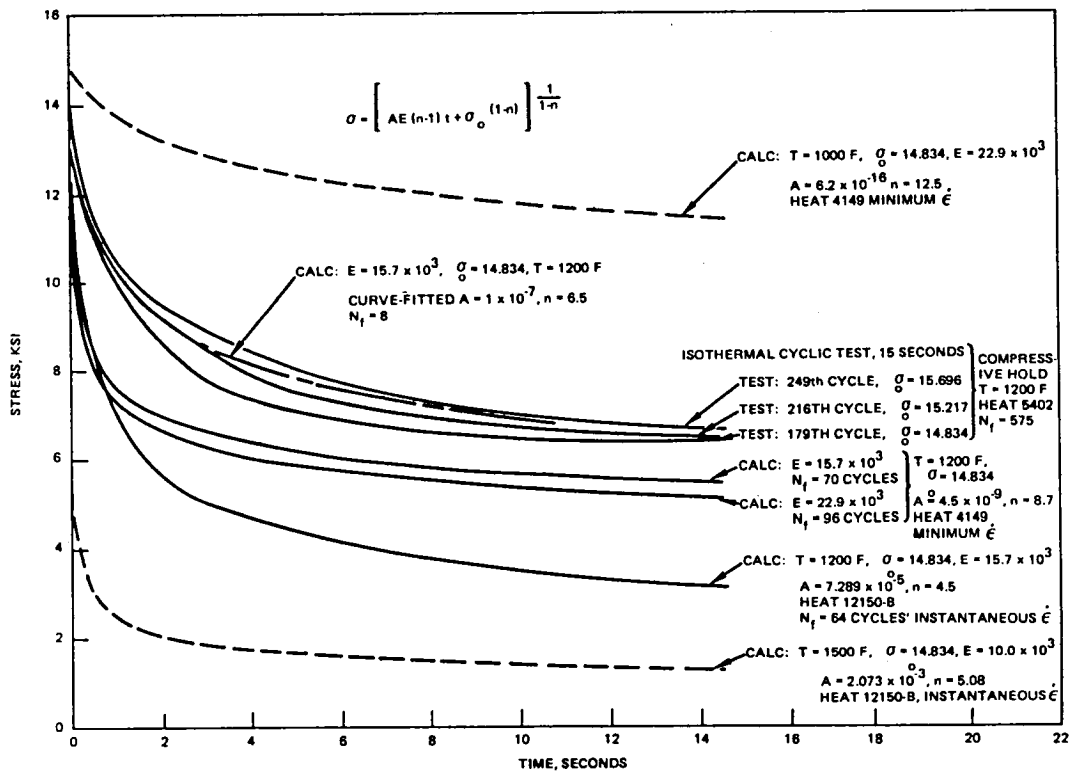

Figure 46. NARloy-Z Stress Relaxation Curves, Comparison of Calculated vs Experimental Data

Duty Cycle Analysis Procedure

The duty-cycle analysis may require tens or hundreds of cycles prior to a failure condition. In cases where a stablized condition occurs in one or two cycles, the analysis can be terminated at this point, and the failure or cracking condition accurately extrapolated. For the structural response of the MCC, this is not possible, since the cyclic strain condition does not stabilize; and the gradual geometric distortions are significant in changing the rate of strain cycling and maximum strain. It is also impractical to consider analyzing every duty cycle. A compromise is to utilize the approximate methodology developed under NASA-funded efforts (Ref. 3 and 4), that analyze a series of duty cycles to determine the conditions consistent within a particular portion of the distortion sequence, extrapolates the geometry to a geometric condition further into the deformation pattern, and then analyzes another series of duty cycles to determine local conditions at this point. It should be noted that this is a specialized analysis technique, not a general methodology applicable to a large class of problems. The extrapolation technique requires that the geometric distortions further into the life cycle can be linearly approximated from a sequence of previous distortions. The analysis technique requires a balance of the cost in performing sufficient duty cycles to determine a local, stablized condition and the extent of the extrapolation further into the duty cycle where the rate of cyclic change is not significantly different. This study utilized a standardized approach of developing a 5 duty-cycle detailed analysis followed by a 15 duty-cycle extrapolation of the geometric shape. The model was then rerun based on the distorted geometry for the next sequence of cycles. This procedure develops the distorted geometry shape for the analysis, but does not track the strain history through the total history. The strain history is tracked only within each of the individual 5 duty-cycle analyses.

STUDY METHODOLOGY

Overview

The SSME MCC is a three-dimensional shell structure. The detailed analysis of the MCC liner was performed using two separate, two-dimensional models one for the jacket boundary conditions and the other for the actual liner analysis. Figure 47 outlines the overall procedure used in this study for structural analyses. This effort consisted of an initial time-phased duty-cycle analysis for both the jacket and liner. Since the jacket loading and displacements were insensitive to the variations in thermal conditions or geometry changes in the liner, only one analysis is required to develop the boundary conditions for the liner model. The coolant liner loading and model varied as required in each task of this study.

A summary of the analysis basis is furnished in Fig. 48. The two models and duty cycle are outlined, as well as the structural parameters that were considered in the analysis. Loadings include temperatures, pressures, jacket restraints, and the initial fabrication gap between the liner and jacket. The models were an axisymmetric jacket model and a generalized plane strain cross-section model of the liner. The liner model analysis included kinematic hardening creep material characteristics and geometric distortion effects. The basic analysis of the liner for each configuration was a series of 5 duty-cycle analyses, followed by a 15-cycle extrapolation.

Figure 49 is a block diagram of the liner analysis procedure for each geometry or thermal condition analyzed. The loads for each model or condition were defined and applied to the basic liner model. The 5 duty-cycle analysis was complete, results reviewed, and life predictions made as required. Next, the geometry was updated to represent the extrapolated shape at a point 15 cycles further into the analysis. This information was then combined with the basic input for the initial finite-element model, and the analysis repeated.

Duty Cycle Definition

At full power level (FPL) conditions, the 100% hg case represents the normal design conditions for the liner, and is representative of tempertures in the liner in over 95% of its surface area. In the local hot-spot regions, the temperatures are significantly hotter, and are represented by the 135 percent hg thermal analysis case. The 135% hg condition was chosen as the baseline duty cycle for establishing the analysis technique and verifying that the overall methodology would demonstrate the cyclic creep phenomenon. The duty cycle was defined and evualated, and divided into 11 discrete time slices to establish the analytical representation of the cycle. Figure 50 is a plot of hot-gas wall temperature, jacket temperature, P_{fuel} and P_{HGW} vs time, and shows graphically the time history of the significant events for the start/steady-state/shutdown cycle, as well as the 11 discrete time-slice points.

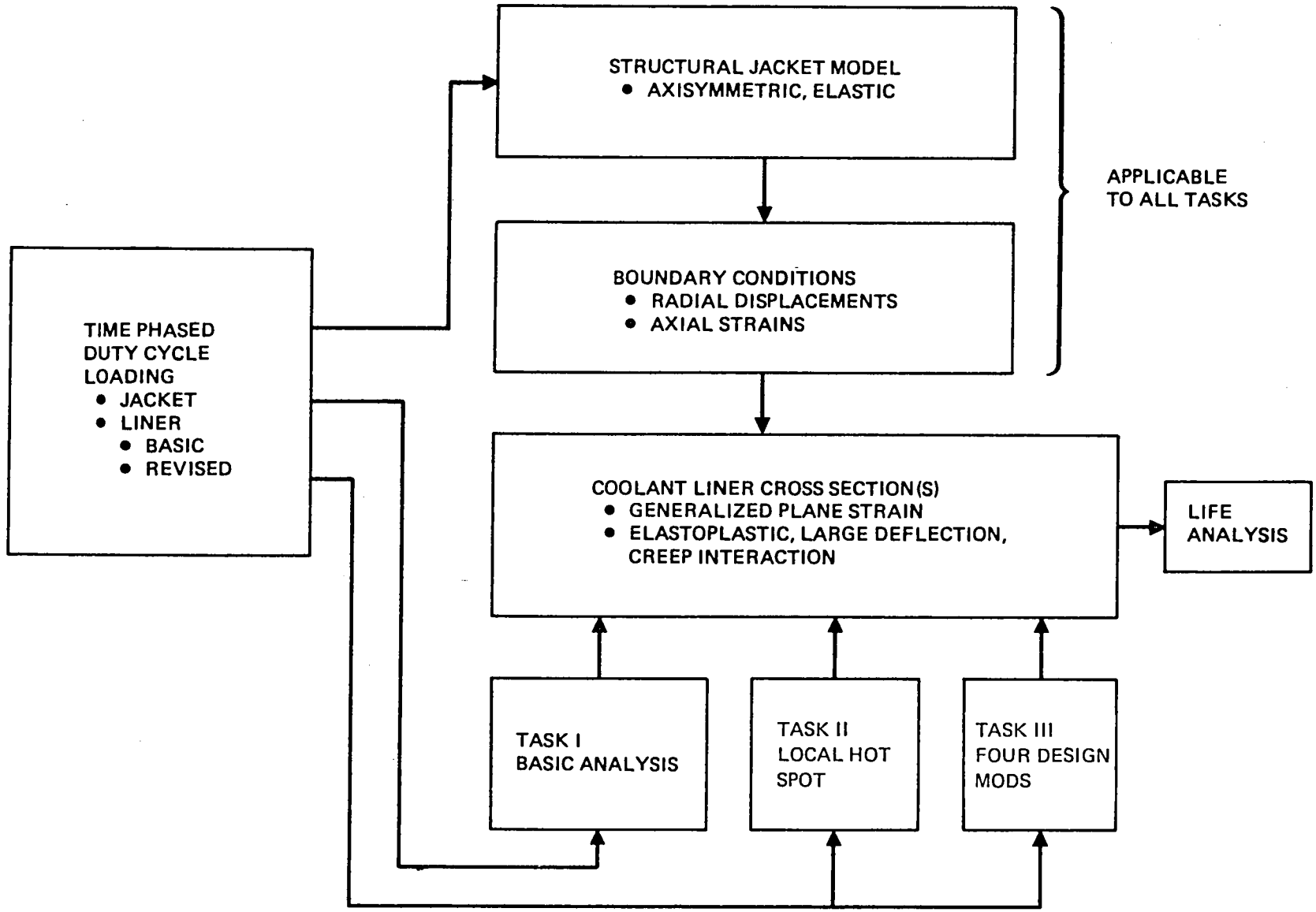

Figure 47. Overall Structural Analysis

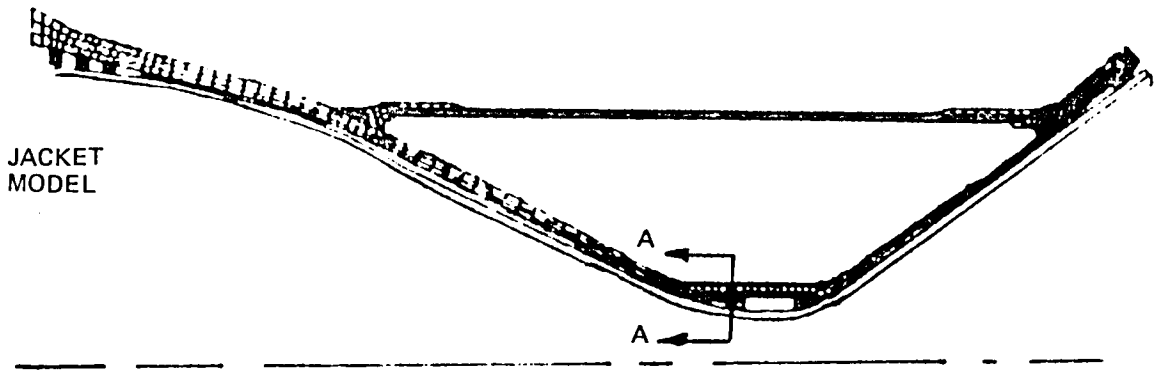

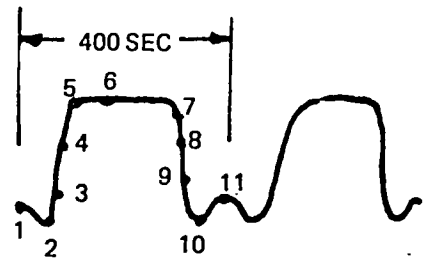

TYPICAL DUTY CYCLE

- DUTY CYCLE – 11 INCREMENTS
- CONSIDER
  - TEMPERATURES AND PRESSURES
  - JACKET RADIAL DISPLACEMENTS AND AXIAL RESTRAINT
  - INITIAL RADIAL LINER GAP 0.508 mm (0.020 IN.)
  - STRUCTURAL MODEL
    - PLANE STRAIN CROSS SECTION
    - INELASTIC MATERIAL – KINEMATIC HARDENING
    - GEOMETRIC DISTORTIONS
    - CREEP/RELAXATION
  - 5-CYCLE DUTY CYCLE ANALYSIS
  - EXTRAPOLATION TO 20-CYCLE GEOMETRY
  - RESTART WITH NEW GEOMETRY AT 21 CYCLE
  - ETC.

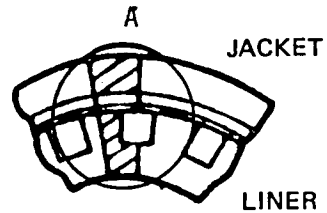

+

SEC A-A

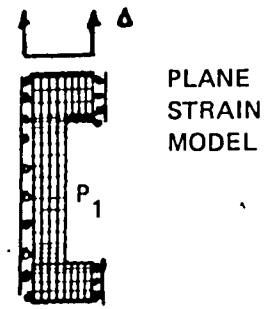

VIEW A

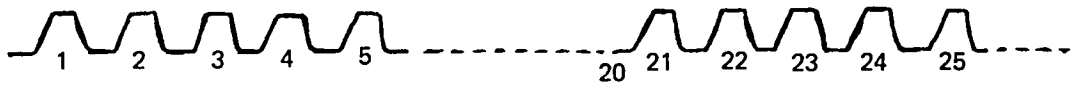

Figure 48. Analysis Approach

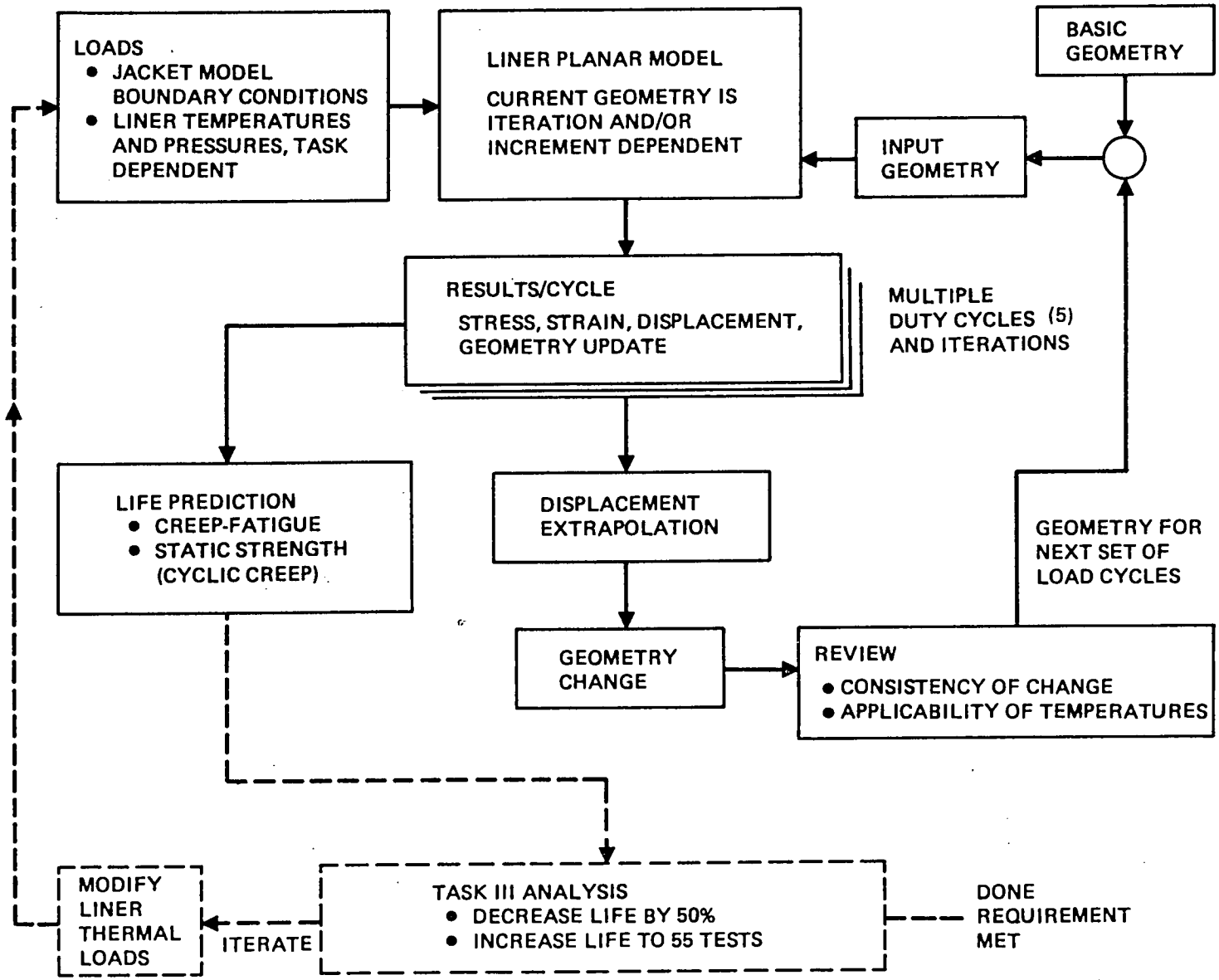

Figure 49. Liner Analysis Block Diagram

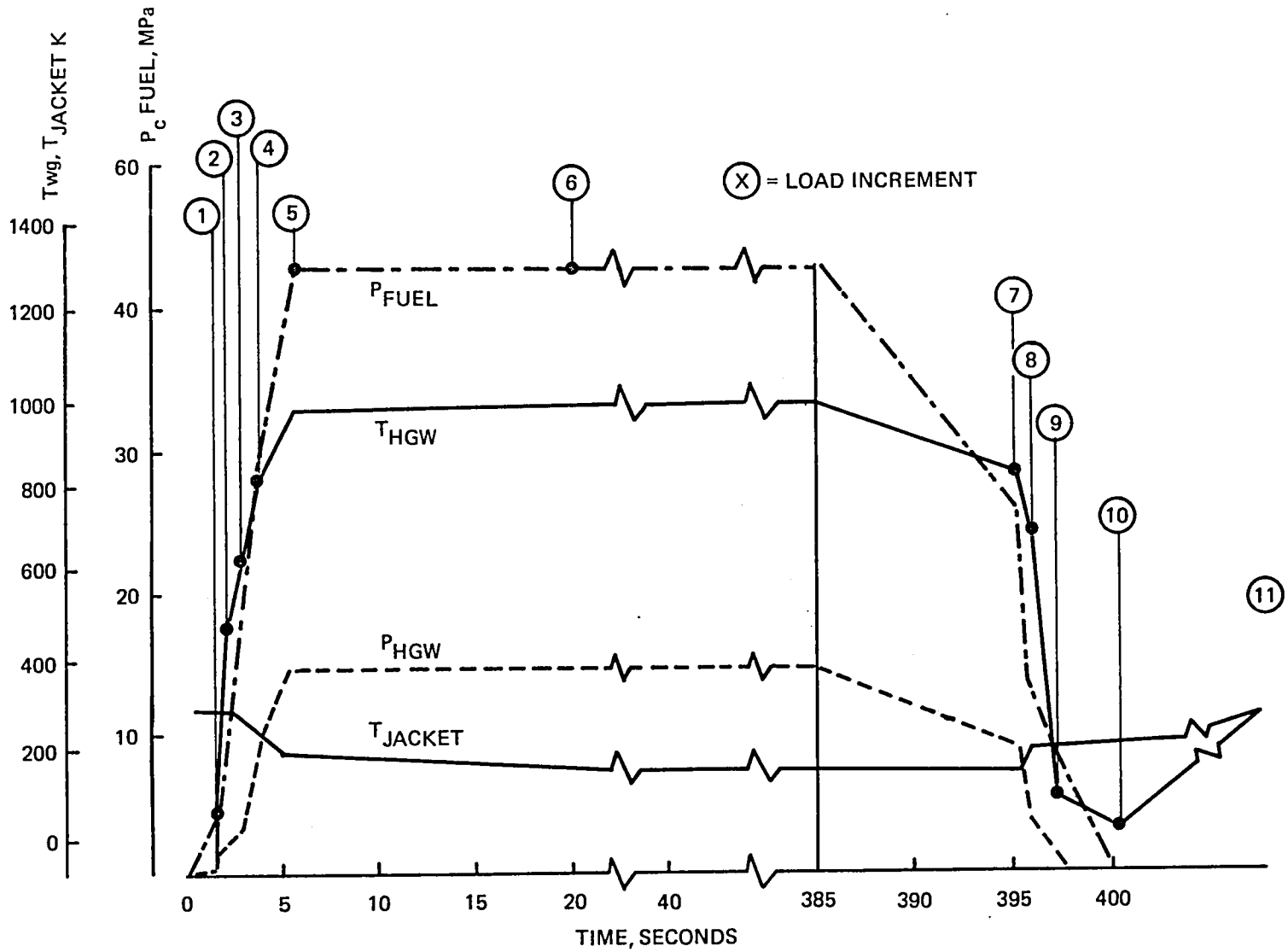

Figure 50a. SSME MCC Life Analysis Duty Cycle and Pressure Display With Time Slices Noted (SI Units)

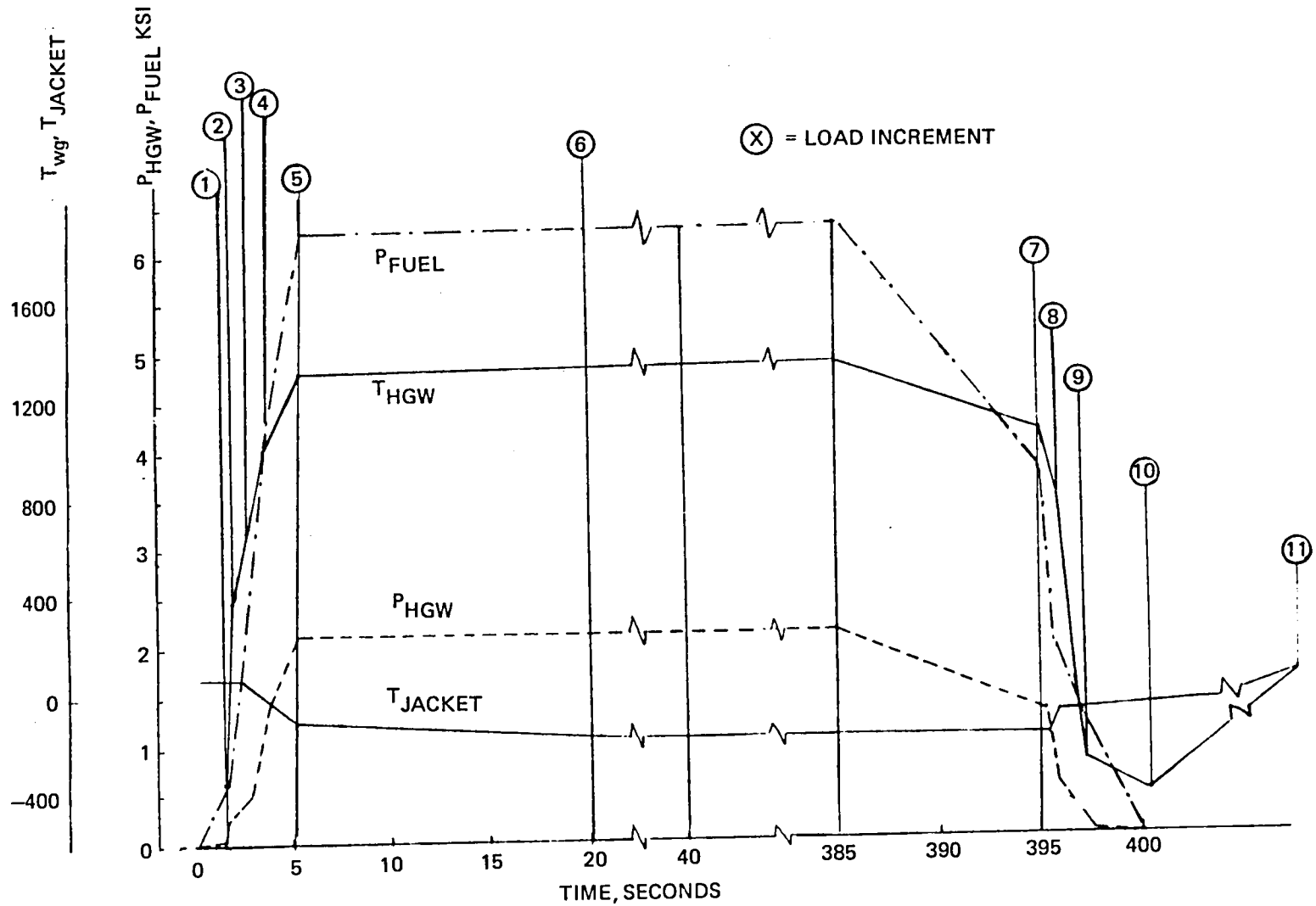

Figure 50b. SSME MCC Life Analysis Duty Cycle and Pressure Display With Time Slices Noted (English Units)

Jacket Model and Duty Cycle Motion

The MCC jacket model was run to establish radial displacement and axial strain influence coefficients for both combustion chamber pressure and average jacket temperature. Using heat transfer data generated from the 100% hg case FPL duty cycle run, compatible time slice values of jacket temperatures and combustion chamber pressure were established, which in turn were used to define the compatible radial displacements and axial strains of the jacket used for the liner cross-section model boundary conditions.

A verbal description of the sequential events helps to understand the time-temperature-pressure relationships between the liner and jacket. The MCC as manufactured can have a maximum radial gap between the liner OD and structural jacket ID of 0.5 mm (0.020 inch). During the start prechill, the cold hydrogen gas flowing through the liner coolant channels causes a thermal contraction of the liner which increases the liner/jacket radial gap. During this time, there is a negligible cooling effect on the jacket due to the cold radiation from the liner. Then, upon ignition, the combustion pressure increases and the weak liner expands radially, like an inner tube in a tire, at a fairly low pressure until it contacts the jacket inner diameter. Once liner/jacket contact is made, the jacket mean temperature experiences a fairly rapid drop in temperature to approximately 200 K (-100 F), while combustion pressure is increasing to its steady-state value. During this time, there is a net radial growth of the jacket from the positive radial displacement of the jacket due to combustion pressure. This displacement is partially offset by the negative radial motion of the jacket as it drops in temperature. After steady-state combustion pressure is reached at 4.9 seconds, the jacket continues to get colder over the next 15 seconds, resulting in a decrease in the jacket radial displacement and axial strain.

At this point, pressure and thermal equilibrium loads in the jacket have been achieved. During shutdown, combustion pressure is throttled down to 65% of rated power level, and then the engine is shut down. During shutdown, the purge flow of hydrogen through the coolant channels rapidly chills the liner to 33 K (-400 F), and the liner separates from the jacket. When combustion pressure reaches zero, the mean temperature of the jacket has warmed up to approximately 211 K (-80 F). The jacket eventually warms back up to room temperature, and returns to essentially a line-to-line contact position with the jacket.

Liner Cross-section Model

The local generalized plane strain model for the current SSME configuration is shown in Fig. 51. This model has gap-type (compression only) elements at the liner-to-jacket interface. Only radial constraint that varies with the jacket displacements was considered at this interface.

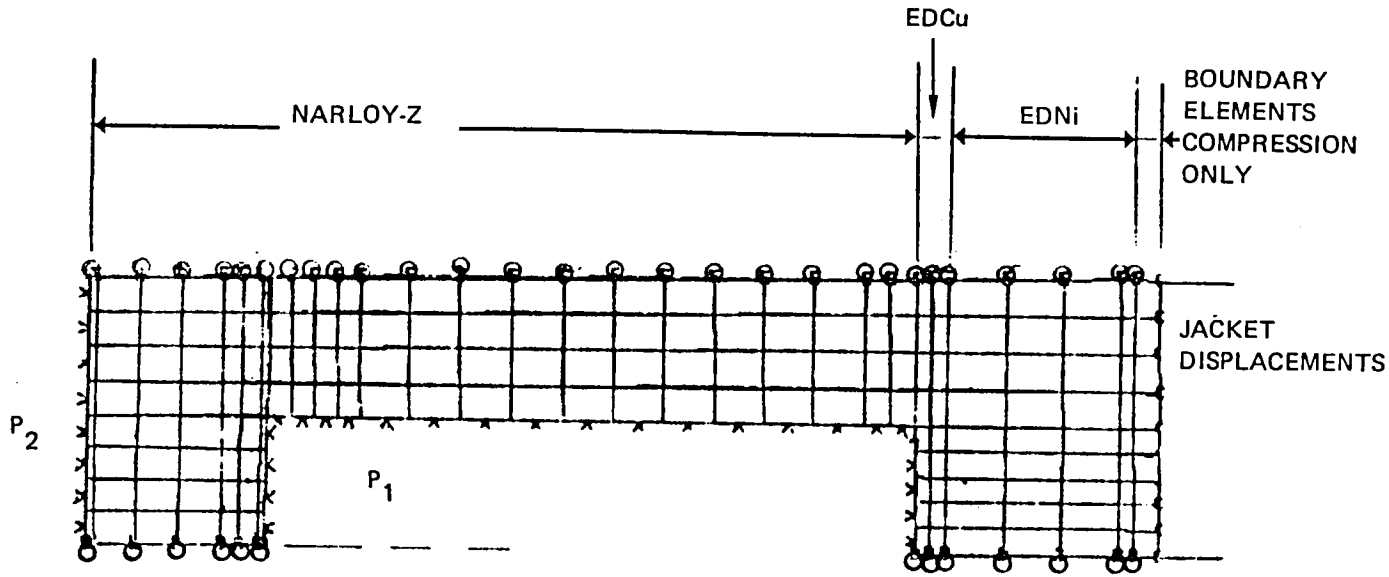

Figure 51. SSME MCC Liner Model Cross-Section

This model is consistent with previous SSME MCC models and previous work performed for NASA-LeRC on cyclic creep analysis. All models analyzed used the same symmetry and boundary conditions. As previously stated, the jacket is the dominant structure, and the liner must follow its movements when the two are in contact. This model and loading technique is a good representation of the major portion of the liner that is unaffected by the local hot spots. When analyzing for the hot-spot condition (135% hg thermal profile), it is assumed that the hot spot occurs each duty cycle at the same position on the liner, the hot-spot covers a large enough zone, and other restraints are such that the jacket symmetry and boundary conditions are maintained in the center of the hot spot, as will be discussed later. Both analysis conditions were used for demonstrating the cyclic creep phenomenon and the 135% hg case in ranking the potential design improvements.

Material Properties

The four materials that make up the liner cross-section, INCO 718, EDNi, EDCu, and NARloy-Z; were represented in the structural model with temperature-dependent, elastic and inelastic properties (see the Materials Section for detailed materials data). The nonlinear behavior was represented with a bilinear stress-strain curve and the analysis used kinematic strain hardening. Since NARloy-Z in the condition used for the MCC is cyclically stable, i.e., it has a relatively small increase in load at constant cyclic strain range, strain hardening was not part of the analysis. Monotonic tensile stress-strain curves were used in developing the bilinear curves. Creep/relaxation constants consistent with available data were used in the analysis.

Large Displacement (Updated Geometry)

A significant change from previous SSME MCC analysis is the inclusion of geometric updating of the structural model. This is accomplished analytically within the computer code analysis for each increment of the duty cycle analyzed, and through an extrapolation code which defines a distorted shape for restarting the finite-element analysis 15 duty cycles further into the analysis.

The geometric distortions are accumulated throughout the analysis and total mid-channel thinning was used as a measure of the total (maximum) strain condition.

The finite element analyses were performed with the APSAC code (Finite Element Axisymmetric and Planar Structural Analysis with Loading and Creep Duty Cycles, Ref. 5). The APSAC code was used for the jacket analysis where an adequate operational model was in existence and was rerun to develop the detailed radial and axial displacements for the incremental loading cycle. APSAC was also used for the liner hot-gas wall analysis.

APSAC is an in-house developed program for finite element analysis. Temperature-dependent material properties, inelastic analysis using bilinear representation of stress-strain curves, and either kinematic or isotropic strain-hardening theory are incorporated in the program.

Large displacement (updated geometry) analysis is available as an option. In addition to the quadrilateral axisymmetric or planar element, a compression-only gap element is available for uses such as the liner/jacket interaction. A secondary-type creep law, $\varepsilon y = A\sigma^n$, is implemented for creep or relaxation effects. An efficient mesh generation scheme is available as a portion of the basic program. Grid and displacement plots, contour plots, and graphical plots are available through a postprocessing program. Information for geometric updates or geometry extrapolation can be performed using data-sets generated by the program.

Rocketdyne has used APSAC and earlier versions of the program since 1969. This program was the primary analysis tool used for the many inelastic analyses performed on the various SSME components. The original MCC liner analysis used the APSAC code prior to implementation of the large-displacement option. Other Rockwell divisions use the program, and it is implemented and used by NASA-MSFC for SSME hardware analysis and other in-house analyses. APSAC has been verified against classical analyses; other codes such as ANSYS and a variety of specimen and test hardware with strain-gage verification, as well as production hardware usage experience.

Displacement Extrapolation

To reduce both engineering and computer costs, a displacement extrapolation program was used. A Rocketdyne code was developed for accomplishing this task, and is discussed in detail in Appendix C. The extrapolation technique used was a standard linear least-squares approximation for the computed rate of change of displacement.

Analysis Strategy

The completion of this study required a minimum of 36 runs consisting of a 5-duty-cycle run plus an extrapolation run and many plot runs. In the course of the work, approximately 50 runs were made. Each 5-duty-cycle analysis consisted of 55 load increments with different temperatures, pressures, and boundary conditions applied in each increment. The temperatures and pressures were obtained from separate heat transfer studies using the REGEN and DEAP analysis codes. Considerable planning and strategy were required to develop techniques to track each run and increment, simplify input data required by the user, and minimize costs in manhours, computing, printout, and graphical output. The intent was to develop techniques usable not only for this study, but applicable as a standard analysis methodology for advance design studies, as well as detail design variations and analysis. Details of these techniques are included in Appendix D as part of the example input data for the 135% hg case baseline analysis.

Creep Fatigue Analysis - Life Prediction

General Methodology. The method of analysis used included a summation of incremental damage caused by fatigue and creep mechanisms at progressive stages of thrust chamber operation (life). Fatigue is the dominant component in this study, but the general creep fatigue methodology is presented, since its proportion may vary from one MCC configuration to another.

Creep fatigue damage is determined from the stress-strain-time history of the structure. Low cycle fatigue damage, ϕ_f, and creep rupture damage, ϕ_c, are considered. The total damage, ϕ_t, is represented in equation form as

$$\phi_t = A\,\phi_f + B\,\phi_c$$

where A and B are damage interaction coefficients.

Predicted life is found as the reciprocal of total damage. The method of analysis is shown schematically in Fig. 52. This is the manner originally proposed by Robinson (Ref. 6) and followed by Taira (Ref. 7), Manson and Halford (Ref. 8), and Spera (Ref. 9). A similar procedure has been finalized and incorporated into the ASME Pressure Vessel Code for creep-fatigue evaluation of nuclear power components, Code Case 1592, Appendix T.

Channel Wall Fatigue Analysis. The fatigue analysis of the channel wall is performed using peak local strains and temperatures. The cyclic range and mean value of the strain were determined at progressive stages of thrust chamber life. The results from the duty-cycle load increments for the most critically strained element are used in a formulation (Ref. 10) analogous to the von Mises criterion to find the strain range, ϵ_t, and the mean strain, ϵ_m.

The values of the strain range components, $\Delta\epsilon_i$, are calculated from the differences in each of the strain components, ϵ_i, for ϵ_t, and the sum of each of the strain components, ϵ_i, for ϵ_m are the strain components at the duty cycle of interest. The values for $\Delta\epsilon_i$ are determined from the maximum and minimum strain conditions in the cyclic analysis, as was previously mentioned. The initial duty cycles adjust the computer model for the inelastic stress and strain state. The formulations for ϵ_t and ϵ_m are as follows:

$$\Delta\epsilon_t = \frac{\sqrt{2}}{3}\sqrt{(\Delta\epsilon_1 - \Delta\epsilon_2)^2 + (\Delta\epsilon_2 - \Delta\epsilon_3)^2 + (\Delta\epsilon_3 - \Delta\epsilon_1)^2 + 3/2\,(\Delta\gamma_{13}^2 + \Delta\gamma_{21}^2 + \Delta\gamma_{23}^2)}$$

$$\epsilon_m = \frac{\sqrt{2}}{3}\sqrt{(\epsilon_1 - \epsilon_2)^2 + (\epsilon_2 - \epsilon_3)^2 + (\epsilon_3 - \epsilon_1)^2 + 3/2\,(\gamma_{13}^2 + \gamma_{21}^2 + \gamma_{23}^2)}$$

Von Mises effective strain defines the uniaxial equivalent for the multiaxial strain state.

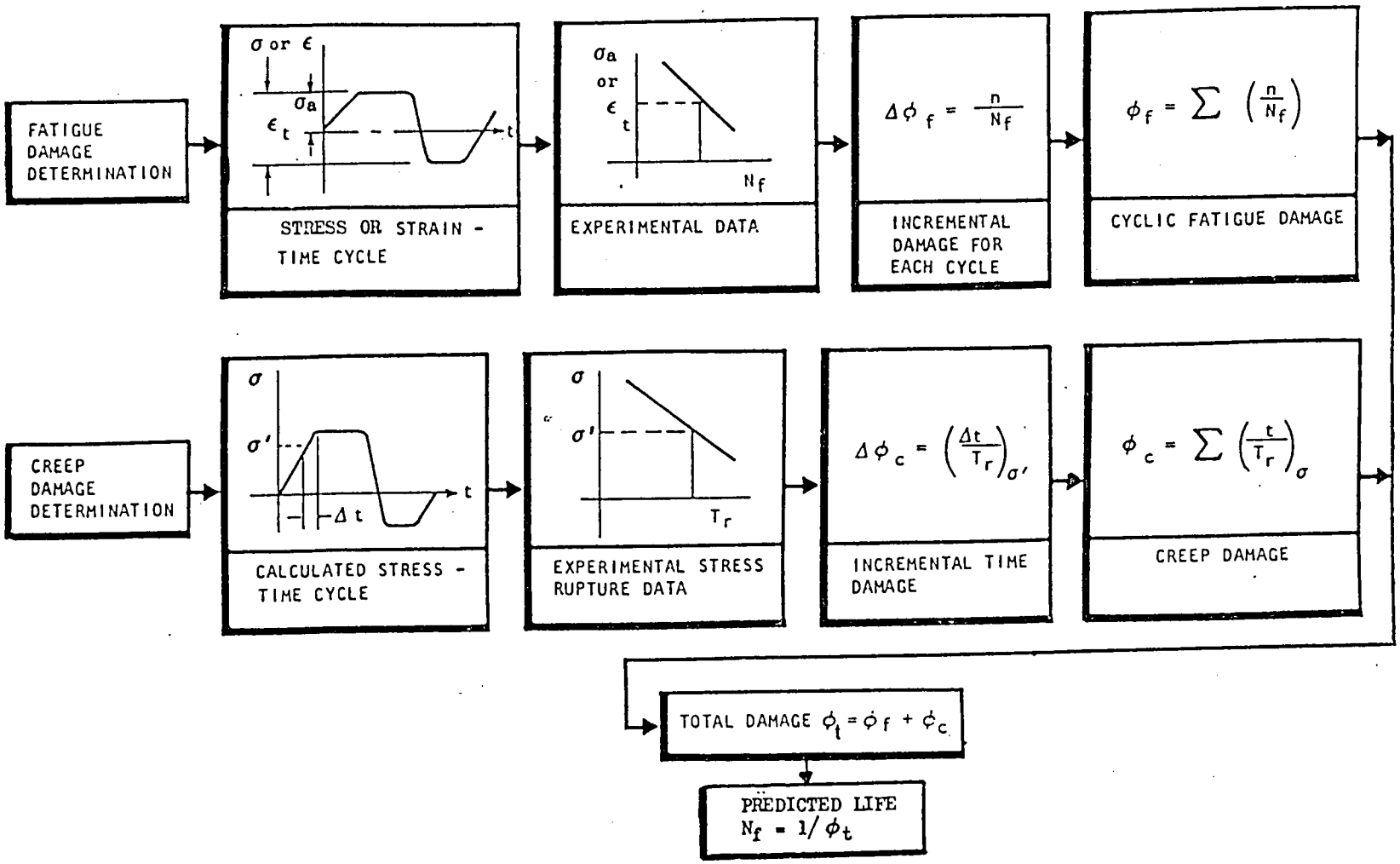

Figure 52. Life Analysis Schematic

Creep Rupture Analysis. Creep damage for the total duration is determined by the summation of the ratios of time spent at a particular stress to the time to rupture at that stress.

$$\phi_c = \frac{t}{T_R}$$

An illustration of the summation process is given in Fig. 52. If the temperature varies simultaneously with the stress, the time-to-rupture curve for the specific temperature is used for each stress increment. The time-to-rupture data that are used are obtained from monotonic load-based creep rupture tests.

As long as the creep rupture damage component is kept small, little inaccuracy is introduced using monotonic creep rupture data. Constants for the primary and secondary creep laws were used in the finite element solution to calculate wall creep deformation.

Static Strength Analysis. The static strength of the thrust chamber channel walls was reduced by the thinning and bulging during the cyclic process. The wall-thickness adequacy to withstand tensile loads occurring during the duty cycle was verified as an additional check of life capability.

Strain Limit

The maximum strain capability of the NARloy-Z material is approached from the tensile instability failure criterion. The maximum hoop strain is related to the radial strain and the thinning of the channel wall. Tensile instability is defined in this case as where the incremental strain hardening of the deforming metal of the wall is less than the incremental increase of true stress due to local wall thinning. Once the instability condition is reached, further increase in load results in rapid failure of the channel wall. The criterion defines a critical strain limit for the material. The analysis method for determining the strain at the onset of instability (called critical strain) is based on the work of Svensson (Ref. 11). The MCC section between lands is modeled as a thin shell plate that has an axial strain of zero during the tensile instability portion of the duty cycle. This strain condition occurs during inelastic straining in a 2:1 (hoop to axial) stress field, which is consistent with tensile instability of a pressurized thin cylinder. This stress state is only a first order approximation of the true-stress state, since the actual hardware has a more complex stress ratio due to the overall duty-cycle response to thermal load variations. The maximum tensile stress state occurs during the cutoff portion of the duty cycle as the temperatures start to fall off and there is still pressure in the channel.

The section of the hot-gas wall between the lands is shown in Fig. 53 with the stated stresses and strain condition.

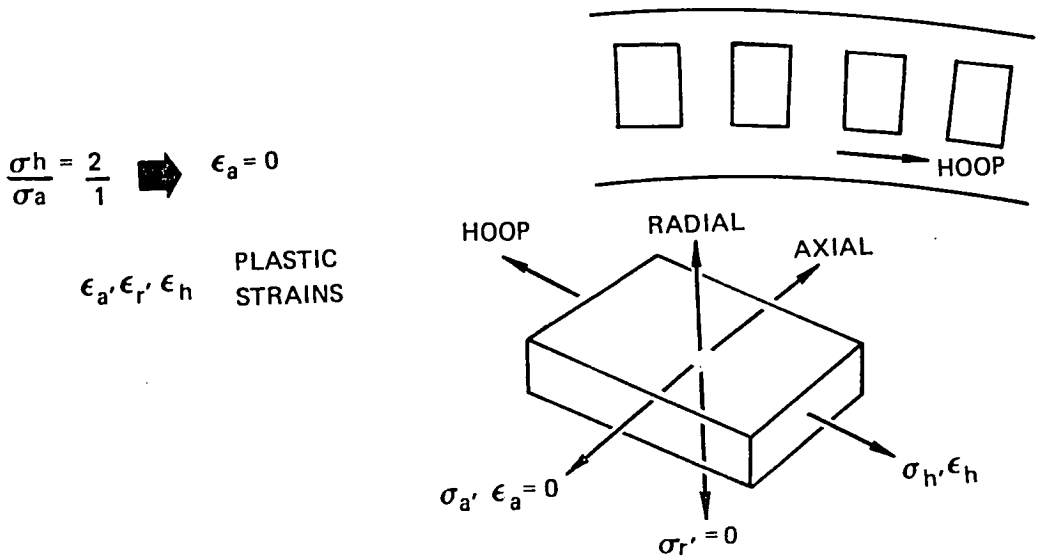

Figure 53. Critical Conditions at Tensile Instability

The critical tensile strain in the hoop direction at instability is equal to the material strain hardening coefficient, n, divided by 2. Once the critical tensile strain in the hot-gas wall is known, the corresponding change in wall thickness, or thinning, is determined from the radial strain, ϵ_r.

The sum of the inelastic strain components is zero, based on a constant volume criterion. Since the axial strain $\epsilon_a = 0$, and the tensile strain in the hoop direction $\epsilon_h = n/2$, at instability the radial strain is found by solving the following:

$$\epsilon_r + \epsilon_h + \epsilon_a = 0$$

$$\epsilon_r + n/2 + 0 = 0$$

$$\epsilon_r = -n/2$$

$$\epsilon_r = \ln \frac{t_{cr}}{t_o} = \frac{-n}{2}$$

or

$$t_{cr} = t_o \, e^{\frac{-n}{2}}$$

where

t_{cr} = thickness of hot-gas wall for tensile instability
t_o = original wall thickness
$\ln \frac{t_{cr}}{t_o}$ = definition of strain in the radial direction

Using this tensile instability methodology, the critical strain or thinning at failure can be calculated knowing the value of n, the exponent in Ludwig's Law. When stress-strain data are not available, a reasonable approximation for n can be determined using the tensile yield and ultimate values. Using the equation

$$n \approx .2 \left(\frac{FTU - FTY}{FTY} \right)^{0.6}$$

Figure 54 plots the value of n versus temperature and thinning at instability for NARloy-Z, based on Boeing and Rocketdyne strength data plus the analysis criteria developed above.

For the MCC, the maximum tensile stress occurs in the 590 to 700 K (600 to 800 F) temperature range and generates a range of thickness reduction of 5 to 8% at tensile instability.

A review of typical cross-sections from hot-fired MCCs show that failure can occur at an estimated 5 to 10% thinning of the channel wall. There is a wide variation in this thinning for different MCC chambers data base, but a 5 to 8% thinning limit is a reasonable criterion for the minimum strain at failure for the SSME. The variation in test results may be attributed to conditions in the heat input at hot spots, flow variation in a specific combustor and the sensitivity of instability analysis to small changes in material orthotropic properties. The 5 to 8% strain limit compared to the uniaxial strain limit of 50% is consistent with a literature survey study Rocketdyne has previously made of available biaxial test results vs uniaxial test results.

Ultimate elongations of 12 metals were obtained at room temperature in the 1:0 (hoop/axial), 1:1, and 2:1 tensile modes (Ref. 2 and 3). The specimens were made from steel, aluminum, and titanium sheet. Plots of the results (Fig. 55, 56, and 57) indicate a large decrease in available uniaxial elongation due to the biaxial mode even for such ductile metals as 301 stainless steel.

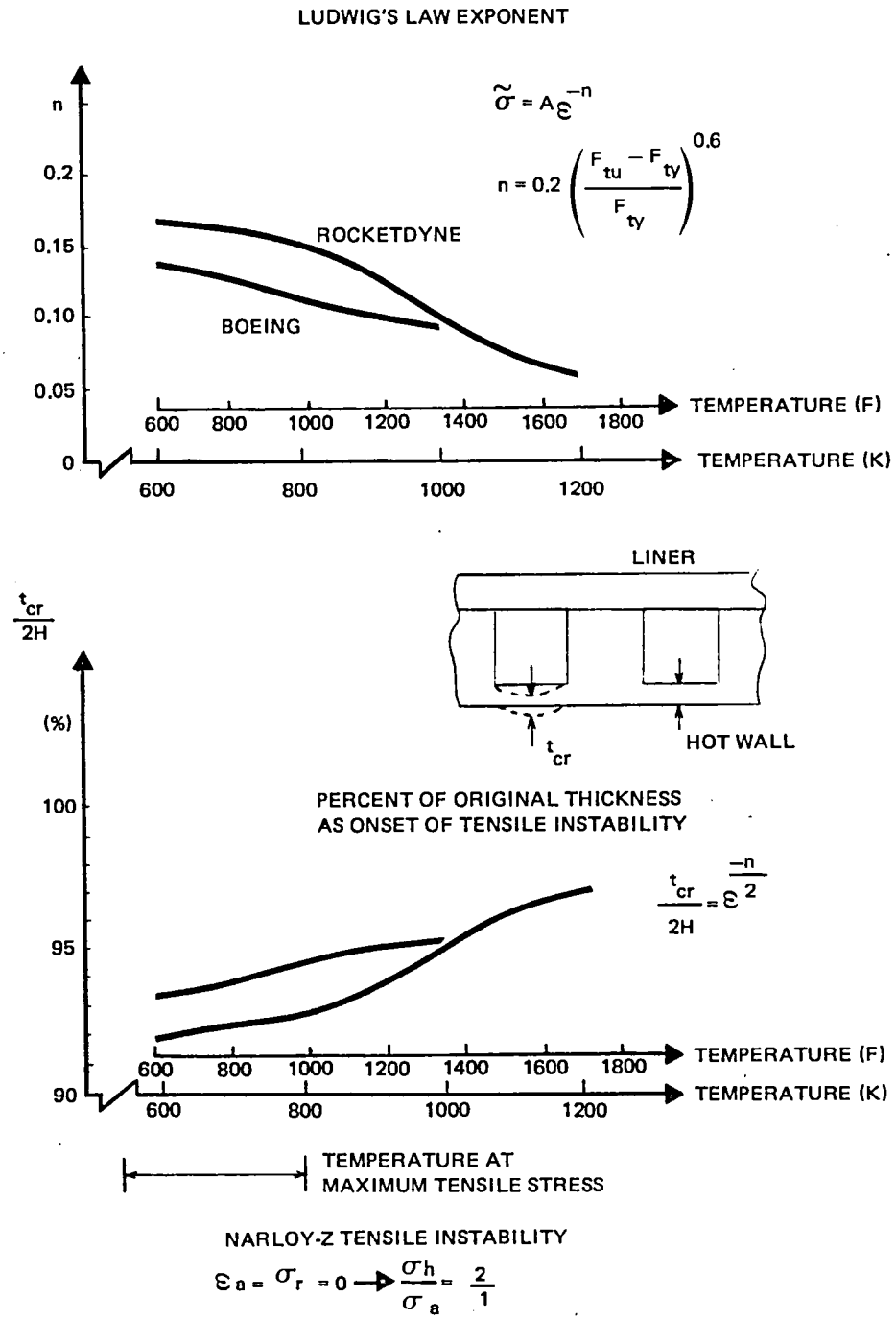

Figure 54. The Value of n vs Temperature and Thinning at Instability for NARloy-Z

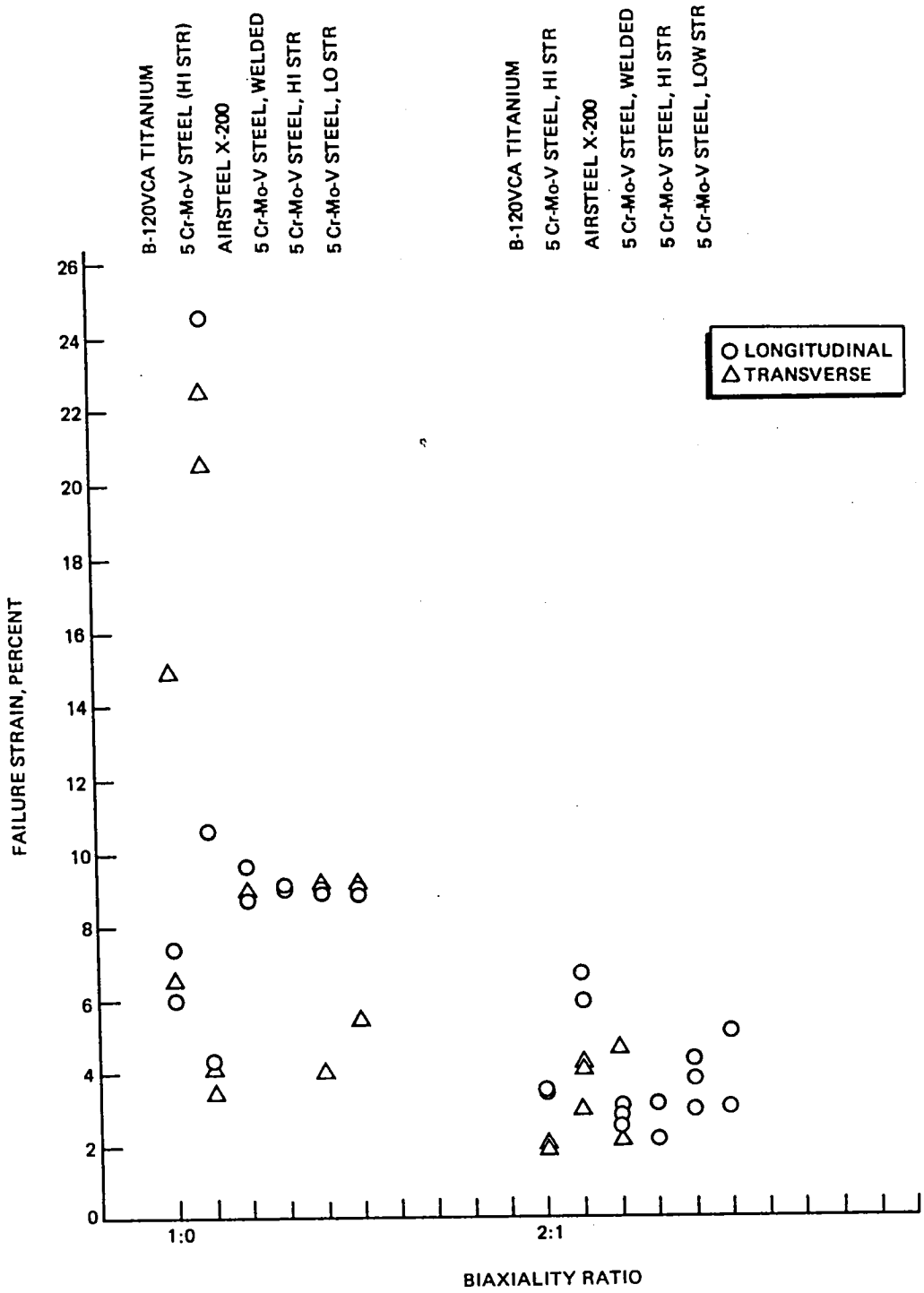

Figure 55. Biaxiality Ratio Failure Strain Data

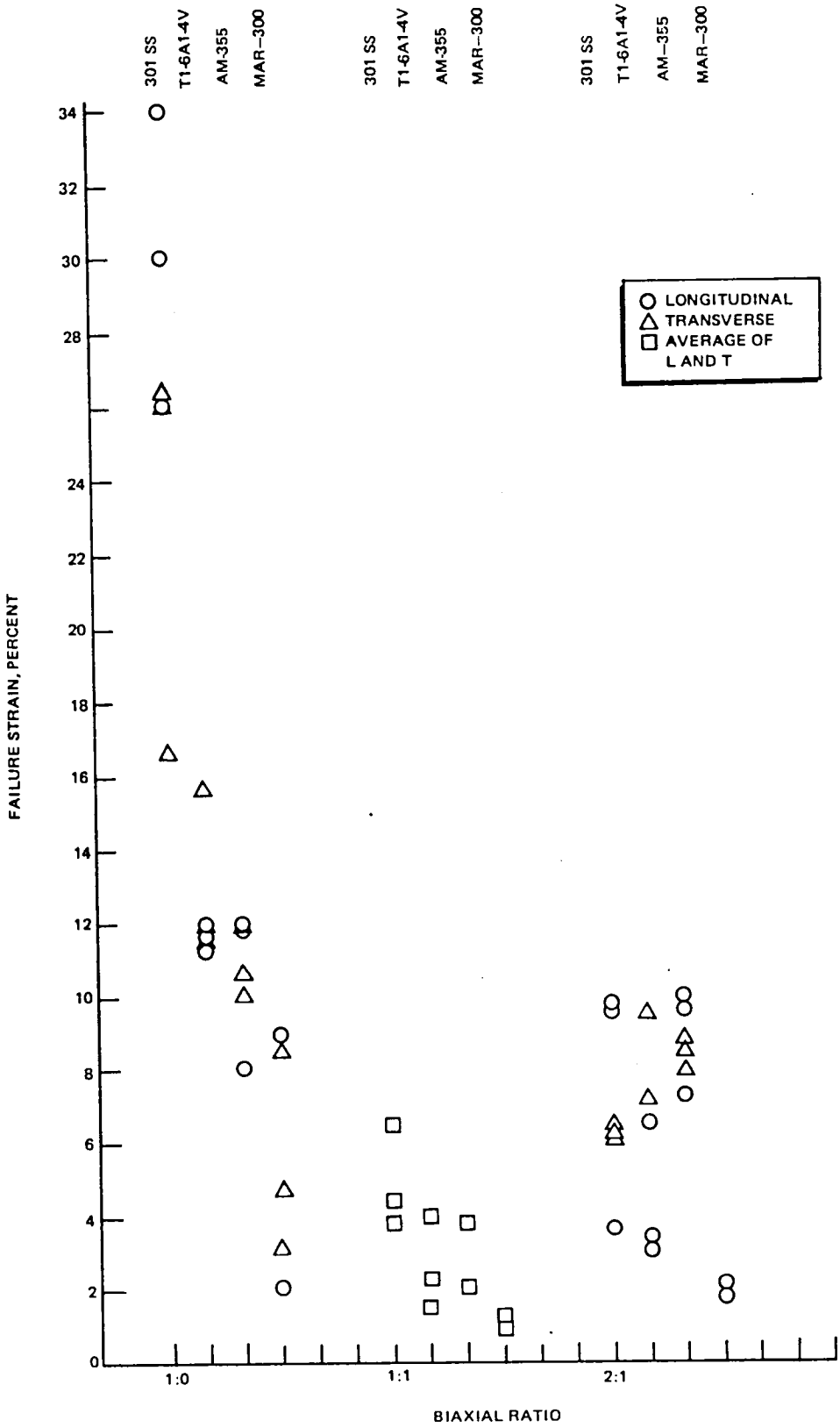

Figure 56. Biaxiality Ratio Failure Strain Data

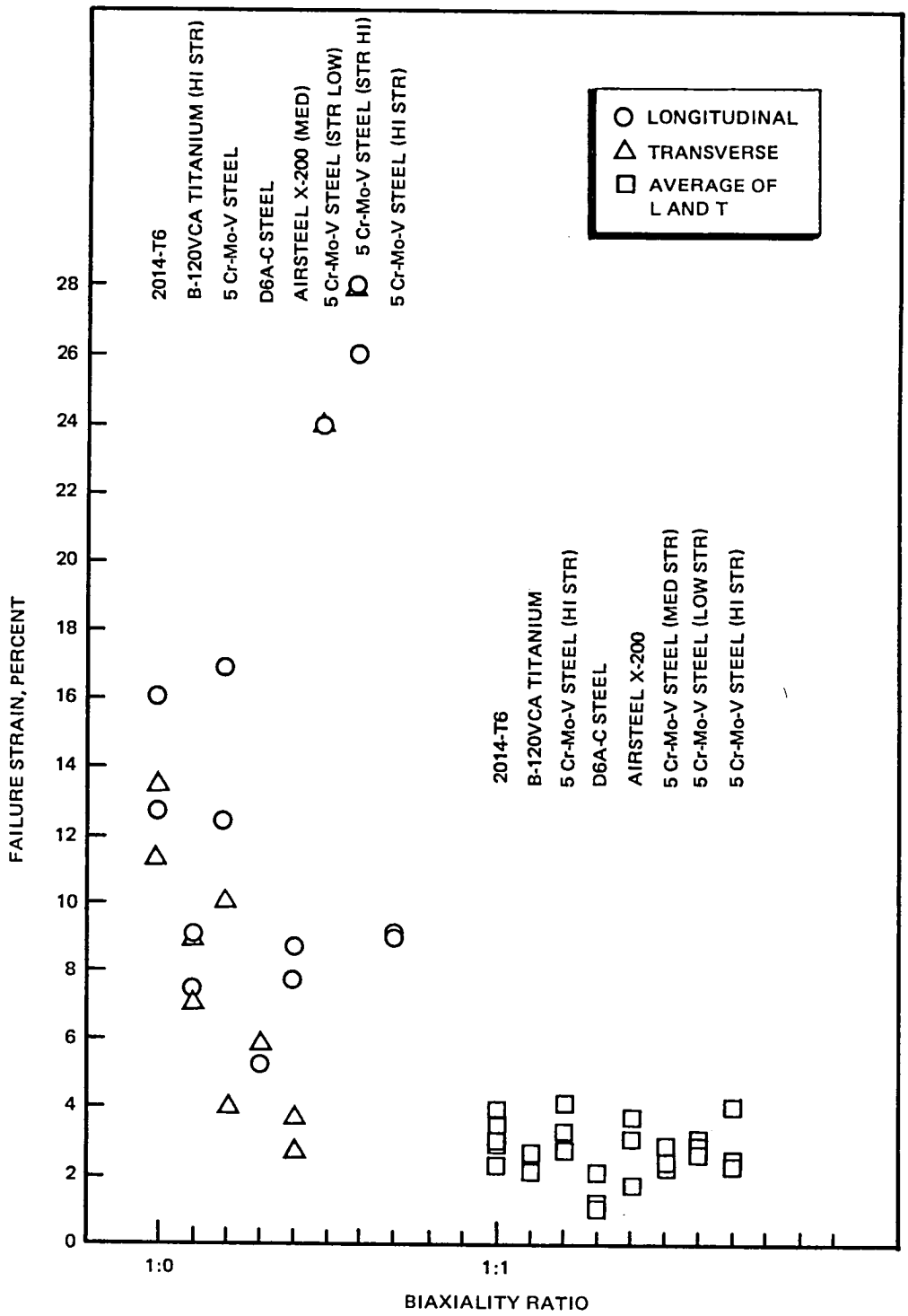

Figure 57. Biaxiality Ratio Failure Strain Data

ANALYSIS RESULTS

As previously mentioned, the 135% hg thermal load case was used as a baseline, so that cyclic creep effects would be a sensitive influence in the structural analysis. Also, it more closely reflects conditions in a hot spot where known cracking occurs. The 100% hg condition--away from hot spots on the MCC--has not shown the channel cracking mode to date. Not knowing what to anticipate from the computer analysis, and desiring maximum sensitivity for evaluating the various recommended life enhancement designs, the hotter condition (135% hg) was the more logical choice for the baseline analysis, especially since cyclic creep was the primary interest of this study.

To date, there is no detailed textbook explanation of how cyclic creep takes place or the relative importance of individually biased loads or geometric shape on cyclic creep. A simplistic sensitivity study was run on various geo- metric and property variations to try to better understand individual vari- ables. Whereas this technique was quite successful in the thermal analysis, it was inconclusive in the structural analysis. The structural boundary con- ditions from the operational duty cycle forces the entire hot wall of the liner well into the inelastic regime. This seems to require accurate shape changes or property variations that are truly representative of the geometric distortions and materials to furnish usable results; i.e., only computerized analysis utilizing updated geometries produced acceptable information for judging life enhancement.

So, to obtain an overall perspective of cyclic creep, the basleline-analysis results have been studied in several ways. One class of studies was from an overall standpoint that is related to observable hardware-channel distortions and cracks. These results are:

1. Overall distorted shape versus test cycle
2. Thinning and cracking versus accumulated duty cycles
3. Thinning versus radial distortion difference between mid-channel and midland

The other class of studies related to trying to understand calculated stress-and-strain conditions and distortions from the standpoint of how to improve a design or evaluate a configuration before a detailed analysis. This effort required a detailed study of start, steady state, cutoff, and posttest increments within a 5 duty-cycle analysis. Areas investigated included:

1. Stress and strain distribution
2. Critical strain locations for LCF analysis
3. Distorted shape throughout the duty cycle
4. Incremental stress-strain hysteresis loops for a critical point

5. Simplified correlation of biaxiality-strain distortion
6. Definition of maximum gross tensile-stress condition in the duty cycle when cracking actually occurs

The baseline analysis will first be discussed completely, followed by correlations with the remaining studies.

Distorted Shape

The shape change with accumulated duty cycles gives a perspective of how well the analysis procedure predicts the type of distortions observed from cross-sections of the SSME MCC. Figure 58 is a composite of the finite-element model distorted shape at the end of each 5 duty-cycle analysis (5, 25, 45, 65, 85, 105). A gradual change in the cross-section is noted as the cycling progresses. The midchannel point thins and the initial sharp corner at the land to channel gradually thickens and smooths. There is only a small permanent set inward (toward the centerline) at the midchannel point relative to the midland position. These geometric changes are typical of what has been observed on the SSME MCC cross-sections in the regions of local hot spots.

Thinning and Cracking Versus Duty Cycles

The maximum channel thinning versus accumulated duty cycles was used as the measure of the total average strain on the channel wall. Because of the approximation technique (updating the geometry, but losing the strain state) used for determining the restart condition after a 15 cycle extrapolation, the total strain in each element is not directly available. However, it is a rather simple task to track the accumulated thinning of the channel wall. The geometric updating is all part of the extrapolation code discussed in Appendix C). There was still additional judgments required to utilize this information. Figure 59 depicts the baseline 135 hg analysis results and shows the shakedown condition that occurred in each 5 duty cycles, and the method of adjusting the raw analysis results to account for the shakedown. Each configuration and operating condition analyzed had similar shakedown conditions. For the first 5 duty cycles, the adjustment of the residual stress and strain conditions during the load cycling resulted in a realistic shakedown condition. The first shakedown condition also included the gross distortion of the liner as it permanently yields through the 0.51 mm (0.020 inch) tolerance gap and touches the jacket. Thereafter, at the steady-state posttest condition, the liner remains virtually in line-to-line contact with the jacket, so the first shakedown is larger than the remaining ones. The other shakedown condition, where there is a rapid change in thickness for the first 1 or 2 cycles, followed by a much slower change in cycles 3, 4, and 5, occur because of the approximations made. Each new 5 duty cycles start with a stress-and-strain-free distorted geometry rather than a shakedown continuation of the previous cycling. If the raw analysis results were used directly, a significant error in thinning would be obtained.

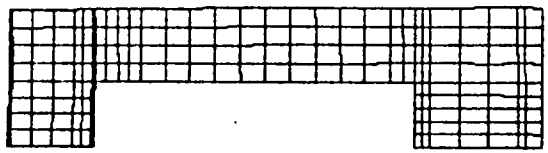

CYCLE 5

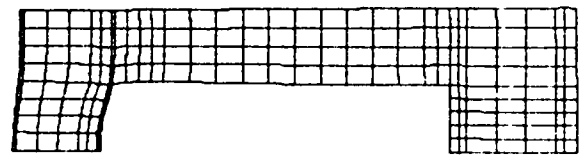

CYCLE 65

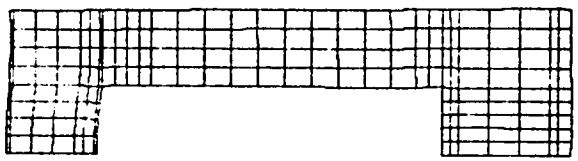

CYCLE 25

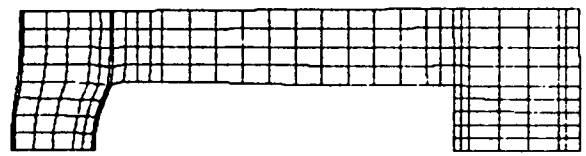

CYCLE 85

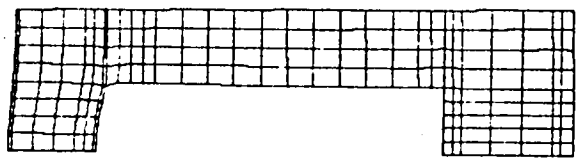

CYCLE 45

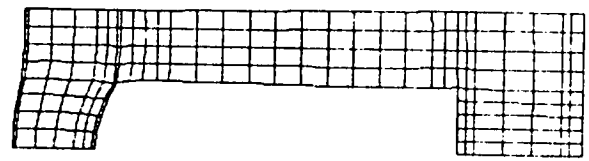

CYCLE 105

Figure 58. Geometric Shape Change With Cycling of Basic SSME Channel Configurations at 135% FPL hg

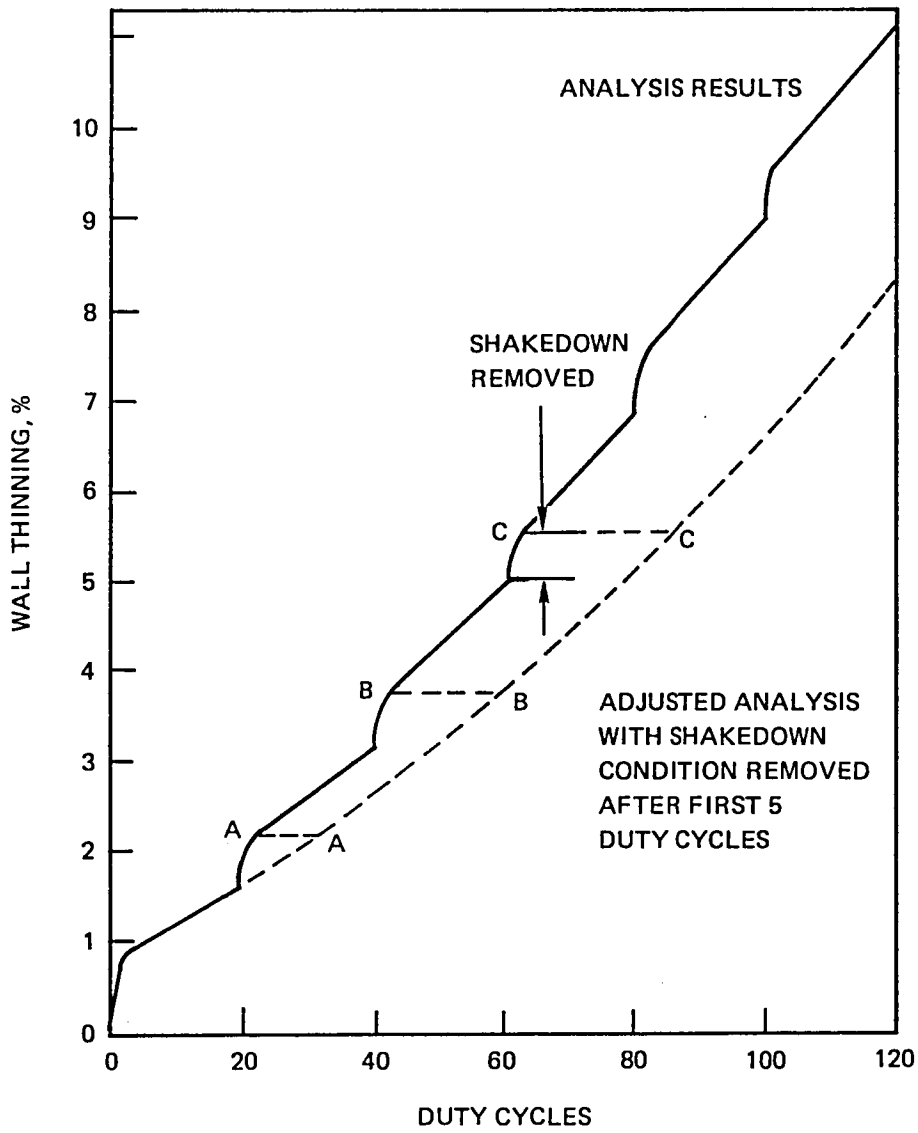

ANALYSIS METHODOLOGY
5 DUTY CYCLE + 15 CYCLE EXTRAPOLATION
RESTART WITH
- DISTORTED GEOMETRY
- VIRGIN MATERIAL(NO RESIDUAL STRAINS)
- MCC LINER IN CONTACT WITH JACKET

INITIAL "SHAKEDOWN" ONLY REALISTIC FOR 1-5 DUTY CYCLES

"SHAKEDOWN" EFFECT SUBTRACTED OUT

Figure 59. SSME MC Life Prediction - Baseline 135% hg

The final methodology chosen to eliminate the shakedown effect was to assume that the distortions from the first cycles in the 5-cycle analysis were equivalent to a series of thinning cycles at the rate of change used for extrapolation to the restart condition. This is effectively obtained by extending the last 5-20-cycle extrapolation line (e.g., A) until it intersects with a horizontal line drawn from the end of the shakedown condition, B. At this point, the B slope applies until the C slope horizontal line intersects. This technique was used to adjust all the raw analysis results in this study. As one would expect, it has the largest effect on slowly thinning analyses with larger shakedown conditions. The raw analysis results for all analyses are located in Appendix G.

The adjusted results for the baseline configuration 135% hg and 100% hg and the strain limitations are shown in Fig. 60. The plot is developed as a percent of thinning versus cycles for two reasons. One is that various channel-wall thicknesses are used in the analyses, and a common baseline is desirable; and the other is the percent thinning is equal to the accumulated radial strain, and is within 10% of the accumulated effective strain. The results show, as expected, significant differences in thinning for the two conditions 1600% hg and 135% hg). The hot-spot condition (135% hg) failure life is between 80 and 125 duty cycles. SSME test history puts this at somewhere between 5 and 30, so there is still a significant difference between the cyclic-creep analysis and hot-fire test data. The most likely reason for this discrepancy is the approximation required to model the hot-spot condition as a plane strain model. The analysis assumes the hot spot occurs in a total circumferential band around the MCC. In reality, the hot spot is a local condition over a range of 5 to 10 channels. Appendix discusses in detail a refined approach to more accurately analyze a local hot spot and presents the results of a preliminary study. From a heat transfer standpoint, however, the size of a hot spot is negligible, as long as it covers several channels and is reasonably long, as has been experimentally evidenced.

From a structural standpoint, relative to the remainder of the liner, the hot spot tends to act like a solid material for the start and cutoff conditions (when it is cool), and an elliptical hole filled with soft material (when it is not) during the steady-state firing conditions. This condition can significantly increase both the out-of-plane axial strain condition and the hoop strain. The detail modeling of a hot spot requires a complex 3D inelastic analysis that is well beyond the scope of this study. The basic correlations and analysis, though, of this study's methodology are useful for correlation between models and temperature changes, but are not considered to be exact answers. The 100% hg condition relates to a circumferentially uniform temperature condition, and the planar model is a more accurate representation. The calculated life of 290 to 445 duty cycles, for the lower temperature nominal SSME-MCC condition has not yet been verified by test data in that individual MCCs have not been tested more than 80 to 100 duty cycles.

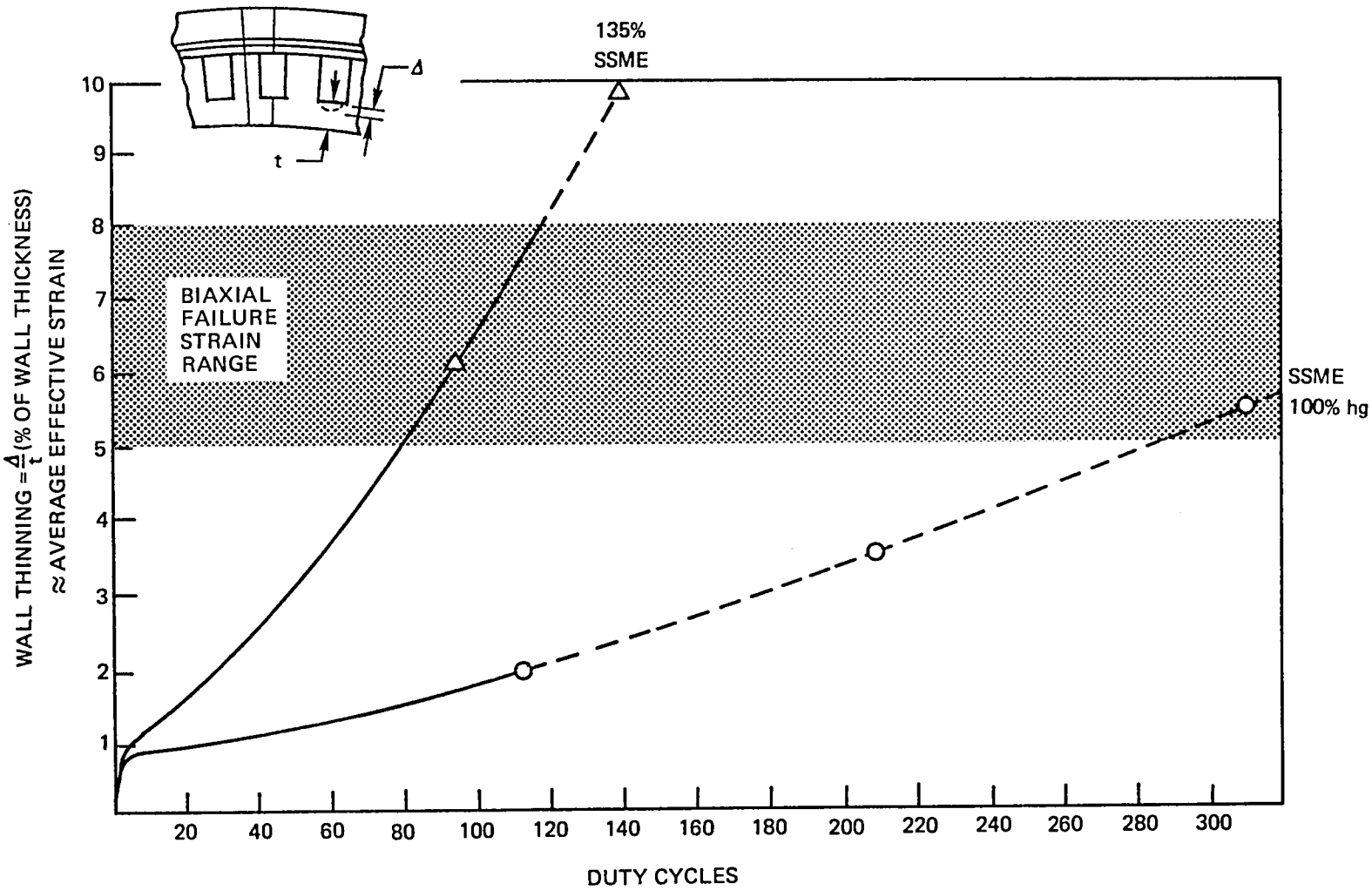

Figure 60. Midchannel Permanent Deformation (Thinning) vs Number of Duty Cycles

Detail Duty Cycle Review

This review presents detailed information and observations gleaned from an intense study of the 135% hg baseline analysis. Its intent is to furnish additional information to aid analysts in understanding possibly how cyclic creep occurs, how to improve a design, strain distributions, and how a typical 5-cycle hysteresis loop looks. These results were specifically used in developing the contoured life-enhancement design.

For the review, the hot wall was separated into three zones: midland (ML), channel to land (LC), and midchannel (MC). Figure 61 defines the characteristics, from a structural analogy, for the three zones. Figure 62 and Table 3 describe the zonal thinning in a relative manner and list the thickness changes for the different key load incremenets per cycle. Figure 63 is a composite of critical time-slice distorted shapes.

TABLE 3. SUMMARY OF CHANNEL WALL THICKNESS PER CYCLE FOR THREE KEY LOAD INCREMENTS (135% hg)

LOAD INCREMENT	LOCATION	CHANGE IN THICKNESS,*	
		mm	INCH
INCREMENT 6, STEADY STATE	ML	0.0196	$+7.7 \times 10^{-4}$
	LC	0.0218	$+8.6 \times 10^{-4}$
	MC	0.0183	$+7.2 \times 10^{-4}$
INCREMENT 10, POST CHILL	ML	-0.0053	-2.1×10^{-4}
	LC	-0.0053	-2.1×10^{-4}
	MC	-0.0091	-3.6×10^{-4}
INCREMENT 11, ROOM TEMPERATURE	ML	-0.0017	-0.67×10^{-4}
	LC	-0.0017	-0.68×10^{-4}
	MC	-0.0053	-2.1×10^{-4}

ML = MIDLAND
LC = LAND/CHANNEL TRANSITION
MC = MIDCHANNEL
*CHANGE IN THICKNESS FROM ORIGINAL GEOMETRY (ABSOLUTE) = $\Delta R_{(1)} - \Delta R_{(2)}$

Table 3 shows that during steady state (increment 6), even though the hot wall is getting thicker due to $\alpha\Delta t$ and compressive hoop load, the MC is getting less thick than ML or LC, or relatively speaking, MC becomes thinner than ML and LC.

DESIRABLE TO SEPARATE INTO 3 ZONES

ML, LC, MC – MID-LAND, CHANNEL TO LAND & MID-CHANNEL

EACH ZONE HAS DIFFERENT CHARACTERISTICS

ML – 3D ZONE OF MATERIAL WITH FREE SURFACE (BIAXIAL RESTRAINT)
(ANALOGY – THICK CYLINDER INSIDE SURFACE)

MC – 2D ZONE OF MATERIAL WITH 2 FREE SURFACES (LOWEST RESTRAINT)
(ANALOGY – THICK PLATE/BEAM WITH ZERO STRESS THROUGH THICKNESS)

LC – NOTCH ZONE WHERE 2D TO 3D EFFECTS TRANSITION (HIGH SHEAR)
(ANALOGY – σ-CONCENTRATION IN STEPPED BAR OR CYLINDER)

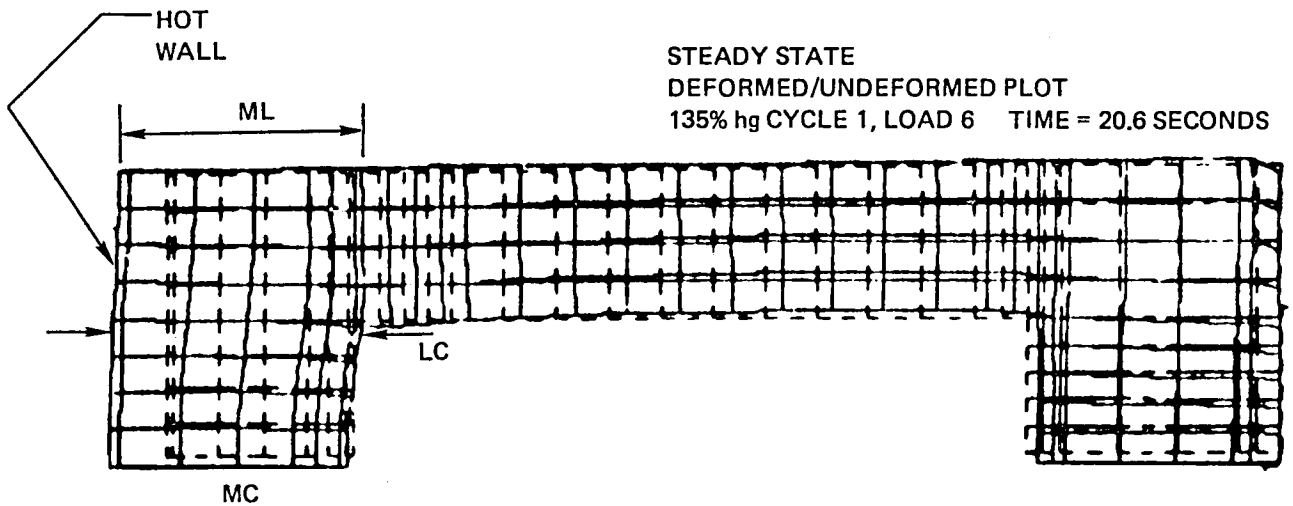

Figure 61. 135% hg MCC Analysis Detail Review, Zone Definition

- THINNING/RELATIVE THINNING/CYCLIC CREEP
  - RELATIVE THINNING APPARENT THROUGHOUT CYCLE
    - RATIO OF THICKNESSES AT ML, LC AND MC ZONES
  - DURING DUTY CYCLE
    - ABSOLUTE THICKNESSES INCREASE UNDER STEADY STATE
      - COMPRESSION LOADING
      - $\alpha \Delta T$ GROWTH
    - ABSOLUTE THICKNESSES THIN DURING PRECHILL AND C/O
      - TENSION LOADING
      - $\alpha \Delta T$ SHORTENING
    - RELATIVE THINNING – MC THINS MORE THAN LC OR ML THROUGHOUT DUTY CYCLE. FUNCTION OF
      - BIAXIAL RESTRAINT AT ML
      - NOTCH RESTRAINT AT LC

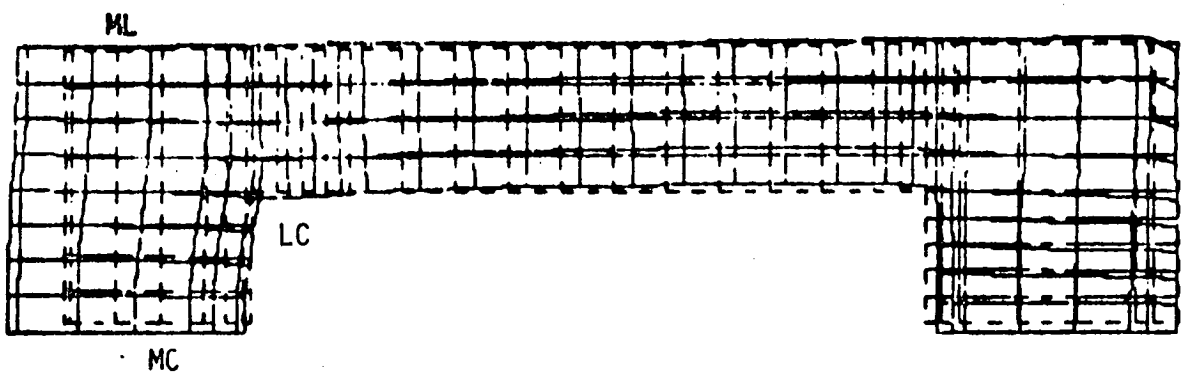

Figure 62. 135% hg MCC Analysis Detail Review, Thinning

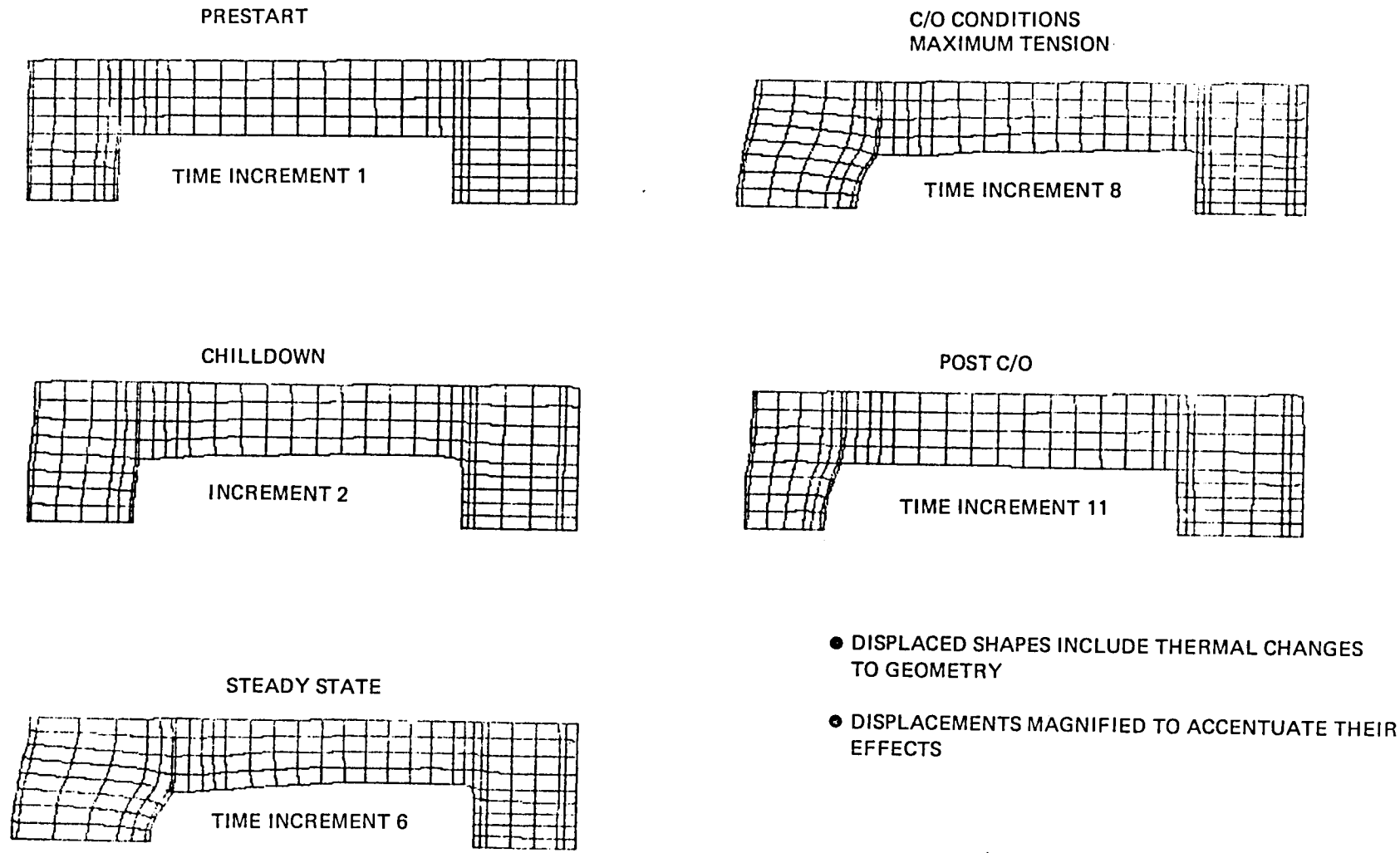

Figure 63. Geometry-Scaled Distortions for a Typical Duty Cycle Basic Configuration at 135% hg

This was a rather interesting result. If one ignores the biased loading effects, the large tension/compression thermal loading of a restrained beam could thin under tension and thicken under compression. The relative thinning under steady-state compression, time increment 6, is probably due to the land/channel transition notch effect and midland high biaxiality, plus the biased loading from the differential pressure.

Figure 63 gives a distorted-shape perspective for the cycle, and shows that the general shapes are as expected, based on the hardware cross-sections.

Table 4 presents an overall summary of the stresses and strains of the key load increments. This basically reinforces the general observations of the previous discussion on the biaxial restraints and shear conditions in the cross-section. It is interesting to note the large difference in mechanical strain across the channel wall from the 1090 K (1500 F) thermal gradients. This makes the hot-wall strain about twice that of the cold-wall strain. Figure 62 shows the yield stress versus temperature across the wall ranging from 20.68 MPa (3 ksi) at the hot surface, to 137.9 MPa (20 ksi) at the inner surface. This demonstrates the significant strength capability of the inner half of the channel wall that was alluded to as previously mentioned in the structural analysis.

It also makes a hand-solution methodology, such as Ref. 12, more difficult with these kind of stress-strain gradients. This reference only assumes average temperatures and, therefore, average yield strengths are rapidly increasing. The channel remains in high tension during the remaining portion of the cutoff cycle. After test, steady-state conditions have the channel wall in a high tension stress in the axial direction with low stresses in plane in the hoop and radial directions.

The primary purpose of Fig. 64 was to point out the stress state that occurs at the hot surface during steady state and what happens during creep relaxation. The material yield strength at 1090 K (1500 F) is only slightly higher than the surface pressure stress (i.e., P_c = 2/3 FTY). This means that the pressure stress is a significant part of the total stress state, and that the stress component in the radial direction must always equal the P_{HGW} value. At the steady-state condition, the top half of the channel wall goes through a creep relaxation process, which shifts the differential pressure primary load to the stronger (cooler), inner-half of the wall. At the hot wall, the stress state equilabrates to primarily a bulk compression equal to the P_{HGW} pressure 14.54 MPa (2109 psi), plus a small component that develops a combined effective stress of 5.52 MPa (800 psi). This is a rather unusual stress condition in that rarely does a surface pressure equal twice the effective stress on the part.

Figure 65 simply restates, in summary format, important observations made during this discussion.

TABLE 4. SUMMARY OF 135% hg APSAC PROGRAM RESULTS

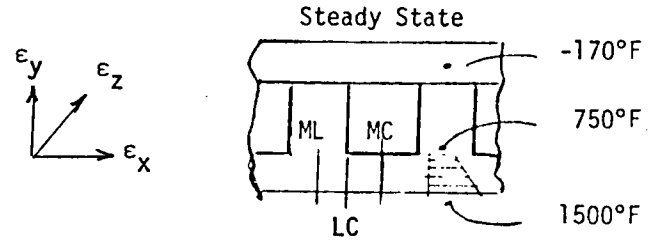

CONDITION	MID-CHANNEL (MC)	CHANNEL-LAND INTERFACE (LC)	MID-LAND (ML)
General Comments	2D Stress State 2 Free Surfaces Plate/Beam Analogy	Notch Zone High Local Shear Stepped Plate Analogy	3D Stress State Free Surface Biaxial Restraint
Steady State (INCR 6)	$\varepsilon_z=-\alpha\Delta T$ =-.017 HW Range =-.0075 CW	$\varepsilon_z=\bar{\alpha}\Delta T$ $\tau<$ 2 ksi	$\varepsilon_z=-\alpha\Delta T$
Hotwall - 1500 F	$\varepsilon_x=1.2\alpha\Delta T$, $\varepsilon_y=.4\alpha\Delta T$ $\tilde{\varepsilon}=1.3\alpha\Delta T$	$\varepsilon_x=1.5\alpha\Delta T$, $\varepsilon_y=-.7\alpha\Delta T$ $\tilde{\varepsilon}=1.5\alpha\Delta T$	$\varepsilon_y=\varepsilon_z=-\alpha\Delta T$ $\tilde{\varepsilon}=1.8\alpha\Delta T$
Coldwall - 750 F	$\varepsilon_x=1.6\alpha\Delta T$, $\varepsilon_y=.8\alpha\Delta T$ $\tilde{\varepsilon}=1.7\alpha\Delta T$	$\varepsilon_x=1.2\alpha\Delta T$, $\varepsilon_y=-.4\alpha\Delta T$, $\gamma=1.2\alpha\Delta T$, $\tilde{\varepsilon}=1.73\alpha\Delta T$	$\varepsilon_y=0$, $\varepsilon_z=-\alpha\Delta T$ $\tilde{\varepsilon}=1.\alpha\Delta T$
Steady State to Cutoff	Large Bending σ, ave. axial σ=-6 ksi	τ < 2 ksi	
HW-1047 F(INCR7)			
HW-739 F (INCR 8)	Minimal Bending σ ave. axial σ=12 ksi	$\tau \approx$ 4. ksi	
HW-300 F (INCR 9)	No Bending σ ave. axial σ=28 ksi	σ_x=40 ksi $\tau \approx$ 4. ksi } @ Notch	

1 in. = 25.4 mm
1 psi = 6894.8 Pa
°F = $\frac{9°K}{5}$ - 460

TABLE 4. (Concluded)

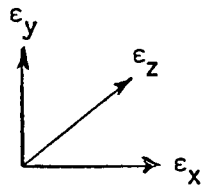

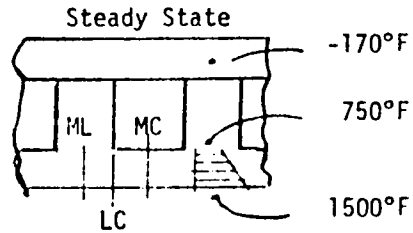

CONDITION	MID-CHANNEL (MC)	CHANNEL-LAND INTERFACE (LC)	MID-LAND (ML)
Minimum Cutoff HW~-400°F (INCR 1	σ_x=25 ksi, No Bending $\tilde{\sigma}$ 32 ksi σ_z=35 ksi ε_x=-1% γ_{xy}=.1% ε_y=.8% $\tilde{\varepsilon}$=1.1% ε_z=.35% Constant Strains 2X Mid-land or LC Interface except for Local Notch Zone	No Bending Throughout End (Constant Temp., no Pressure) ε_y=-.5% γ_{xy}=1.4% @ Notch ε_x=-1.% @ Notch $\tilde{\varepsilon}$=1.3 @ Notch ε_y=.3% ε_z=.35% Constant	ε_x=-.4% γ_{xy}=0 ε_y=.2% ε_z=.35% Constant $\tilde{\varepsilon}$=.5% @ Notch
Room Temp. INCR 13 70°F	No Bending Throughout End (70°F Constant, no Pressure) $\sigma_x=\sigma_y=\tau_{xy}=0$ & $\sigma_z=\tilde{\sigma}$=23 ksi on Whole X-Section @ End ε_x=-.8% ε_y=.8% γ_{xy}=.1% $\tilde{\varepsilon}$ = 1% ε_z=0 on Whole X-Section	ε_x=-.33% → ε_x=-.7% @ Notch ε_y=.3% → ε_y=.7% @ Notch γ_{xy}=.7% → γ_{xy}=1.33% @ Notch ε=.6% → $\tilde{\sigma}$=1.2% @ Notch	ε_x=-.2% γ_{xy}=0 ε_y=.2% $\tilde{\varepsilon}$=.2%

1 in. = 25.4 mm
1 psi = 6894.8 Pa
°F = $\frac{9°K}{5}$ - 460

- STEADY STATE LOADING
  - $P_c \approx 2/3$ FTY $\approx 2\sigma$ RELAX
  - UNUSUAL LOADING ON HOT WALL SURFACE, SOMEWHAT LIKE A FORMING STATE
  - $P_f < 1/3$ FTY MINOR EFFECT ON σ-STATE
  - THERMAL DOMINATES σ-STATE

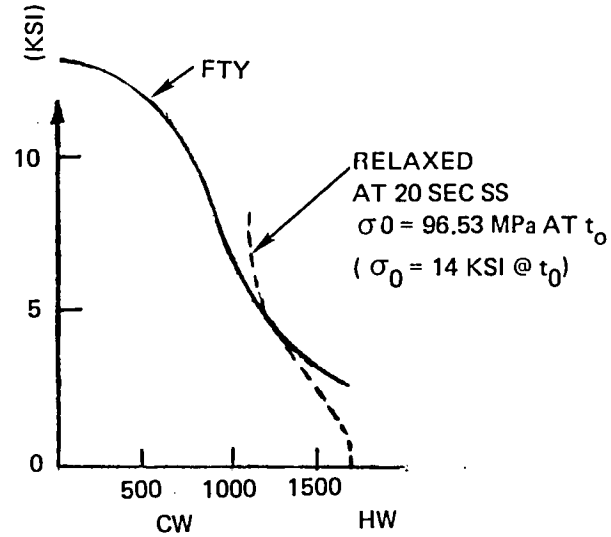

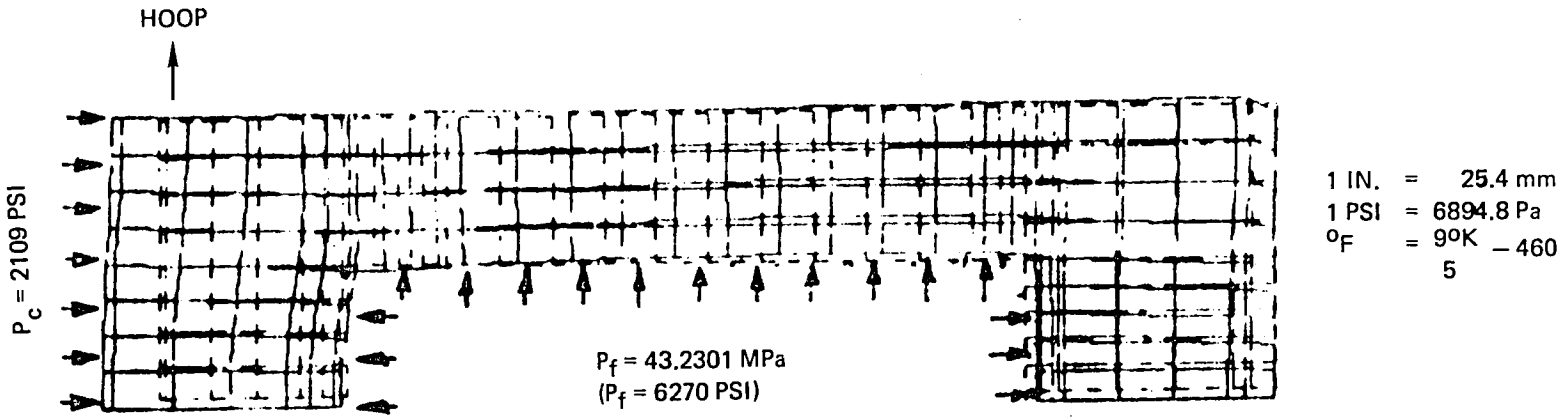

Figure 64. 135% hg MCC Analysis Detail Review

- STEADY STATE RESULTS
  - CYCLES 1 AND 5 REVIEWED
  - SIMILAR RESULTS
  - DISPLACEMENTS AND STRAINS SHOW CONSISTENT RESULTS
    - MID-CHANNEL (MC) DISPLACEMENT AND STRAINS LESS THAN MIDLAND (ML) WHICH ARE LESS THAN THE LAND TO CHANNEL (LC) VALUES
    - AXIAL STRAINS (ε_z) UNIFORM AT POINTS ALONG THE HOOP DIRECTION
    - THINNING STRAINS (ε_x) $\rightarrow f(\varepsilon_y, \varepsilon_z, \alpha_{yz})$
    - AT MC LOWEST RESTRAINT WITH LOW SHEAR RESULTING IN SMALLEST ε_x
    - AT ML, $\varepsilon_x \approx \varepsilon_y + \varepsilon_z$ ($\alpha_{yz} \approx 0$) DEMONSTRATING HIGH BIAXIAL RESTRAINT
    - AT LC, α_{yz} is HIGH AND RESTRAINT IS MODERATE YIELDING THE LARGEST DISPLACEMENTS
    - CONTOUR, DIGITAL & GRAPHICAL PLOTS ALL CONFIRM THIS CONDITION
  - THERMAL GRADIENT THROUGH THICKNESS LARGE (1500 F to 750 F) (1089 K to 672 K)
    - LARGE $\alpha\Delta T$ GRADIENT - FACTOR OF 2
    - MAXIMUM ε VARIES ALONG HOT WALL DUE TO VARYING RESTRAINT
    - HOT WALL CREEPS & RELAXES TO $\tilde{\sigma} \approx \sigma_y$, COMPONENTS $\approx \sigma_y$
    - STRESS GRADIENT THROUGH WALL TEMPERATURE DEPENDENT - α, F_{TY} NOT STRAIN DEPENDENT
    - GRADIENT FORCES MAXIMUM ε ON HOT SURFACE 3%

Figure 65. Observations of 135% hg Basic Geometry, SSME MCC APSAC Analysis Detail Review

Figure 66 is a typical multiple duty cycle plot of the stress-and-strain history of the element located midchannel at the hot wall. The efective stresses and strains are plotted with their sign obtained from the hoop-stress components (note: effective stress and strain are only magnitude quantities).

The duty cycle increments and hot-wall temperatures are noted on the first cycle to help follow the duty cycle. The point first goes in tension during the prechill operation, followed by a rapid drop to a high compressive state, then reduces in stress magnitudes as the material strength decreases with temperature and, from creep/relaxation effects, to the maximum compressive strain (point 6). The stress decrease from increment 2 to 6 is mainly due to changes in yield stress with temperature. During the throttle back to 65% of thrust, the point moves to a tension stress state even though the total strain is a high compressive plastic strain. As cutoff starts, the element is driven to a high-tension, high-positive strain point. Finally, after the test duty cycle and the part is stabilized at room temperature, the element is in compression with a large tensile, plastic strain.

Each duty cycle progressively shifts to a more positive strain position. This is indicative of a thermal ratchet or cyclic-creep phenomenon and resultant channel-wall thinning.

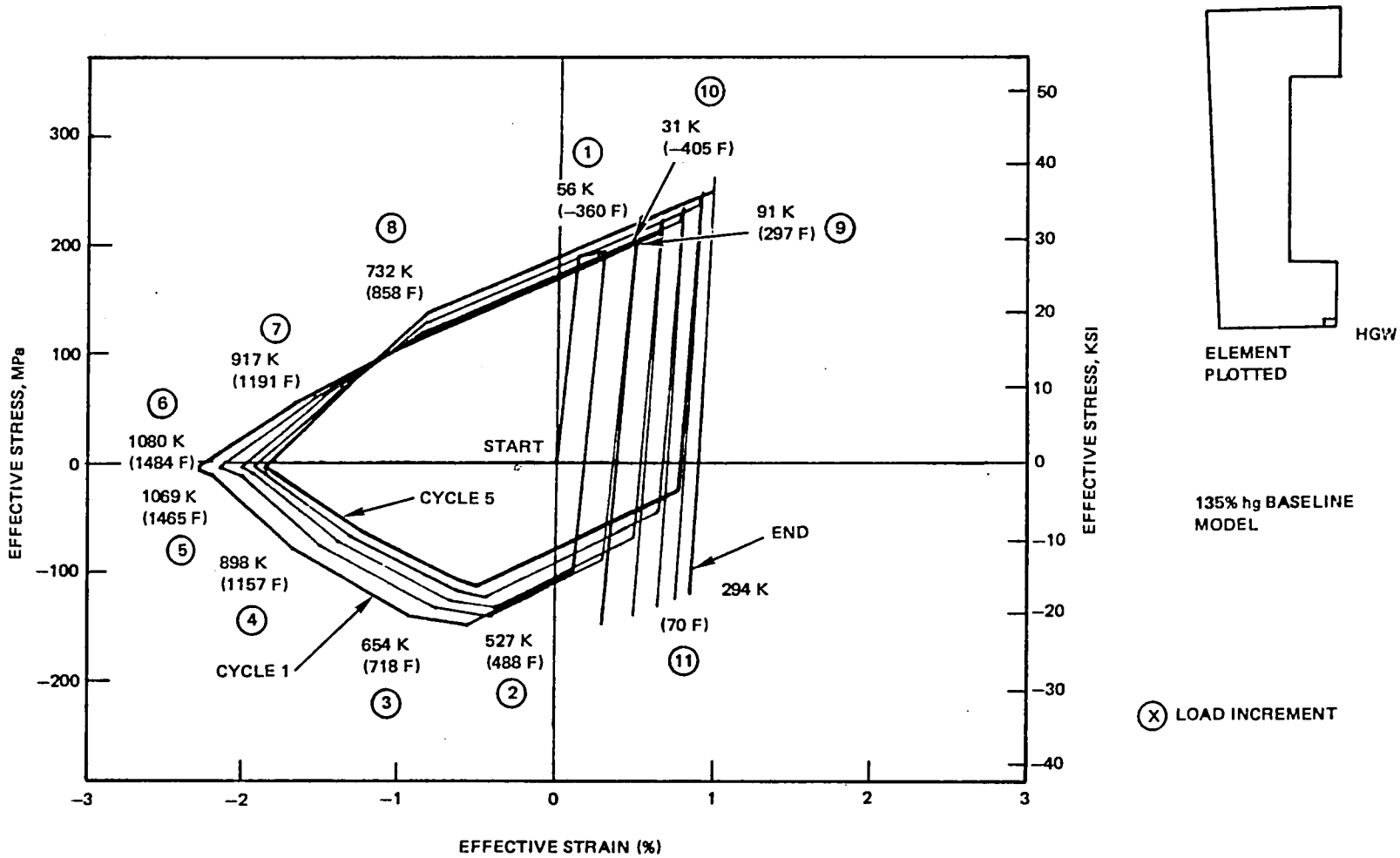

Figure 66. Midchannel Hot-Gas Wall Multiple Duty Cycle Stress/Strain History

LIFE-ENHANCED DESIGNS

General

Task III of this study consisted of evaluating four life-improvement designs using the developed methodology. The requirements were to select two designs with minimum changes from the current MCC configuration; one best concept that could be a radical change, and one combination configuration or second-best concept configuration. In addition, concepts where coatings were required were declared outside the scope of the study.

The total concept evaluation addressed manufacturing, thermal, structural, and operational considerations. Some of these are discussed in other sections of the report. The discussion herein is primarily limited to the structural considerations. The goals for the life enhancement were to:

1. Reduce the cyclic creep deformation rate and extend the life to crack initiation

2. Reduce the hot-wall surface and overall temperature. This lowers the thermal strains, increases the strength capability, and minimizes the sensitivity of the channels to creep or relaxation. This also minimizes the onset of surface-roughness changes that occur on the hot-gas-wall surface and increases the hot gas heat transfer rates. This condition further bootstraps local thermal conditions from a minor hot-spot to a significant local hot-spot that produces accelerated cyclic creep cracking

3. Reduce the cyclic strain range and increase the low-cycle fatigue life of the part

4. Maximize the available elongation or strain capability of the material by using designs with preferrential biaxial ratios, i.e., close to uniaxial stress states

Figure 67 summarizes the four designs selected. The first design--contoured configuration--has essentially the same temperatures as the baseline configuration, but the thickness has been varied as a mirror image of the thickness changes that occur with cyclic creep. The thickness at the corner has been reduced by 0.038 mm (0.0015 inch) and thickened in the center by 0.025 mm (0.001 inch), making a total thickness change of approximately 10% of the nominal 0.71 mm (0.028 inch). The second design--increased number of channels--has reduced wall thickness and more channels. This design is similar to one of the proposed SSME uprated designs, and reduces the surface temperatures by over 83 K (150 F). The third design--the keel rib--essentially adds a fin in the center of the channel to pull more heat from the hot wall.

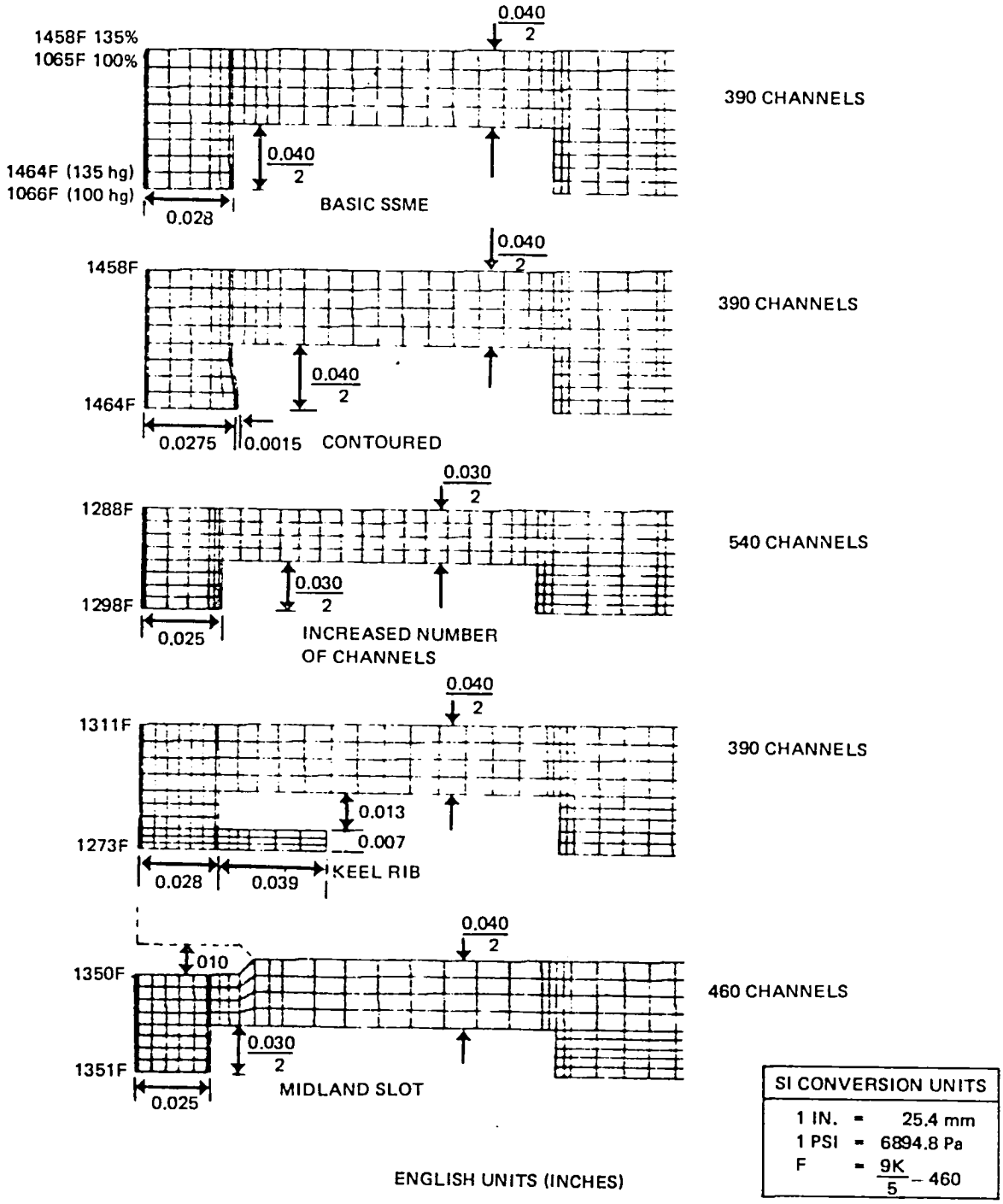

Figure 67. Analyzed Channel Configuration

The channel height has also been increased to maintain the baseline crosssectional area. Structurally, this does not change the load path in the chan- nel wall markedly, since the rib is too narrow to allow the load to diffuse into the total thickness; but it does change the biaxiality strain picture and affect the rate of thinning. The lower temperatures for a keel rib design will also minimize the thermal strain state, but the channel still carries the same differential pressure-primary load. The fourth design concept--slotted mid-land--essentially interrupts the hoop continuity of the structure, thereby reducing the biaxial strains. The added notch is of concern, but its base is located in a cooler portion of the structure, which should reduce some of the local strain concentration. At this time, it is believed that a slot any thinner than 0.25 mm (0.010 inch) could not be fabricated on a repetitive basis with sufficient reliability. The channel width and hot-wall thickness of 0.75 mm (0.030 inch) and 0.63 mm (0.025 inch), respectively, provide opti- mum heat transfer capability, and with a 1.02 mm (0.040 inch) land width, the slotted ligament thickness of 0.38 mm (0.015 inch) provides a thermally effi- cient channel/land ratio. The mid-land slot interrupts the hoop continuity of the hot wall, which will greatly reduce the thermally induced cyclic strain range in that direction. For flexibility, a slot depth of 1.02 mm (0.040 inch) was chosen. This creates a 0.38 x 0.38 mm (0.015 x 0.015 inch) ligament on each side of the channel to absorb the hot wall thermal displacements. During steady-state operation, the hot wall will expand and reduce the slot width by 0.025 mm (0.001 inch).

In order to prevent high temperatures in the slot region, it was assumed that the slot was filled with a material such as felt metal or sintered screen mesh, which was attached by brazing at the bottom of the slot. A maximum operating slot/filler gap of 0.051 mm (0.002 inch) was assumed for the thermal analysis.

The life enhancement designs should be viewed as a first-order approximation, since they have been optimized from only a thermal or structural standpoint. An actual design study would include further modifications and iterations to better optimize the life of the total design.

Structural Analysis

These concepts were evaluated using the analysis techniques that were developed for the baseline analysis. The 135% hg case (hot-spot) was used for the evaluation, since it more accurately reflects the temperature conditions when channel cracking normally occurs. Three of the four concepts required additional thermal analysis to optimize the geometry and furnished detail temperatures for the time slices of interest. The contoured channel design used the same temperatures as the baseline 135% hg condition. The jacket displacements and other boundary conditions were the same for all design analyses. Figure 65 showed CRT pictures of the five designs studied, including the maximum surface temperatures during steady state from the heat transfer analysis. From a simplistic maximum temperature and resulting thermal strain condition, the keel rib, increased number of channels and slotted mid-land configurations have essentially the same hot-gas-wall temperature 987 to 1003 K (1315 to 1345 F). The SSME baseline design and the contoured channel design are approximately 89 K (160 F) hotter at 1083 K (1489 F).

The analysis procedure consisted of running the first 5 duty cycles plus a 15 cycle extrapolation, resulting in detail plots for each design. These results were carefully reviewed to ensure modeling accuracy and general observations about which would be the best design. The rest of the analysis was then completed. The primary methods of correlation of the designs were through cyclic creep life evaluation, LCF evaluation, maximum surface temperature, and a gross estimation of fabrication difficulty. Figure 68 furnishes a comparison of mid-channel wall thinning vs duty cycle for the various design concepts for the first 5 duty cycles, plus 15 cycle extrapolation. The life-enhancement designs were then extended to 120 duty cycles and beyond, by estimation, based on being bracketed by actual analysis data for the basic design 135% and 100% hg cases out to 120 and 100 duty cycles, respectively. These results are depicted in Fig. 69. The set of information available after the completion of the first five duty-cycle results for each life-enhancement design was utilized as a test to determine how well the final results of the study could be extrapolated from this limited data. If good accuracy was obtainable, future sensitivity studies could potentially be made with only this information. The 540-channel configuration and the contoured channel should give the best extrapolations, since they are only varients of the standard channel design. The keel rib and slotted configuration are more geometrically different, although the keel rib itself does not grossly affect the primary load path. Figure 69 shows the 120 duty cycle extrapolated results, and orders the configurations from the highest thinning to the lowest thinning as baseline 135% hg, slotted, keel rib, contour wall, 540 channels, and 100 percent hg baseline. The actual order of the life enhanced designs, as will be shown later, is only correct for the 540-slot design, the most similar design to the baseline configuration. Figure 68 shows another variable that was not completely assessed in this study. This is reflected by the rate of change of thinning which has not completely stabilized after 5 duty cycles for some of the configurations. The baseline 135% hg and the 540 channel design have the same rate of mid-channel deformation for between cycle 4 and 5, and therefore the extrapolation to 20. The other three design results are somewhat ratty, and would have required more duty cycles to completely stabilize. For this effort, this variation was judged relatively unimportant to the overall objectives of the study within the available time and cost restraints. Figure 70 plots the peak strain at four critical locations in the models. The maximum strains across each configuration vary roughly as a function of maximum temperature, except for the slotted design, which does radically drop the strains due to the interruption of the hoop continuity.

Two other plots were made to verify that the maximum rate of thinning was being used for the two designs that had variable-channel wall thicknesses (contoured and keel rib). Figure 71 is a plot of the thinning along the contoured design channel wall, in a circumferential direction (Nodes 1 through 9). As expected, the thinning rate is still the maximum at the center of the channel. Figure 72 is a similar plot for the keel rib design, and shows that the maximum thinning over a length that includes the keel rib and the channel-wall intersection with the rib. These results were also checked at the 100 to 120 duty-cycle point and substantiated the methodology of using the same thinning concept for ranking the configurations.

CYCLE DIFFERENTIAL	DEFORMATION RATE/CYCLE in. X 10^{-4} µm											
Configuration % hg	Basic 100		Basic 135		Contoured 135		540 Channels 135		Slotted 135		Keel Rib 135	
	in.	µm	in.	µm	in.	µm	in.	µm	in.	µm	in.	µm
2-1	.219	.556	.270	.686	.223	.566	.256	.650	.228	.579	.321	.815
3-2	.074	.188	.140	.356	.103	.261	.099	.251	.163	.414	.164	.416
4-3	.030	.076	.110	.279	.074	.188	.055	.140	.100	.254	.118	.300
5-4	.017	.043	.110	.279	.060	.152	.055	.140	.084	.213	.098	.249
20-5	.023	.058	.110	.279	.067	.170	.052	.132	.101	.257	.109	.277

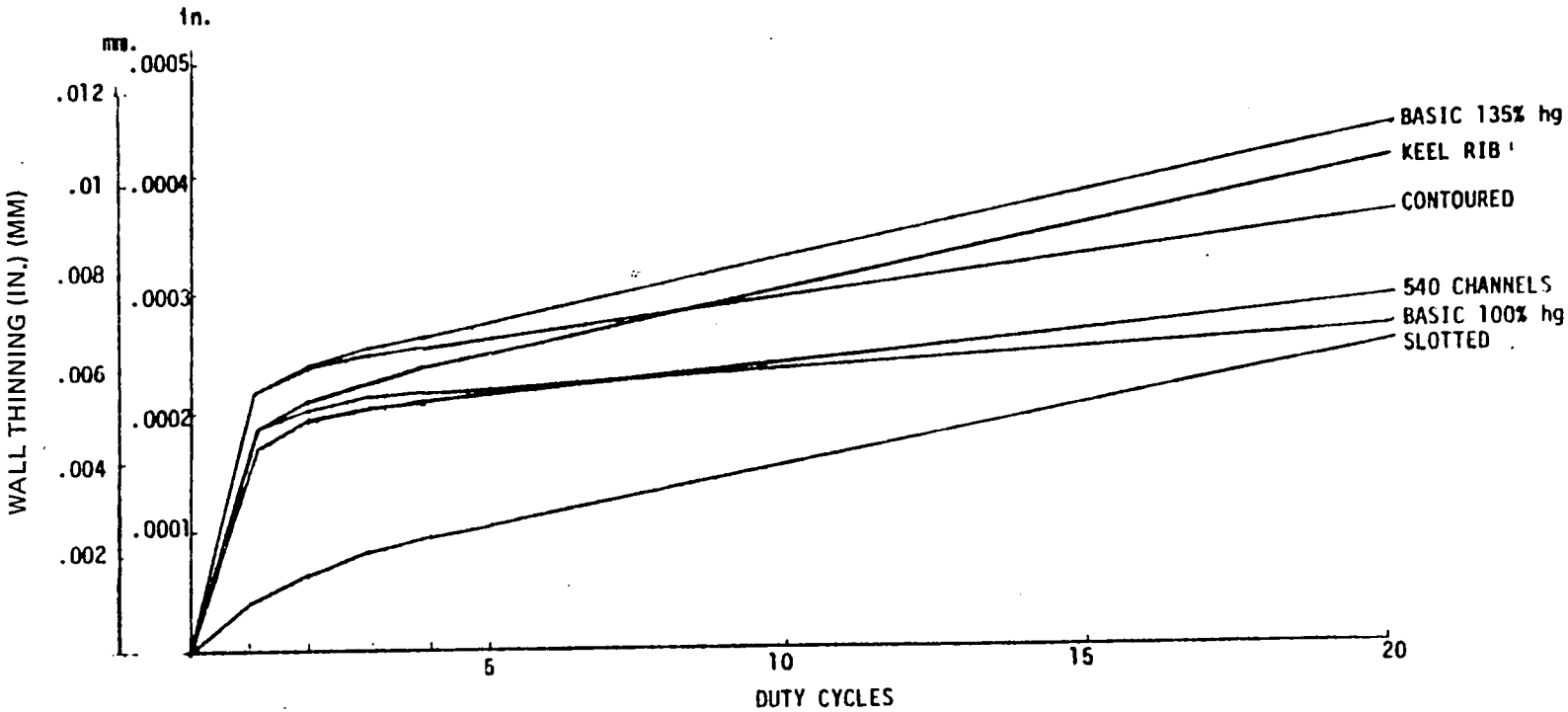

Figure 68. SSME MCC Life Enhancement Sensitivity Study, 5 Duty Cycle Comparison

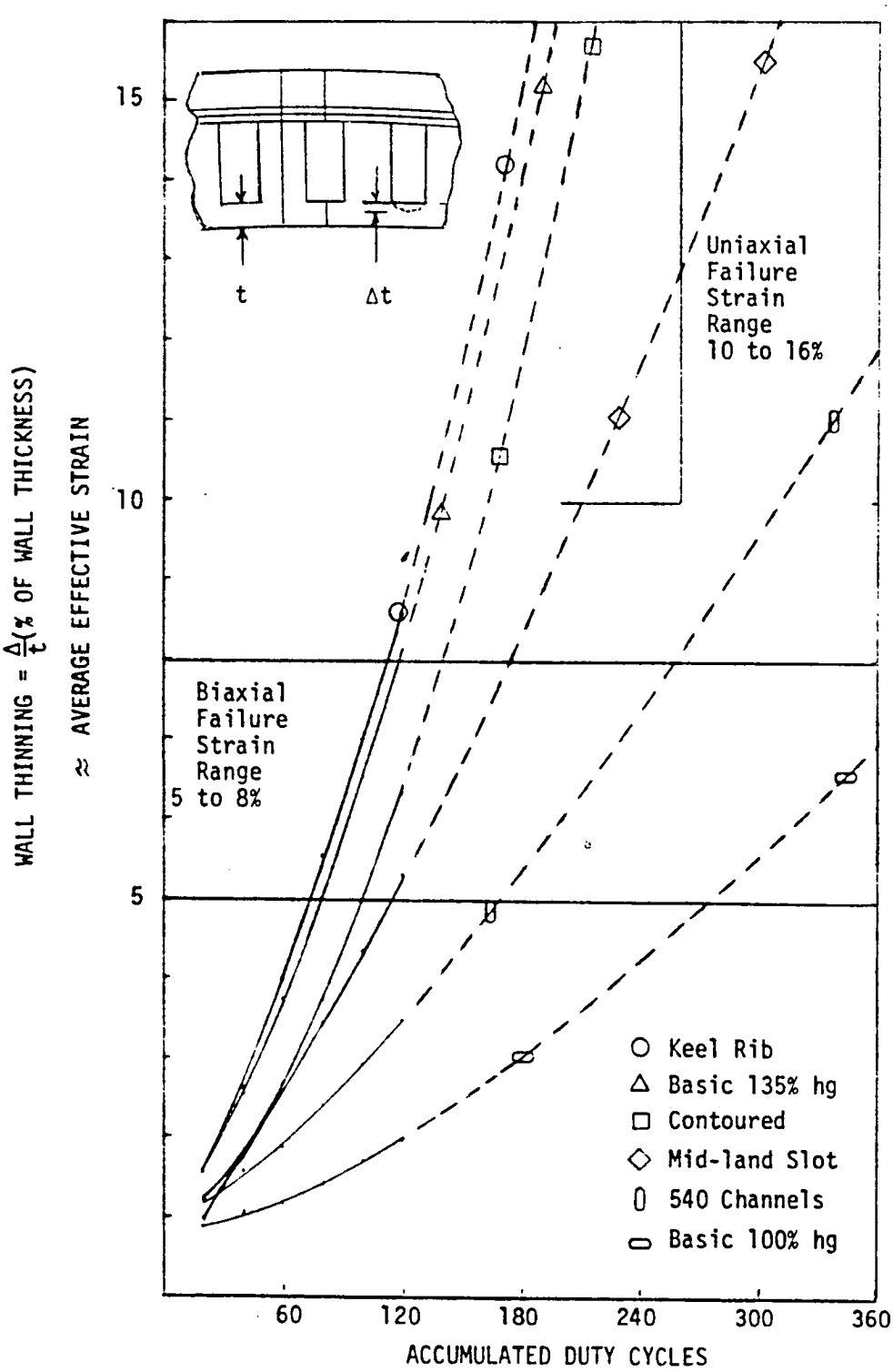

Figure 69. Life Enhancement Sensitivity Study, 120 Duty Cycle Plus Extension Comparison

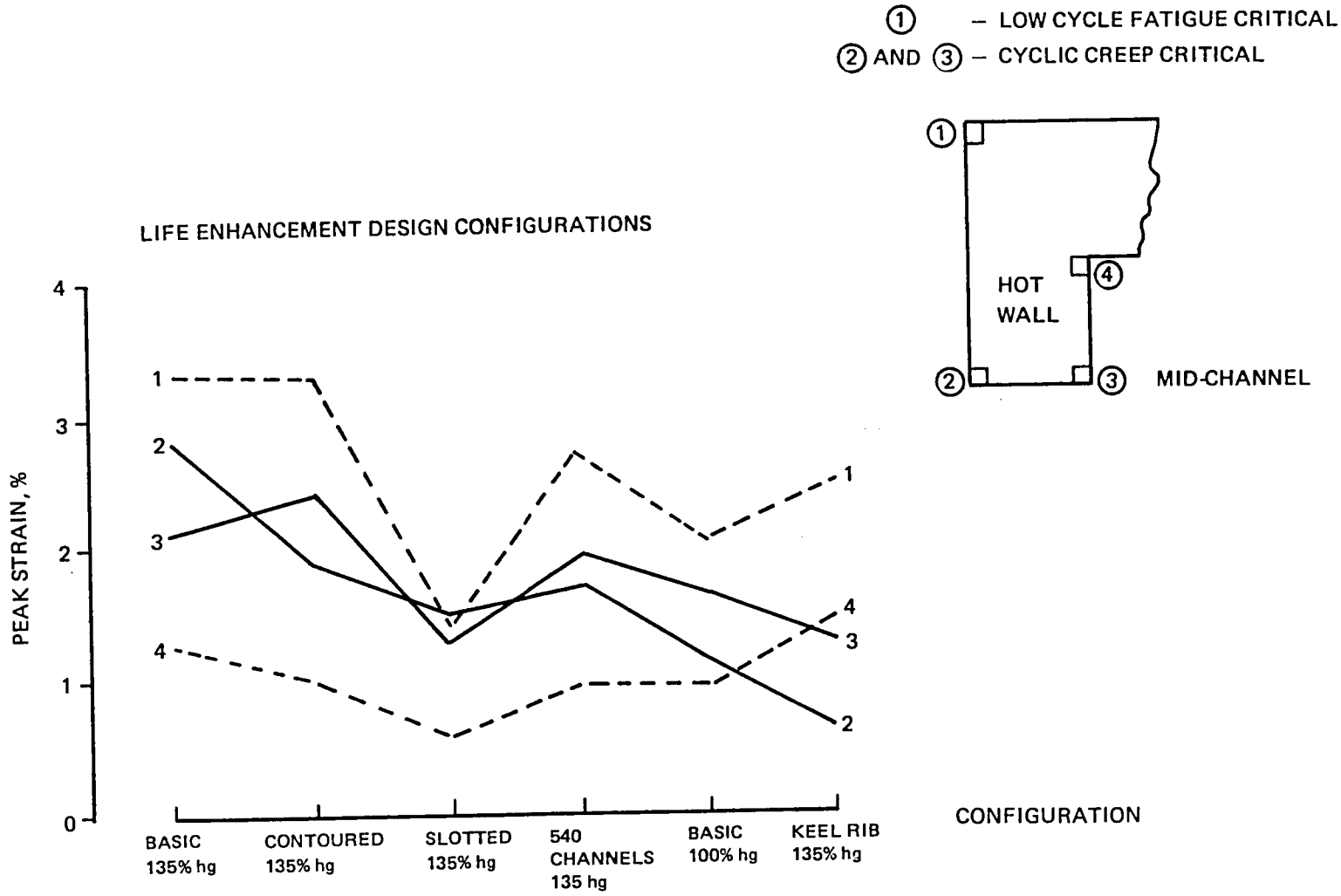

Figure 70. SSME MCC Life Prediction Sensitivity Study Peak Strain vs Life Enhancement Configuration

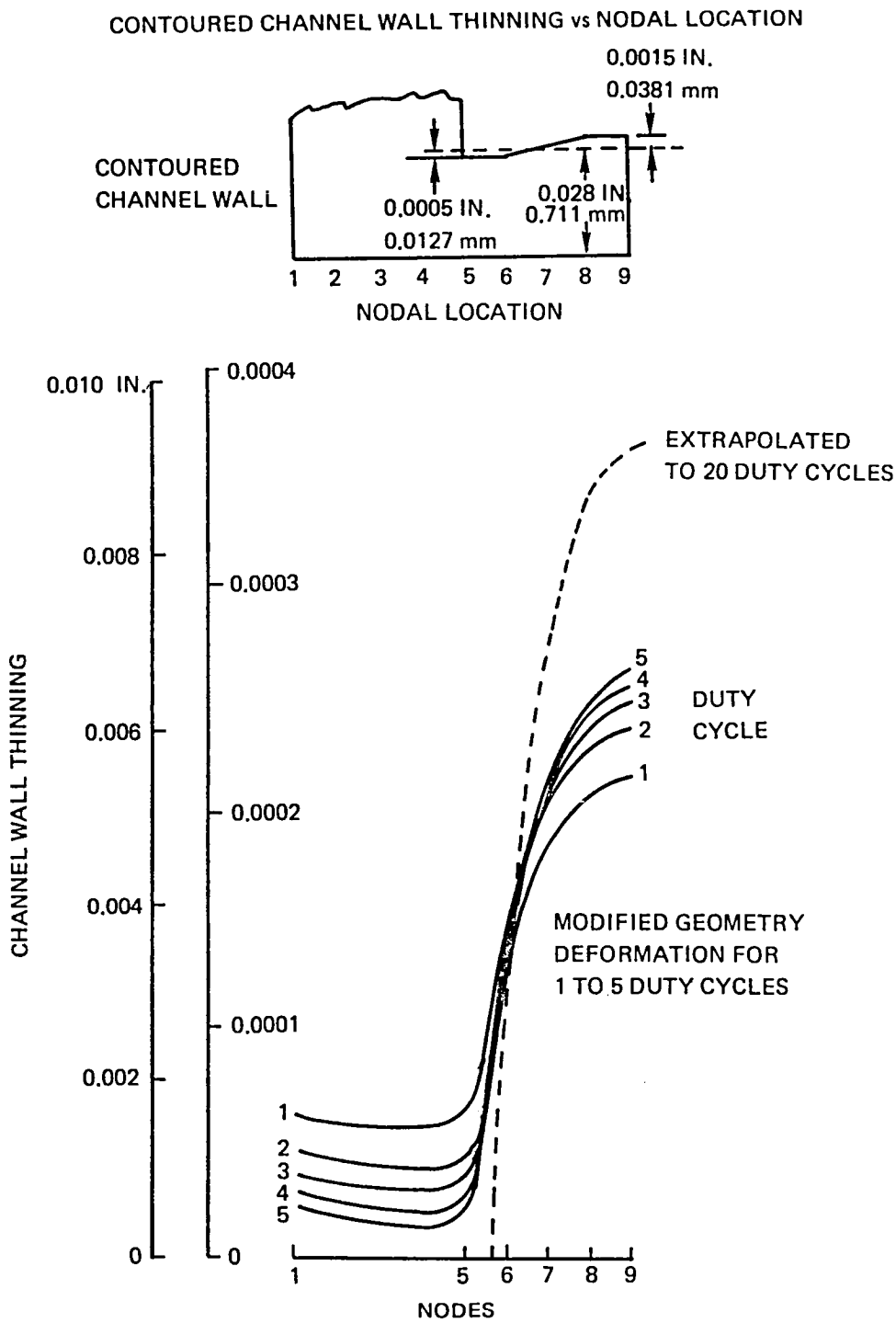

Figure 71. Contoured Wall Thinning vs Nodal Location

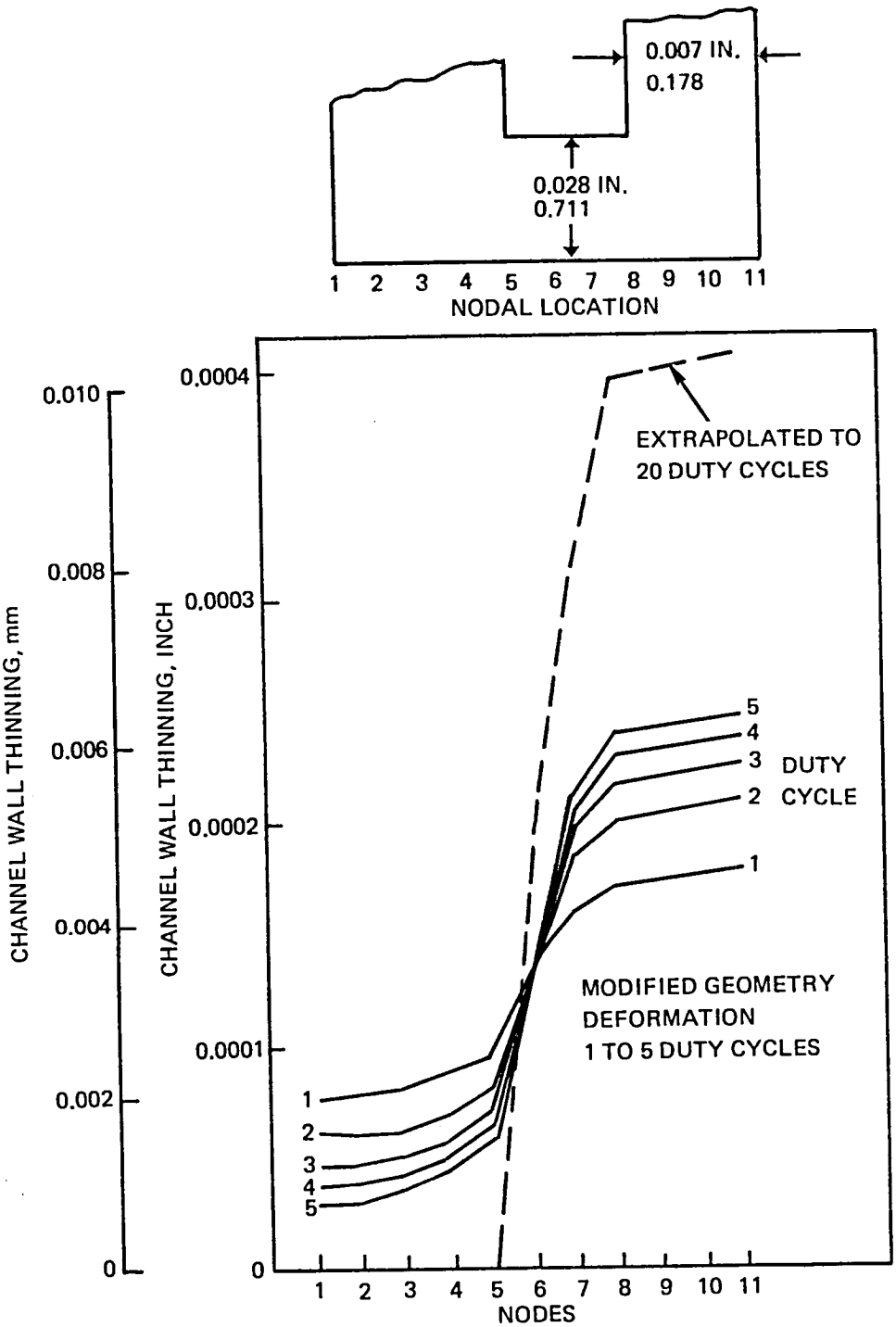

Figure 72. Keel Rib Thinning vs Nodal Location

The finite-element wall thinning analysis results of the five configurations through 120 duty cycles is presented in Fig. 73. The results are also extrapolated beyond the 120-cycle point with dashed lines. The 5 duty cycle analysis thinning rates (Fig. 73) are significantly different than the 120-cycle rates for all configurations. The ranking of the designs, by analysis, as a func- tion of thinning from maximum thinning to minimum thinning is the keel rib, baseline 135% hg, contoured, 540 channels, and the baseline 100% hg. Table 5 summarizes this information, plus other notable variables to allow assessment of all the configurations. The analyses were all made at a 135% hg, except for the baseline 100% hg. In all cases, the cyclic creep life is less than the typical LCF-life calculation. The keel-rib design and the baseline 135% hg are very close to each other from a cyclic creep standpoint, although the lower keel-rib temperatures would be less sensitive to hot-spots and surface roughing. The high thinning rates of the keel rib design are attributed to subtle changes in strain biaxiality, caused by the addition of the keel rib.

The 80 to 115 duty-cycle life of the baseline 135% hg case is still considerably different than the actual cracking of 5 to 30 cycles. As previously mentioned, the best estimation of the reason for this discrepancy is the potential error in simulation of local strains in a hot-spot. Appendix discusses this in detail. The channel contouring seems to have a more significant effect for the first few duty cycles up to 60 or 80, but then has similar thinning rates to the baseline analysis. The 540-slot design is by far the best design of the more standard configurations. The slotted design has a high thinning rate, but because its biaxial restraint is closer to a uniaxial case, the allowable thinning for this configuration is assessed as twice the other configurations (10 to 16%). This configuration also has a significantly lower strain range. On the negative side, the slot-filler material and the heat transfer analysis accuracy for this model are in question. The filler material was added to eliminate unknowns associated with heat transfer characteristics within the slots.

Copper and AMZIRC normally have more radial motion and thinning than is obtained with NARloy-Z. In some cases, such as the 40K chamber, NARloy-Z has shown large amounts of radial deformation and wall thinning prior to failure.

As shown in Fig. 74 the amount of mid-channel radial deformation and mid-channel wall thinning is quite variable. The four basic channel wall cases--100% hg SSME, 135% hg SSME, increased number of channels, and contoured channel wall--show similar and consistent solutions. The higher surface temperature cases radially deform faster per cycle and the basic spread of data is reasonable. The slotted results furnish the most linear curve. The keel rib configuration has very small radial deformation, but one of the highest rates of thinning.

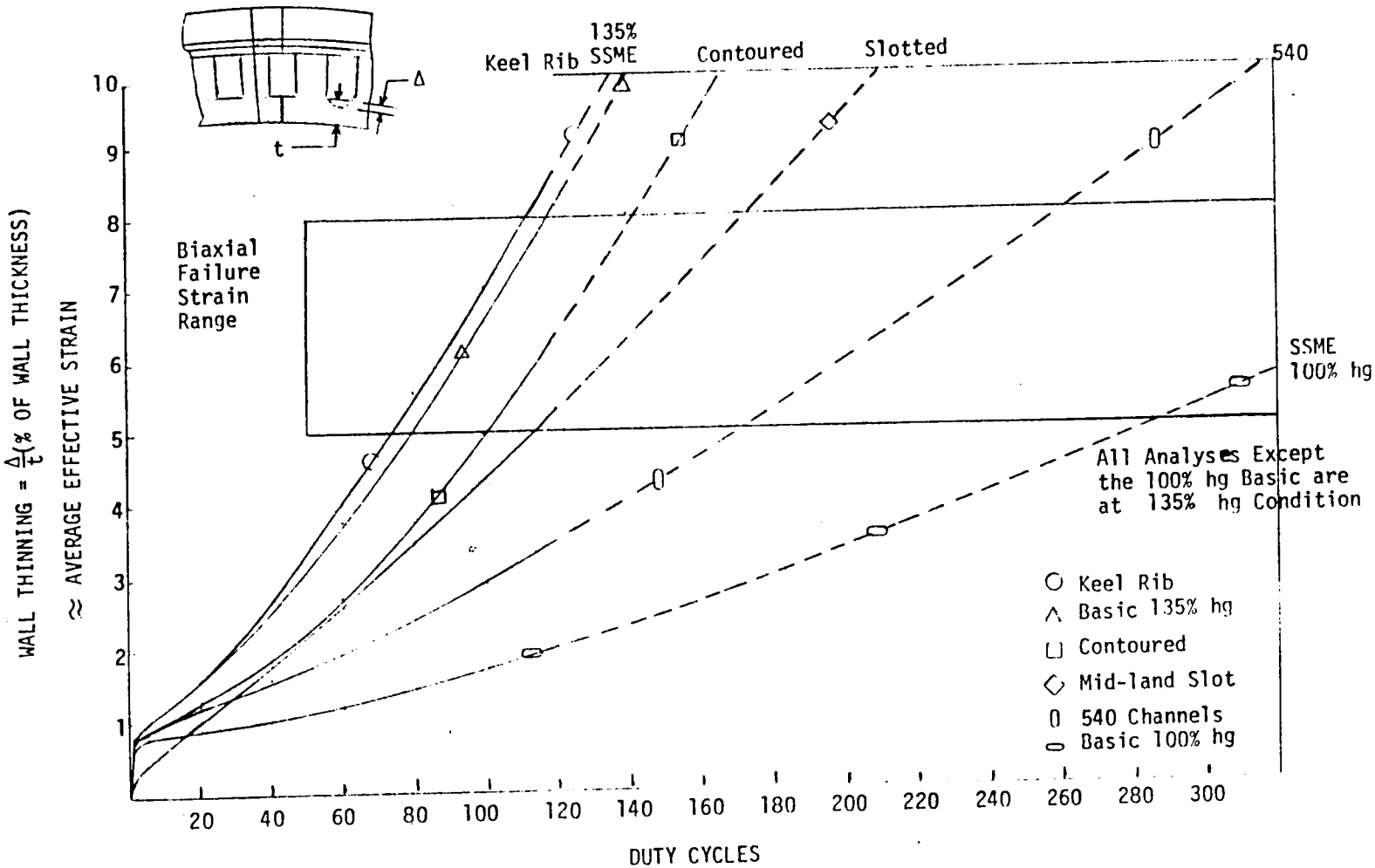

Figure 73. Mid-Channel Wall Permanent Deformation (Thinning) vs Number of Duty Cycles

TABLE 5. SSME MCC LIFE PREDICTION CONCEPT COMPARISON

	% Hg	LCF LIFE, DUTY CYCLES (TYPICAL)	CYCLIC CREEP LIFE, DUTY CYCLES	MAXIMUM TEMPERATURE, F	MAXIMUM TEMPERATURE, K	FABRICATION DIFFICULTY	COMMENT
SSME	100	660	290 TO 445	1087	859	--	BASELINE ANALYSIS
SSME	135	300	80 TO 115(1)	1484	1080	--	MAXIMUM HOT-SPOT CONDITION
1. CONTOURED	135	300	100 TO 140	1484	1080	LOW	
2. 540 CHANNELS	135	400	170 TO 260	1313	985	MODERATE	SIMILAR TO SSME UPRATED
3. KEEL RIB	135	400	75 TO 110	1337	998	MODERATE	SIMILAR TO PROPOSED OTHER HARDWARE
4. SLOTTED	135	550	210 TO 320(2)	1346	1003	HIGH	NEW

(1) ACTUAL CRACKING 10 TO 30 CYCLES

(2) TWICE THE ALLOWABLE STRAIN LIMIT USED FOR LOW BIAXIAL RESTRAINT CONDITION

GOALS FOR LIFE ENHANCEMENT

- REDUCE DEFORMATION RATE (THINNING)
- REDUCE TEMPERATURE
- REDUCT CYCLIC STRAIN RANGE
- MAXIMIZE AVAILABLE ELONGATION BY PREFERENTIAL BIAXIALITY RATIO

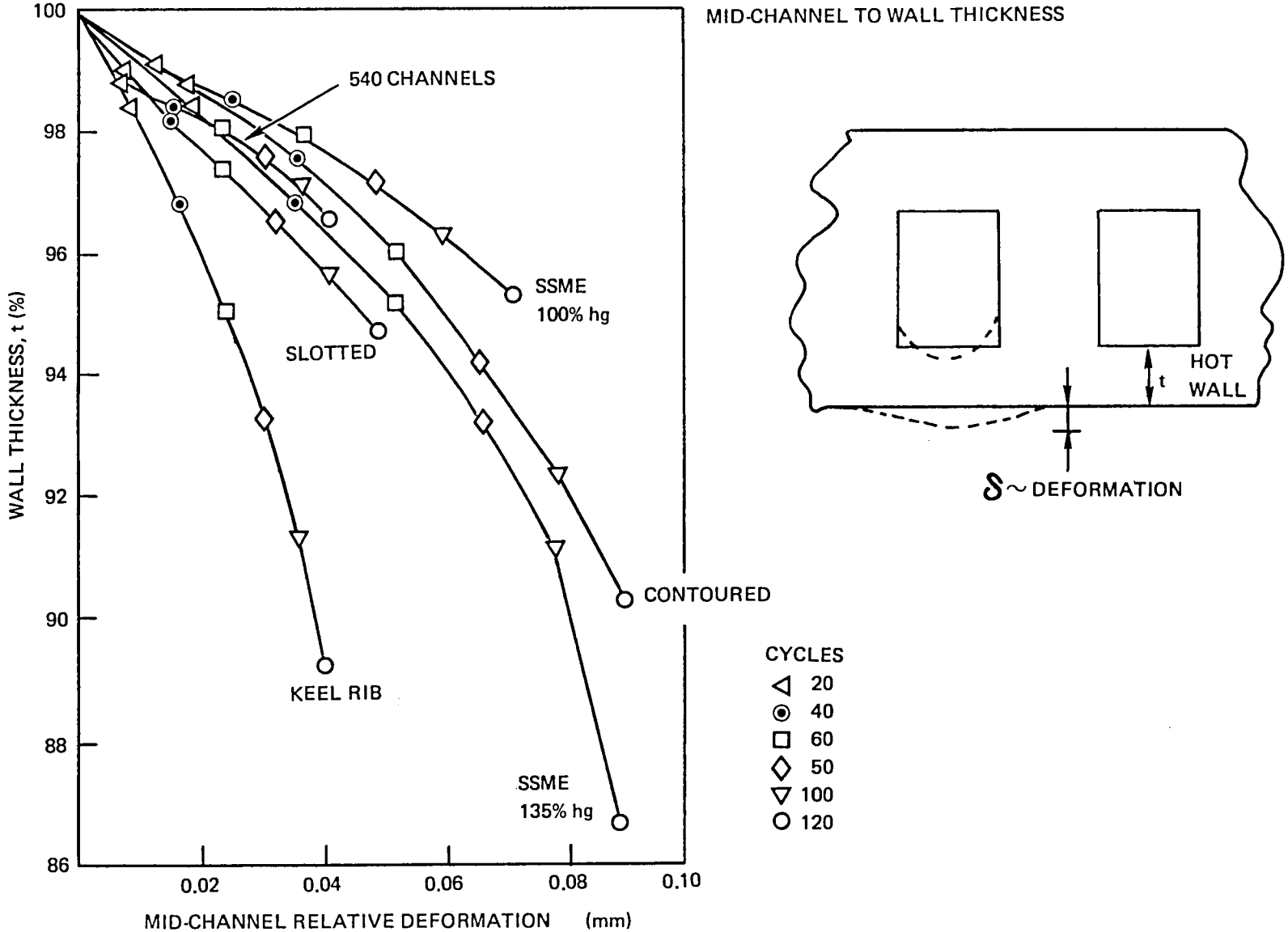

Figure 74. Relative Hot-Wall Deformation vs Duty Cycle Mid-Channel to Wall Thickness

It is interesting to note the highly nonlinear shape of the curve with cycling. During the initial sensitivity study previously discussed, the distorted results from the first 5 duty-cycle analysis was extrapolated to a 10% thinning condition. This required an accumulated duty cycle of approximately 400 cycles, and a radial distortion of 3.81 mm (0.15 inch). As previously mentioned, trying to use estimated geometries, etc., led to conditions both in cyclic life and geometric distortions that were grossly inconsistent with test hardware history and/or detailed duty-cycle analysis.

This type of plot is of interest for two other reasons. NASA has previously used these plot parameters for evaluation of measurements from test hardware (Ref. 2), and a closed-form solution technique for channel wall analysis (Ref. 12) uses radial deformation to relate to thinning. A markedly nonlinear relationship is not projected by the closed-form methodology, since the total analysis is based on a 1/2 duty-cycle consideration with no shakedown effects.

TECHNOLOGY IDENTIFICATION

Recommended technology items to be considered for follow-on work are summarized below. These suggested areas requiring experimental investigation are based on the results of this analytical study.

PROPOSED FOLLOW-ON EFFORTS

1. MCC Analysis Improvements (Strain History and Extrapolation Methodology)

2. Materials Laboratory Testing

3. Hot Spot Analysis Development

4. Midland Hot Wall Slot Manufacturing Verification

5. Hot-Fire Test Program

MCC ANALYSIS IMPROVEMENTS

The current SSME MCC life prediction study has demonstrated that cyclic creep and the use of a biaxial strain failure mode can be used to predict channel cracking using currently available analytical tools, i.e., FE (finite element) codes such as APSAC, extrapolation procedures, and appropriate failure criteria. This effort is a worthwhile step toward accurate MCC life prediction, but there are several areas where the life analysis procedure and methodology can be improved. Specific items include the following:

1. Improved extrapolation methodology

2. More acurate representation of material properties in FE codes

3. Better postprocessing to mechanize tracking of thinning, strain, and stress history, etc.

4. Investigation of the cold-wall fracture mode that can occur after hot-wall cracking

5. Improved hand analysis methodology

The current SSME MCC cyclic-creep analysis is an implementation of methodology developed in other LeRC supported work. The procedure includes a 5-duty-cycle FE analysis followed by an extrapolation of the geometry to the shape projected at 15 additional duty cycles. The new shape is then used as a basis for additional analysis using the 5 + 15 additional duty cycles concept. The procedure is continued until failure occurs based on low-cycle fatigue or biaxial strain limits.

The resultant thinning for the basic SSME configuration is shown in Fig. 75. The basic technique loses the strain history in the extrapolation procedure, since only the geometry shape is projected. This causes the rounded stepped shape at the first 1 of 2 cycles of the detailed duty-cycle analysis. The material gradually increases in maximum strain from geometric changes and biased loading during the duty cycle. This shakedown effect can be removed from the results by subtracting out the bias, but more accurate methods are recommended.

An improved extrapolation methodology would add the strain history as part of the procedure. This can be accomplished in at least two ways. One is to extrapolate the strains as well as the geometry. The other is to use the modified geometry as a rigid distorted shape relative to the original geometry and calculate the resulting strains. This loading would be a prestart condition for a succeeding 5-duty-cycle analysis. Either methodology requires careful attention to the mechanized procedure in the FE code for accounting for the distorted shape throughout the total part history. This latter procedure will be tested in the next month on Rocketdyne funds to partially prove-out the technique.

The analysis methodology also can be improved by using cyclic stress-strain curves and more accurate creep relaxation information (discussed in a separate section) as well as a more accurate representation of the stress-strain curve. Currently, only a bilinear representation is utilized for the stress-strain curves. To demonstrate a necking or true tensile instability phenomena, the stress-strain curve representation must have a maximum point. Therefore, addition of a multilinear representation is required to the APSAC code. Addition of cyclic strain hardening would be desirable, but is not a critical item because the cyclic strain hardening for NARloy-Z is relatively small ($\leq$20%), and its effect will be partially considered by using cyclic stress-strain curves.

Another area for improving the evaluation and understanding of the computerized analysis would be some additions to the postprocessing plot and output code. Additional features are recommended to summarize data across the 5 duty cycles of information. Currently, all processing is done on a single increment and the code has no features for collecting data for multiple increments.

Plotting the element strain cycling loop, summarizing nodal displacements, thinning and element strain information are additional needs to minimize hand plotting and allow a more thorough understanding of results.

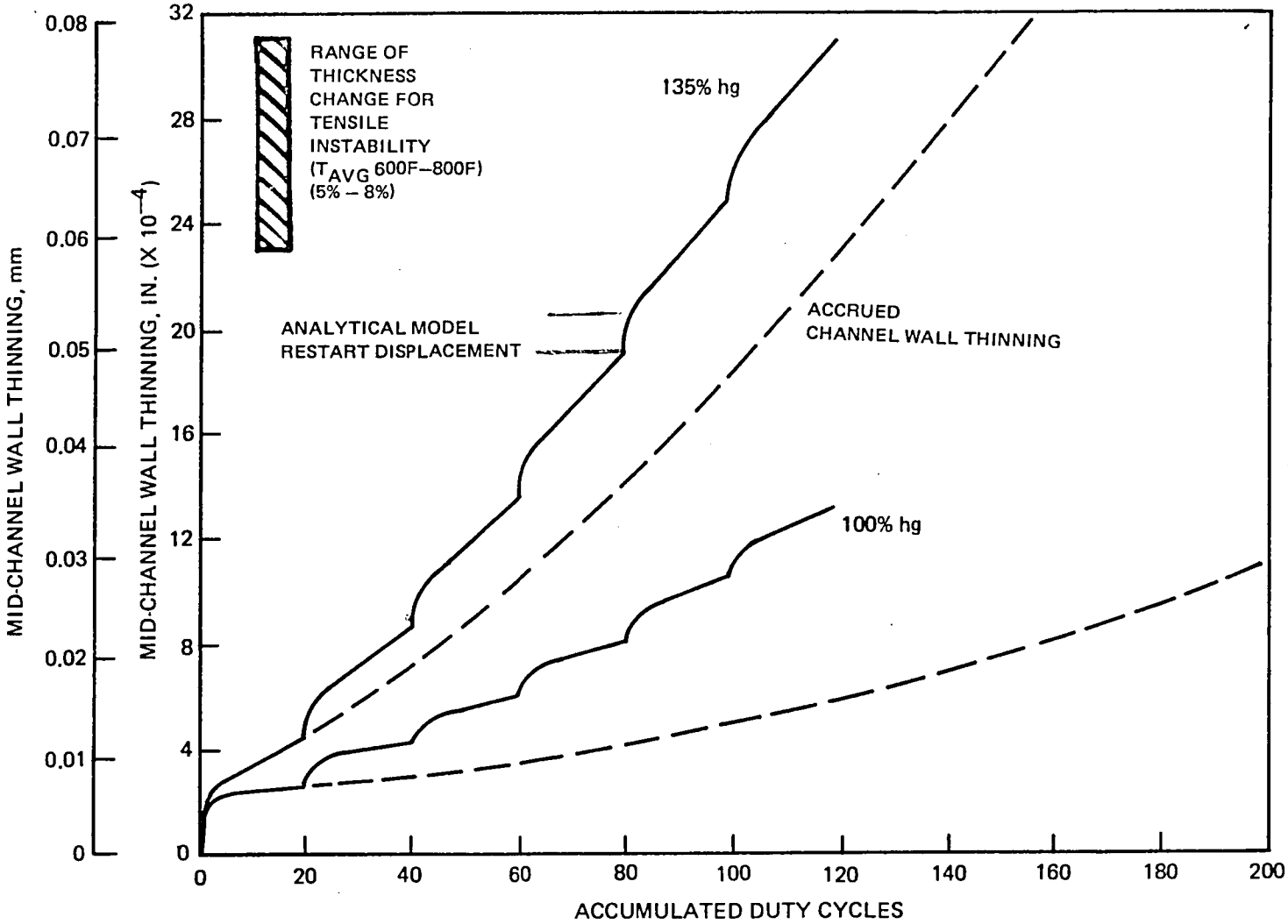

Figure 75. Coolant Channel Cyclic Creep (Wall Thinning) for SSME MCC at 100% FPL hg and 135% hg

Another area where improvements are needed is the incorporation of cyclic creep into the hand analysis methodology. Rocketdyne has hand solution methods considering hot-wall temperature gradients, pressure, etc., for determining factor of safety and LCF life. The cyclic creep methodology (Ref. 12) NASA CR-165585, "The Development of a Simplified Procedure for Thrust Chamber Life Prediction," can be upgraded to consider such items as hot-wall temperature gradients, associated strains, and material property variations. This methodology could then be included as part of the hand solution for MCC channel wall life and factor of safety. It can be used for initial sizing and sensitivity studies.

MATERIALS LABORATORY TESTS TO IMPROVE THE ANALYSIS EFFORT

Information on the cyclic stress-strain response, ductility, and creep/relaxation of NARloy-Z needs to be developed to verify and calibrate the life analysis of the SSME MCC channel wall liner for the cyclic creep failure mode. The cyclic response of the material would be investigated through the determination of cyclic stress-strain curves. Large mean strain effects should be considered to relate to the hardware strains. Availability of ductility would be investigated through the testing of multiaxial specimens to obtain elongation at onset of tensile instability. Creep relaxation data would be obtained from conventional test specimens. Information is required over a temperature range of -400 to 1500 F. Some background on the development of the desired information follows.

Cyclic stress-strain curves would be obtained over a wide temperature range to a maximum cyclic strain range dictated by analysis. Consideration would be given to the strain rate corresponding to hardware operation. The program testing would be limited to isothermal uniaxially loaded, deflection controlled tests. The curves would be run to get information on the material strain hardening exponent used in instability analysis for determining biaxial strain limits and to provide elastic/inelastic stress/strain data for the finite-element analysis of the main combustion chamber channel wall.

Ductility defined by elongation would be measured under isothermal conditions using multiaxial monotonically loaded specimens. A review of the literature indicates biaxial loading through the use of cylindrical pressure vessels or cross specimens is feasible (Ref. 13). The influence of cycling and nonisothermal conditions is recognized, but investigation would not be part of this program. The available elongation obtained from test would be used to evaluate elongation at onset of tensile instability.

Creep/relaxation data would be used to support life analysis of combustion chamber channel wall hot spots. At the present time, no information exists on NARloy-Z creep behavior in the temperature regime to 1089 K (1500 F). Data on creep rupture ductility, creep deformation, and relaxation would be obtained from tests of uniaxially loaded specimens. A theoretical adjustment to the data would have to be made to account for material strain cycling and multiaxiality.

DEVELOPMENT OF HOT SPOT ANALYSIS TECHNIQUE

The 135% hg thermal load case being used to evaluate and compare the various MCC life enhancement design concepts represents an operating environment that generates a 1089 K (1500 F) hot-gas wall temperature 167 K (300 F) above nominal operating conditions). This condition typically occurs due to injector anomalies, and on the actual MCC hardware shows up as local hot spots that generally have a 2:1 to 4:1 elliptical pattern.

The current analysis technique used for the finite element channel/land/closeout model treats the overtemperature condition as occurring axisymmetrically around the entire ID circumference. This generates more total circumferential growth of the hot wall that is restrained by the structural jacket and the EDNi closeout; however, the generated strain is shared uniformly by all the channels around the circumference. In reality, the local hot-spot area channels are much weaker than the remaining normally heated hot-wall channels around the circumference. Although there is less total circumferential growth to be restrained, the hot spot is a weaker material that acts like a hole in the total liner with a #/£ concentration factor causing local distortions that force more strain into the local weak zone.

A preliminary APSAC analysis of a plate with a 4:1 elliptical hot spot (135% hg hot-wall temperature) showed peak strains and strain ranges that were a factor of 2 to 4 times higher than the remainder of the plate (100% hg hotwall temperature).

The axisymmetric modeling technique only shows an increase in peak cyclic strains of 15 to 20% when comparing the 100% hg and 135% hg thermal load cases. Therefore, the local hot spot appears to provide a mechanism that could generate significantly higher strain and midchannel deformation rates that would cause the cyclic creep failure mode to occur in a number of cycles that would more closely match the hardware failures observed to date.

The optimum hot-spot analysis technique would utilize a three-dimensional program with inelastic, creep, and incremental load case capabilities. The cost and difficulty involved in completing this type of analysis would not be practical as a standard analytical tool, and this follow-on effort would be directed toward the development of a simplified analysis approach that would simulate the increased localized hot-spot effects.

The current 2-D model of the channel cross section would be supplemented by a second 2-D plate model that would generate the membrane hot-spot effects. Simplistically, this could be an APSAC plate model of just the hot-gas wall, or could be a more involved ANSYS plate model incorporating multiple layers that would simulate the hot wall, lands, and cold wall. The plate model hot-spot effects would be imposed on the channel cross-section model in the form of displacement boundary conditions or as pseudo material properties such as #, E, etc., and then the model would be subjected to the typical 5-cycle PSAC multi-increment duty cycle analysis plus the 15-cycle extrapolation to

establish the cyclic strain range and channel deformation rate (tensile instability mode). To verify the technical adequacy of the simplified approach, it is recommended that a one-time 3-D model be generated. The 3-D model would be used to compare with the 2-D model(s) results to ensure that the hot-spot effects have been properly simulated. Once good correlation is achieved between the 2-D and 3-D models, the simplified approach could be used as a standard analytical tool for determining life of combustor hot-wall channels that are subjected to local hot-spot injector anomalies.

HOT-FIRE TEST PROGRAM

A hot-fire test program is proposed using 20 K size test hardware to substantiate life prediction techniques and evaluate life-enhancement channel redesigns. The proposed program consists of five technical tasks:

Task I - Establish measuring techniques to define channel geometry history (deformation/thinning) of test hardware.

Task II - Design and fabrication of test hardware. A minimum of two life-enhanced channel concepts will be utilized and compared to the baseline SSME MCC design.

Task III - Hot-fire testing, including facility build and/or modification and installation of test hardware.

Task IV - Data correlation and empirical cyclic life relationships established.

Task V - Analytical life cycle model upgrading culminating in a versatile computer code (to NASA).

A new combustion chamber with axisymmetric coolant passages would be designed and fabricated for the hot-fire testing. The combustion chamber would be designed with different coolant passages in three or more sectors of the chamber. Each sector would be independently manifolded and instrumented to measure the total section heat load. Thermocouples would be installed, at selected locations at the throat plane to measure the hot gas side surface temperature and the temperature at the midpoint of the lands. The test matrix would include varied operating points and injector configurations to allow investigation of the effects of local mixture ratio zones on the wall, chamber pressure, established during Task I, coolant flowrates, and coolant fluids. Posttest hardware inspections would be performed to allow correlation of channel life as a function of the accumulated exposure of thermal and structural loading conditions. The proposed program effort would colminate in the development of a versatile computer-code capable for cyclic life prediction of any convectively cooled channel-configured heat exchanger.

LIFE ENHANCEMENT MIDLAND HOT-WALL SLOTS (LIFE ENHANCEMENT CONCEPT NO. 4) MANUFACTURING VERIFICATION

A manufacturing feasibility demonstration is proposed to support life enhancement Concept No. 4 (Fig. 75). This concept relaxes the biaxial strain in the tangential direction, thereby increasing the MCC cyclic life. This life enhancement concept creates a substantial manufacturing challenge. Manufacturing areas of concern are: (1) machining narrow slots of 0.010-inch width, (2) identification of midland locations and numerical indexing, and (3) machining on an internal contoured surface (ID of the MCC). The latter requires a special machine or adaptation to current types of milling machines.

The proposed experimental program consists of four Tasks:

Task I

Verification of slot dimensional control and cutter life. This effort would be conducted on inexpensive flat plate NARloy-Z or AMZIRC (OFHC copper-base alloys) samples.

Task II

Search for cutting machine (or adaptation of existing machines) capable of cutting slots on the MCC contoured internal hot-wall surface (MCC ID). The milling cutter needs to be affixed to an arm with a minimum reach of several feet. It must also be capable of contour tracing and indexing with extreme accuracy.

Task III

Demonstrate machining of midland hot-wall slots on existing SSME design full size hardware (Fig. 76). As a minimum, the axial location of the slots will be from 4 inches upstream of the MCC throat to 1 inch downstream of the geometric throat. Inspection techniques will be established to identify slot dimensions and location relative to midland and adjacent coolant channels. Quality control will be emphasized.

Task IV

Evaluation of thermal barrier slot filler materials. Concepts to be evaluated will be low-density flexible filler materials, such as felt metal construction. Usable surface temperature range will be >2480 K (4000 F) and accommodate a LOX/H_2 combustion gas environment. The purpose of the slot filler is to retard or negate convective heating of the slot side walls. Bonding (brazing) of the selected slot filler materials at the slot-base is to be established during this task effort.

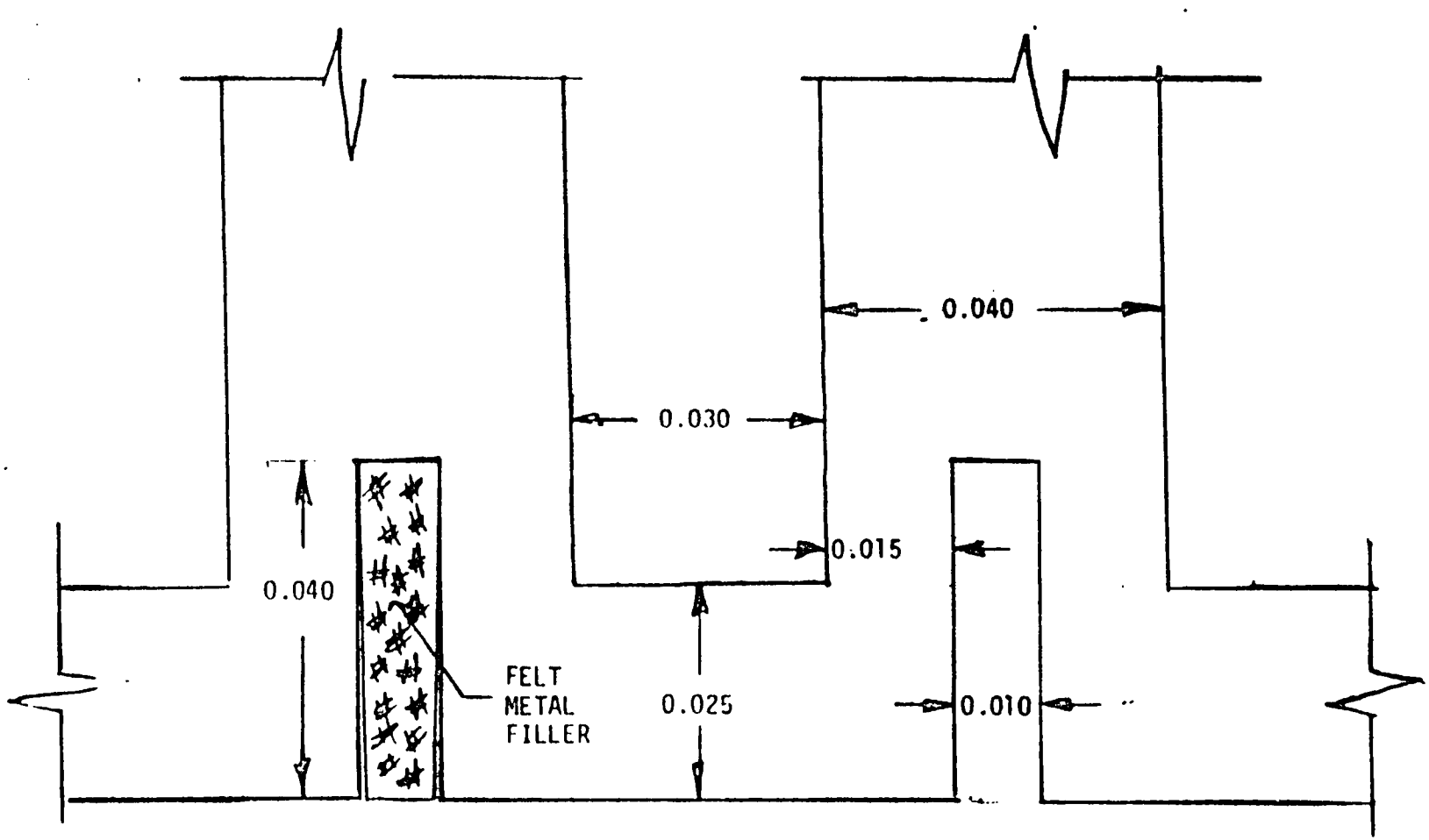

Figure 76. Midland Slotted Geometry

CONCLUSIONS

1. Cyclic-creep in the form of channel wall thinning is the dominating factor in defining the reusable life of channel configured combustion chambers.

2. The predicted cyclic-creep life is typically between 30 and 50% of the predicted low-cycle-fatigue (LCF) life.

3. The analysis methodology used in this study predicts the correct failure mode, including midchannel cyclic-creep deformation patterns.

4. The predicted midchannel wall thinning rate is less than indicated by hot-fire test results. However, a preliminary 3-D hot-spot analysis indicates a potential for generating higher local strain levels and an accelerated thinning rate.

5. The most feasible approach to increasing the SSME-MCC usable life is increasing the number of coolant channels. Increasing the number of channels from 390 to 540 doubles the usable life. Channel dimensions (channel width, land width, and wall thickness) are typical of those used for advanced engine design studies.

6. A maximum usable SSME-MCC life benefit of a factor of three was shown for the maximum risk design which incorporated two life enhancement features. This included increasing the number of channels from 390 to 460/and slotting the midland hot-gas wall to minimize the transverse strain.

APPENDIX A

SSME-MCC EXPERIMENTAL BACKGROUND

Substantial hot-fire testing has been conducted on the SSME and 40K main combustion chamber with similar configurations. As a result of this testing, a considerable number of thermal cycles has been accumulated. This section presents an overview of this test effort related to combustion chamber thermal cyclic life.

SPACE SHUTTLE MAIN ENGINE

The following case histories are presented indicating the hot-gas wall thermal crack histories as a result of Space Shuttle Main Engine testing.

MCC 0008, Engine 0009

Main combustion chamber 0008 accumulated 21 tests and 9000 seconds total operation at the time of its first noted hot-gas wall crack. The crack was located approximately 2.54×10^{-2} m (1 inch) above the throat centerline and was unusual in that it ran perpendicular to the direction of hot-gas flow rather than parallel. Prior to crack initiation, that area of the chamber had endured discoloration and blanching, with a general trend of increasing roughness, throughout the chamber's test history. Roughness readings of the area increased from the 7.62×10^{-1} to 1.016×10^{-6} m (30 to 40 μin.) range to 5.08×10^{-6} to 6.36×10^{-6} m (200 to 250 μin.) in the tests immediately preceding crack initiation. Radiographic examination following the test in which the crack was noted revealed no signs of obvious contamination.

Following two additional 520-second flight profile tests, two more longitudinal cracks were reported in the same general plane as the first, each downstream of other elements. All three cracks were 5.08 x 10-5 to 1.27 x 10-4 m (0.002- to 0.005-inch) wide by 7.62×10^{-4} m (0/030-inch) long at this point in the testing. In addition, a small, vertical, three-pronged crack had grown upward from the horizontal crack and two 1.27×10^{-4} meters (0.005-inch) diameter holes had appeared slightly to the right of the horizontal crack in a single coolant channel.

Four short-duration tests had no apparent effect on the cracks. Following the next test, 823 seconds, the chamber had a total of 10,900 seconds with five observable cracks. The original horizontal crack was unchanged in size; however, the other three existing cracks had increased to approximately 2.54×10^{-2} m (1 inch) in length. In addition, one of the cracks had developed a neighbor, approximately two or three channels away at a slightly different height. Liner roughness in the immediate area was only 2.0324×10^{-6} m (80 μin.), indicating the fuel being vented into the combust-i.on zone helped cool locally.

MCC 0007, Engine 0008.

This chamber developed a hot-gas wall crack very early in its test history (5 tests, 1143 seconds) and none since. The crack developed from an area which exhibited only minor discoloration after the first main stage test (third

hot-fire test) and relatively rough surface following the second main stage test. On the following test, the fifth (third main stage), there was a small eyelid-like channel rupture approximately 8.89 x 10^{-4} m (0.035 inch) long in the converging radius of the combustor zone. The surrounding area was very rough, approximately 5 x 10^{-6} m (200 μin.). Radiographic examination 1.27 x 10^{-1} m (5 inches) fore and aft of the throat revealed no obstructions in the cooling channels.

The general area of the crack has exhibited intermittent overheating since crack generation. This has apparently not been entirely eliminated by enlargement of the three overhead film coolant hoyes in the main injector primary faceplate.

Another area of the chamber exhibited higher than normal roughness subsequent to the second main stage test, and finally reached severe enough proportions to warrant coolant hole enlargement. The one hot fire test since shows the area to have apparently been cured of overheating. To date, the chamber has accumulated 21 tests and 6750 seconds hot-fire duration with more than 1400 seconds at 107% RPL or higher.

MCC 2007, Engine 2008 (2018).

The first instance of hot-gas wall distress on this MCC was noted after its seventh test (fifth main stage) and 1020 seconds. Not coincidentally, this was the first long-duration (520 seconds) test and first test in excess of RPL (102%). Following two additional long-duration tests, the chamber exhibited two areas of severe roughness. Four film coolant holes were enlarged, which totally relieved the surface distress. No further signs of distress were noted during the remainder of the engine's 102% RPL certification series.

Following rebuild of engine 2008 as 2108, the engine was employed for a series of FPL tests. Two added distressed areas required additional film cooling. In one area, the remedy worked totally, however, in the second area, the distress appeared even rougher after film coolant hole enlargement and exhibits fine surface cracking.

MCC 0005, Engine 0005

Numerous blanched areas appeared randomly dispersed throughout the convergent and throat sections of the chamber. Five areas of parent metal erosion appeared on the second hot-fire test on.the. engine. Maximum roughness in these areas was 5.08 x 10^{-6} m (110 μin.).

Surface cracking appeared after the next test in two of the areas eroded on the previous test. One crack originated in the convergent region, and one just upstream of the throat. The fourth test resulted in rough blanching beneath 12 elements; two elements have two blanched areas each. Two more cracks appeared in and just above the throat beneath the convergent region crack. All three cracks penetrated the hot-gas wall, and all three were in different, adjacent channels.

Two tests later, there were two additional areas showing surface cracking. The next four tests resulted in no apparent further degradation. The fourth test ended in a main injector failure which eroded the hot-gas wall and coated it with flame spray and slag.

MCC 0005, Engine 0006

The first two tests on this engine resulted in no reported anomalies. After the third test, there were two areas of moderate to severe blanching. The next test resulted in a new through-crack underneath one element. There was no obvious change to the other cracks. Flame spray on the chamber came from FPB wall burn-through.

Two tests later, there were five areas of light to moderate blanching, and two additional tests later, it was the same. Three tests later, there was one moderate to severe blanched spot. Following ten additional tests, primarily relatively short-duration, resulted in no more distressed areas, and all cracks appeared unchanged.

RECENT SSME MCC TEST HISTORY

Main combustion chamber (MCC) hot-gas wall failure in the form of channel cracks in the more recent phase of the test program is essentially the same as in the earlier phases and subscale testing. A noticeable trend during full power level (FPL) testing has been for cracking to occur faster in terms of number of engine tests and test durations (Tables 6 and 7). Cracks have developed in as little as three tests on a chamber during the FPL test phase. It is presumed that the crack failure modes are similar to those experienced on subscale chambers and earlier testing of the SSME, but no destructive analysis has been performed on an FPL MCC.

Circumferentially, liner distress most frequently occurs downstream of main injector baffle elements due to decreased mass flux in these areas. In attempt to minimize this distress, it has become standard practice to enlarge the 10 main injector boundary layer coolant holes adjacent to the baffles following the first or second test of an FPL engine.

One new form of hot gas wall distress, known as pimpling, has been noted on several recent MCCs operating at FPL. Circular areas of raised material up to about 1.27×10^{-3} m (0.050 inch) base diameter and 5.08×10^{-4} m (0.020 inch) high appear in hot spots where blanching or roughness has already occurred. A small pinhole may open at the peak of these pimples, producing what resembles a tiny volcano. Enlarging appropriate main injector film coolant holes seems to help prevent pinholes from developing and generally relieves this distress similarly to the case of blanching and channel cracks.

The following case histories are presented indicating the hot-gas wall thermal distress histories of some recent high-time SSME main combustion chambers.

TABLE 6. MCC INITIAL CRACK HISTORY-RECENT ENGINES AT FULL POWER LEVEL (FPL)

MCC/U/N	ENGINE NO.	TESTS BEFORE FIRST CRACK	TEST TIME (SECONDS) NOMINAL/FPL	CIRCUMFERENTIAL CRACK LOCATION (DOWNSTREAM OF OUTER ROW INJECTOR ELEMENT NO.)
0010	0010/0107	6	735/440	36 (BAFFLE)
9004	0204	7	750/440	56/57
2011	2010	7	2600/1890	76 (HIGH VELOCITY AREA)
9005	2013	3	600/760	36 AND 68 (BAFFLES AND LONGITUDINAL WELD)
2015	2014	6	1910/1310	36 (BAFFLE)
0007	0008/2308	5	1145/945	68 (BAFFLE AND LONGITUDINAL WELD)
2015	2011	4	128/0	53
2017	2012	6	802/390	76 (HIGH VELOCITY AREA)
4001	2017	4(PINHOLE)	1094/0	72
2014	2015	NO CRACKS		

*85 INJECTOR ELEMENTS IN OUTER ROW, WHERE NO. 1 IS AT FUEL TURBOPUMP HOT-GAS TRANSFER DUCT (COUNTING CLOCKWISE LOOKING FORWARD).

TABLE 7. MCC INITIAL CRACK HISTORY-RECENT ENGINES, FIRST MANNED ORBITAL FLIGHT (FMOF) ENGINES AT RPL OPERATION

MCC/U/N	ENGINE NO.	TESTS BEFORE FIRST CRACK	TEST TIME (SECONDS) NOMINAL	CIRCUMFERENTIAL CRACK LOCATION (DOWNSTREAM OF OUTER ROW INJECTOR ELEMENT NO.)
0006	2004	6	220	21
2005	2005	NO CRACKS	3840	
2004	2000	NO CRACKS	3760	
0009	2007	NO CRACKS	4210	

MCC 2015, Engine 2014 (FPL)

The 10 film coolant holes adjacent to baffles were enlarged as a precautionary measure following the second test. The second and third tests on this engine resulted in blanching which required the enlargement of nine additional film coolant holes. A surface crack developed after the fifth test in a previously blanched area and grew to 58.4 x 0.28 mm (2.3 x 0.011 inch) by the sixth test. Blanching increased such that two more film coolant holes were enlarged after the seventh test.

Following the eighth test and 2411.5 seconds, blisters appeared in a blanched area. Four through cracks developed after the ninth test. the next test, one of the through cracks grew and two merged and extended. Pinholes and pimples developed after the 16th test (3868.1 seconds) in a previously blanched area and became four small holes with a crack following the 20th test. A channel crack appeared after the 21st test. One film coolant hole was opened after the 24th test, and three more after the 31st test. Blanching has been evident throughout this MCC's test history to date (36 tests, 11590.31 seconds)

MCC Unit 2011, Engine 2010 (FPL)

Blanching (measuring 100μinch surface roughness) first occurred after the third test and 601.5 seconds. Blanching increased in five areas such that film coolant holes were enlarged by the fifth test. The next test revealed that four out of the five blanched areas became rougher and one area became eroded and cracked because of element contamination. Subsequent tests revealed more blanching and the need to open more film coolant holes. A 1.27×10^{-3} m (1/2-inch) long crack developed in an area that was previously blanched after the seventh test. Five tests later (seven tests, 2601.5 seconds), a crack 2.54×10^{-3} m x 2.54×10^{-4} m (1 x 0.01 inch) developed and stabilized. A new crack developed adjacent to the previous crack six tests later.

Six cracks and two pinholes were noted after the 17th test. The cracks extended longitudinally and the pinholes stabilized after six tests. Pimples appeared after the 27th test. A crack connected the pinholes after the 37th test and 11,197.5 seconds. Two new cracks occurred after the 40th test, one at the throat and one in the upper convergent region.

MCC 0006, Engine 2004 (FMOF)

The first instance of hot-gas wall distress, which was minor, was noted early in the chamber's test history (four tests, 5.6 seconds). A surface crack at the throat was noticed following the fifth test. Following the eighth test, the hotspot near the first surface crack, when viewed under magnification, showed molten Narloy-Z and slight erosion.

After six additional tests (14 tests, 321.4 seconds), another hot spot revealed a channel with a small 7.94×10^{-4} m (1/32 inch) long rupture 5.08×10^{-2} m (2 inches) above the throat centerline and a total of five channels with 1.905×10^{-2} m (3/4 inch) long channel cracks. Blanching with a blister in this area occurred during the next test. After the 16th test, there was some disturbance at a longitudinal weld, a 0.51 mm (0.02 inch) hole, and some cracking was visible in this area.

Seven test later, the cracks seemed to stabilize. A new 7.94 mm (5/16 inch) long crack was discovered after 30 test and 4587.5 seconds. This crack propagated to 9.53 mm (3/8 inch) long. A blanched area with high roughness (300 μin.) developed a small crack after the 44th test. Blanching was evident between the 44th and 49th tests.

SSME SUBSCALE THRUST CHAMBER

A 1.8143 x 104 kilograms (40,000 pound) thrust subscale SSME thrust chamber was fabricated to demonstrate the cyclic life of its larger counterpart. The thrust chamber is designed to operate at 2.0684 x 107 pascal (3000 psia) with liquid oxygen and fuel-rich O_2/H_2 combustion products for fuel. The combustion chamber is copper alloy with a nickel electro-formed closeout to complete the channel wall flow passages. These coolant passages duplicate the geometry of the full scale thrust chamber to obtain realistic cycle life data.

A staged combustion cycle was employed to simulate accurately injector combustion chamber heat transfer relationship. The primary goals of the program were to: (1) accumulate 100 main stage thermal cycles on a hydrogen cooled combustion chamber, and (2) demonstrate the equivalent thermal strain damage of 60 SSME missions on the main injector oxidizer posts.

The combustion system assembly (Fig. 77A) consisted of a single preburner assembly, a hot-gas transfer manifold, a main injector, and a main combustion chamber. The preburner assembly and hot-gas transfer manifold designs were workhorse in nature; however, the main injector and main combustion chamber incorporated key design features of the flight-type SSME hardware.

The main injector assembly (Fig. 77B) consisted of 58 recessed coaxial main injection elements, 3 baffle injection elements, and a transpiration cooled, dual faceplate configuration. The injection elements and faceplates duplicated the full scale injector design relative to propellant injection parameters and cooling. Demonstration of the injector body and oxidizer post material to withstand the thermal cycle strains induced by ducting both high-temperature (hot-gas) and cryogenic temperature (liquid oxidizer) fluids through the injector was one of the two design verification items included in the subscale program. Main combustion chamber test hardware includeded both water- and hydrogen-cooled units and are shown in Fig. 77C and 77D, respectively.

The 1.8143 x 10 kilogram (40K pounds) subscale primary goals were met by accumulating more than 100 main stage thermal cycles on the regeneratively cooled chamber.

Analysis of Test Results and Posttest Hardware Evaluation

The subscale program's primary goals were met by accumulating more than 100 main stage thermal cycles on the first regenerative chamber (U/N 2).

The service life of the SSME main combustion chamber, as demonstrated by 40K subscale chamber hot-fire testing, is 103 starts and cutoffs. This is based on the demonstrated 109 thermal cycles of the subscale chamber (U/N 2) prior

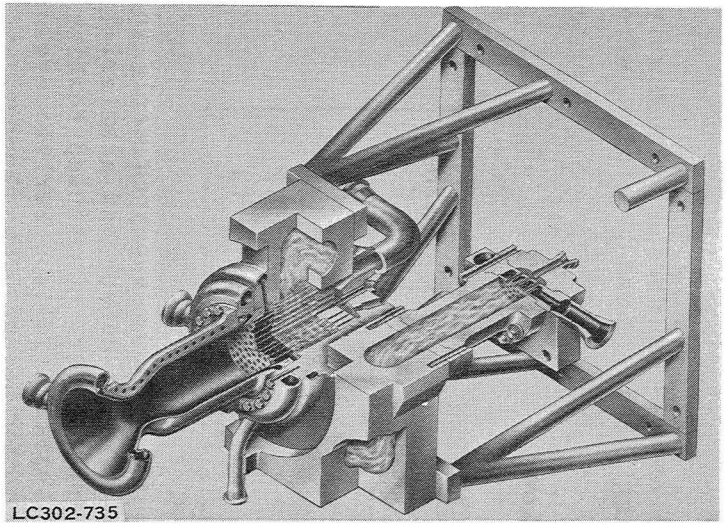

(A) SYSTEM

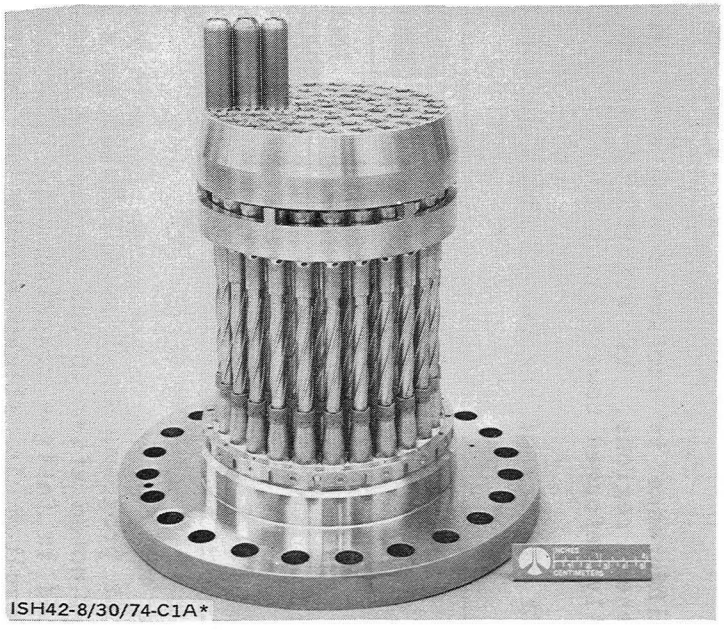

(B) INJECTOR

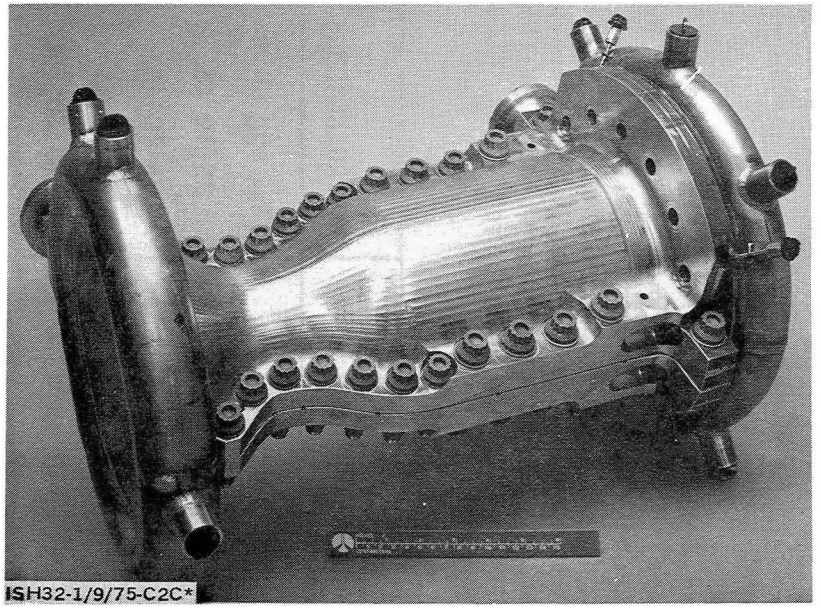

(C) WATER COOLED CHAMBER

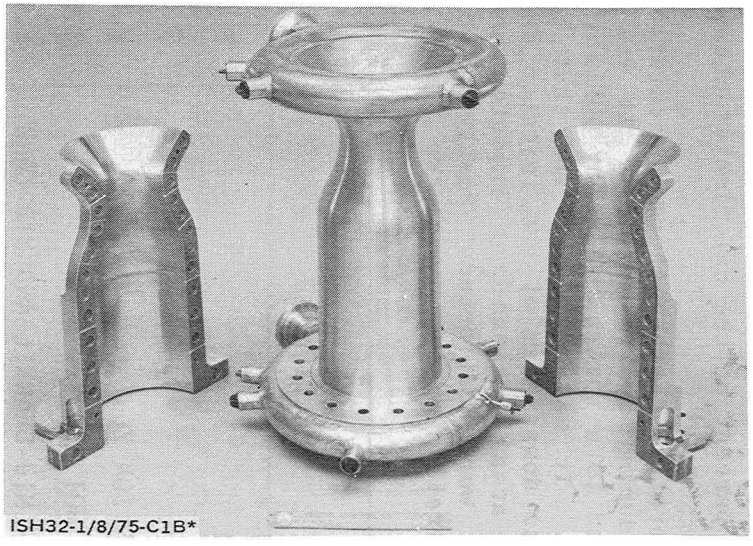

(D) HYDROGEN COOLED CHAMBER

Figure 77. SSME Subscale Thrust Chamber

to attaining a low cycle fatigue crack in the NARloy-Z liner. The life analysis utilized nominal heat transfer operating conditions of the regenerative chamber, where the average heat load during the test series was established to be 95 percent of the calorimeter chamber heat load.

Regenerative chamber thermal escalation was noted by an increase in total heat load during cyclic testing. It was determined that the heat load could be reduced to a nominal value by polishing the hot-gas wall surface with a crocis cloth. It was also observed that local regions located 1.016×10^{-1} m (4 inches) downstream of the injector and at the throat were roughened more than other areas between the injector and throat. All areas downstream of the throat were unaffected. Posttest hot-gas wall surface finish values for the regenerative chamber U/N 2 are summarized below:

REGION	SURFACE FINISH METERS	MICROINCHES
NOZZLE	5.08×10^{-7}	20
THROAT	$2.54 \times 10^{-8} - 4 \times 10^{-5}$	35 TO 45
COMBUSTION ZONE	$2.54 \times 10^{-8} - 4 \times 10^{-5}$	35 TO 45
LOCAL HOT SPOTS	$2.54 \times 10^{-8} - 4 \times 10^{-5}$	35 TO 45
OVER MID-CHANNEL AND MID-LAND	$6.35 \times 10^{-6} - 8.89 \times 10^{-6}$	250 TO 350
OVER CHANNEL TO LAND CORNERS	1.524×10^{-6}	60

The difference in surface finish over land to channel corners in the highly roughened regions, is attributed to polishing since these surfaces were slightly deformed toward the hot-gas.

The LCF history of the two chambers is noted below:

CHAMBER NO.	TOTAL NUMBER OF TESTS	LOCATION LFC CRACKS	CHANNEL NO.*	THERMAL CYCLE NO.
002	118	10 INCH	98	109
		THROAT	98	112
		THROAT	121	112
001	57	THROAT	121	53

On the 40K chamber U/N 2 (Fig. 78) two hot-gas wall cracks appeared early in the test program, which were related to a manufacturing defect and a material defect; noted after 10 and 29 thermal cycles, respectively. Continued testing resulted in fatigue cracking after 109 and 112 thermal cycles. Further cycling resulted in slight growth of existing cracks before the chamber was retired after a 118 thermal cycle test program (Fig. 79 and 80).

1SH35-3/22/76-CIE

Figure 78. 40K MCC Showing Anomalous Injector Effects

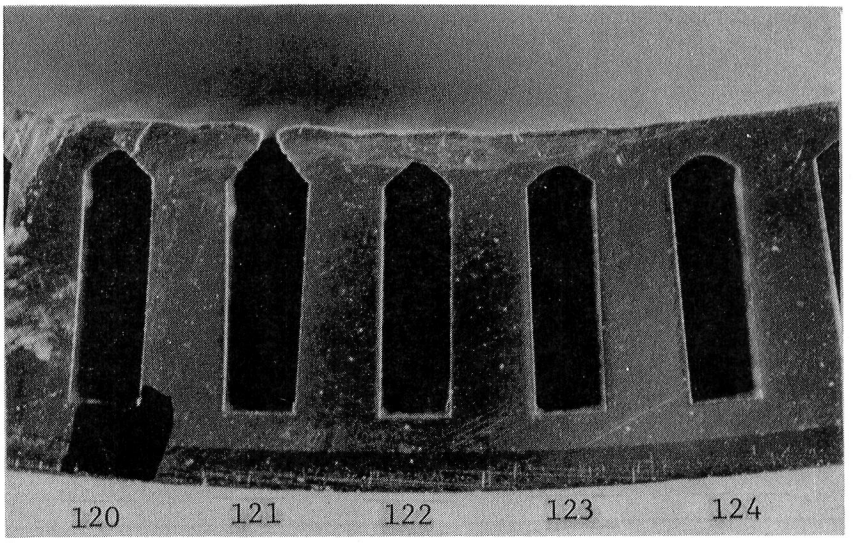

Figure 79. 40K Chamber Section Through a Hot Spot Near the Throat

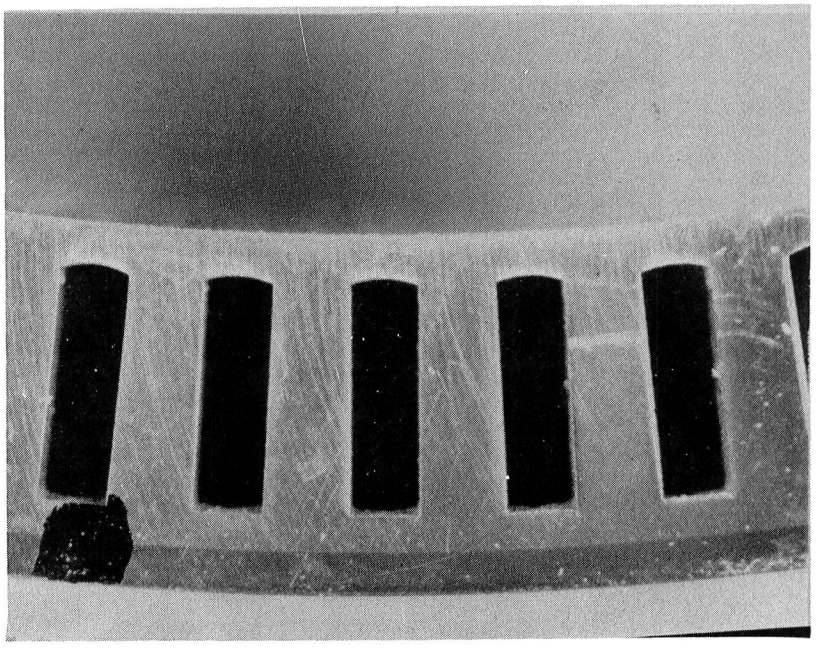

Figure 80. 40K Chamber Section Showing Typical Channel Deformation Near the Throat

On the 40K chamber U/N 1 a low-cycle fatigue through crack appeared in the throat region after 53 thermal cycles. The chamber was then tested for four more additional thermal cycles. The crack grew from approximately 1.27 x 10^{-2} m to 1.91 x 10^{-2} m (0.5 to 0.75 inch) in length. The 57 thermal cycles completed the test program on the 40K chamber.

3.3K Program

The 3.3K chamber (Fig. 81) underwent 1013 hot-fire test cycles prior to leakage through the hot-gas wall. The failure analysis summary, MPR 74-904, attributes failure to fatigue initiating from the coolant side of the hot-gas wall surface. The distortion and cracking are symptomatic of significant temperature variations between identical axial locations.

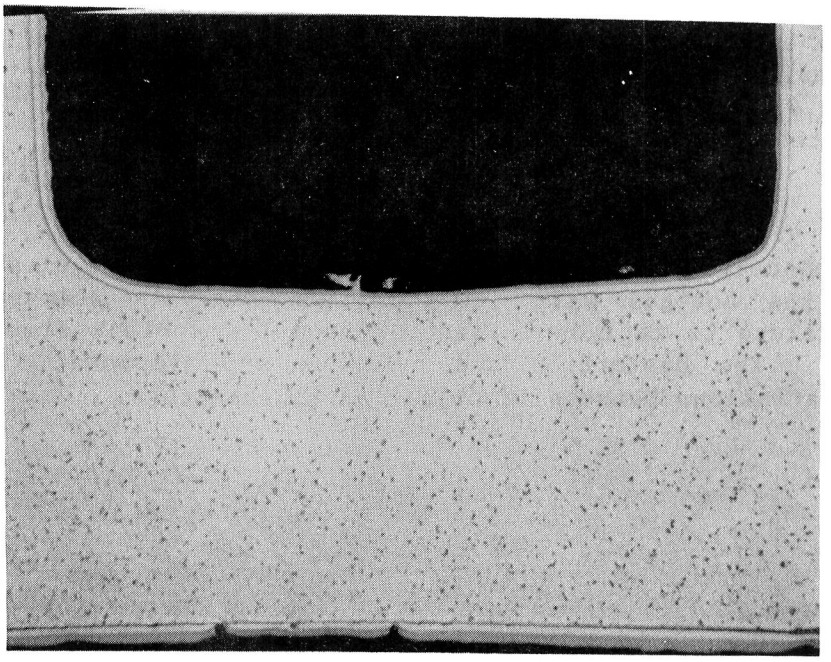

(A) CHANNEL NO. 9 50 X

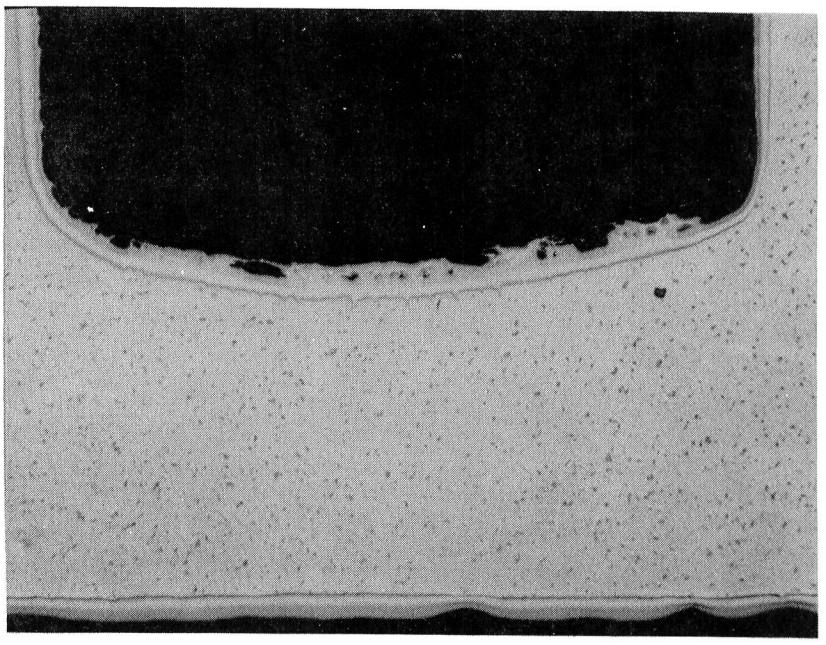

(B) CHANNEL NO. 11 50 X

Figure 81. Sections From 3.3K Chamber Near the Throat Showing Two Nearby Channels--One With and One Without Hot-Gas Wall Bulging

APPENDIX B

MATERIAL PROPERTIES

SSME MCC (REF. 14) MATERIALS DEFINITION

NARloy-Z is a copper base, silver, zirconium-containing alloy developed by Rocketdyne specifically for high heat flux combustion chamber applications. The material has excellent thermal conductivity and can develop good strength and ductility up to 922 K (1200 F) by a simple heat treatment. The slotted liner requires a material which has good strength at elevated temperatures to resist coolant pressures and superior thermal fatigue resistance to accommodate the severe thermal strains generated during hot firing. NARloy-Z has demonstrated that it offers the best combination of characteristics to satisfy these requirements.

Electrodeposition of nickel (EDNi) having an initial barrier of electrodeposited copper (EDCu) for hydrogen environment protection was selected as the method for closing out the coolant channels in the slotted liner. The deposited structure has excellent bonding actions with the NARloy-Z liner material and makes a good structural closeout. The properties of electrodeposited nickel are good making it suitable for containing the coolant pressures in the channels while providing a transition metal for welding the jacket to the liner.

EDCu is deposited initially to provide a barrier to the embrittling effects on EDNi of high-pressure hydrogen in the coolant passages. This barrier has imparted excellent low cycle fatigue life to EDNi in the presence of hydrogen.

The material requirements to support the MCC life predictions for this study are summarized in Table 8. The materials considered are NARloy-Z, electrodeposited-nickel (EDNi) and electrodeposited-copper (EDCu). Available test data were compiled (Ref. 15) and the material properties curves extrapolated to the ranges of interest. In the absence of test data, various prediction methods were used.

1. Thermal-Physical Properties

The elastic.modulus and Poisson's ratio data for NARloy-Z had to be extrapolated from test data between 978 to 1089 K (1300 to 1500 F). For EDNi and EDCu, the elastic modulus and Poisson's ratio was extrapolated between 294 to 78.6 K (70 to -320 F) from test data. Thermal expansion data was available for all three alloys in the temperature range of interest.

2. Structural Properties

Tensile test data were available for all three materials. However, stress-strain curves at various temperatures were also needed. MIL-HDBK-5 suggests two methods for determining stress-strain curves (Ref. 16). They are the Strain-Departure Method and the Ramberg-Osgood Method. The elastic modulus and the yield strength at the required temperature plus stress-strain curves at other temperatures to determine a representative shape are needed.

TABLE 8. MATERIAL PROPERTIES SUMMARY

MATERIAL	PROPERTY	TEMPERATURE, K	TEMPERATURE, F	FIGURE NO.	COMMENTS
NARloy Z	ELASTIC MODULUS	78 TO 1089	-320 to 1500	82	EXTRAPOLATED AT TEMPERATURES ABOVE 978 K (1300 F)
	POISSON'S RATIO	78 TO 1089	-320 TO 1500	83	EXTRAPOLATED AT TEMPERATURES ABOVE 922 K (1200 F)
	THERMAL EXPANSION	78 TO 1089	-320 TO 1500	84	--
	TENSILE PROPERTIES	78 TO 1089	-320 TO 1500	85, 86	EXTRAPOLATED AT TEMPERATURES ABOVE 1033K (1400 F)
	STRESS-STRAIN DIAGRAM	78 TO 1089	-320 TO 1500	87	PREDICTED AT 78 K (-320 F) AND 1089 K (1500 F)
	LOW CYCLE FATIGUE	78 TO 1089	-320 TO 1500	88	PREDICTED AT 978 K (1300 F) AND 1089 K (1500 F)
	STRESS EXPONENT n	644 TO 1089	700 TO 1500	89	EXTROPLATED AT 1089 K (1500 F)
	MATERIAL CONSTANT A	644 TO 1089	700 TO 1500		EXTROPLATED AT 1089 K (1500 F)
	CREEP-RUPTURE	644 TO 1089	700 TO 1500	90	--
EDNi	ELASTIC MODULUS	78 TO 422	-320 TO 300	91	EXTRAPOLATED AT TEMPERATURES BELOW 294 K (70 F)
	POISSON'S RATIO	78 TO 422	-320 TO 300	92	EXTRAPOLATED AT TEMPERATURES BELOW 294 K (70 F)
	THERMAL EXPANSION	78 TO 422	-320 TO 300	93	--
	TENSILE PROPERTIES	78 TO 422	-320 TO 300	94, 95	--
	STRESS-STRAIN DIAGRAM	78 TO 422	-320 TO 300	96	PREDICTED AT 78 K (-320 F)
	LOW CYCLE FATIGUE	78 TO 422	-320 TO 300	97	--
EDCu	LASTIC MODULES	78 TO 478	-320 TO 400	98	EXTRAPOLATED AT TEMPERATURES BELOW 78 K (-320 F)
	POISSON'S RATIO	78 TO 478	-320 TO 400	99	EXTRAPOLATED AT TEMPERATURES BELOW 78 K (-320 F)
	THERMAL EXPANSION	78 TO 478	-320 TO 400	100	--
	TENSILE PROPERTIES	78 TO 478	-320 TO 400	101	--
	STRESS-STRAIN DIAGRAM	78 TO 478	-320 TO 400	102	PREDICTED
	LOW CYCLE FATIGUE	294 TO 617	70 TO 617	103	PREDICTED - MUS ÷ 3 IS BASED ON PREDICTED DUCTILITY VALUES

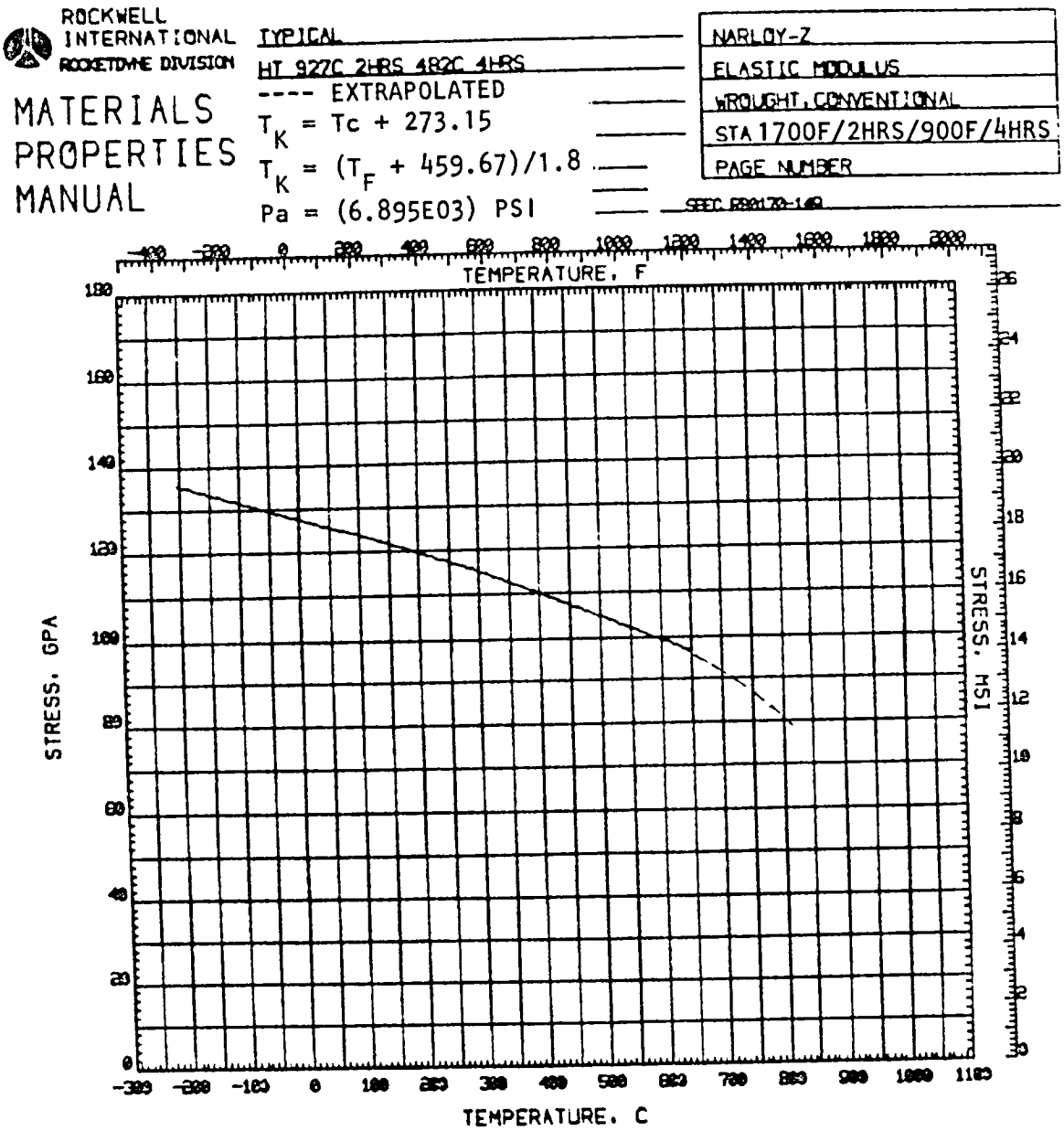

Figure 82. NARloy-Z Elastic Modulus As a Function of Temperature

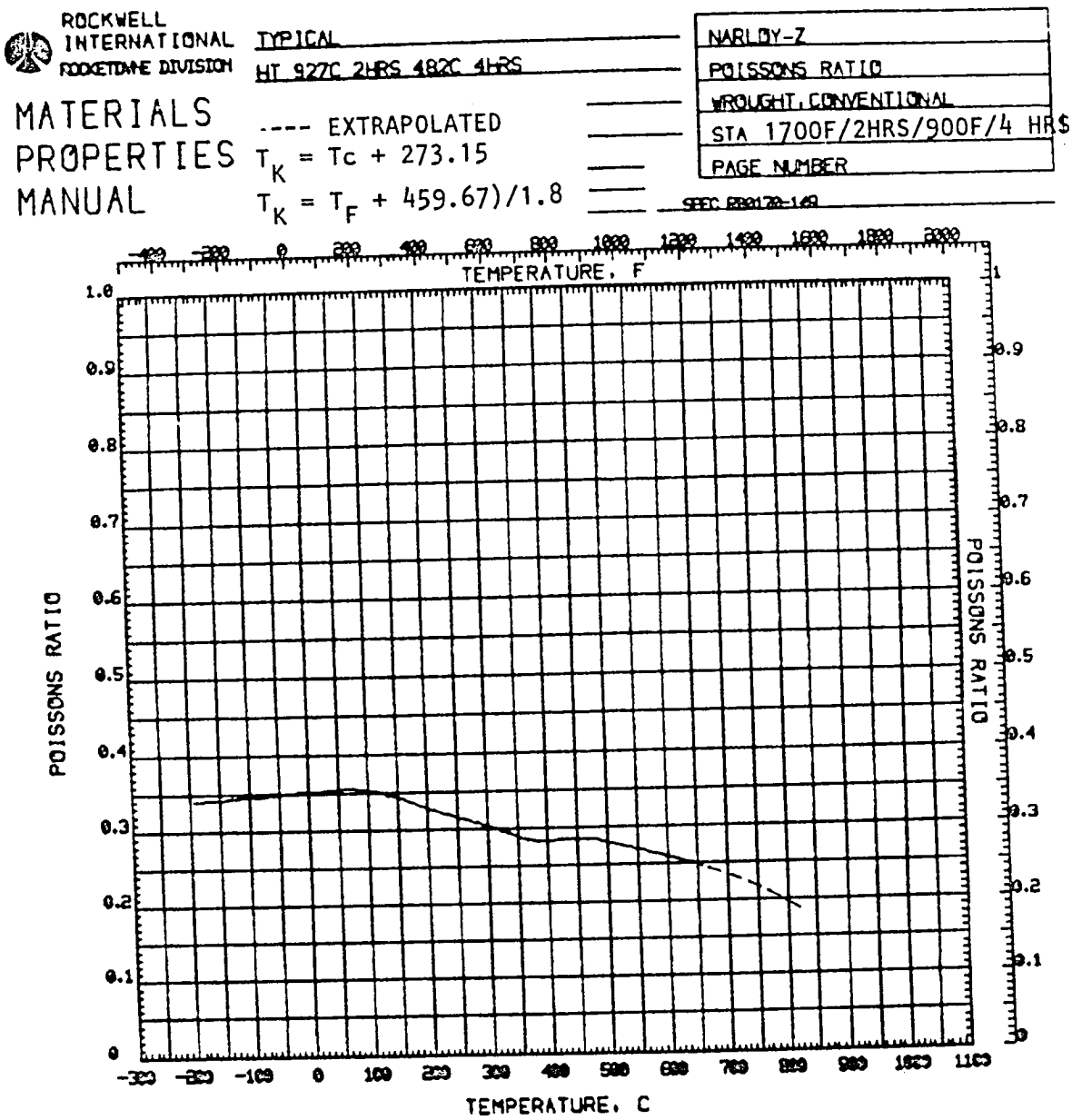

Figure 83. NARloy-Z Poisson's Ratio as a Function of Temperature

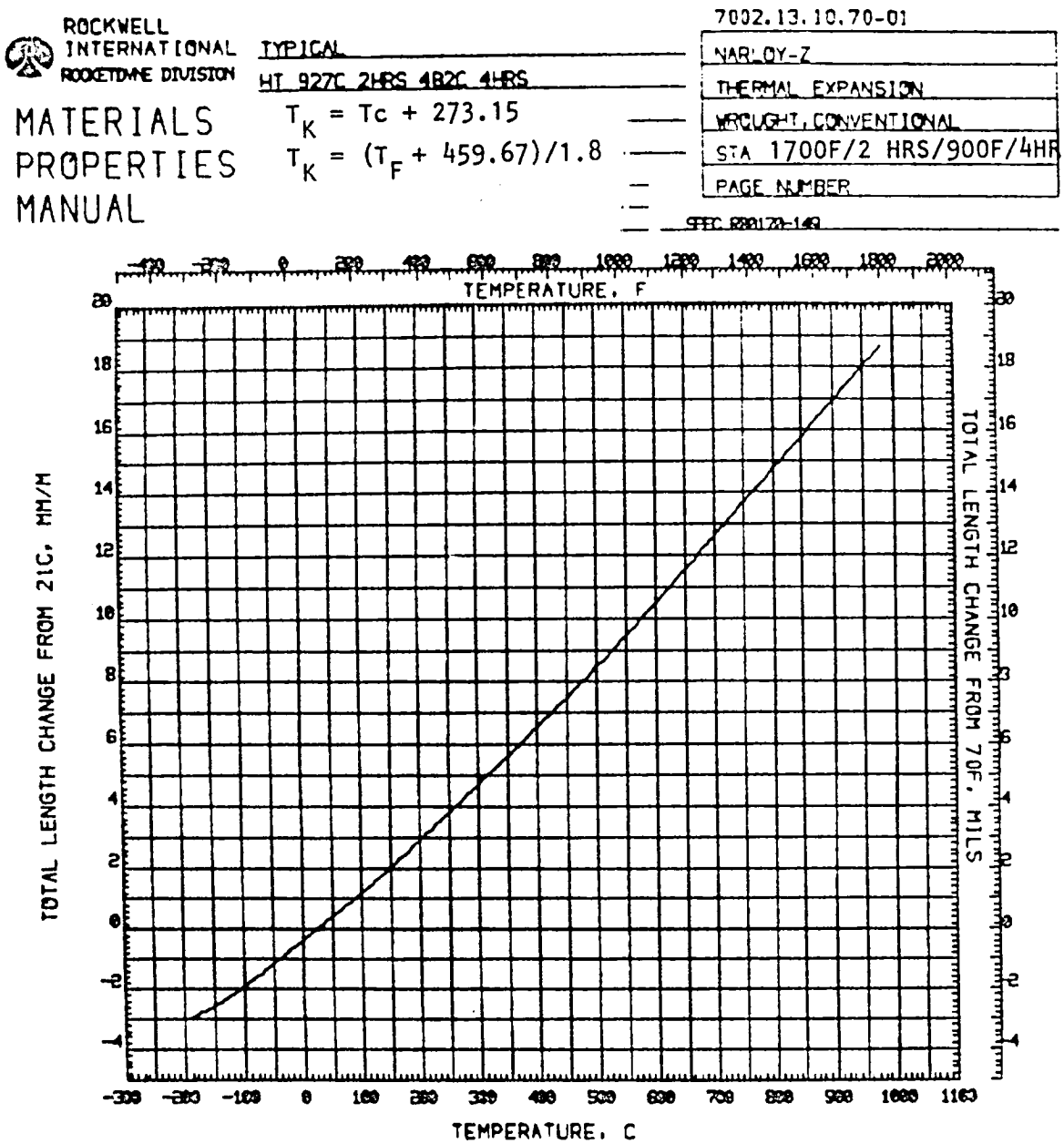

Figure 84. NARloy-Z Thermal Expansion as a Function of Temperature

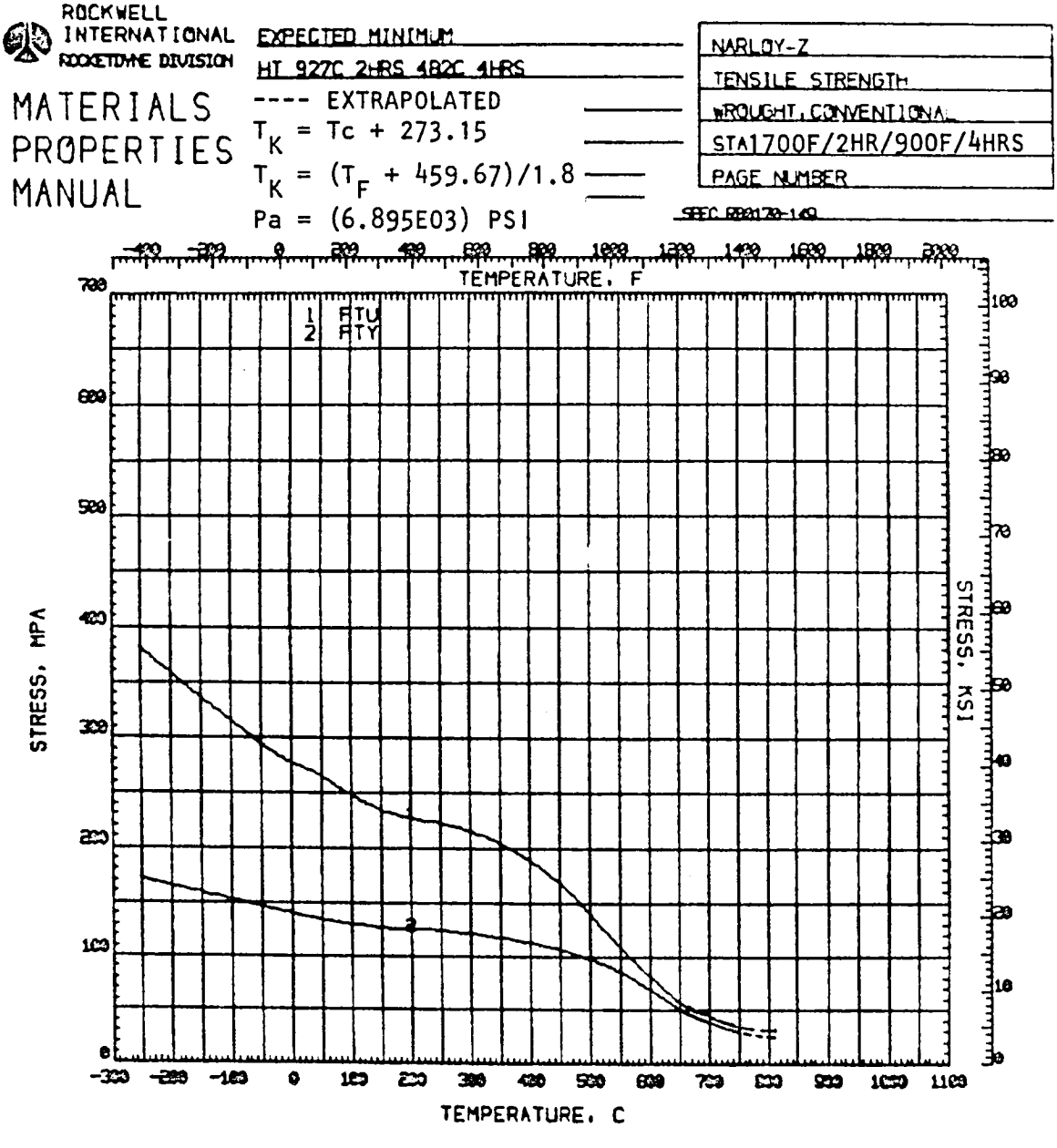

Figure 85. NARloy-Z Tensile Strength as a Function of Temperature

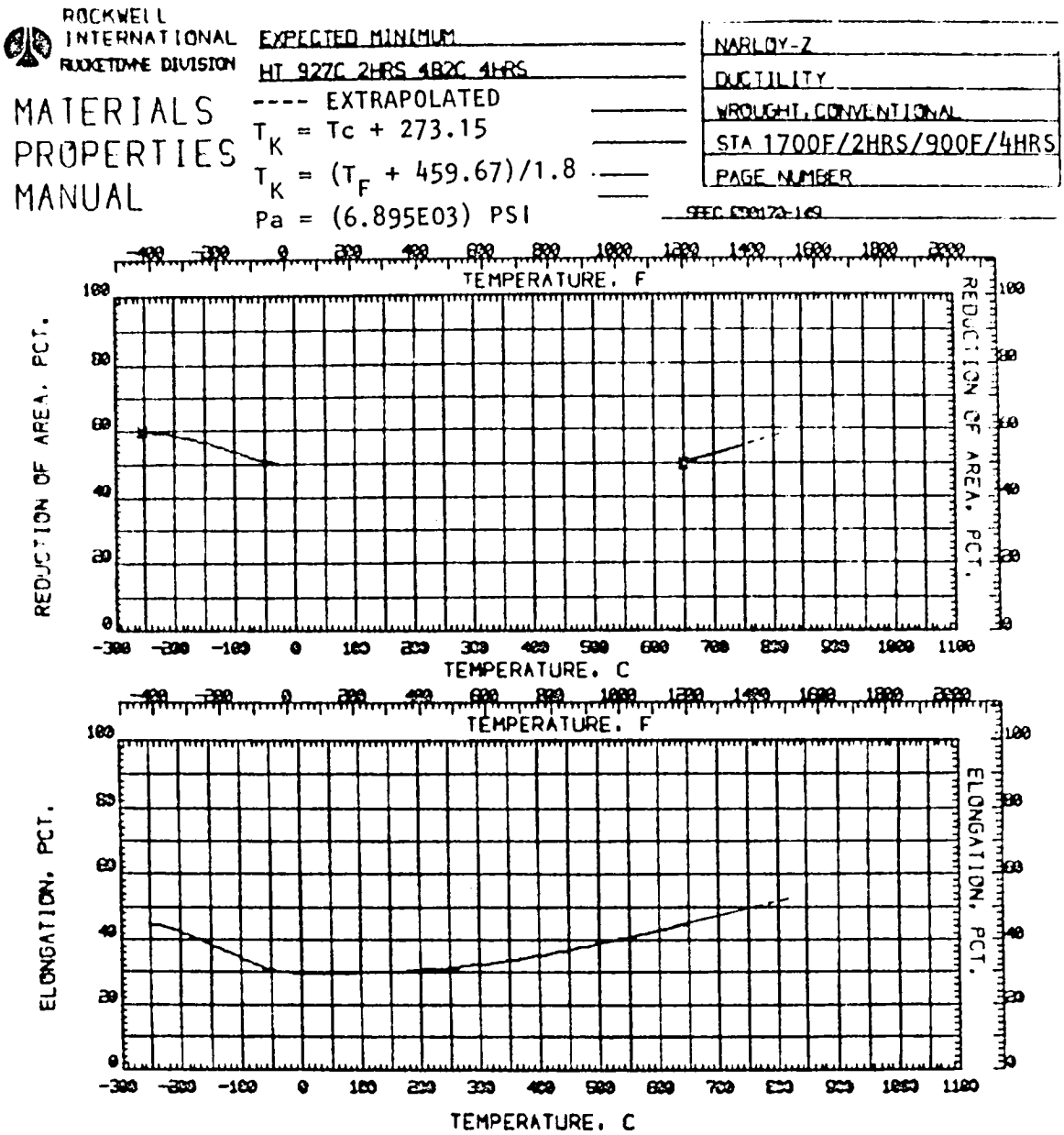

Figure 86. NARloy-Z Ductility as a Function of Temperatue

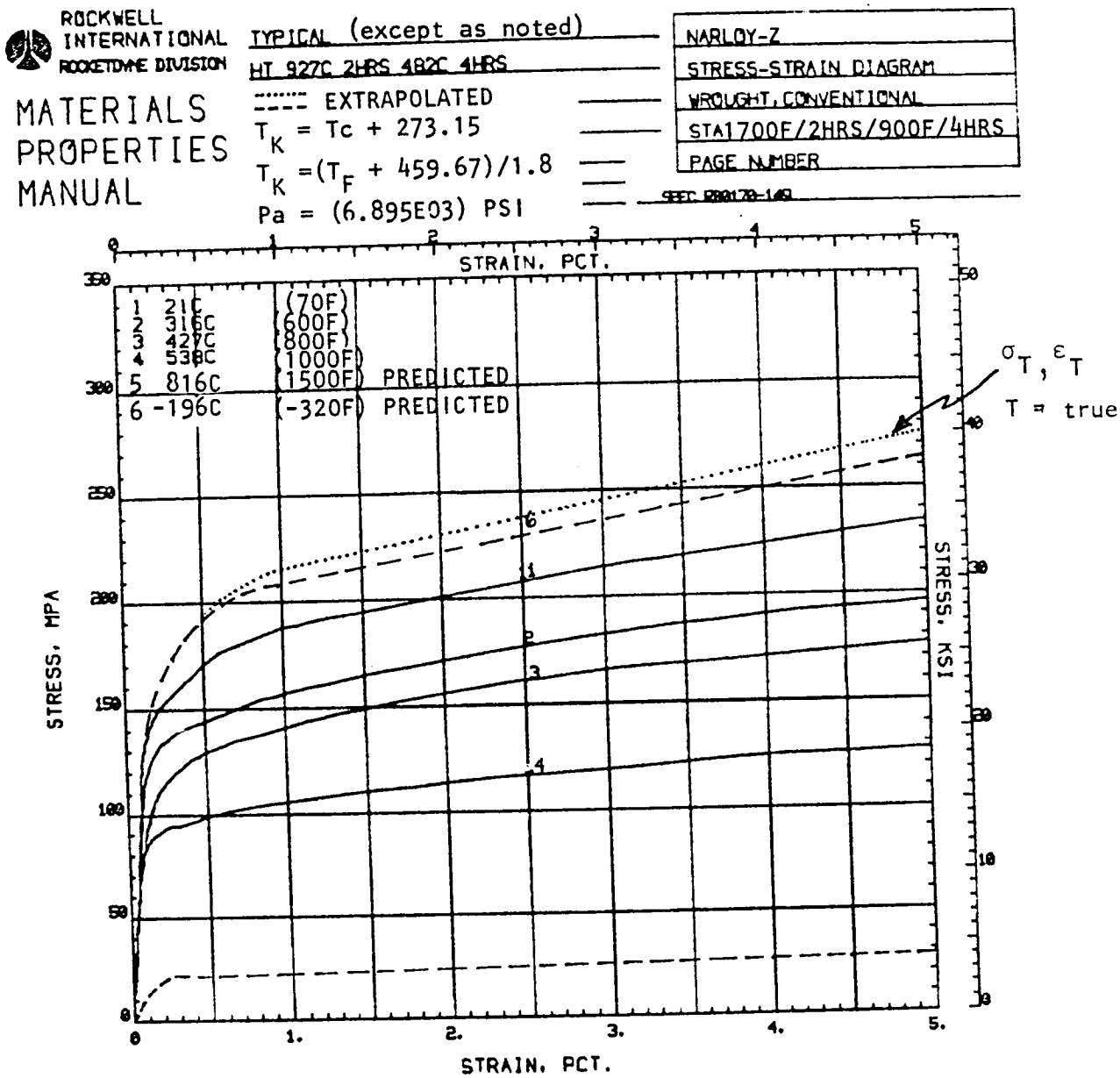

Figure 87. NARloy-Z Stress-Strain Diagram

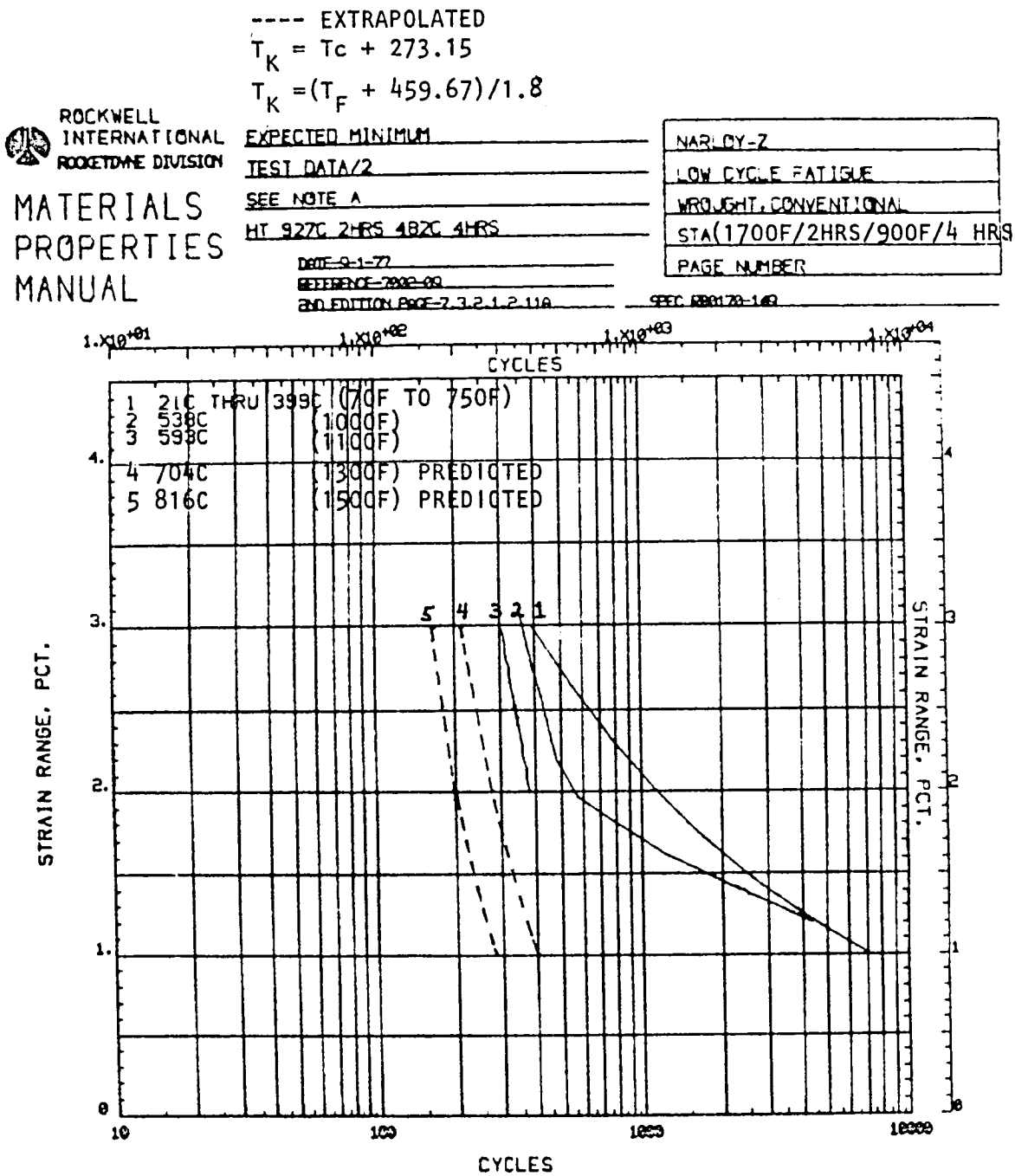

Figure 88. NARloy-Z Low Cycle Fatigue

WROUGHT - STA (1144 K/2 HOURS/755 K/4 HOURS) (1600 F/2 HOURS/900 F/4 HOURS)			
TEMPERATURE, K	TEMPERATUE, F	'e	A
644	700	19.2	2.9×10^{-31}
700	800	16.1	9.6×10^{-25}
755	900	13.9	1.0×10^{-19}
811	1000	12.5	6.2×10^{-16}
922	1200	8.7	4.5×10^{-9}
1089	1500	5.08	2.073×10^{-3}
FROM TENSION CREEP DATA (SOURCE: MPTR 70-902)			

Figure 89. NARloy-Z Stress Exponent 'e and Material Constant A as a Function of Temperature

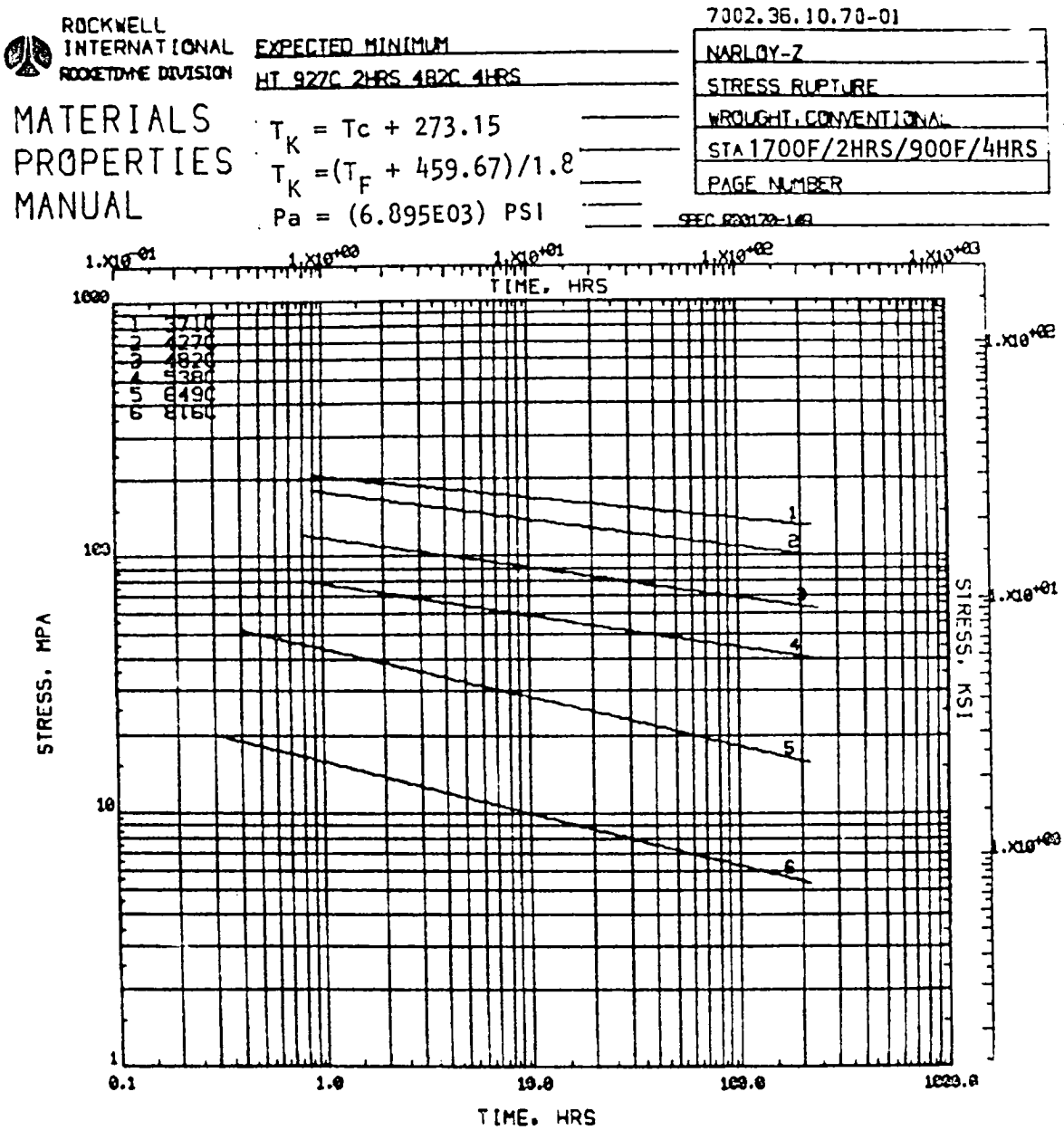

Figure 90. NARloy-Z Stress Rupture

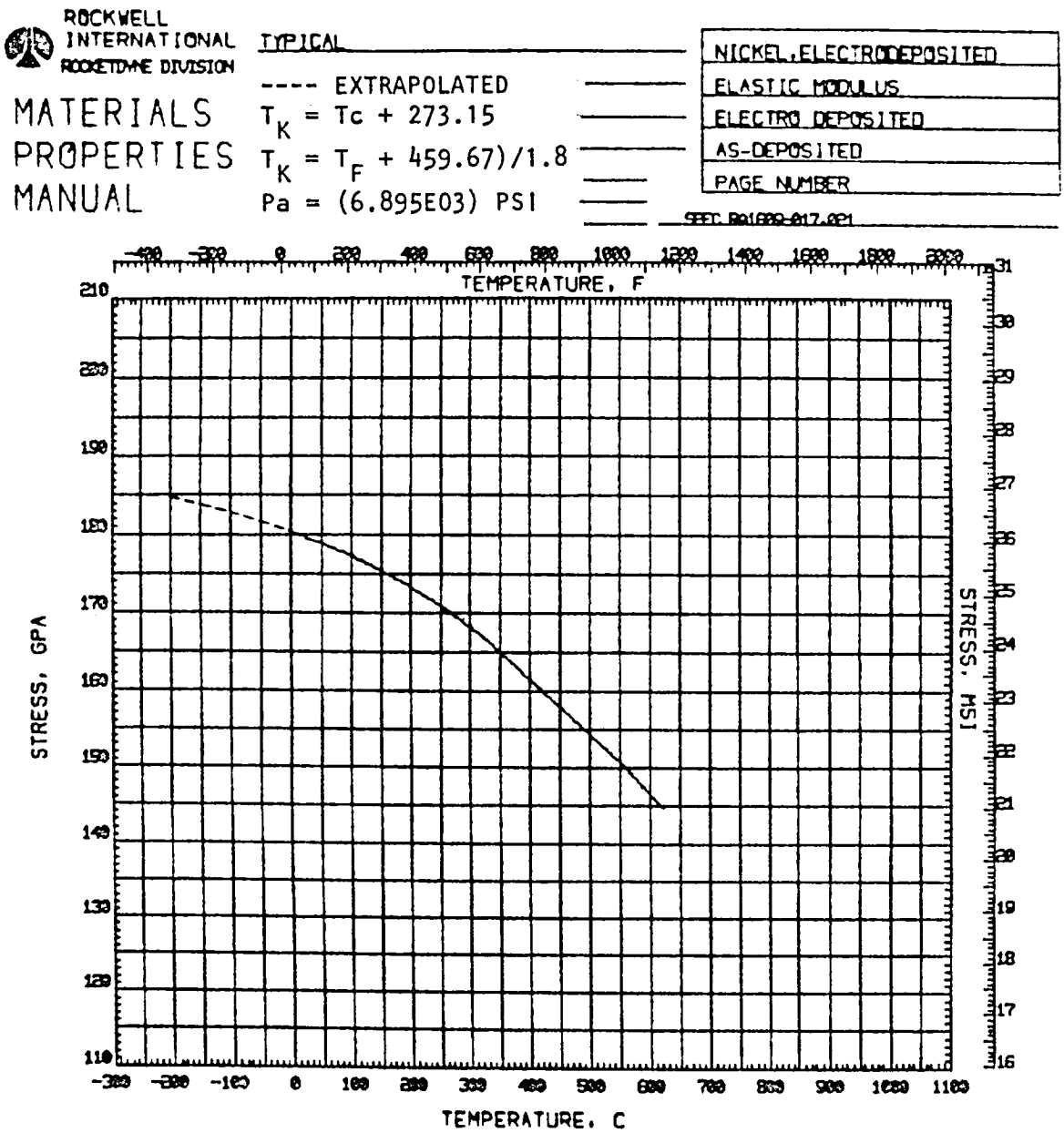

Figure 91. EDNi Elastic Modulus as a Fucntion of Temperature

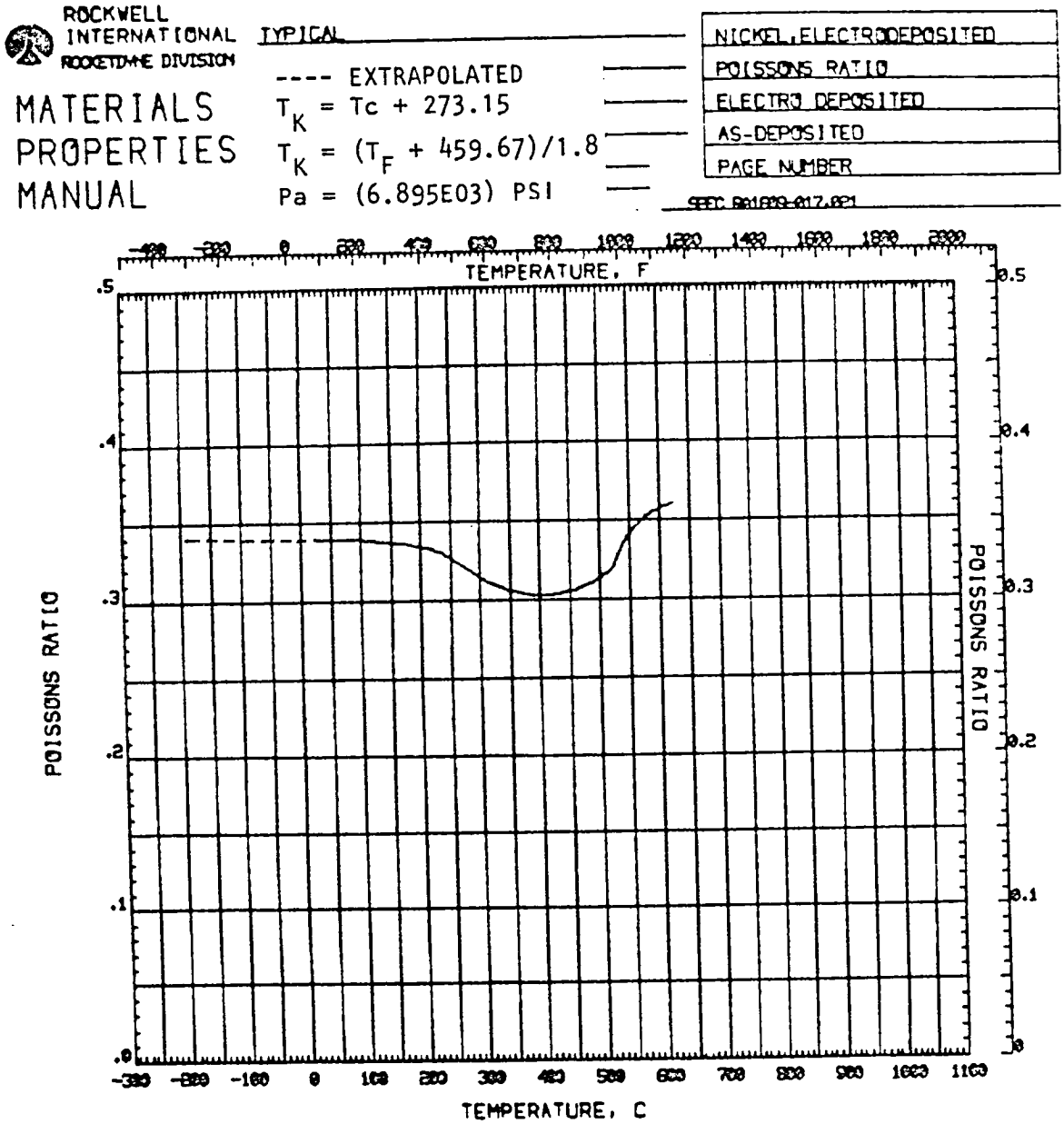

Figure 92. EDNi Poisson's Ratio as a Function of Temperature

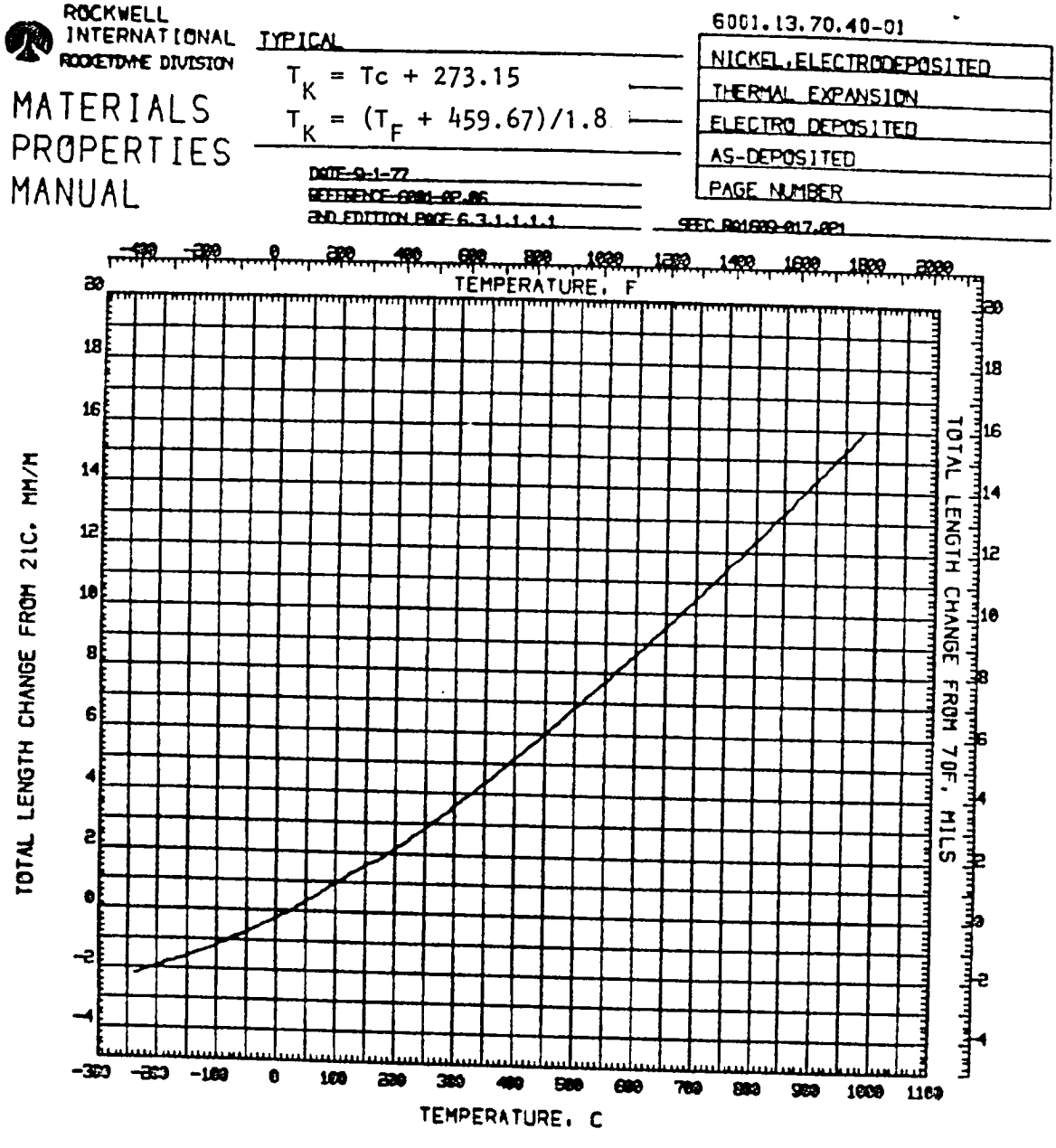

Figure 93. EDNi Thermal Expansion

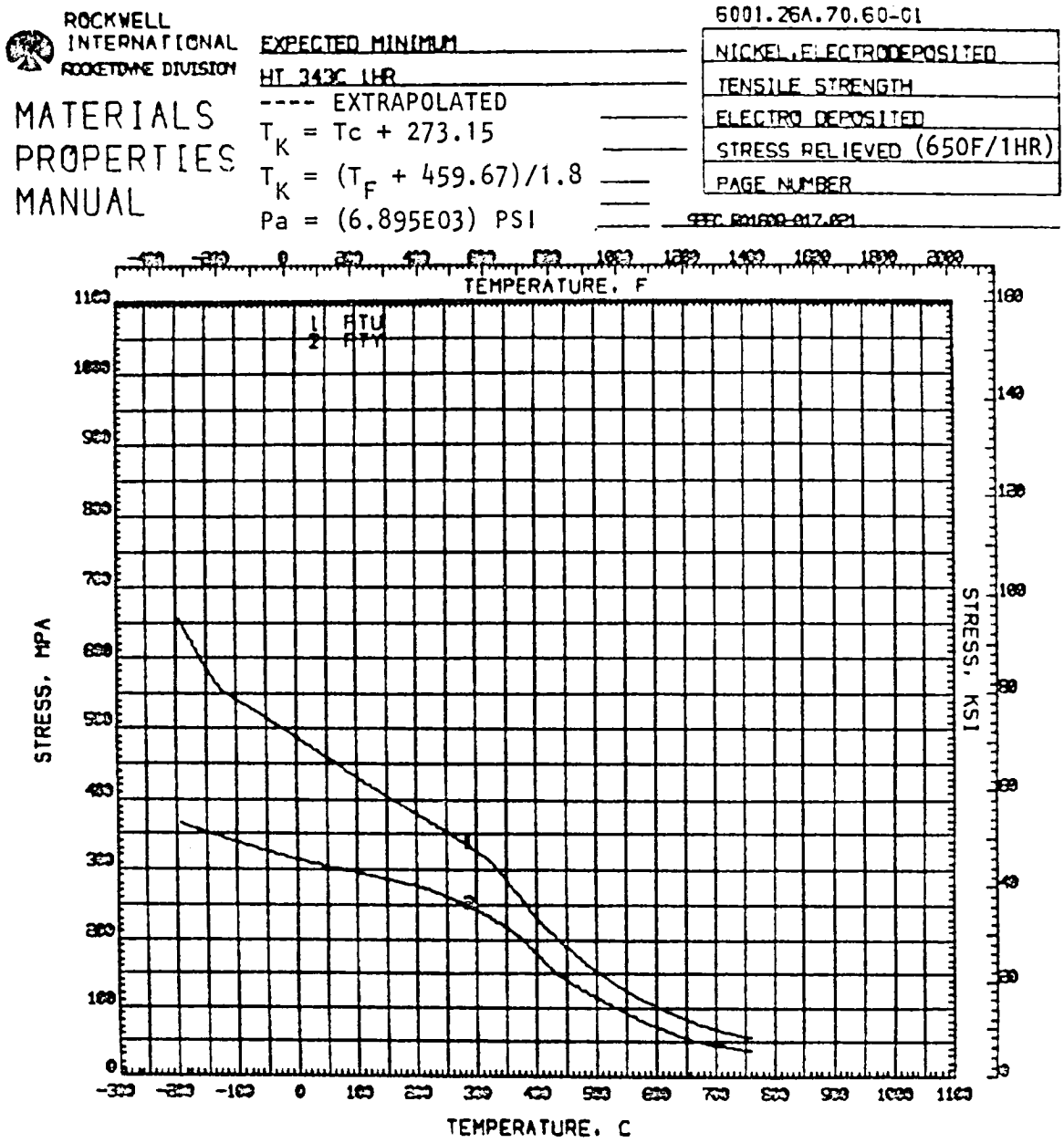

Figure 94. EDNi Tensile Strength as a Function of Temperature

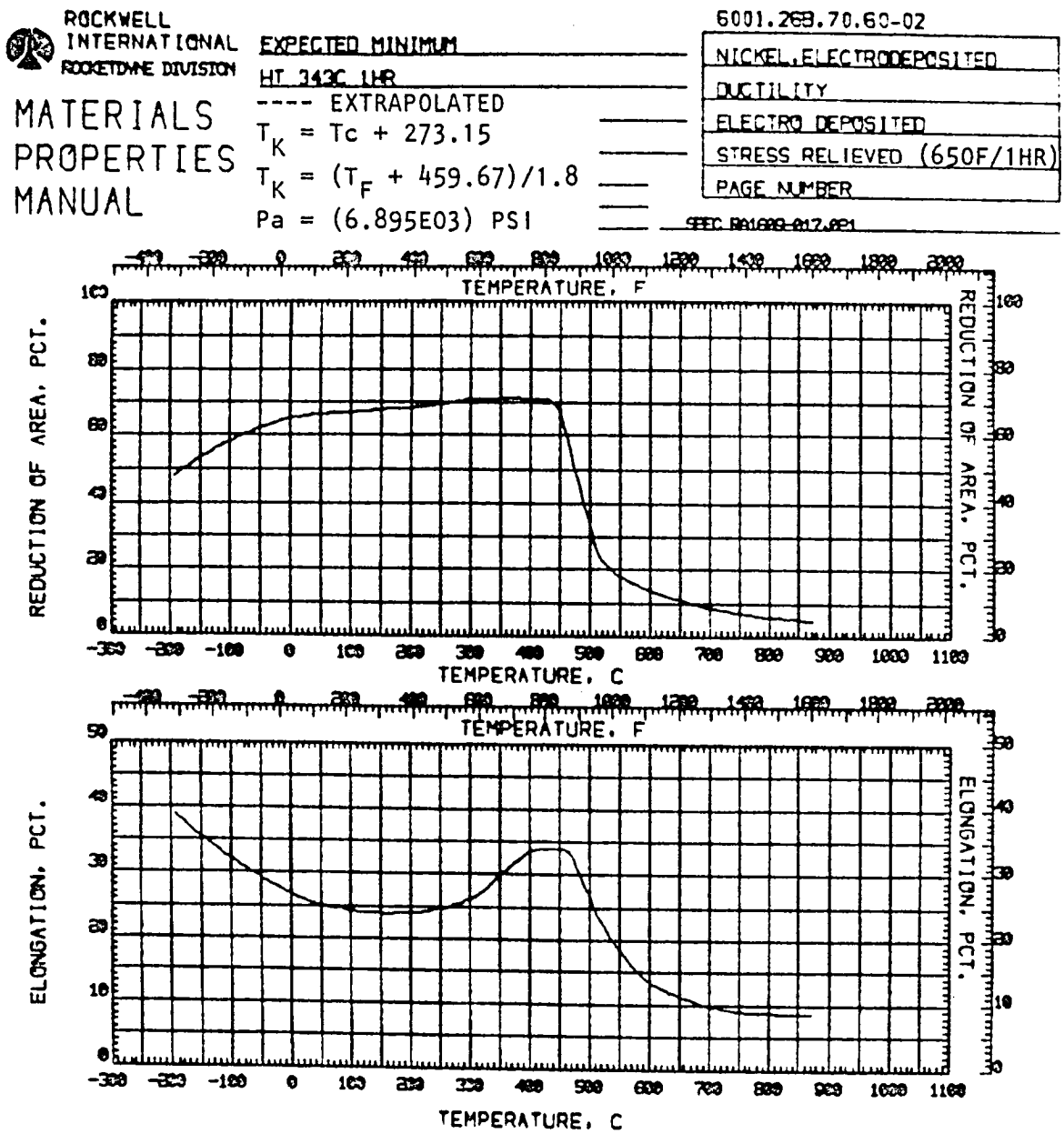

Figure 95. EDNi Ductility as a Function of Temperature

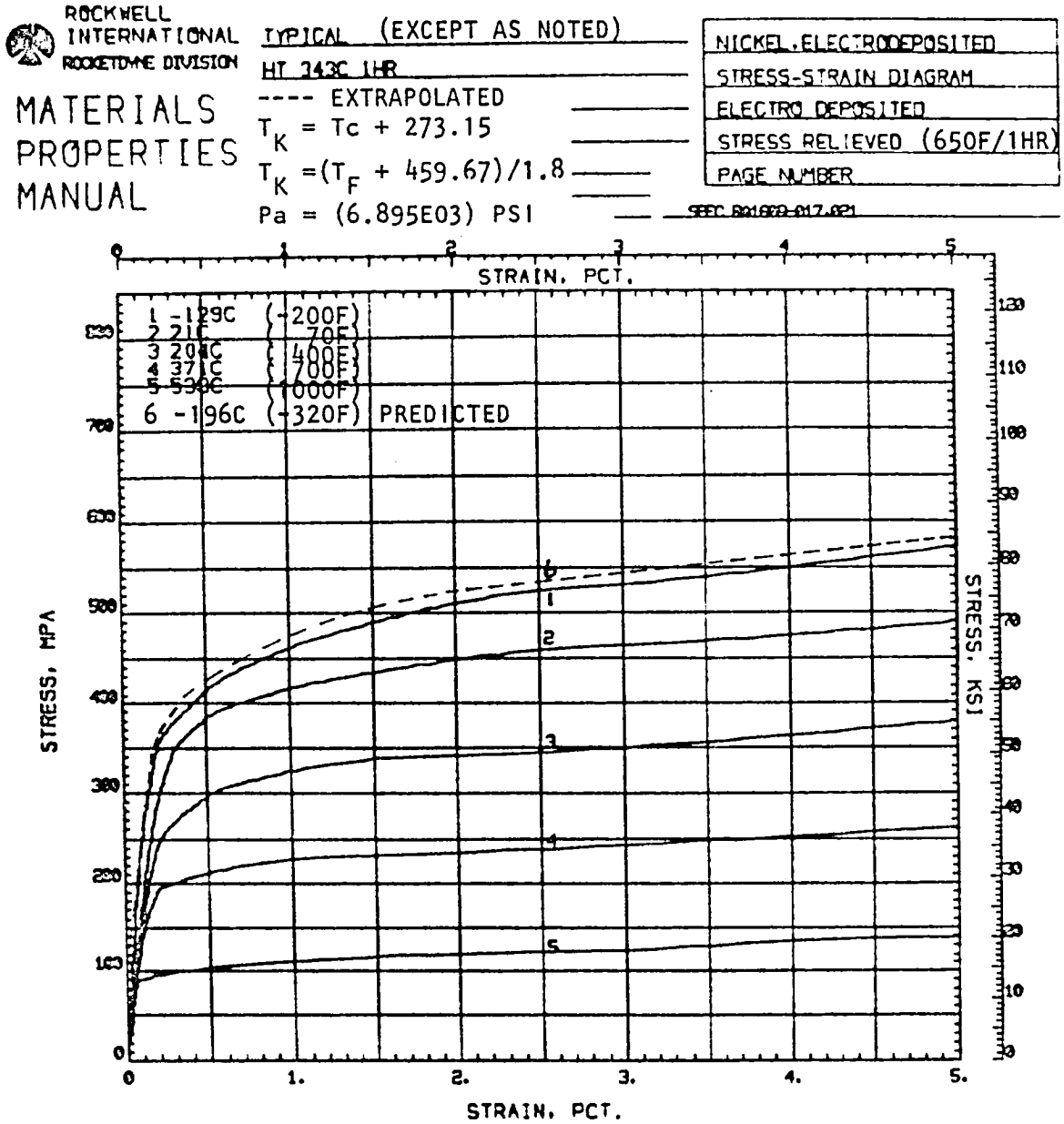

Figure 96. EDNi Stress-Strain Diagram

$T_K = Tc + 273.15$

$T_K = T_F + 459.67)/1.8$

Pa = (6.895E03) PSI

ROCKWELL INTERNATIONAL
ROCKETDYNE DIVISION

MATERIALS PROPERTIES MANUAL

PREDICTED MINIMUM HT 343C 1HR TEST DATA/GREATER THAN 2 FOR -196C THRU 21C MJS/GREATER THAN 3 FOR 260C TO 538C SEE NOTE A

DATE-9-1-77
REFERENCE-C321-63
2ND EDITION PAGE-6.3.1.1.2.78

6001.34.70.60-01

NICKEL,ELECTRODEPOSITED
LOW CYCLE FATIGUE
ELECTRO DEPOSITED
STRESS RELIEVED (650F/1HR)
PAGE NUMBER

SPEC PA1000-017.0P1

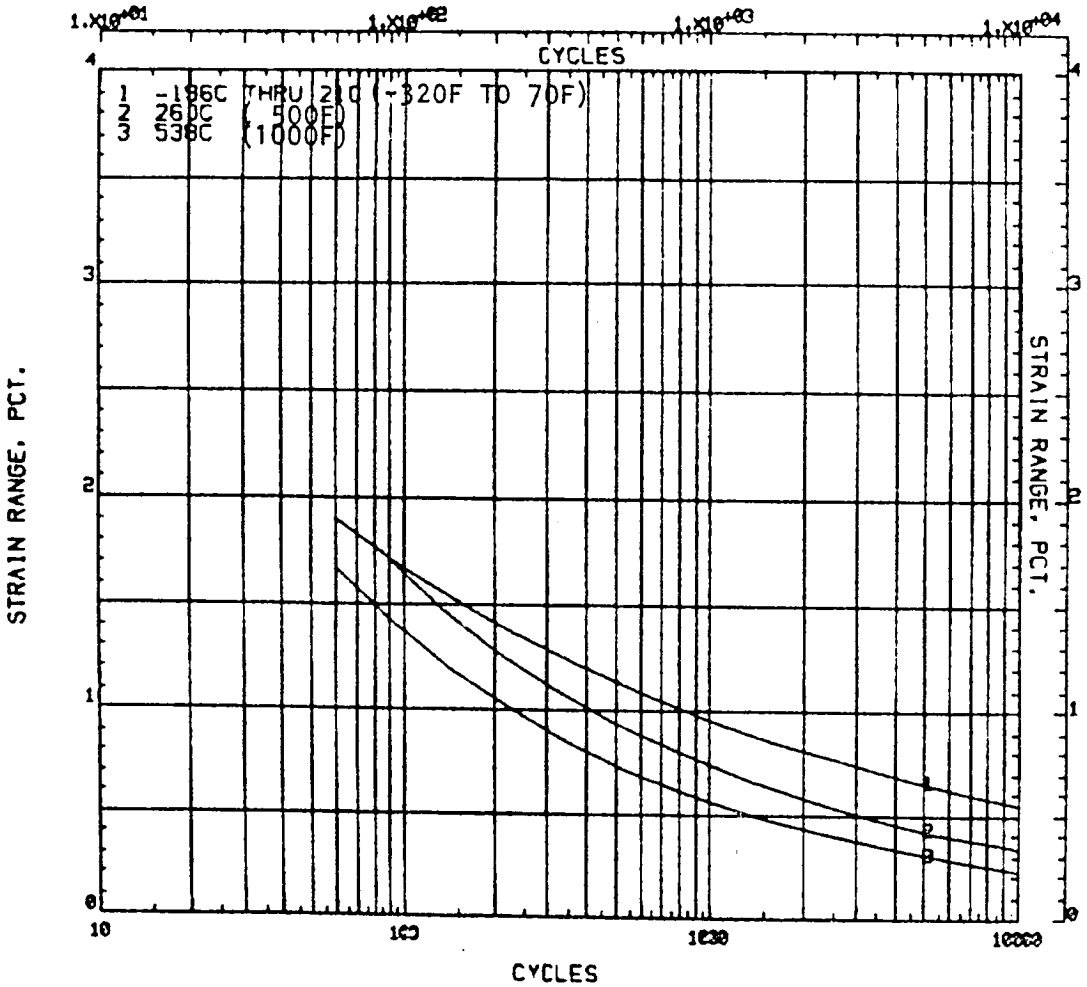

Figure 97. EDNi Low Cycle Fatigue

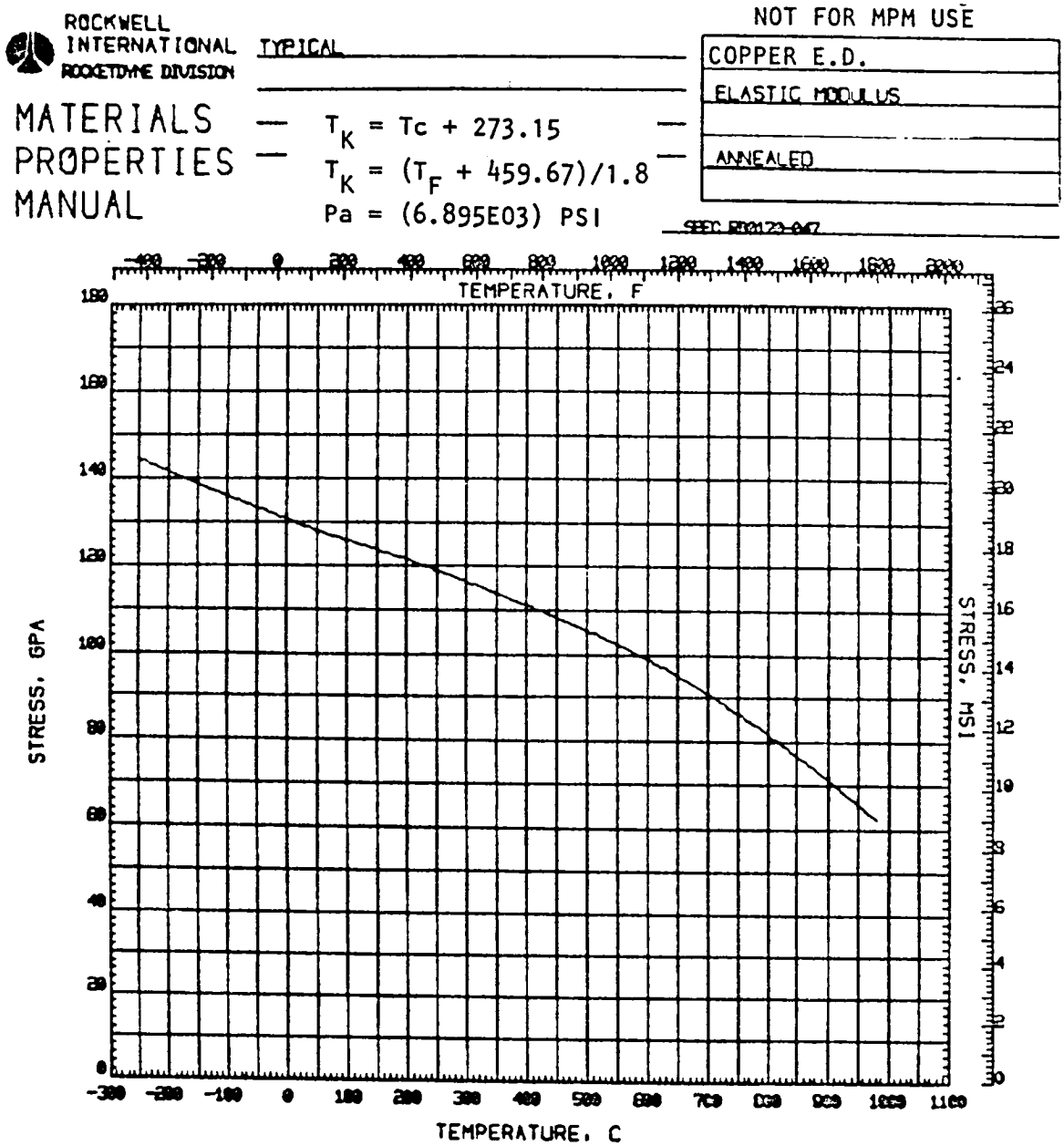

Figure 98. EDCu Elastic Modulus

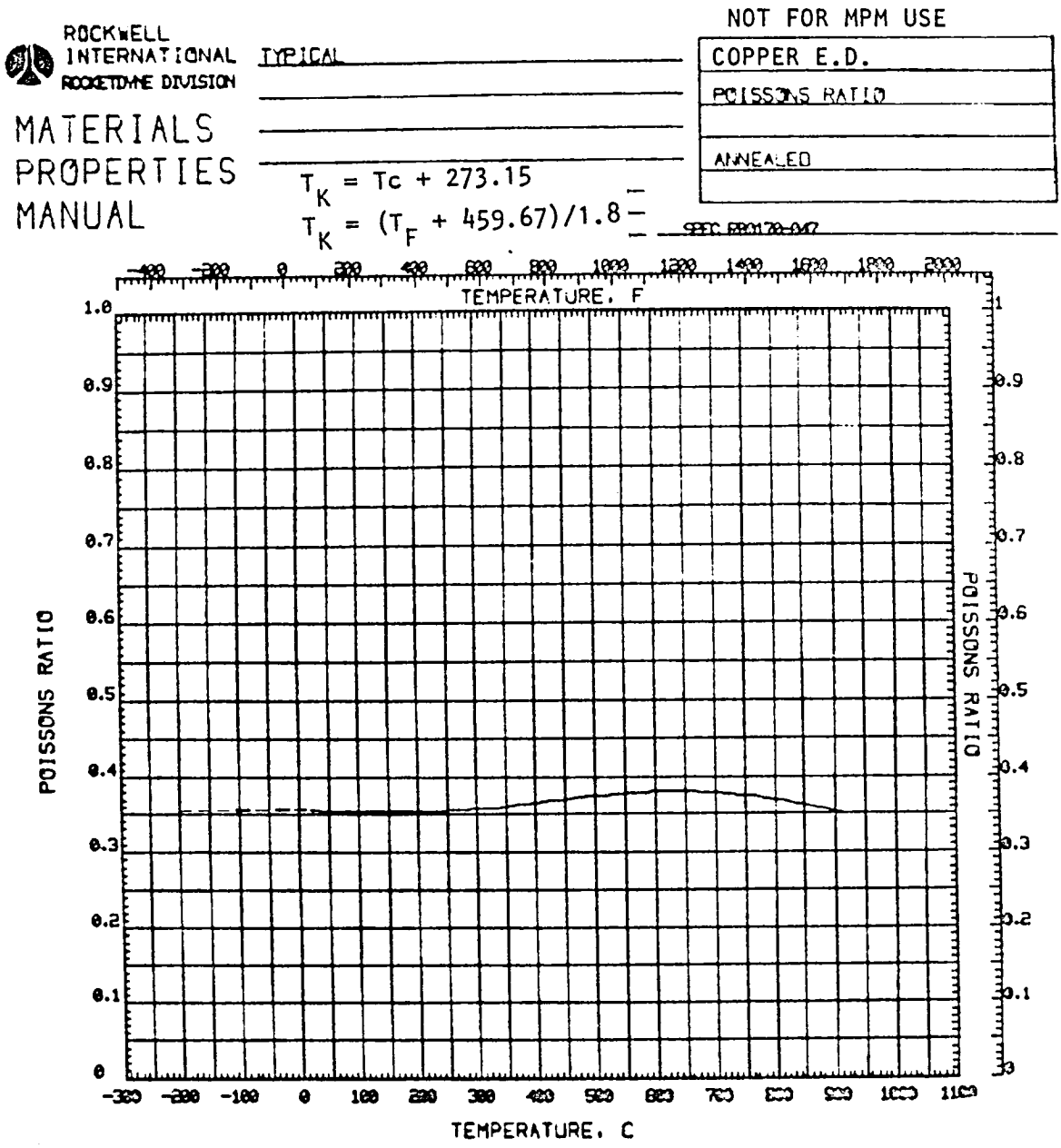

Figure 99. EDCu Poisson's Ratio

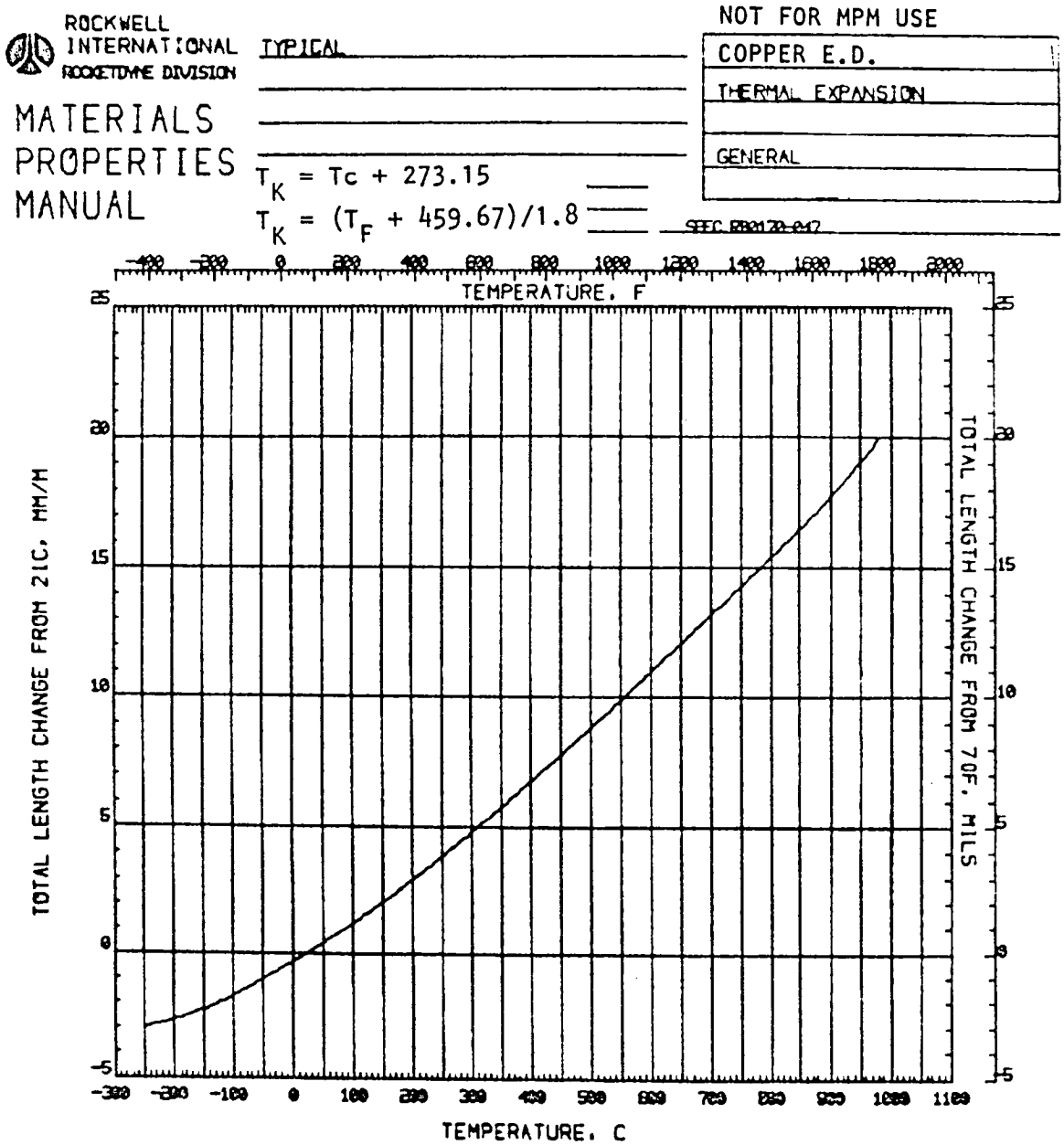

Figure 100. EDCu Thermal Expansion

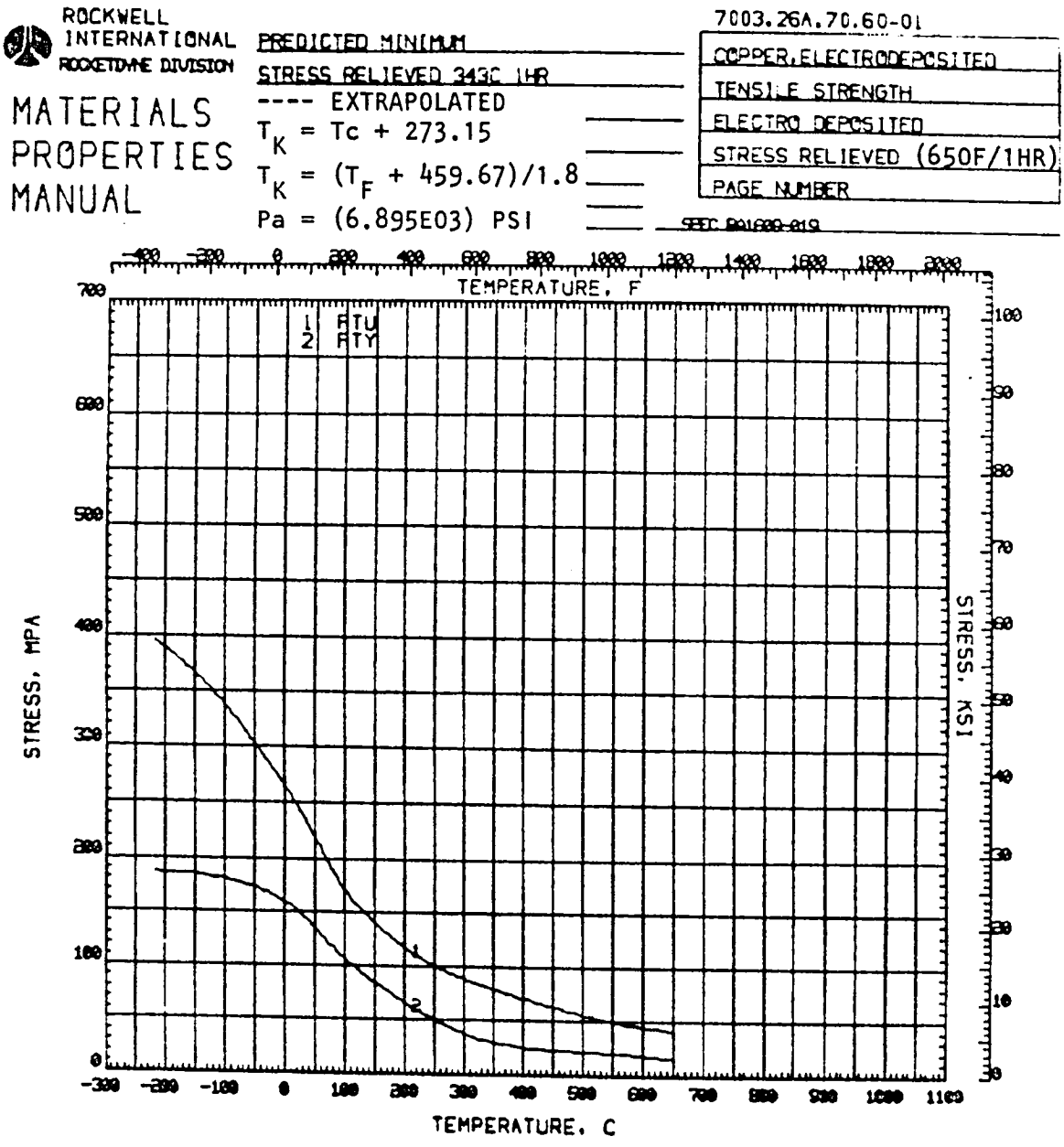

Figure 101. EDCu Tensile Strength

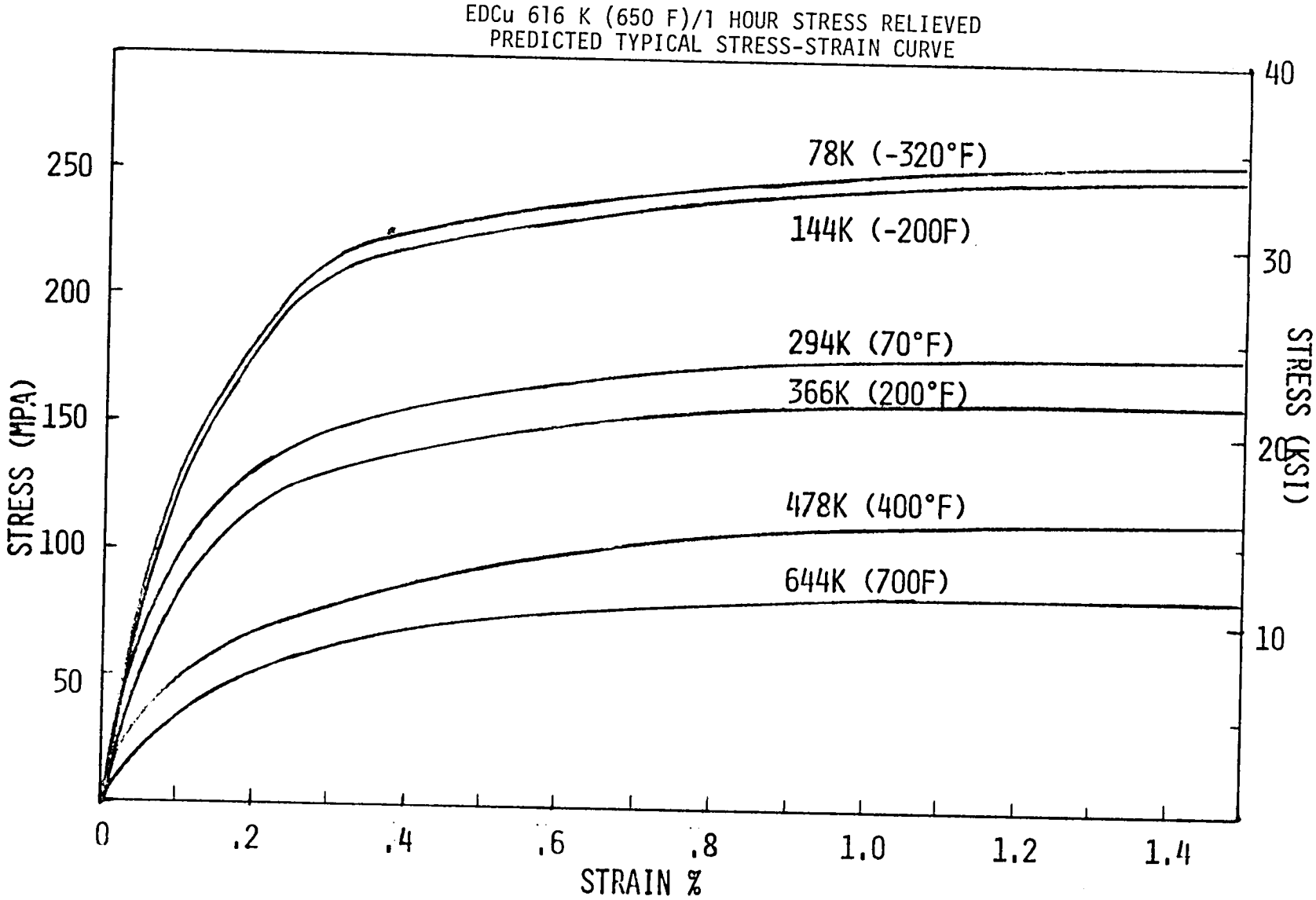

Figure 102. EDCu Stress-Strain Diagram

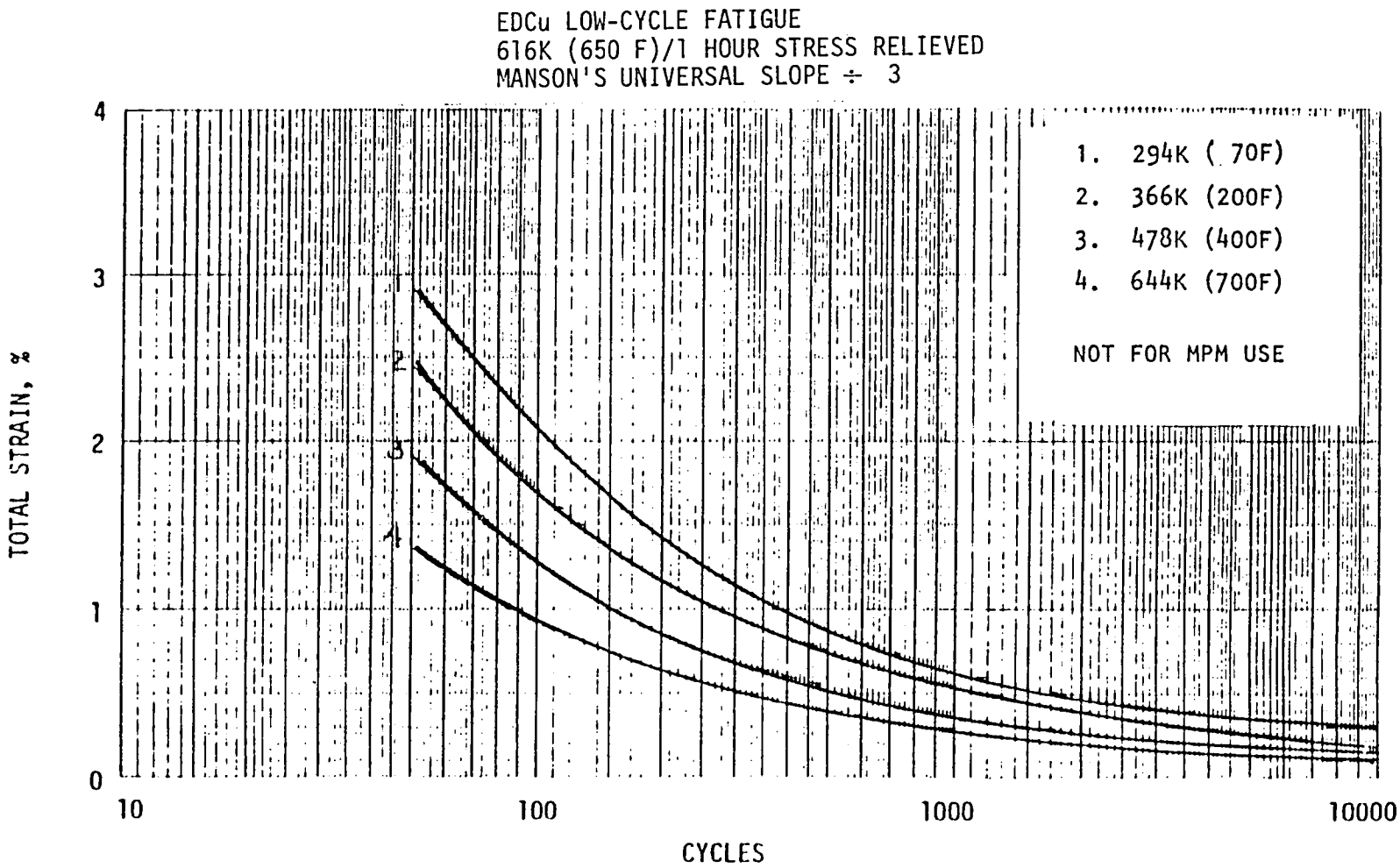

Figure 103. EDCu Low-Cycle Fatigue

Usually, when nominal materials properties are evaluated, the concepts of engineering stress (s) and engineering strain (e) are employed. However, since dimensions do change as the load is applied, calculations of engineering stress and strain are subject to errors. To provide a more accurate measure of stress and strain, the quantities true stress (σ) and true strain (ε) have been defined in the following way: True stress S is the actual stress based on the actual area A corresponding at every instant to the current value of load P.

The relationship between true stress and strain and engineering stress and strain can be expressed as follows:

$$\sigma = S\ (1 + e) \qquad \text{(valid up until necking)}$$

$$\varepsilon = n\ (1 + e)$$

Using the above relationship, a comparison of the true stress/strain curve versus the engineering stress/strain curve showed only a small difference for NARloy Z (Fig. 87). Engineering stress/strain curves were used for the structural analysis.

3. Life Prediction

a. Low Cycle Fatigue

The low cycle fatigue life was predicted for NARloy-Z in the STA condition at 978 K (1300 F) and 1089 K (1500 F) based on Manson's Universal Slopes (MUS) equation. However, service at such a high temperature is well into the creep range of the material. Also, tensile properties for all the temperatures of interest are not available since 1500 F is close to the solution temperature of NARloy-Z. Therefore, extrapolated values were used. But even if tensile properties were available, tensile strength and ductility is very sensitive to strain rate in the creep range and their values would depend on the rate at which the strain is applied in the tensile test. Therefore, it is reasonable to assume that some time factor would have to be introduced into the analysis. Manson's Universal Slopes method does not take this into account.

In general, attempts to predict high temperature fatigue behavior in the creep range by using tensile test properties at the temperature of interest result in predictions of unconservative lives that are obtained by fatigue test. Part of this discrepancy is due to the large creep component at high temperatures. As an attempt to account for creep-fatigue interactions, Manson suggests a 10% rule at high temperatures (Ref. 17). LCF life is taken as 10% of the predicted value. But for NARloy-Z, MUS yields an unconservative slope which crosses test data. Available test data from 294 to 866 K (70 to 1100 F) show an increasing slope with temperature for a log percent total strain range versus log cycles to failure plot (Fig. 88). This is probably due to an increase in the amount of creep damage at the higher temperatures.

Another approach to high temperature life prediction is based on linear summation of time dependent creep damage and cycle dependent fatigue damage, with failure anticipated when the total damage, equals a given value (in many cases unity for convenience (Ref. 18). This model assumes that fatigue and creep are linearly interactive. But for high temperature life prediction, the linear damage summation rule must be used carefully since it depends upon the amount of mixing of the damage components, as well as the order of damage for a given material and temperature. Plumtree and Abdel-Raouf studied the effects of first imposing one type of damage (e.g., fatigue) followed by the other type of damage (e.g., creep-type) to failure (Ref. 19). It was found that the amount of damage which occurred during the first operative damage mechanism had no influence on the amount of damage accumulated in the following block if the two mechanisms were different. For OFHC copper at 811 K (1000 F), linear summation to failure may vary from less than 0.4 for maximum interaction to greater than unity for little or no interaction of the damage mechanisms.

Hirschberg-Halford-Manson predicted life during high temperature fatigue by partitioning the creep and plastic strains in each hysteresis loop and linearly summing their respective damage contribution (Ref. 20). An attempt at using this method yielded appproximately the same results as MUS. Also, there was not enough data to predict all the damage fractions. But this, too, is an idealized method, because only damage associated with plastic strains are summed.

Since none of the life prediction methodologies can accurately account for creep-fatigue interactions, the NARloy-Z prediction at 978 K (1300 F) and 1089 K (1500 F) are merely a best-guess estimate taking into account the slope determined from test data.

b. Creep

Creep in many materials at intermediate stress levels can be described by a power law creep expression (Ref. 21 - 23).

$$\varepsilon = K \sigma_a^n \exp(-Q_{app}/RT) \quad (1)$$

where ε_s the steady state creep rate, K is a material constant, σ_a is the applied stress, n is the stress exponent for creep, Q_{app} is the apparent activation energy for creep, R is the gas constant, and T is the absolute temperature. At a given temperature, the above equation can be reduced to the following assuming K to be independent of creep strain:

$$\varepsilon_s = A \sigma^n \quad (2)$$

where A is a constant at a given temperature

$$\therefore A = K \exp. \frac{-Q}{R} \quad (3)$$

A plot of log creep rate versus log stress will generate a straight line with the slope being the value of the stress exponent if Eq. 2 holds.

Values of the stress exponent n and the material constant A of NARloy Z for the temperature range 644 to 922 K (700 to 1200 F) were taken from Ref. 24. The values were based on test data. Values at 1089 K (1500 F) were estimated.

Exponent n at 1089 K (1500 F) is based on extrapolation of the stress exponent versus temperature data given in Ref. 24. Extrapolation resulted in a value of 4.6 at 1089 K (1500 F).

The constant A at a given temperature can be calculated from the following relationship:

$$A = K \exp \frac{-Q}{R}$$

where,

K, for NARloy Z $\simeq 1.6 \times 10^{16}$
Q, activation energy = 110×10^{3} cal/mole
R, Universal Gas Constant = 1.98 cal/mole K
T, Temperature = 1089 K (1500 F)

Substitution of these values in the above equation yields the value of A as 1.10×10^{-6}.

APPENDIX C

EXTRAPOLATION IMPLEMENTATION*

The APSAC analysis system accounts for deformed geometry and inelasticity through a total Lagrangian approach that utilizes the geometry changes from the previous loadings and the historical information related to inelastic strains and yielded surface. The overall capability already existed for sequential analysis of a duty cycle through the use of a restart dataset, so the incorporation of the extrapolated geometry into the analysis was rather straightforward. The most important point was to define the overall extrapolation requirements and determine how to best implement them into the available programs. The requirements for this task included:

1. Being able to output a displacement dataset at the end of specified duty cycles
2. Combining and merging separate displacement datasets for use in the extrapolation
3. Extrapolation from a series of duty cycles to a specified future duty cycle
4. Plotting extrapolated geometry
5. Generation of an equivalent dataset for use with the APSAC code to restart the next analysis sequence

After reviewing the available codes and how they interact, the block diagram strategy was developed for the extrapolation, as shown in Fig. 104. The top half of the page outlines the current applicable codes and their interaction. Basically, a dataset was output from APSAC that included all information for future identification of the job (input dataset), all necessary arrays for restarting the job for the next load increment, and output results for plotting. This dataset also has other uses such as the input to the STAMP code to generate geometric data for the DEAP thermal code. This methodology was used for this analysis so that the thermal and structural models were identical, and the temperatures could be properly accessed from the DEAP datatape.

The output dataset is currently accessed by APSAC for two separate purposes: one (Tape 11) is for restarting a job for additional loading increments or changing the geometry, and the other (Tape 13) is for reading in a field of displacements that can be used as fixed boundary displacements. This dataset is also used in the plot code as part of the displacement accumulation.

The simplest method for accomplishing the extrapolation technique was to incorporate it as an option of the plot program. This code already read and searched the dataset for displacement information, and would be readily changed to output displacements and generate a modified dataset for plotting and for generating a restart dataset with the proper displacements.

*This effort was funded by Rocketdyne.

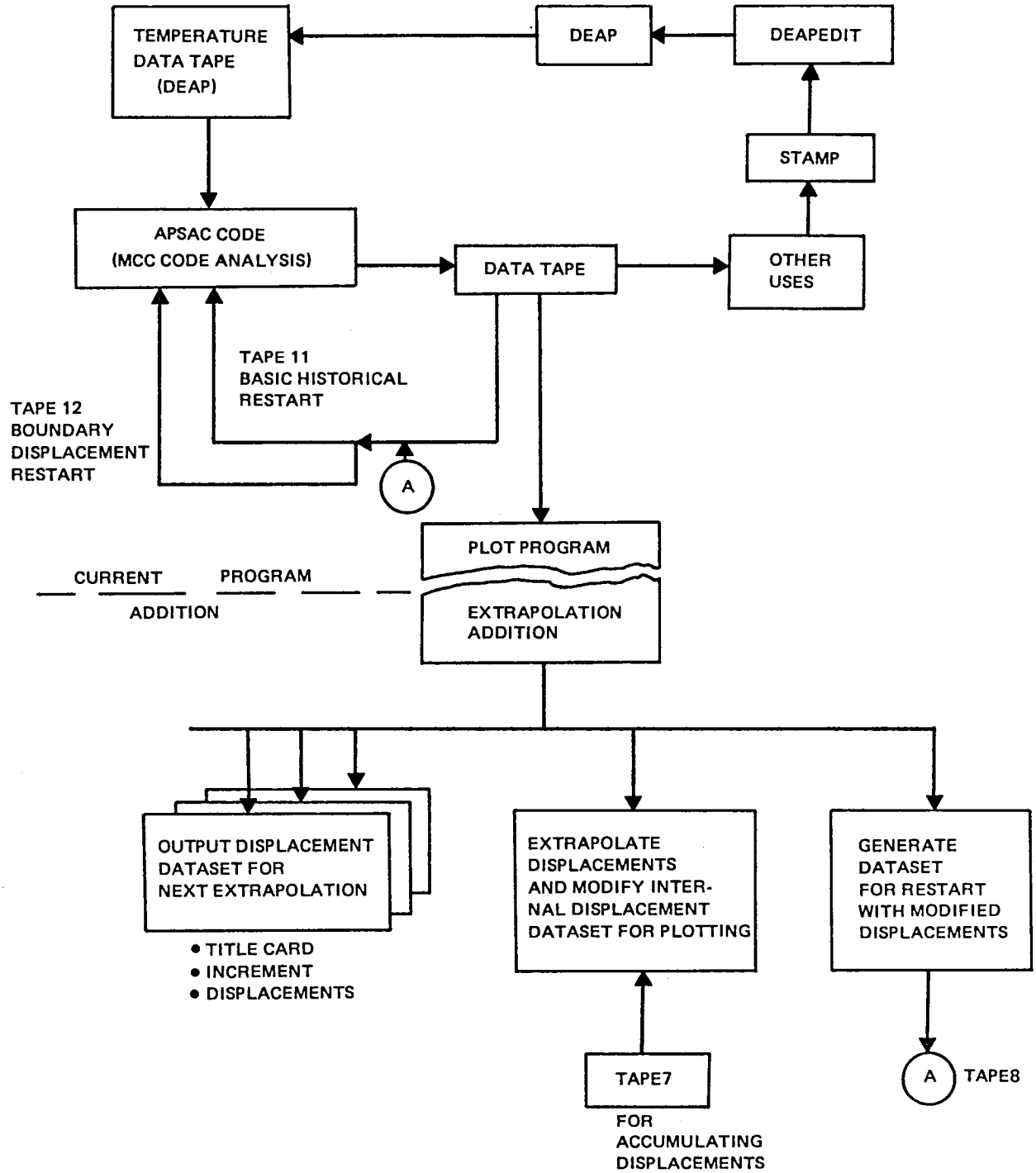

Figure 104. Block Diagram of Strategy for Incorporating Extrapolation Technique

Figure 105 shows the concept of the duty cycle analysis for five increments, an extrapolation and the restart for the next series of increments. Two options are listed, but only option 1 has been used for the contract analysis. The accumulated displacements from the extrapolation tape were added to the initial geometry, and the stresses and strains on the part were initialized to zero. Essentially, a new analysis with a distorted geometry and no strain history.

Option 2 is for experimental use to evaluate whether a forced distorted shape with or without the history of strains from the last increment prior to the extrapolation can be used to minimize or eliminate the restart shakedown observed in the analysis. A future option could be to add extrapolation of inelastic strains, etc., to get a more accurate restart condition.

The extrapolation code evolved through the addition of several options to allow flexibility in positioning the model in the appropriate radial displaced position. Working through the first model from 1 to 120 duty cycles identified the need for this flexibility to account for the initial liner gap and the liner movement away from the jacket during multiple duty cycles. These considerations were required since the liner is not attached to the jacket, except at its ends. At the start of the analysis, there is an initial 0.020 tolerance gap. During the first duty cycle, the liner cross-section yields and radially displaces to meet the jacket motion. At the end of the first duty cycle, the liner is firmly compressed against the jacket. During the succeeding cycles, the liner has additional relaxation that reduces the compression against the jacket. This was essentially a small rigid body motion of the total model. Even though this motion is small, it was significant compared to the displacements of the rest of the geometry. During the extrapolation process, both this rigid body motion, as well as local distortions, were extrapolated and pulled the liner away from the jacket. The actual hardware, though, only relaxes the liner to some stable point--where the gross yielding of the liner is balanced by the relaxation effects. The actual liner motion is nonlinear, whereas the basic extrapolation technique is linear. Options have been added to the extrapolation code to subtract out rigid body motion, move the model into position, and adjust fixed boundary node positions to properly adjust for the true hardware motions. Essentially what was done was to allow the liner to yield up against the jacket in the first 1 to 5 duty cycles. Then, as part of the extrapolation technique, a rigid body motion was added to the model, such that one of the nodes in the liner that touches the gap element was held against the jacket. The gap element node positions were also adjusted to a compatible position. These displacements were then used to update the geometry for the 21st duty cycle. The same procedure was used as part of the next extrapolation with the addition of the accumulation of the current extrapolated displacements and the displacements that were used to start the 21st cycle. The latter technique is repetitively applied for the remainder of the analysis to develop the distorted geometry. This procedure is pictorially shown in Fig. 106.

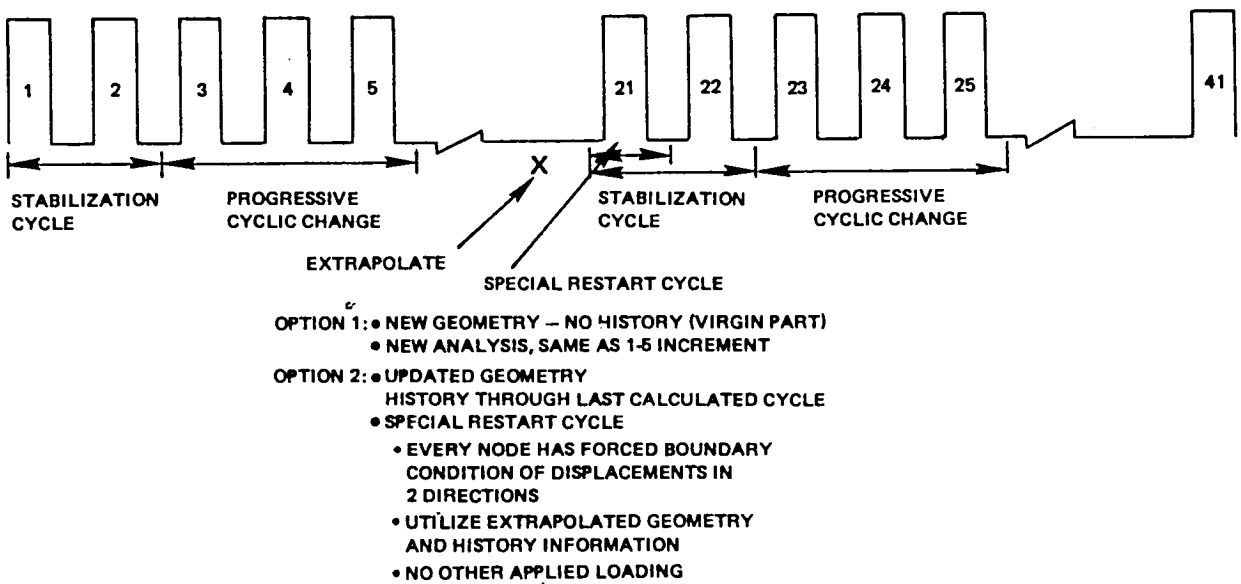

Figure 105. Duty Cycle Analysis Concept

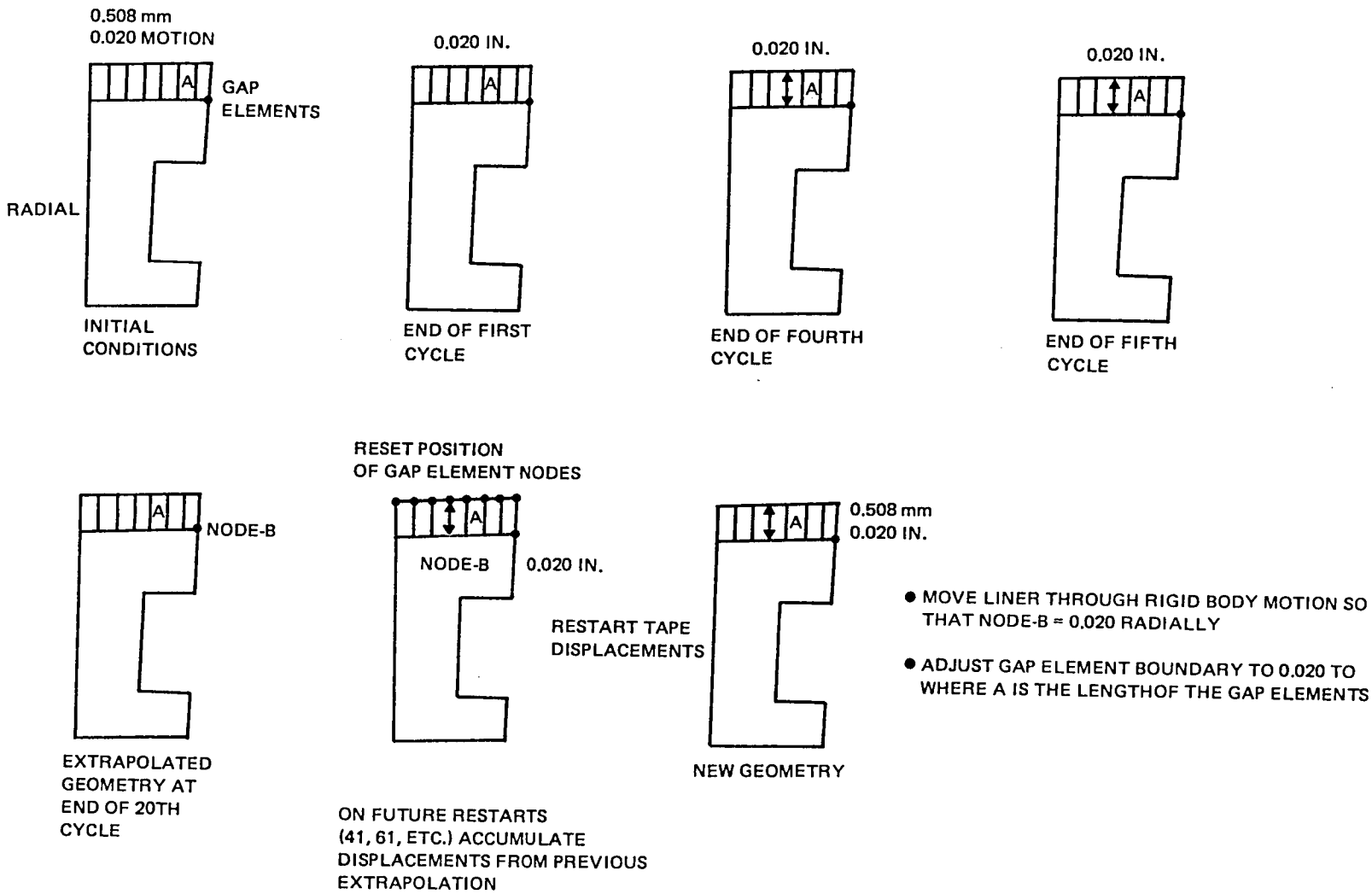

Figure 106. Extrapolation Detail Model Runs

The plot program input revisions to add the extrapolation technique are included in the following pages. These can be run as a separate job or intermixed with a standard plot data deck. For traceability, it is simpler to run the extrapolation as a separate computer job.

The details of the data card inputs follow.

CARD 1:	TITLE CARD
NO. REQUIRED:	One card per load increment of APSAC analysis. Title and terminater card must be present whether or not increment is considered for extrapolation or plotting.
FUNCTION:	Title used on each CRT within the current load increment
FORMAT:	18A4

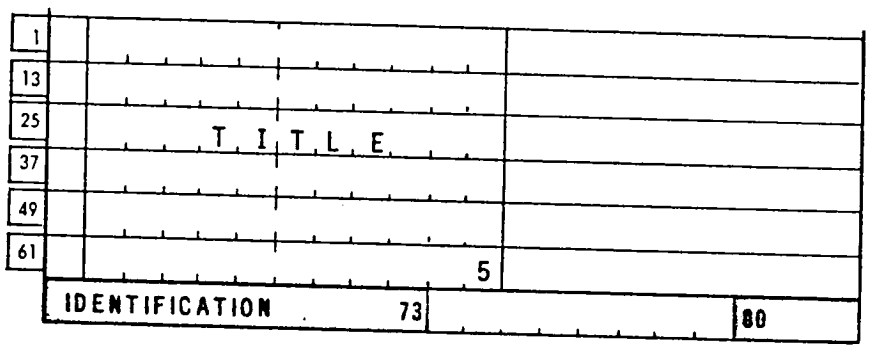

CARD 1: TITLE CARD

"5" in column 72 must be present on the title card for the first increment (first card in data deck) to write displacements on Tape 4 for later use in extrapolation procedure.

EXTRAPOLATION

CARD 2: CONTROL CARD

NO. REQUIRED: One card for each increment from which displacements are to be written to Tape4

FORMAT: (I4, 2I1, I2, I3, 4E6.0, 9A4)

Column	Format	Variable	Description
1 - 4	I4	LDEL	u_z Ref. node as described in Table G-1.
5 IGRID = 6, 7, or 8, read in card 2	I1	IGRID	IGRID=5 - Displacements for current increment are written on Tape4. =6 - Extrapolate displacements to Nth increment, using this and the previous increments from Tape4 =7 - Extrapolate to Nth increment using this and the previous increments from Tape4. Subtract the rigid body displacement =8 - Extrapolate to Nth increment using this and the previous increments from Tape4. Options include: 1)node no. to keep to a specified displacement (DISP) 2)nodal displacements to directly replace the extrapolated value.
6	I1	ITYPE	ITYPE=value=order of extrapolation for IGRID=6, 7, or 8
7 - 8	I2	IFUN	Not Used
9 - 12	I4	NNC	NNC=value=increment identification for Tape4
13 - 36			Not Used
37 - 72	9A4	LABEL	Title Printed

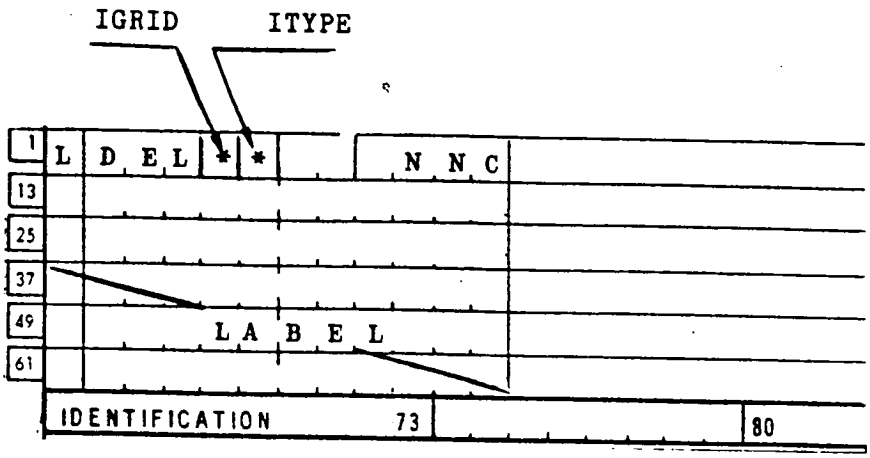

CARD 2 One for each increment where displacements are to be written on Tape4

CARD 3: EXTRAPOLATED CYCLE CARD

FUNCTION: Immediately follows any extrapolation card where IGRID=6, 7, or 8, to define the number of the cycle where extrapolated data is desired.

1		NINCR, MINCR	
13		NODE, NDISP	
25		UXDISP	
37		UXDISP	
49		IFLAG	
61			
	IDENTIFICATION	73	80

DISPLACEMENT data from the current increment and displacement data from TAPE4, either from previous increments of same job, or saved from a previously run job, and the selected order of extrapolation are used to calculate the displacements at "NINCR." These may be saved on "TAPE8" and used for restart purposes. "TAPE8" has the same format as "TAPE10," generated by APSA or APSAC. TAPE8 then has accumulated displacements up to the duty cycle at the end of the current extrapolation. Only 1 increment is generated on TAPE8*. When accessing this tape for restart, request the first increment.

*TAPE8 has the stress and strains from the local increment from which the extrapolation is generated, plus the extrapolated displacements.

CARD 3

REQUIRED FOR IGRID							
6	7	8	COLUMN	FORMAT	VARIABLE	DESCRIPTION	
X	X	X	1-6	I6	NINCR	INCREMENT WHERE EXTRAPOLATED DATA IS DESIRED	
	X		7-12	I6	MINCR	INCREMENT TO BE USED AS REFERENCE ZERO FOR RIGID BODY DISPLACEMENT REMOVAL (MINCR=0, USE AVERAGE OF ALL PREVIOUS INCREMENTS)	
	X	X	13-18	I6	NODE	IGRID=7, NODE NUMBER TO BE USED AS REFERENCE ZERO FOR RIGID BODY DISPLACEMENT REMOVAL, IGRID=8, NODE NUMBER TO BE KEPT TO A SPECIFIED DISPLACEMENT (UXDISP, UYDISP)	
		X	19-24	I6	NDISP	NUMBER OF DISPLACEMENTS TO BE READ IN AND DIRECTLY REPLACE THE EXTRAPOLATED VALUES (SEE NEXT CARD)	
		X	25-36	E12.0	UXDISP	FIXED DISPLACEMENT VALUES WHICH WILL BE ASSIGNED TO NODE "NODE" CAUSING THE REST OF THE DISPLACEMENTS TO BE TRANSLATED BEFORE EXTRAPOLATION	
		X	37-48	E12.0	UYDISP		
X	X	X	49-54	I6	IFLAG	IFLAG=1, READ IN DISPLACEMENTS FROM TAPE7 (OLD TAPE8) AND ADD TO CURRENT EXTRAPOLATED DISPLACEMENTS	

CARD 4: DISPLACEMENT CARD

NUMBER REQUIRED: "NDISP"

FUNCTION: To replace displacement values after extrapolation with the specified input value

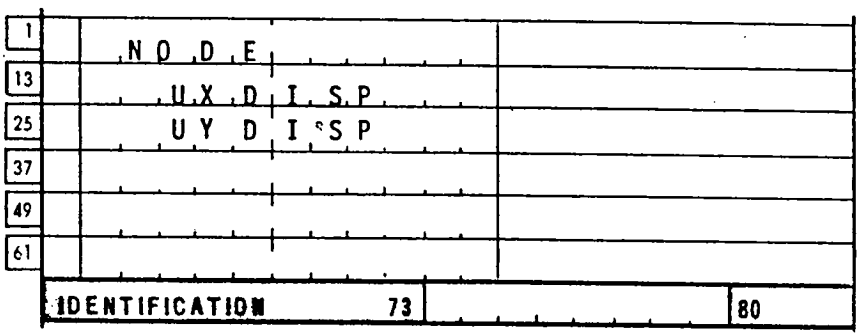

CARD 4

COLUMN	FORMAT	VARIABLE	DESCRIPTION
1-6	I6	NODE	NODE NUMBER FOR REPLACING THE DISPLACEMENT UX (OR UR) AND UV (OR UZ) AFTER EXTRAPOLATION
7-12	I6	--	NOT USED
13-24	E12.0	UXDISP	NEW UX DISPLACEMENT VALUE FOR NODE "NODE"
25-36	E12.0	UYDISP	NEW UY DISPLACEMENT VALUE FOR NODE "NODE"

Increment Termination

CARD 5: Increment End Card for APSAC

NO. REQUIRED: One to end each load increment

FUNCTION: Terminates a load increment. Terminates the repeat plot card set. Specifies that the repeat plot set is to be used in this load increment

Column	Format	Variable	Description
1 - 4	I4		Not used
5	I1	IGRID	IGRID = 2 Terminate the load increment
6	I1	ITYPE	ITYPE Non Blank, Plot the repeat dataset in the current increment
6 - 36			Not used
37 - 48	A12		"END PLOT SET" specified on the end card used to terminate the repeat plot card data set
49 - 72			Not used

INCREMENT END CARD FOR APSAC

IGRID ITYPE

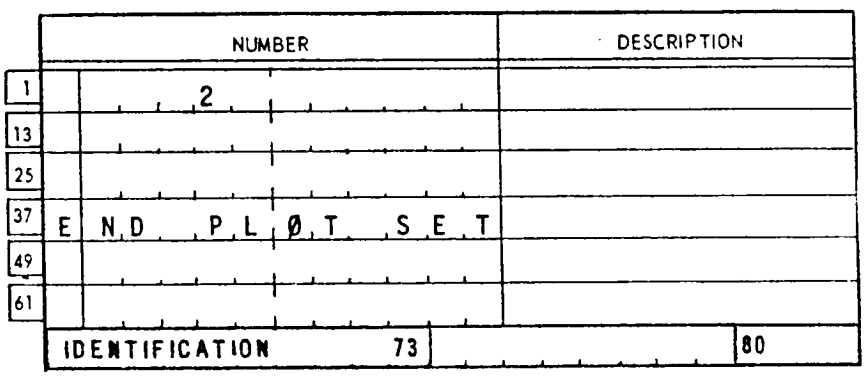

APPENDIX D

FINITE ELEMENT MODEL

INTRODUCTION

The APSAC--Axisymmetric and Planar Structural Analysis (APSAC) with Creep code and associated system of programs were utilized for this study. Ths code has the capability (options) for accounting for deformed geometry and inelasticity through use of a total Lagrangian approach that utilizes the geometric changes through a duty cycle, as well as a kinemetic strain hardening flow rule for tracking the stress and strain history of the analysis. The code is part of an integrated set of codes for structural and thermal analyses that allowed optimization of the entire analysis. This was an important factor in being able to complete the study within cost and time constraints. The total analysis requires a large number of individual model runs, plus extrapolations. In order to accomplish these objectives, the overall study was reviewed, and a strategy developed to efficiently set up, track, and process the models. The basic philosophy was to organize the study so that it could be used, not only for this effort, but for future use on advance design or production analysis. This appendix discusses the details of the finite element model (FEM) and the strategy for processing the jobs. The thermal model is closely related to the structural model in that the same finite element model is used to develop the nodes, connectors, volumes, etc. for the thermal analysis. This results in an efficient one-to-one correspondence between nodes of the two models, and allows the structural model to assign temperatures to nodes from specified time slices in the thermal duty-cycle analysis. The one-to-one node match was used in an APSAC code modification to allow the thermal field to track the structural model as it distorts.

Structural Model

The primary structural model of concern is the 2D generalized plane strain model of the coolant liner. The jacket model will not be discussed in detail, since it is only used to furnish boundary displacements and the out-of-plane total strain for the various duty-cycle increments. The basic model and analysis considerations are summarized in Fig. 107. The FEM model is one-half of a channel cross-section (Fig. 108). The model has symmetry boundaries on both circumferential edges. The basic model subtends an angle of 0.46154 degrees, since it is one-half of one of the 390 channels that comprise the 360 degrees total circumference (1/2 x 360/390). The inner edge (inside diameter) of the model is pressurized at chamber pressure, P2, and the coolant channel is pressurized to hydrogen coolant pressure, P1. The pressures are consistent with a location that is 1.2 inch forward of the MCC throat. Pressure is denoted by a V on the model pointing in the direction of positive pressure. The B and E signify the sliding boundary condition definition, and the C signifies the structural jacket boundary condition.

The liner has three materials--NARloy-Z (1), EDNi (2), and EDCu (3),--note the ( ) values are the material nomenclature used in the code. A fourth material (4) is used to specify the gap element identified as ISO=4 material in the

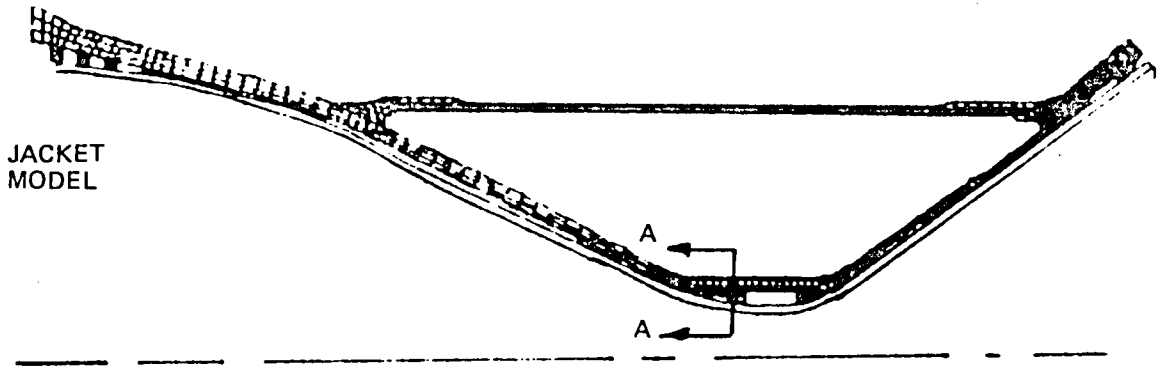

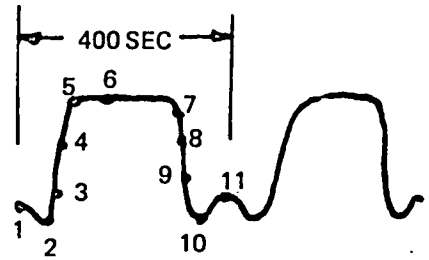

TYPICAL DUTY CYCLE

- DUTY CYCLE – 11 INCREMENTS
- CONSIDER
  - TEMPERATURES AND PRESSURES
  - JACKET RADIAL DISPLACEMENTS AND AXIAL RESTRAINT
  - INITIAL RADIAL LINER GAP 0.508 mm (0.020 IN.)
  - STRUCTURAL MODEL
    - PLANE STRAIN CROSS SECTION
    - INELASTIC MATERIAL – KINEMATIC HARDENING
    - GEOMETRIC DISTORTIONS
    - CREEP/RELAXATION
  - 5-CYCLE DUTY CYCLE ANALYSIS
  - EXTRAPOLATION TO 20-CYCLE GEOMETRY
  - RESTART WITH NEW GEOMETRY AT 21 CYCLE
  - ETC.

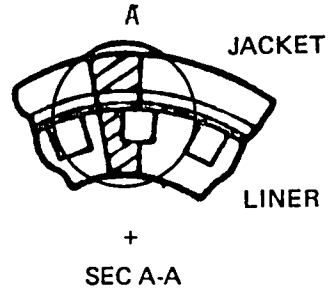

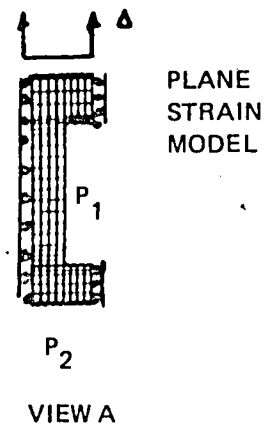

Figure 107. Analysis Basis

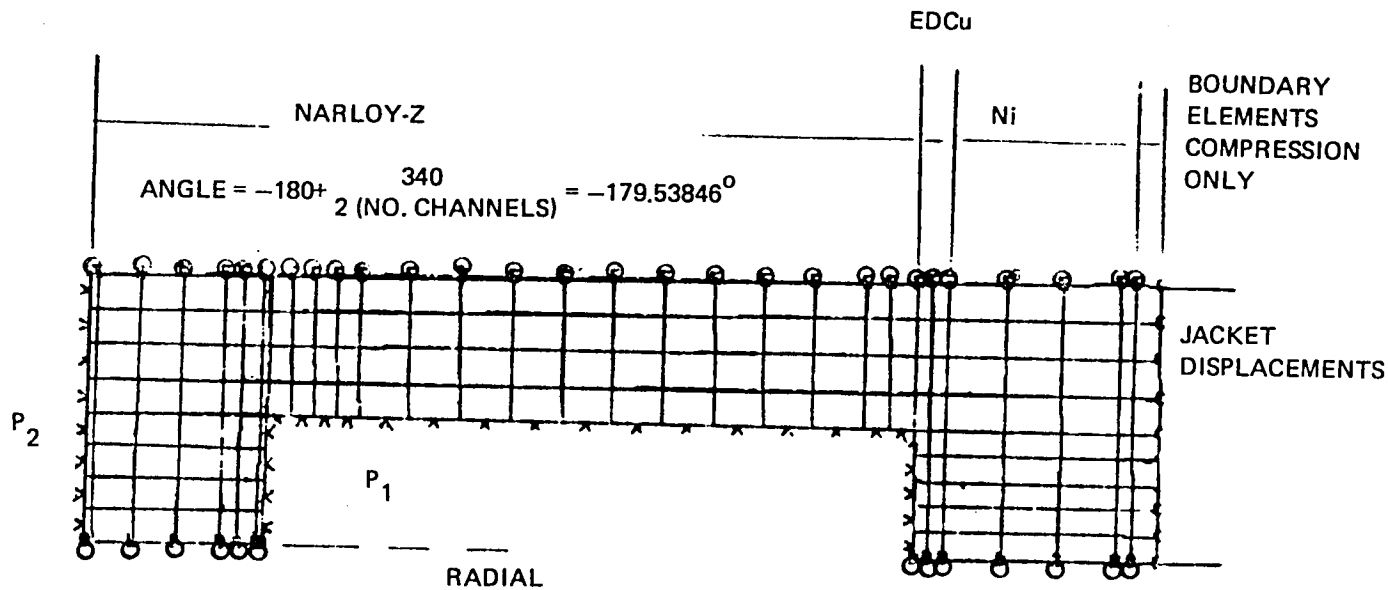

Figure 108. Cross-Section SSME MCC Liner

code. This material is stiff in compression but weak in tension and shear, which allows proper simulation of the liner-jacket interface. The model node and element numbers and material numbers are shown in Fig. 109. The materials used are isotropic, with bilinear stress-strain curve representation, which require temperature-dependent properties over the range of temperatures the model sees throughout the duty cycle. Each material has up to 8 sets of input specifying temperature, modulus, Poisson's ratio, coefficient of expansion, yield stress and tangent modulus ratio. The temperature increments are selected to best approximate the total set of properties that will be linearly interpretted for actual values of elements at intermediate temperatures. The bilinear stress-strain curves used are furnished in Fig. 110 and 111.

Where applicable, secondary creep constants are input for the materials. Only NARloy-Z has temperatures above the creep activation temperature, and has creep constants specified. Again, the creep properties are input at discrete temperatures to properly control the temperature interpolation. The material constants and creep relaxation data are obtained from the material curves included in this study. Table 9 shows the details in setting up the NARloy-Z creep constants in the format used by the code.

The rest of the model geometry definition consists of defining an (I, J) topology numbering system to relate the model grid and coordinates. Input to define materials and boundary conditions are then specified, and the code develops the node and element sequencing for the above information. Other inputs include the out-of-plane strain, displacements, pressures, and temperatures. For all runs, the temperatures are recovered from a thermal DEAP code datatape for every time slice, except the room temperature posttest increment 11. Each analysis run consisted of 55 increments used to define the 5 duty cycles (11 increments per duty cycle). Table 10 summarizes the duty cycle loading on the structure, except for thermal conditions.

Title and Control cards are input to specify analysis options. For these runs, the large deflection codes to control the analysis are specified as shown in Table 11. The codes define how the large deflection option is to be processed on each increment of load, and for restarting from a datatape. The creep increments are handled slightly different from the load-only increments, due to a code limitation that both creep and large deflections are not allowed within the time-dependent portion of the total increment. This is not a significant limitation in that the geometry is updated at the end of the creep increments--5 and 6. In the other loading increments, the geometry is updated throughout the calculation process.

The model was optimized and thoroughly checked as part of the initial study. This optimization included varying the model refinement to achieve acceptable accuracy in stresses and strains, as well as temperatures. The model, as was shown in Fig. 108 has variable size elements in the x-direction to pick up representative surface strains and strains in the channel wall to land-notch area. The same type variation was included in the EDCU notch zone to properly represent the inelasticity that occurs during the duty cycle. The model was exercised through a series of small deflection duty cycles with and without creep, and large deflection duty cycles with and without creep, to build up

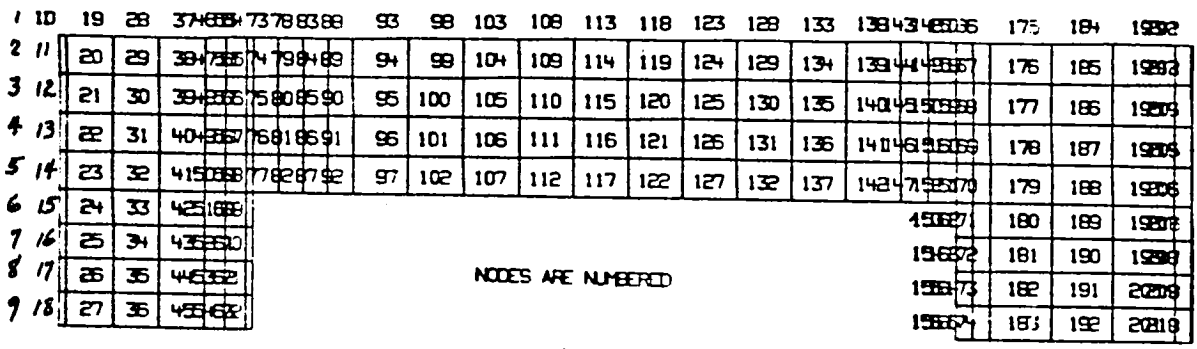

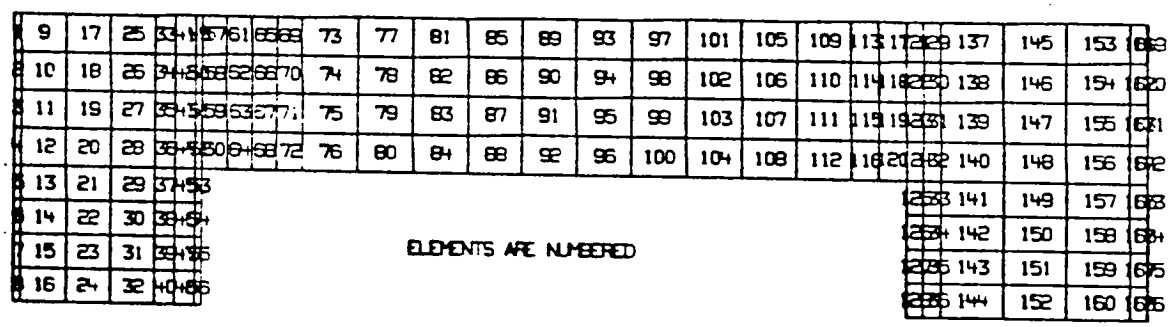

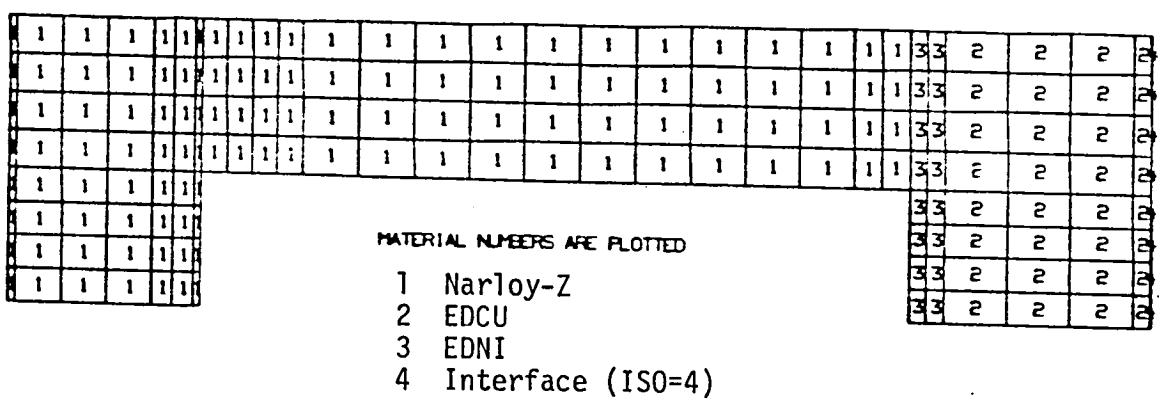

Figure 109. Nodal Network and Materials Identification

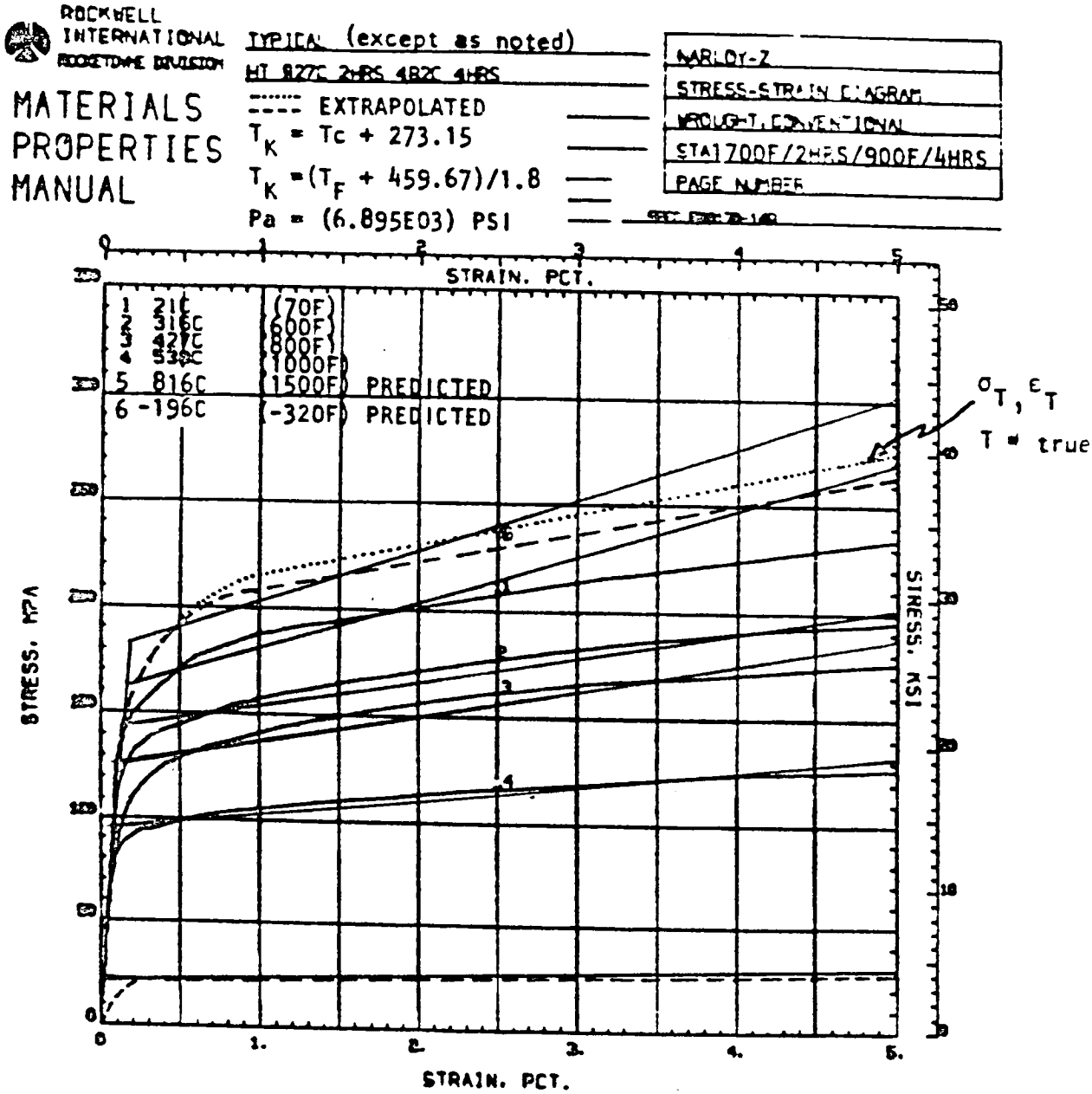

Figure 110. NARloy-Z Stress-Strain Diagram With Bilinear Curves

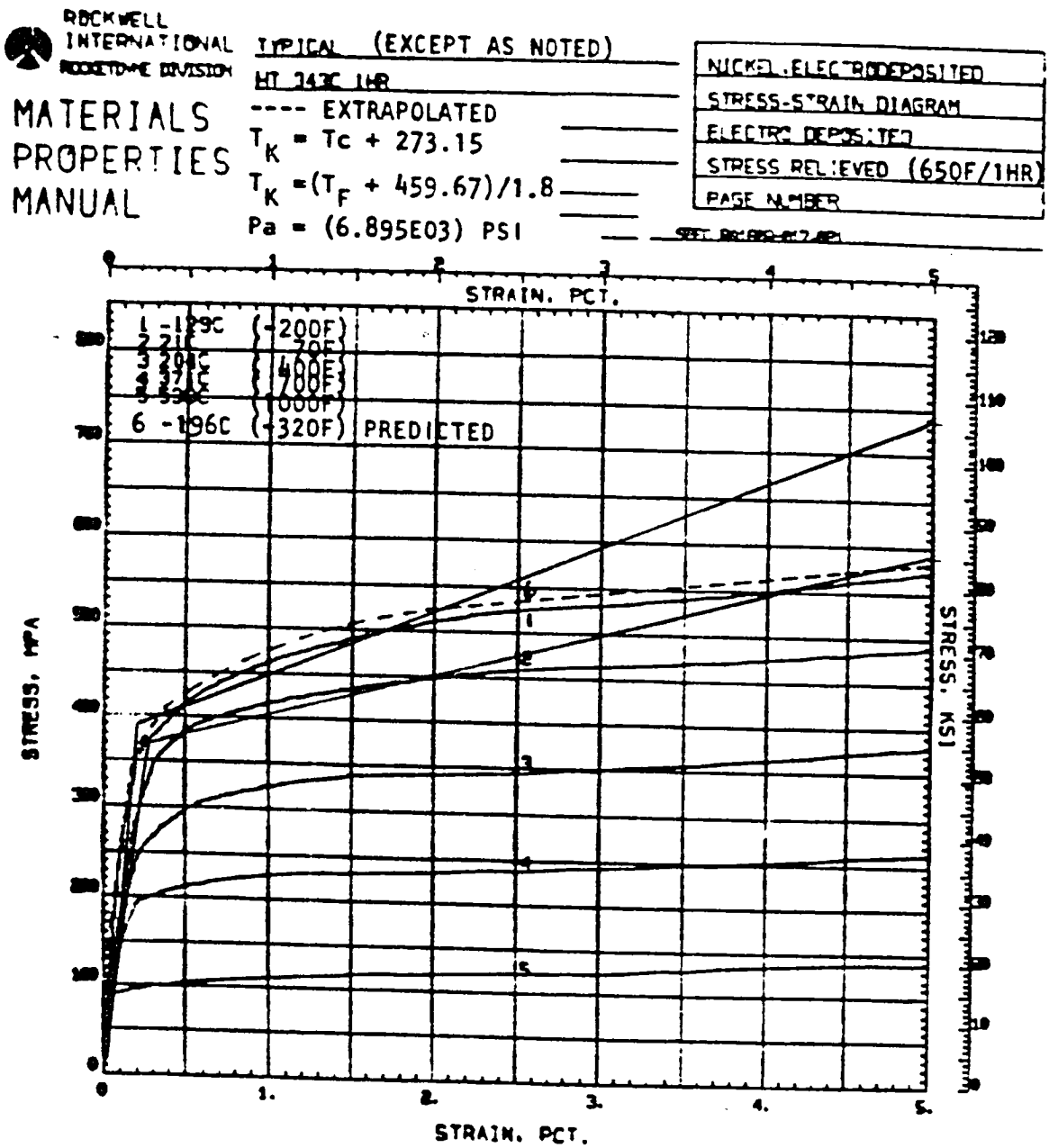

Figure 111. ED Nickel Stress-Strain Diagram With Bilinear Curves

TABLE 9. STRESS RELAXATION (CREEP) CONSTANTS

TEMPERATURE		E YOUNG'S MODULUS		n	A	A
K	F	MPTR 70-902	MATERIAL PROPERTIES MANUAL		MPTR70-902	ADJUSTED BY E*
22	-420		20.0×10^{6}	19.2	1.0×10^{-50}	1.0×10^{-50}
644	700.		16.2×10^{6}	16.1	2.9×10^{-31}	2.9×10^{-31}
811	1000.	22.9×10^{6}	14.9×10^{6}	12.5	6.2×10^{-16}	$\frac{22.9}{14.9}$ $(6.2 \times 10^{-16}) = 9.529 \times 10^{-16}$
922.	1200.	15.7×10^{6}	14.0×10^{6}	8.7	4.5×10^{-9}	$\frac{15.7}{14.0}$ $(4.5 \times {}^{-9}) = 5.046 \times 10^{-9}$
1089.	1500.	10.0×10^{6}	11.5×10^{6}	5.08	2.073×10^{-3}	$\frac{10.0}{11.5}$ $(2.073 \times 10^{-3}) = 1.803 \times 10^{-3}$

THE STRESS RELAXATION FORMULA $\sigma = \left[AE(n-1)t + \sigma_o^{(1-n)}\right]^{\frac{1}{1-n}}$ SHOWS THE DEPENDENCY OF THE CONSTANT, A, UPON THE VALUE USED FOR YOUNG'S MODULUS. FOR THIS ANALYSIS, A WAS ADJUSTED TO REFLECT THE TRUE VALUE OF E.

TABLE 10a. SSME DUTY CYCLE INCREMENTS THERMAL, PRESSURE, BOUNDARY CONDITIONS DATA FOR ANALYSIS (ENGLISH)

LOAD INCREMENT	DEAP TIME SLICE NO.	TIME, SECONDS	T_{HGW}, F	T_{JACK}, F	$P_{HOT\ WALL}$, PSIA	$P_{COOLANT}$, WALL PSIA	JACKET BOUNDARY CONDITIONS	
							Δ_R, INCH	ϵ_Z, INCH/INCH
1	15	1.4	-365	R.T.	40	525	0.00016	-0.000013
2	19	1.6	404	R.T.	384	909	0.00149	-0.000122
3	35	2.4	610	R.T.	518	2150	0.00202	-0.000165
4	55	3.4	1015	-23	1436	4035	0.00310	-0.000404
5	58	4.9	1306	-100	2109	6270	0.00370	-0.000578
6	60	20.5	1324	-175	2109	6270	0.00175	-0.000540
7	79	395.0*	1047	-175	1267	3629	-0.00149	-0.000275
8	85	395.6	739	-100	537	1930	-0.00234	-0.000084
9	100	397.1	-297	-84	109	1028	-0.00354	0.0000403
10	129	400.0	-405	-82	9	0	-0.00386	0.0000730
11			70	70	0	0	0	0

*DEAP DATATAPE TEMPERATURE INPUT ONLY CHANGE IN INPUT LOADS FROM MODEL TO MODEL

TABLE 10b. SSME DUTY CYCLE INCREMENTS THERMAL, PRESSURE, BOUNDARY CONDITIONS DATA FOR ANALYSIS (METRIC)

LOAD INCREMENT	DEAP TIME SLICE NO.	TIME, SECONDS	T_{HGW}, K	T_{JACK}, K	$P_{HOT\ WALL}$, MPa	$P_{COOLANT\ WALL}$, MPa	JACKET BOUNDARY CONDITIONS	
							Δ_R, (mm)	ϵ_Z, (mm)
1	15	1.4	53	R.T.	0.2758	3.6197	0.004064	-0.00033
2	19	1.6	480	R.T.	2.6476	6.267	-0.037846	-0.003099
3	35	2.4	594	R.T.	3.5646	14.824	0.051308	-0.004191
4	55	3.4	546	243	9.9009	27.820	0.07874	-0.010262
5	58	4.9	819	200	14.541	43.230	0.09398	-0.014681
6	60	20.5	991	158	14.541	43.230	0.04445	-0.013716
7	79	395.0*	837	158	8.7356	25.021	-0.037846	-0.006985
8	85	395.6	666	200	3.7024	13.307	-0.059436	-0.002134
9	100	397.1	90	209	0.7515	7.0878	-0.089916	0.001024
10	129	400.0	30	210	0.0621	0	0.98044	0.001854
11			R.T.	R.T.	0	0	0	0

*DEAP DATATAPE TEMPERATURE INPUT ONLY CHANGE IN INPUT LOADS FROM MODEL TO MODEL

TABLE 11. SUMMARY OF APSAC CONTROL CODES FOR MCC LARGE DEFLECTION ANALYSIS

	CYCLE	INCREMENT	NEWRZ	LGDFL	AO	TOLLD	LDOPT	LDRST	CREEP
Initial 5-Cycle Analysis	1	1		-1	.7	.0005	2	1	
		2			.7	.0005	2	3	
		3			.5	.0005	2	3	
		4			.7	.0005	2	3	
		5, 6					1	2	1
		7-11			.7	.0005	2	3	
	2	1			.7	.0005	2	3	
		2-11		Same as Cycle 1					
	3-5	Repeat Cycle 2							
Restart for Succeeding 5-Duty Cycles	21	1	1	-1	.7	.0005	2	1	
	Etc.								

APSAC

LGDFL	$\neq 0$	Large deflection analysis for some increment of this job. Read in additional card to define type of analysis (to be performed this iteration) and start geometry.
	< 0	Change temperature coordinates read from DEAP datatape for this increment to nodal coordinates for this increment. There must be an exact correlation between nodes.
NEWRZ	> 0	Displacements from a previous duty cycle are added to basic nodal geometry. Used to restart after first 5 cycles and extrapolation to cycle 20.
AO		Factor to limit amount of geometry change per iteration in large deflection analysis.
TOLLD		Large deflection iteration convergence number
LDOPT		Type of analysis to be performed this increment =1 elastic-plastic =2 elastic-plastic and large deflection simultaneously =3 elastic and large deflection simultaneously
LDRST		Geometry to start this increment =1 start geometry is basic geometry =2 start geometry is basic geometry + U from previous increment =3 start geometry is basic geometry + U from previous increment, U' equals U' from previous increment =4 start geometry is basic geometry + U from previous increment, U' equals U' from previous increment Previous increment is stored on tape 11, increment number = |NREAD|

overall confidence in the total methodology. The initial duty cycle had been divided into 13 increments, but two increments were eliminated when model testing deomonstrated that the two additional increments in the steady-state portion of the cycle were not significant in defining the stress and strain and displaced conditions. Elimination of these increments reduced computer run costs by about 10%.

This model checkout also showed that the compression only elements must be carefully sized when used with this type of large deflection analysis. The APSAC code performs an iteration process, and the geometry distortion is accounted for during these iterations. If too large a load increment is used as the liner displaces toward the jacket boundary, the model can overshoot during the iteration; and the boundary elements can turn inside-out, which is not allowable in the code. To minimize this problem, the boundary elements were sized to be almost square. Usually for small displacement analysis, thin elements are used; but the size is inconsequential to the analysis, except for a code restraint that the longest side must be normal to the stiff direction of the element. The problem of too large a displacement within a load increment, as the liner deformed through the 0.508 mm (0.020 inch) initial gap and touched the jacket, occurred in two of the models. This was readily eliminated through adjusting the displacement relaxation factor, AO. Input datacard image listing of the 1-5, 21-25, and 41-45 duty cycles and extrapolations are included for examples of the procedure used to run all the models. Other geometries are only minor variations of these runs. These listings show all the detailed code input required, and the methodology used for control, tracking and changing the input from the terminal.

Model Stragegy

The model strategy used for this study was to standardize the input so that only a minimum number of changes were required to submit individual jobs and to develop a naming convention for datasets saved and processed in the analysis sequence. The other major technique was to utilize the terminal and editor for making all job submittals and input data changes. This procedure effectively eliminated job submittal errors and reduced the time to review and process a 5 duty-cycle analysis to less than 4 manhours effort.

The decks were setup so that only two job-control cards, the title cards for each increment and one or two other cards, need modification. The changes on the cards are also standardized so that all changes to the data deck can be made with a few (less than 10) editor commands. This is accomplished with the naming convention of datasets and identification on title cards. The dataset-naming conventions are as shown in Table 12. For instance, using the editor feature of replacing character sets, by replacing A001 by A021 changes all the dataset names in a submittal from the first-cycle input convention to the 21st-cycle input convention. Since the rest of the duty-cycle definition and the temperature dataset did not change, the only other change dealt with adjusting large deflection control flags from an initial submittal to a continuing analysis, and adjusting the displacements in the 21st cycle load increments to account for the rigid body motion of the structure of 0.508 mm (0.020 inch) that occurs between the first and 21st duty cycles.

TABLE 12. DATASET NAMING CONVENTIONS USED FOR COMPUTER RUNS

JOB NAME	TITLE	PERMANENT FILE NAME	FILE USAGE
QMCCA	AOONOX	TAOONOX	TAPE10
		PAOONOX	PRINT
		CAOONOX	CRTS

WHERE A IS THE CODE DESCRIBING THE TYPE OF ANALYSIS BEING RUN -

- BASIC SSME ANALYSIS 100Δ HG CASE
- BASIC SSME ANALYSIS 135Δ HG CASE
- CONTOURED GEOMETRY
- SLOTTED
- KEEL RIB
- 540 CHANNELS

N IS THE INITIAL CYCLE OF EACH ANALYSIS, AND X IS THE INCREMENT WITHIN THAT CYCLE CYCLE THAT THE JOB IS INITIATED. THE RESTART, PRINT, AND CRT FILES ARE CODED CONSISTENTLY TO SIMPLIFY JOB TRACKING.

For the standard analysis, all results were obtained from the postprocessing plotting code, either as in graphical or pictorial format, or as printouts of selected displacements, stresses or strains. Other detailed information from job runs were scanned at the terminal from saved datasets.

This overall strategy ended up saving considerable costs from computing, man-hours, and overall lapsed time. As previously mentioned, it also virtually eliminated job reruns from data errors.

The remaining pages of this section furnish examples of the card images for running typical APSAC and APSAPLOT/EXTRAPOLATION codes. The first set of card images show the setup for the first 5 duty cycle analysis that accounts for the initial liner to structural jacket gap. The next set of card images show the setup of the analysis runs where the liner is in contact with the jacket at the start of the duty cycle. The extrapolation card images for the first and second extrapolation cores are next. This set of card images was used to obtain plots and output summaries.

```
QHPEG.T3C
USER(QC030,MAGGI)
CHARGE,*.
ACCT(HAVEN      000454512?*0554056  )
ATTACH,TAPE20=MCCT135.
GET,PROCPMR/UN=Q0828.
BEGIN,APSAC,PROCPMR,STAPE10=TH00101,SPRINT=PH00101,NPPLOT,NOCRT.
```

APSAC CODE USED FOR INITIAL FIVE DUTY CYCLES,
STARTING WITH BASIC GEOMETRY AND A 0.508 mm
(0.020 INCH) GAP BETWEEN THE LINER AND JACKET

DUTY CYCLE LOADING

```
MH00101 ..35HG  CYCLE001 TC001+4  T=0 TO 400 SEC
   -2                 4          -15 70.0        -.000013
                   15 .01                    1 0009      1   -1
                                                        2         1
        55

NARLOYZ    1  5  1     7
 -420.0        1.0      -50 -57.6       19.2        .03                  2
  700.0        2.9      -31 -57.6       19.2        .03                  2
 1000.0        9.529    -16 -37.5       12.5        .03                  2
 1200.0        5.046    -09 -26.1       8.7         .03                  2
 1500.0        1.803    -03 -15.24      5.08        .03                  2
-420.0         20.0     +06                         .335
                                 6.94    -06                  28.2    +03
                                 .01796
 -320.0        19.6     +06                         .34
                                 7.7     -06                  26.7    +03
                                 .01796
 70.0          18.4     +06                         .355
                                 7.6     -06                  23.5    +03
                                 .01783
 600.0         16.6     +06                         .3
                                 9.4     -06                  20.7    +03
                                 .01024
 800.0         15.7     +06                         .28
                                 9.7     -05                  18.5    +03
                                 .01121
 1000.0        14.9     +06                         .27
                                 9.9     -06                  14.0    +03
                                 .00671
 1500.0        11.5     +06                         .185
                                 10.7    -06                  3.0     +03
                                 .00261
EDNI       2  2  1     4
-420.0         1.0      -50 -57.6       19.2        .03                  2
 700.0         2.9      -31 -57.6       19.2        .03                  2
-420.0         27.0     +06                         .34
                                 4.49    -06                  61.0    +03
                                 .03947
-320.0         26.6     +06                         .34
                                 4.62    -06                  58.0    +03
                                 .03947
-200 0         26.5     +06                         .34
                                 4.81    -06                  57.0    +03
                                 .03962
 70.0          26:0     +06                         .34
                                 6.0     -06                  53.0    +03
                                 .02577
EDCU       3  2  1     8
 -420.0        1.0      -50 -57.6       19.2        .03                  2
 700.0         2.9      -31 -57.6       19.2        .03                  2
-420.0         21.0     +06                         .355
                                 6.1     -06                  29.0    +03
                                 .0270
-320.0         20.6     +06                         .355
                                 6.92    -06                  29.0    +03
                                 .02780
-200.0         20.0     +06                         .355
                                 7.78    -06                  28.1    +03
                                 .0293
 70.0          19.7     +06                         .355
                                 8.5     -05                  18.8    +03
```

```
                              .03320
ISO=4       4  2  4     2
 -420.0        1.0     -50  -57.6        19.2        .03                 2
 700.0         2.9     -31  -57.6        19.2        .03                 2
 -420.0


 700.0


            10         31          99        4         4           5
41    9      1  5.2507      0.0        5     1  5.250862    0.02
                0.0         0.0
41    5      1                         1     1  5.25053     0.042296
                0.0         0.0
11    1      1                         1     2  5.25153     0.042304
11    1      2                         1     5  5.27153     0.042465
11    1      5                         1     7  5.27753     0.042513
11    1      7                         1     8  5.27853     0.0425214
11    1      8                         1    12  5.29322     0.04264
11    1     12                         1    22  5.37386     0.04329
11    1     22                         1    24  5.3820      0.043355
11    1     24                         1    26  5.387025    0.043396
11    1     26                         1    29  5.41452     0.04362
11    1     29                         1    30  5.417024    0.0436372
11    1     30                         1    31  5.420924    0.043638
11    1     31                         5    31  5.421119    0.02
11    5     31                        10    31  5.4211      0.0
11   10     31                        10    30  5.4172      0.0
11   10     30                        10    29  5.41470     0.0
11   10     29                        10    26  5.3872      0.0
11   10     26                        10    24  5.3822      0.0
11   10     24                         5    24  5.3822      0.02
11    5     24                         5    22  5.37402     0.02
11    5     22                         5    12  5.29335     0.02
11    5     12                         5     8  5.2787      0.02
11    5      8                         9     8  5.2797      0.0
11    9      8                         9     7  5.2777      0.0
11    9      7                         9     5  5.2717      0.0
11    9      5                         9     2  5.2517      0.0
11    9      2                         9     1
4     1      2                         5     2  5.251662    0.02
                0.0         0.0
4     5      2                         9     2
                0.0         0.0
4     1      7                         5     7  5.27766     0.02
                0.0         0.0
1     5      7                         9     7
4     1      8                         5     8  5.27866     0.02
                0.0         0.0
1     1     12                         5    12
1     1     22                         5    22
1     1     24                         5    24  5.3822      0.02
1     1     26                         5    26  5.3872      0.02
1     5     26                        10    26
4     1     29                         5    29  5.41466     0.02
                0.0         0.0
1     5     29                        10    29
1     1     30                         5    30  5.417119    0.02
1     5     30                        10    30
1     5     29                         5    26
1     5     26                         5    24
```

```
1    5     7                                   5     5  5.271662     0.02
1    5     5                                   5     2  5.251662     0.02
1    1     5                                   5     5
1    5     5                                   9     5
9
     9     9      1     8  2.0
    10    10     24    30  2.0
     1     1      1    30-179.53846
     1    10     31    31    3.0             .02016
           1      1     9     1      24
           3      1    10    24      26
           2      1    10    26      30
           4      1    10    30      31                    -1.0
           9            8   525.0                    5              8   525.0
           5            8   525.0                    5             24   525.0
           5           24   525.0                   10             24   525.0
           1            1    40.0                    9              1    40.0
           1           31  -1.0                     10             31  -1.0
   -19                  1          5             0 2 1  -.000122
                             .7                .0005               2            3
     1    10     31    31   3.0              .02149
           9            8 909.0                      5              8 909.0
           5            8 909.0                      5             24 909.0
           5           24 909.0                     10             24 909.0
           1            1 384.0                      9              1 384.0
           1           31 -1.0                      10             31  -1.0
   -35                  1          4             0 2 1  -.000165
                          .5                 .0005                 2            3
     1    10     31    31   3.0              .02202
           9            8 2150.0                     5              8 2150.0
           5            8 2150.0                     5             24 2150.0
           5           24 2150.0                    10             24 2150.0
           1            1 518.0                      9              1 518.0
   -55                  1          4             0 2 1  -.000404
                          .7                 .0005                 2            3
     1    10     31    31   3.0              .0231
           9            8   4035.0                   5              8   4035.0
           5            8   4035.0                   5             24   4035.0
           5           24   4035.0                  10             24   4035.0
           1            1   1436.0                   9              1   1436.0
   -53                  1          4   1         0 2 1  -.000578
                          .7                 .0005                 1            2
     1    10     31    31   3.0              .02370
           9            8 6270.0                     5              8 6270.0
           5            8 6270.0                     5             24 6270.0
           5           24 6270.0                    10             24 6270.0
           1            1 2109.0                     9              1 2109.0
          30  .0043333    .03                .24           3.0
   -60                  1          4   1         0 2 1  -.000540
                          .7                 .0005                 1            2
     1    10     31    31   3.0              .02175
           9            8 6270.0                     5              8 6270.0
           5            8 6270.0                     5             24 6270.0
           5           24 6270.0                    10             24 6270.0
           1            1 2109.0                     9              1 2109.0
          30  .1041277    .03                .24           3.0
   -79                  1          4                 0 2 1  -.000275
                          .7                 .0005                 2            3
     1    10     31    31    3.0              .01851
           9            8 3629.0                     5              8 3629.0
           5            8 3629.0                     5             24 3629.0
           5           24 3629.0                    10             24 3529.0
```

```
          1              1  1267.0                    9          1  1267.0
  -85                    1          4        0 2 1 -.000084
                            .7          .0005                    2           3
   1     10     31      31  3.0         .01766
         9               8  1930.0                5              8  1930.0
         5               8  1930.0                5             24  1930.0
         5              24  1930.0               10             24  1930.0
         1               1  537.0                 9              1  537.0
  -100                   1          4        0 2 1  .0000403
                            .7          .0005                    2           3
   1     10     31      31  3.0         .01646
         9               8  1028.0                5              8  1028.0
         5               8  1028.0                5             24  1028.0
         5              24  1028.0               10             24  1028.0
         1               1  109.0                 9              1  109.0
  -129                   1          4        0 2 1  .000073
                            .7          .0005                    2           3
   1     10     31      31  3.0         .01614
         9               8  0.0                   5              8  0.0
         5               8  0.0                   5             24  0.0
         5              24  0.0                  10             24  0.0
         1               1  9.0                   9              1  9.0
   4                     1          1        0 2 1  0.0
                            .7          .0005                    2           3
0.0          0.0            70.0
10.0          10.           70.0
10.          0.0            70.0
0.0          10.            70.0
   1     10     31      31  3.0          .020
         1              31  -.1                  10             31  -.1
  -15                    1          4        0 2 1  .000013
                            .7          .0005                    2           3
   1     10     31      31   3.0        .02016
         9               8   525.0                5              8   525.0
         5               8   525.0                5             24   525.0
         5              24   525.0               10             24   525.0
         1               1   40.0                 9              1   40.0
  -19                    1          5        0 2 1 -.000122
                              .7         .0005                   2           3
   1     10     31      31   3.0        .02149
         9               8  909.0                 5              8  909.0
         5               8  909.0                 5             24  909.0
         5              24  909.0                10             24  909.0
         1               1  384.0                 9              1  384.0
         1              31  -1.0                 10             31  -1.0
  -35                    1          4        0 2 1 -.000165
                          .5            .0005                    2           3
   1     10     31      31   3.0        .02202
         9               8  2150.0                5              8  2150.0
         5               8  2150.0                5             24  2150.0
         5              24  2150.0               10             24  2150.0
         1               1  518.0                 9              1  518.0
  -55                    1          4        0 2 1 -.000404
                          .7            .0005                    2           3
   1     10     31      31   3.0        .0231
         9               8   4035.0               5              8   4035.0
         5               8   4035.0               5             24   4035.0
         5              24   4035.0              10             24   4035.0
         1               1   1436.0               9              1   1436.0
  -58                    1          4  1     0 2 1 -.000578
                          .7            .0005                    1           2
   1     10     31      31   3.0        .02370
```

```
         9          8 6270.0                  5          8 6270.0
         5          8 6270.0                  5         24 6270.0
         5         24 6270.0                 10         24 6270.0
         1          1 2109.0                  9          1 2109.0
        30 .0043333     .03        .24             3.0
-60                 1          4  1       0 2 1 -.000540
                               .7        .0005                1.          2
 1   10    31    31  3.0        .02175
         9          8 6270.0                  5          8 6270.0
         5          8 6270.0                  5         24 6270.0
         5         24 6270.0                 10         24 6270.0
         1          1 2109.0                  9          1 2109.0
        30 .1041277     .03        .24             3.0
-79                 1          4          0 2 1 -.000275
                               .7        .0005                2          3
 1   10    31    31  3.0        .01851
         9          8 3629.0                  5          8 3629.0
         5          8 3629.0                  5         24 3629.0
         5         24 3629.0                 10         24 3629.0
         1          1 1267.0                  9          1 1267.0
-65                 1          4          0 2 1 -.000084
                               .7        .0005                2          3
 1   10    31    31  3.0        .01766
         9          8 1930.0                  5          8 1930.0
         5          8 1930.0                  5         24 1930.0
         5         24 1930.0                 10         24 1930.0
         1          1 537.0                   9          1 537.0
-100                1          4          0 2 1  .0000403
                               .7        .0005                2          3
 1   10    31    31  3.0        .01646
         9          8 1028.0                  5          8 1028.0
         5          8 1028.0                  5         24 1028.0
         5         24 1028.0                 10         24 1028.0
         1          1 109.0                   9          1 109.0
-129                1          4          0 2 1  .000073
                               .7        .0005                2          3
 1   10    31    31  3.0        .01614
         9          8 0.0                     5          8 0.0
         5          8 0.0                     5         24 0.0
         5         24 0.0                    10         24 0.0
         1          1 9.0                     9          1 9.0
    4                1          1          0 2 1 0.0
                               .7        .0005                2          3
  .0         0.0          70.0
10.0         10.          70.0
 10.         0.0          70.0
 0.0         10.          70.0
 1   10    31    31  3.0        .020
         1         31  -.1                   10         31  -.1
-15                 1          4          0 2 1 .000013
                               .7        .0005                2          3
 1   10    31    31  3.0        .02016
         9          8  525.0                  5          8  525.0
         5          8  525.0                  5         24  525.0
         5         24  525.0                 10         24  525.0
         1          1   40.0                  9          1   40.0
-19                 1          5          0 2 1 -.000122
                               .7        .0005                2          3
 1   10    31    31  3.0        .02149
         9          8 909.0                   5          8 909.0
         5          8 909.0                   5         24 909.0
         5         24 909.0                  10         24 909.0
```

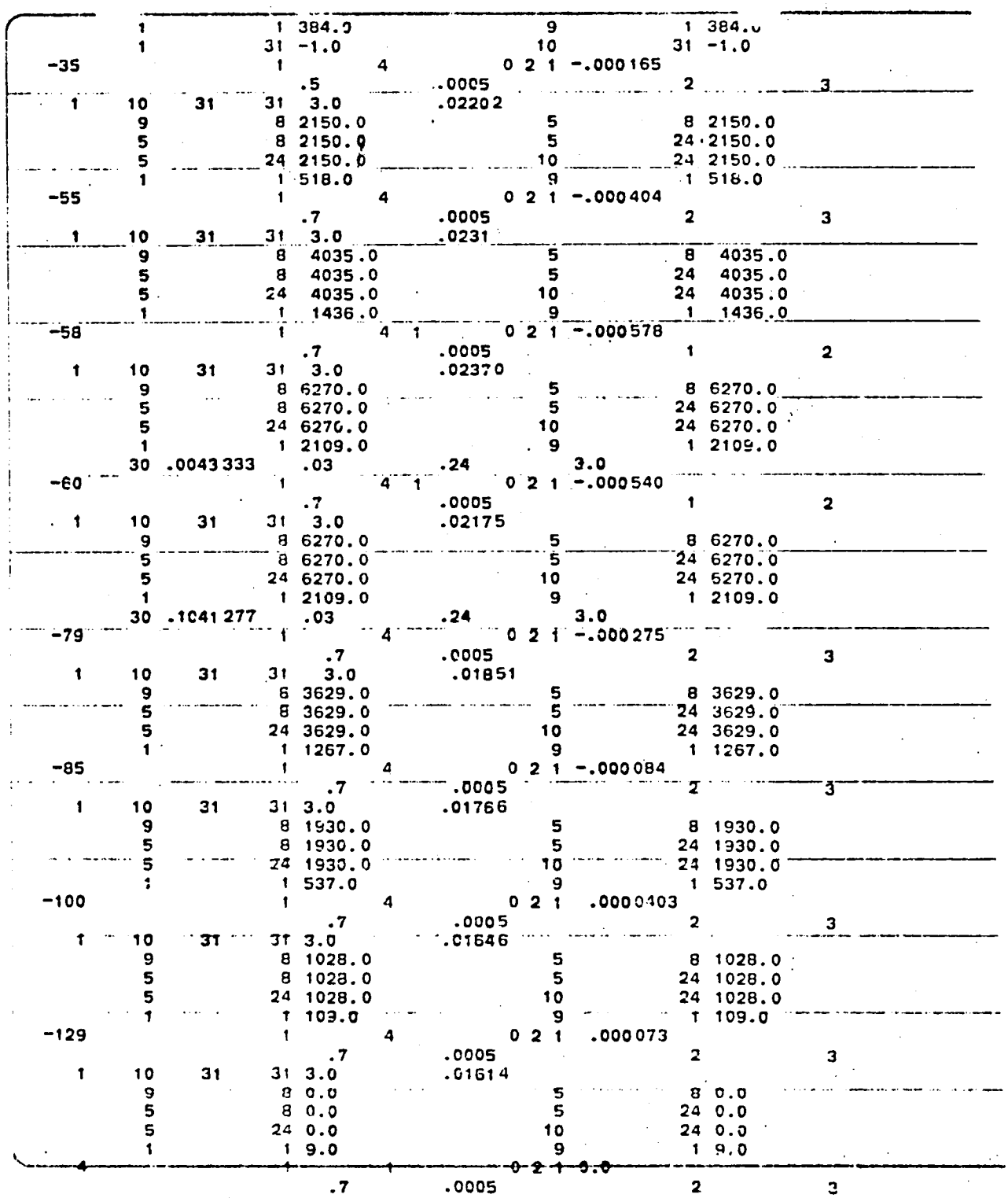
1 1 384.0 9 1 384.0
1 31 -1.0 10 31 -1.0
-35 1 4 0 2 1 -.000165
.5 .0005 2 3
1 10 31 31 3.0 .02202
9 8 2150.0 5 8 2150.0
5 8 2150.0 5 24 2150.0
5 24 2150.0 10 24 2150.0
1 1 518.0 9 1 518.0
-55 1 4 0 2 1 -.000404
.7 .0005 2 3
1 10 31 31 3.0 .0231
9 8 4035.0 5 8 4035.0
5 8 4035.0 5 24 4035.0
5 24 4035.0 10 24 4035.0
1 1 1436.0 9 1 1436.0
-58 1 4 1 0 2 1 -.000578
.7 .0005 1 2
1 10 31 31 3.0 .02370
9 8 6270.0 5 8 6270.0
5 8 6270.0 5 24 6270.0
5 24 6270.0 10 24 6270.0
1 1 2109.0 9 1 2109.0
30 .0043333 .03 .24 3.0
-60 1 4 1 0 2 1 -.000540
.7 .0005 1 2
1 10 31 31 3.0 .02175
9 8 6270.0 5 8 6270.0
5 8 6270.0 5 24 6270.0
5 24 6270.0 10 24 6270.0
1 1 2109.0 9 1 2109.0
30 .1041277 .03 .24 3.0
-79 1 4 0 2 1 -.000275
.7 .0005 2 3
1 10 31 31 3.0 .01851
9 8 3629.0 5 8 3629.0
5 8 3629.0 5 24 3629.0
5 24 3629.0 10 24 3629.0
1 1 1267.0 9 1 1267.0
-85 1 4 0 2 1 -.000084
.7 .0005 2 3
1 10 31 31 3.0 .01766
9 8 1930.0 5 8 1930.0
5 8 1930.0 5 24 1930.0
5 24 1930.0 10 24 1930.0
1 1 537.0 9 1 537.0
-100 1 4 0 2 1 .0000403
.7 .0005 2 3
1 10 31 31 3.0 .01646
9 8 1028.0 5 8 1028.0
5 8 1028.0 5 24 1028.0
5 24 1028.0 10 24 1028.0
1 1 109.0 9 1 109.0
-129 1 4 0 2 1 .000073
.7 .0005 2 3
1 10 31 31 3.0 .01614
9 8 0.0 5 8 0.0
5 8 0.0 5 24 0.0
5 24 0.0 10 24 0.0
1 1 9.0 9 1 9.0
4 1 0 2 1 0.0
.7 .0005 2 3

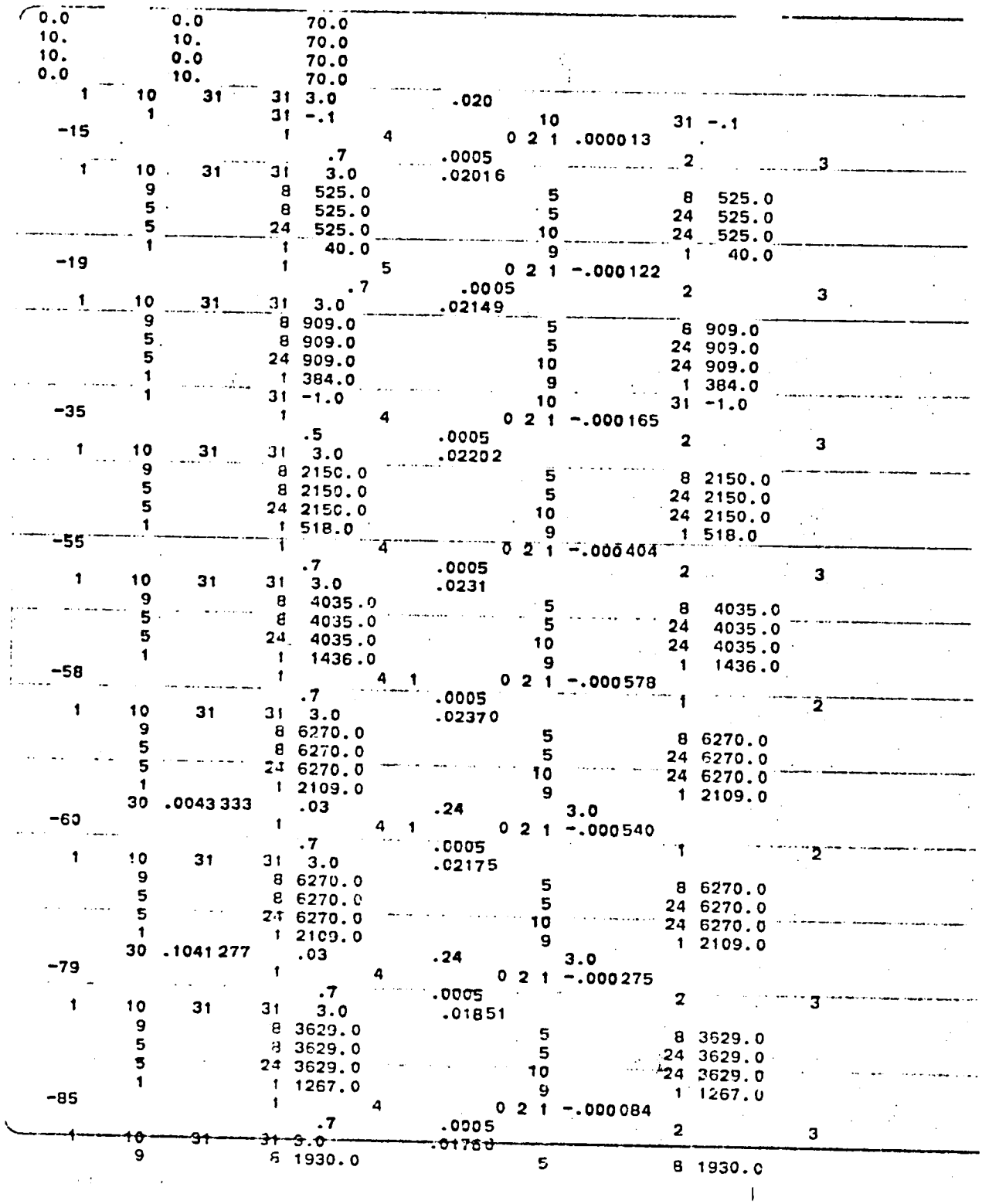
0.0 0.0 70.0
10. 10. 70.0
10. 0.0 70.0
0.0 10. 70.0
1 10 31 31 3.0 .020
1 31 -.1 10 31 -.1
-15 1 4 0 2 1 .000013
.7 .0005 2 3
1 10 31 31 3.0 .02016
9 8 525.0 5 8 525.0
5 8 525.0 5 24 525.0
5 24 525.0 10 24 525.0
1 1 40.0 9 1 40.0
-19 1 5 0 2 1 -.000122
.7 .0005 2 3
1 10 31 31 3.0 .02149
9 8 909.0 5 8 909.0
5 8 909.0 5 24 909.0
5 24 909.0 10 24 909.0
1 1 384.0 9 1 384.0
1 31 -1.0 10 31 -1.0
-35 1 4 0 2 1 -.000165
.5 .0005 2 3
1 10 31 31 3.0 .02202
9 8 2150.0 5 8 2150.0
5 8 2150.0 5 24 2150.0
5 24 2150.0 10 24 2150.0
1 1 518.0 9 1 518.0
-55 1 4 0 2 1 -.000404
.7 .0005 2 3
1 10 31 31 3.0 .0231
9 8 4035.0 5 8 4035.0
5 8 4035.0 5 24 4035.0
5 24 4035.0 10 24 4035.0
1 1 1436.0 9 1 1436.0
-58 1 4 1 0 2 1 -.000578
.7 .0005 1 2
1 10 31 31 3.0 .02370
9 8 6270.0 5 8 6270.0
5 8 6270.0 5 24 6270.0
5 24 6270.0 10 24 6270.0
1 1 2109.0 9 1 2109.0
30 .0043333 .03 .24 3.0
-60 1 4 1 0 2 1 -.000540
.7 .0005 1 2
1 10 31 31 3.0 .02175
9 8 6270.0 5 8 6270.0
5 8 6270.0 5 24 6270.0
5 24 6270.0 10 24 6270.0
1 1 2109.0 9 1 2109.0
30 .1041277 .03 .24 3.0
-79 1 4 0 2 1 -.000275
.7 .0005 2 3
1 10 31 31 3.0 .01851
9 8 3629.0 5 8 3629.0
5 8 3629.0 5 24 3629.0
5 24 3629.0 10 24 3629.0
1 1 1267.0 9 1 1267.0
-85 1 4 0 2 1 -.000084
.7 .0005 2 3
1 10 31 31 3.0 .01760
9 8 1930.0 5 8 1930.0

	5		8	1930.0				5		24	1930.0	
	5		24	1930.0				10		24	1930.0	
	1		1	537.0				9		1	537.0	
-100			1		4			0 2 1	.0000403			
				.7			.0005			2		3
1	10	31	31	3.0			.01646					
	9		8	1028.0				5		8	1028.0	
	5		8	1028.0				5		24	1028.0	
	5		24	1028.0				10		24	1028.0	
	1		1	109.0				9		1	109.0	
-129			1		4			0 2 1	.000073			
				.7			.0005			2		3
1	10	31	31	3.0			.01614					
	9		8	0.0				5		8	0.0	
	5		8	0.0				5		24	0.0	
	5		24	0.0				10		24	0.0	
	1		1	9.0				9		1	9.0	
4			1		1			0 2 1	0.0			
				.7			.0005			2		3
0.0		0.0		70.0								
10.		10.		70.0								
10.		0.0		70.0								
0.0		10.		70.0								
1	10	31	31	3.0			.020					
	1		31	-.1				10		31	-.1	
-15			1		4			0 2 1	.000013			
				.7			.0005			2		3
1	10	31	31	3.0			.02016					
	9		8	525.0				5		8	525.0	
	5		8	525.0				5		24	525.0	
	5		24	525.0				10		24	525.0	
	1		1	40.0				9		1	40.0	
-19			1		5			0 2 1	-.000122			
				.7			.0005			2		3
1	10	31	31	3.0			.02149					
	9		8	909.0				5		8	909.0	
	5		8	909.0				5		24	909.0	
	5		24	909.0				10		24	909.0	
	1		1	384.0				9		1	384.0	
	1		31	-1.0				10		31	-1.0	
-35			1		4			0 2 1	-.000165			
				.5			.0005			2		3
1	10	31	31	3.0			.02202					
	9		8	2150.0				5		8	2150.0	
	5		8	2150.0				5		24	2150.0	
	5		24	2150.0				10		24	2150.0	
	1		1	518.0				9		1	518.0	
-55			1		4			0 2 1	-.000404			
				.7			.0005			2		3
1	10	31	31	3.0			.0231					
	9		8	4035.0				5		8	4035.0	
	5		8	4035.0				5		24	4035.0	
	5		24	4035.0				10		24	4035.0	
	1		1	1436.0				9		1	1436.0	
-58			1		4	1		0 2 1	-.000578			
				.7			.0005			1		2
1	10	31	31	3.0			.02370					
	9		8	6270.0				5		8	6270.0	
	5		8	6270.0				5		24	6270.0	
	5		24	6270.0				10		24	6270.0	
	1		1	2109.0				9		1	2109.0	
	30	.0043333		.03			.24		3.0			

```
   -60                  1          4   1         0 2 1  -.000540
                           .7             .0005                    1             2
     1     10     31     31  3.0          .02175
           9             8 6270.0                    5             8 6270.0
           5             8 6270.0                    5            24 6270.0
           5            24 6270.0                   10            24 6270.0
           1             1 2109.0                    9             1 2109.0
          30 .1041277     .03          .24          3.0
   -79                  1          4                 0 2 1  -.000275
                           .7             .0005                    2             3
     1     10     31     31  3.0           .01851
           9             8 3629.0                    5             8 3629.0
           5             8 3629.0                    5            24 3629.0
           5            24 3629.0                   10            24 3629.0
           1             1 1267.0                    9             1 1267.0
   -85                  1          4                 0 2 1  -.000084
                           .7              .0005                   2             3
     1     10     31     31 3.0           .01766
           9             8 1930.0                    5             8 1930.0
           5             8 1930.0                    5            24 1930.0
           5            24 1930.0                   10            24 1930.0
           1             1 537.0                     9             1 537.0
  -100                  1          4                 0 2 1   .0000403
                           .7              .0005                   2             3
     1     10     31     31 3.0           .01646
           9             8 1028.0                    5             8 1028.0
           5             8 1028.0                    5            24 1028.0
           5            24 1028.0                   10            24 1028.0
           1             1 109.0                     9             1 109.0
  -129                  1          4                 0 2 1   .000073
                           .7             .0005                    2             3
     1     10     31     31 3.0           .01614
           9             8 0.0                       5             8 0.0
           5             8 0.0                       5            24 0.0
           5            24 0.0                      10            24 0.0
           1             1 9.0                       9             1 9.0
     4                  1          1                 0 2 1 0.0
                           .7             .0005                    2             3
 0.0          0.0          70.0
 10.          10.          70.0
 5.5          0.0          70.0
 5.5           .5          70.0
     1     10     31     31 3.0            .020
           1            31 -.1                      10            31 -.1
           1            31 -.1                      10            31 -.1
```

```
QH002.T1777.
USER(Q0030,MAGGI)
CHARGE,*.
ACCT(HAVEN      000 7545127*0554056    )
ATTACH,TAPE20=MCCT135.
ATTACH,TAPE11=EH82X13.              MH002
GET,PROCPMR/UN=Q0828.
BEGIN,APSAC,PROCPMR,STAPE10=TH02101,SPRINT=PH02101,NPPLOT,NOCRT.
```

APSAC CODE USED FOR SUBSEQUENT DUTY CYCLES.
GEOMETRY IS UPDATED GEOMETRY. NO LINER TO
JACKET GAP.

DUTY CYCLE LOADING

```
MH02101 1.05HG  CYCLE021  TD021+4  T=0 TO 400 SEC
   -2                  4          -15  70.0         -.000013
              15  .01                            1  0009      1  1 -1
                         .5              .0005                  2          1
         55

NARLOYZ    1   5   1     7
 -420.0        1.0      -50  -57.6       19.2       .03                    2
 700.0         2.9      -31  -57.6       19.2       .03                    2
 1000.0        9.529    -16  -37.5       12.5       .03                    2
 1200.0        5.046    -09  -26.1       8.7        .03                    2
 1500.0        1.803    -03  -15.24      5.08       .03                    2
-420.0         20.0     +06                         .335
                             6.94    -06                        28.2    +03
                             .01796
 -320.0        19.6     +06                         .34
                             7.7     -06                        26.7    +03
                             .01796
 70.0          18.4     +06                         .355
                             7.6     -06                        23.5    +03
                             .01783
 600.0         16.6     +06                         .3
                             9.4     -06                        20.7    +03
                             .01024
 800.0         15.7     +06                         .28
                             9.7     -06                        18.5    +03
                             .01121
 1000.0        14.9     +06                         .27
                             9.9     -06                        14.0    +03
                             .00671
 1500.0        11.5     +05                         .185
                             10.7    -06                        3.0     +03
                             .00261
EDNI         2   2   1     4
-420.0         1.0      -50  -57.6       19.2       .03                    2
 700.0         2.9      -31  -57.6       19.2       .03                    2
-420.0         27.0     +06                         .34
                             4.49    -06                        61.0    +03
                             .03947
-320.0         26.6     +06                         .34
                             4.62    -06                        58.0    +03
                             .03947
-200.0         26.5     +06                         .34
                             4.81    -06                        57.0    +03
                             .03962
 70.0          26.0     +06                         .34
                             6.0     -06                        53.0    +03
                             .02577
EDCU         3   2   1     4
 -420.0        1.0      -50  -57.6       19.2       .03                    2
 700.0         2.9      -31  -57.6       19.2       .03                    2
-420.0         21.0     +06                         .355
                             6.1     -06                        29.0    +03
                             .0278
-320.0         20.6     +06                         .355
                             6.92    -06                        29.0    +03
                             .02780
-200.0         20.0     +06                         .355
                             7.78    -06                        28.1    +03
                             .0293
 70.0          18.7     +06                         .355
                             8.5     -06                        18.8    +03
```

```
                                    .03320
ISO=4       4  2  4     2
 -420.0       1.0     -50  -57.6        19.2        .03              2
 700.0        2.9     -31  -57.6        19.2        .03              2
 -420.0

 700.0

          10              31            99               4          4          5
41   9     1  5.2507        0.0               5     1  5.250662    0.02
              0.0           0.0
41   5     1                                  1     1  5.25053     0.042296
              0.0           0.0
11   1     1                                  1     2  5.25153     0.042304
11   1     2                                  1     5  5.27153     0.042465
11   1     5                                  1     7  5.27753     0.042513
11   1     7                                  1     8  5.27853     0.0425214
11   1     8                                  1    12  5.29322     0.04264
11   1    12                                  1    22  5.37386     0.04329
11   1    22                                  1    24  5.3820      0.043355
11   1    24                                  1    26  5.387025    0.043396
11   1    26                                  1    29  5.41452     0.04362
11   1    29                                  1    30  5.417024    0.0436372
11   1    30                                  1    31  5.420924    0.043638
11   1    31                                  5    31  5.421119    0.02
11   5    31                                 10    31  5.4211      0.0
11  10    31                                 10    30  5.4172      0.0
11  10    30                                 10    29  5.41470     0.0
11  10    29                                 10    26  5.3872      0.0
11  10    26                                 10    24  5.3822      0.0
11  10    24                                  5    24  5.3822      0.02
11   5    24                                  5    22  5.37402     0.02
11   5    22                                  5    12  5.2[illegible]3[illegible]5  0.02
11   5    12                                  5     8  5.2[illegible]87  0.02
11   5     8                                  9     8  5.27[illegible]7  0.0
11   9     8                                  9     7  5.2777      0.0
11   9     7                                  9     5  5.2717      0.0
11   9     5                                  9     2  5.2517      0.0
11   9     2                                  9     1
4    1     2                                  5     2  5.251662    0.02
             0.0            0.0
4    5     2                                  9     2
             0.0            0.0
4    1     7                                  5     7  5.27766     0.02
             0.0            0.0
1    5     7                                  9     7
4    1     8                                  5     8  5.27866     0.02
             0.0            0.0
1    1    12                                  5    12
1    1    22                                  5    22
1    1    24                                  5    24  5.3822      0.02
1    1    26                                  5    26  5.3872      0.02
1    5    26                                 10    26
4    1    29                                  5    29  5.41466     0.02
             0.0            0.0
1    5    29                                 10    29
1    1    30                                  5    30  5.417119    0.02
1    5    30                                 10    30
1    5    29                                  5    26
1    5    26                                  5    24
```

```
1    5    7                                   5     5 5.271662    0.02
1    5    5                                   5     2 5.251662    0.02
1    1    5                                   5     5
1    5    5                                   9     5
9
     9    9     1     8 2.0
    10   10    24    30 2.0
     1    1     1    30-179.53846
     1   10    31    31   3.0        .00016
               1     1     9     1    24
               3     1    10    24    26
               2     1    10    26    30
               4     1    10    30    31
               9           8  525.0                5           8  525.0
               5           8  525.0                5          24  525.0
               5          24  525.0               10          24  525.0
               1           1   40.0                9           1   40.0
               1          31 -1.0                 10          31 -1.0
   -19                     1         5          0 2 1 -.000122
                                .5          .0005                2          3
     1   10    31    31   3.0          .00149
               9           8 909.0                5           8 909.0
               5           8 909.0                5          24 909.0
               5          24 909.0               10          24 909.0
               1           1 384.0                9           1 384.0
               1          31 -1.0                 10          31 -1.0
   -35                     1         4          0 2 1 -.000165
                                .5          .0005                2          3
     1   10    31    31   3.0          .00202
               9           8 2150.0               5           8 2150.0
               5           8 2150.0               5          24 2150.0
               5          24 2150.0              10          24 2150.0
               1           1 518.0                9           1 518.0
   -55                     1         4          0 2 1 -.000404
                                .5          .0005                2          3
     1   10    31    31   3.0          .0031
               9           8  4035.0              5           8  4035.0
               5           8  4035.0              5          24  4035.0
               5          24  4035.0             10          24  4035.0
               1           1  1436.0              9           1  1436.0
   -58                     1         4 1        0 2 1 -.000578
                                .5          .0005                1          2
     1   10    31    31   3.0          .00370
               9           8 6270.0               5           8 6270.0
               5           8 6270.0               5          24 6270.0
               5          24 6270.0              10          24 6270.0
               1           1 2109.0               9           1 2109.0
              30 .0043333     .03          .24          3.0
   -60                     1         4 1        0 2 1 -.000540
                                .5          .0005                1          2
     1   10    31    31   3.0          .00175
               9           8 6270.0               5           8 6270.0
               5           8 6270.0               5          24 6270.0
               5          24 6270.0              10          24 6270.0
               1           1 2109.0               9           1 2109.0
              30 .1041277     .03          .24          3.0
   -79                     1         4          0 2 1 -.000275
                                .5          .0005                2          3
     1   10    31    31   3.0          -.00149
               9           8 3629.0               5           8 3629.0
               5           8 3629.0               5          24 3629.0
               5          24 3629.0              10          24 3629.0
```

```
            1              1 1267.0
  -85                      1          4                 9        1 1267.0
                           .5                     0 2 1 -.000084
   1    10    31      31 3.0              .0005              2              3
        9              8 1930.0          -.00234
        5              8 1930.0                       5          8 1930.0
        5             24 1930.0                       5         24 1930.0
        1              1 537.0                       10         24 1930.0
  -100                 1          4                   9          1 537.0
                           .5                     0 2 1  .0000403
   1    10    31      31 3.0              .0005              2              3
        9              8 1028.0          -.00354
        5              8 1028.0                       5          8 1028.0
        5             24 1028.0                       5         24 1028.0
        1              1 109.0                       10         24 1028.0
  -129                 1          4                   9          1 109.0
                           .5                     0 2 1 -.000073
   1    10    31      31 3.0              .0005              2              3
        9              8 0.0             -.00386
        5              8 0.0                          5          8 0.0
        5             24 0.0                          5         24 0.0
        1              1 9.0                         10         24 0.0
   4                   1          1                   9          1 9.0
                           .5                     0 2 1 0.0
 0.0         0.0          70.0            .0005              2              3
 10.0        10.          70.0
 10.         0.0          70.0
 0.0         10.          70.0
   1    10    31      31 3.0
        1             31 -.1
  -15                  1          4                  10         31 -.1
                           .5                     0 2 1  .000013
   1    10    31      31   3.0            .0005              2              3
        9              8   525.0          .00016
        5              8   525.0                      5          8  525.0
        5             24   525.0                      5         24  525.0
        1              1    40.0                     10         24  525.0
  -19                  1          5                   9          1   40.0
                             .5                   0 2 1 -.000122
   1    10    31      31   3.0            .0005              2              3
        9              8 909.0            .00149
        5              8 909.0                        5          8 909.0
        5             24 909.0                        5         24 909.0
        1              1 384.0                       10         24 909.0
        1             31 -1.0                         9          1 384.0
  -35                  1          4                  10         31 -1.0
                         .5                       0 2 1 -.000165
   1    10    31      31   3.0            .0005              2              3
        9              8 2150.0           .00202
        5              8 2150.0                       5          8 2150.0
        5             24 2150.0                       5         24 2150.0
        1              1 518.0                       10         24 2150.0
  -55                  1          4                   9          1 518.0
                         .5                       0 2 1 -.000404
   1    10    31      31   3.0            .0005              2              3
        9              8   4035.0         .0031
        5              8   4035.0                     5          8   4035.0
        5             24   4035.0                     5         24   4035.0
        1              1   1436.0                    10         24   4035.0
  -58                  1          4  1                9          1   1436.0
                         .5                       0 2 1 -.000578
   1    10    31      31 3.0              .0005              1              2
                                          .00370
```

```
          9              8 6270.0                    5              8 6270.0
          5              8 6270.0                    5             24 6270.0
          5             24 6270.0                   10             24 6270.0
          1              1 2109.0                    9              1 2109.0
         30 .0043333      .03          .24              3.0
  -60                    1          4  1        0 2 1 -.000540
                                .5          .0005                   1              2
    1    10    31    31  3.0              .00175
          9              8 6270.0                    5              8 6270.0
          5              8 6270.0                    5             24 6270.0
          5             24 6270.0                   10             24 6270.0
          1              1 2109.0                    9              1 2109.0
         30 .1041277      .03          .24              3.0
  -79                    1          4        0 2 1 -.000275
                                .5          .0005                   2              3
    1    10    31    31  3.0              -.00149
          9              8 3629.0                    5              8 3629.0
          5              8 3629.0                    5             24 3629.0
          5             24 3629.0                   10             24 3629.0
          1              1 1267.0                    9              1 1267.0
  -85                    1          4        0 2 1 -.000084
                                .5          .0005                   2              3
    1    10    31    31  3.0              -.00234
          9              8 1930.0                    5              8 1930.0
          5              8 1930.0                    5             24 1930.0
          5             24 1930.0                   10             24 1930.0
          1              1 537.0                     9              1 537.0
  -100                   1          4        0 2 1  .0000403
                                .5          .0005                   2              3
    1    10    31    31  3.0              -.00354
          9              8 1028.0                    5              8 1028.0
          5              8 1028.0                    5             24 1028.0
          5             24 1028.0                   10             24 1028.0
          1              1 109.0                     9              1 109.0
  -129                   1          4        0 2 1  .000073
                                .5          .0005                   2              3
    1    10    31    31  3.0              -.00386
          9              8 0.0                       5              8 0.0
          5              8 0.0                       5             24 0.0
          5             24 0.0                      10             24 0.0
          1              1 9.0                       9              1 9.0
    4                    1          1        0 2 1 0.0
                                .5          .0005                   2              3
  .0          0.0          70.0
 10.0         10.          70.0
 10.          0.0          70.0
 0.0          10.          70.0
    1    10    31    31  3.0
          1             31 -.1                      10             31 -.1
  -15                    1          4        0 2 1 .000013
                                .5          .0005                   2              3
    1    10    31    31   3.0             .00016
          9              8  525.0                    5              8  525.0
          5              8  525.0                    5             24  525.0
          5             24  525.0                   10             24  525.0
          1              1   40.0                    9              1   40.0
  -19                    1          5        0 2 1 -.000122
                                .5          .0005                   2              3
    1    10    31    31  3.0              .00149
          9              8 909.0                     5              8 909.0
          5              8 909.0                     5             24 909.0
          5             24 909.0                    10             24 909.0
```

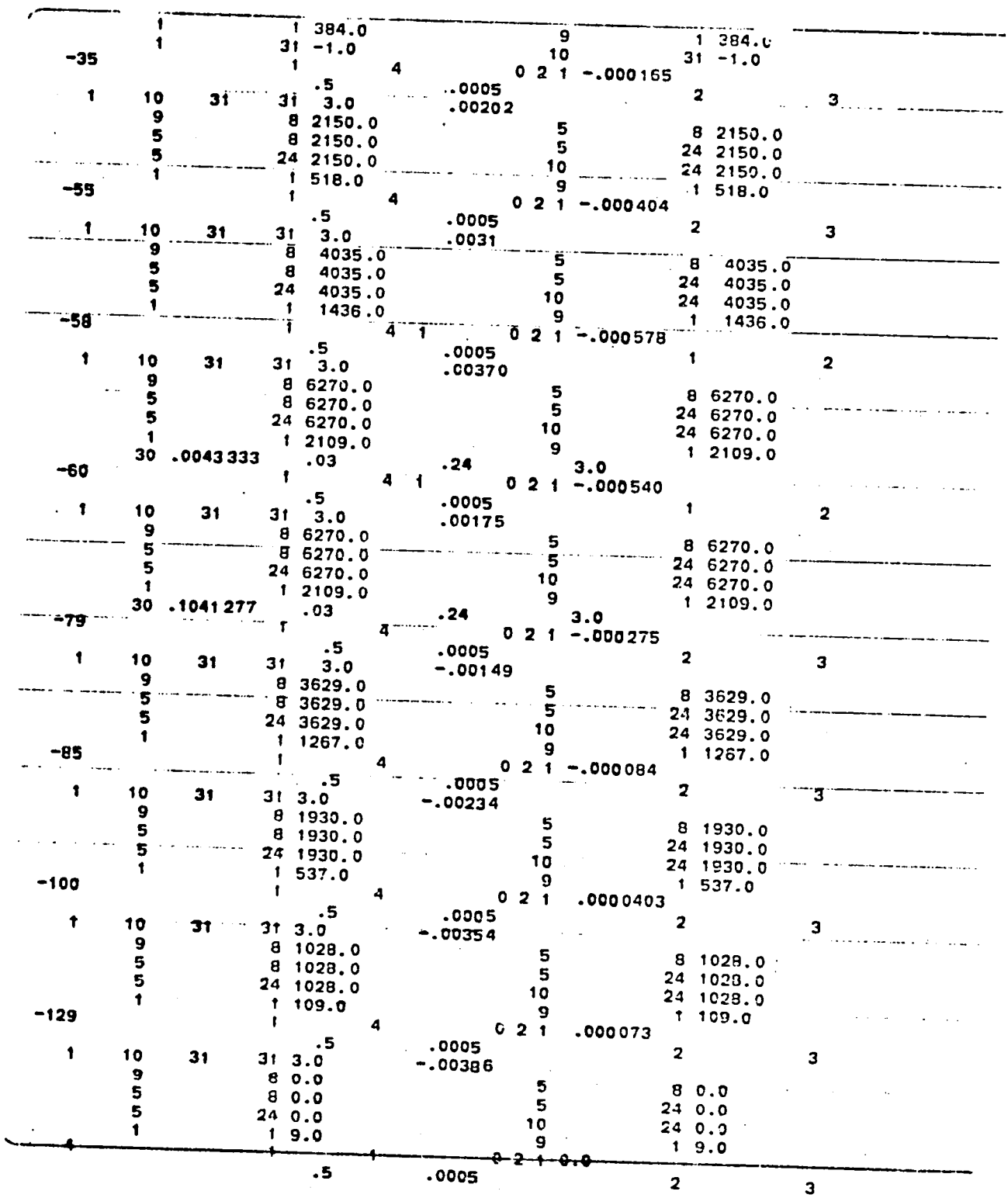

```
 0.0          0.0          70.0
 10.          10.          70.0
 10.          0.0          70.0
 0.0          10.          70.0
    1   10    31    31 3.0
        1              31 -.1                    10          31 -.1
  -15                   1        4          0 2 1 .000013
                          .5          .0005                  2          3
    1   10    31    31   3.0          .00016
        9               8  525.0                  5           8  525.0
        5               8  525.0                  5          24  525.0
        5              24  525.0                 10          24  525.0
        1               1   40.0                  9           1   40.0
  -19                   1        5          0 2 1 -.000122
                             .5          .0005                  2          3
    1   10    31    31   3.0          .00149
        9               8 909.0                  5           8 909.0
        5               8 909.0                  5          24 909.0
        5              24 909.0                 10          24 909.0
        1               1 384.0                  9           1 384.0
        1              31 -1.0                  10          31 -1.0
  -35                   1        4          0 2 1 -.000165
                          .5          .0005                  2          3
    1   10    31    31   3.0          .00202
        9               8 2150.0                 5           8 2150.0
        5               8 2150.0                 5          24 2150.0
        5              24 2150.0                10          24 2150.0
        1               1 518.0                  9           1 518.0
  -55                   1        4          0 2 1 -.000404
                          .5          .0005                  2          3
    1   10    31    31   3.0          .0031
        9               8  4035.0                5           8  4035.0
        5               8  4035.0                5          24  4035.0
        5              24  4035.0               10          24  4035.0
        1               1  1436.0                9           1  1436.0
  -58                   1        4  1       0 2 1 -.000578
                          .5          .0005                  1          2
    1   10    31    31   3.0          .00370
        9               8 6270.0                 5           8 6270.0
        5               8 6270.0                 5          24 6270.0
        5              24 6270.0                10          24 6270.0
        1               1 2109.0                 9           1 2109.0
       30 .0043333      .03          .24          3.0
  -60                   1        4  1       0 2 1 -.000540
                          .5          .0005                  1          2
    1   10    31    31   3.0          .00175
        9               8 6270.0                 5           8 6270.0
        5               8 6270.0                 5          24 6270.0
        5              24 6270.0                10          24 6270.0
        1               1 2109.0                 9           1 2109.0
       30 .1041277      .03          .24          3.0
  -79                   1        4          0 2 1 -.000275
                            .5          .0005                  2          3
    1   10    31    31   3.0          -.00149
        9               8 3629.0                 5           8 3629.0
        5               8 3629.0                 5          24 3629.0
        5              24 3629.0                10          24 3629.0
        1               1 1267.0                 9           1 1267.0
  -85                   1        4          0 2 1 -.000084
                          .5          .0005                  2          3
    1   10    31    31   3.0          -.00234
        9               8 1930.0                 5           8 1930.0
```

```
          5          8 1930.0                  5          24 1930.0
          5         24 1930.0                 10          24 1930.0
          1          1 537.0                   9           1 537.0
  -100               1        4          0 2 1  .0000403
                          .5        .0005                  2          3
    1    10    31   31 3.0        -.00354
          9          8 1028.0                  5           8 1028.0
          5          8 1028.0                  5          24 1028.0
          5         24 1028.0                 10          24 1028.0
          1          1 109.0                   9           1 109.0
  -129               1        4          0 2 1  .000073
                          .5        .0005                  2          3
    1    10    31   31 3.0        -.00386
          9          8 0.0                     5           8 0.0
          5          8 0.0                     5          24 0.0
          5         24 0.0                    10          24 0.0
          1          1 9.0                     9           1 9.0
    4                1        1          0 2 1 0.0
                          .5        .0005                  2          3
0.0         0.0           70.0
10.         10.           70.0
10.         0.0           70.0
0.0         10.           70.0
    1    10    31   31 3.0
          1         31 -.1                    10          31 -.1
  -15                1        4          0 2 1 .000013
                          .5        .0005                  2          3
    1    10    31   31  3.0         .00016
          9          8  525.0                  5           8  525.0
          5          8  525.0                  5          24  525.0
          5         24  525.0                 10          24  525.0
          1          1   40.0                  9           1   40.0
  -19                1        5          0 2 1 -.000122
                          .5        .0005                  2          3
    1    10    31   31  3.0         .00149
          9          8 909.0                   5           8 909.0
          5          8 909.0                   5          24 909.0
          5         24 909.0                  10          24 909.0
          1          1 384.0                   9           1 384.0
          1         31 -1.0                   10          31 -1.0
  -35                1        4          0 2 1 -.000165
                          .5        .0005                  2          3
    1    10    31   31  3.0         .00202
          9          8 2150.0                  5           8 2150.0
          5          8 2150.0                  5          24 2150.0
          5         24 2150.0                 10          24 2150.0
          1          1 518.0                   9           1 518.0
  -55                1        4          0 2 1 -.000404
                          .5        .0005                  2          3
    1    10    31   31  3.0         .0031
          9          8  4035.0                 5           8  4035.0
          5          8  4035.0                 5          24  4035.0
          5         24  4035.0                10          24  4035.0
          1          1  1436.0                 9           1  1436.0
  -58                1        4   1      0 2 1 -.000578
                          .5        .0005                  1          2
    1    10    31   31  3.0         .00370
          9          8 6270.0                  5           8 6270.0
          5          8 6270.0                  5          24 6270.0
          5         24 6270.0                 10          24 6270.0
          1          1 2109.0                  9           1 2109.0
         30  .0043333   .03         .24          3.0
```

```
  -60                   1         4  1          0 2 1 -.000540
                            .5            .0005                        1            2
     1    10    31     31   3.0           .00175
          9            8 6270.0                         5            8 6270.0
          5            8 6270.0                         5           24 6270.0
          5           24 6270.0                        10           24 6270.0
          1            1 2109.0                         9            1 2109.0
         30 .1041277    .03               .24                3.0
  -79                   1         4                 0 2 1 -.000275
                            .5            .0005                        2            3
     1    10    31     31   3.0          -.00149
          9            8 3629.0                         5            8 3629.0
          5            8 3629.0                         5           24 3629.0
          5           24 3629.0                        10           24 3629.0
          1            1 1267.0                         9            1 1267.0
  -85                   1         4                 0 2 1 -.000084
                            .5            .0005                        2            3
     1    10    31     31 3.0            -.00234
          9            8 1930.0                         5            8 1930.0
          5            8 1930.0                         5           24 1930.0
          5           24 1930.0                        10           24 1930.0
          1            1 537.0                          9            1 537.0
 -100                   1         4                 0 2 1  .0000403
                            .5            .0005                        2            3
     1    10    31     31 3.0            -.00354
          9            8 1028.0                         5            8 1028.0
          5            8 1028.0                         5           24 1028.0
          5           24 1028.0                        10           24 1028.0
          1            1 109.0                          9            1 109.0
 -129                   1         4                 0 2 1  .000073
                            .5            .0005                        2            3
     1    10    31     31 3.0            -.00386
          9            8 0.0                            5            8 0.0
          5            8 0.0                            5           24 0.0
          5           24 0.0                           10           24 0.0
          1            1 9.0                            9            1 9.0
     4                  1         1                 0 2 1 0.0
                            .5            .0005                        2            3
 0.0          0.0         70.0
 10.          10.         70.0
 5.5          0.0         70.0
 5.5           .5         70.0
     1    10    31     31 3.0
          1           31 -.1                           10           31 -.1
          1           31 -.1                           10           31 -.1
```

```
QPXSS,T
USER(Q          )
CHARGE(,
ACCT(HAVEN      000754512?•OSS          )
GET,PROCPMR/UN=Q08 28.
ATTACH,TAPE10=TH10101.
ATTACH,TAPE7=EH100XX.
DEFINE,TAPE8=EH120XX/CT=PU.          PXSUBS
BEGIN,APSAC,PROCPMR,NAPSAC.
```

PXSUBS - CARD IMAGES FOR APSAPLOT TO EXTRAPOLATE 23RD, 24TH, AND 25TH DUTY-CYCLE RESULTS TO 40TH CYCLE CONFIGURATION AND TO EXTRAPOLATE ALL SUBSEQUENT CYCLES. TAPE 7 CARRIES THE ACCUMULATED DISPLACEMENTS.

```
TH10101         NER 1.35 HG CYCLE101    ,INCR=01 T=  1.4                    $
    2
TH10101         NER 1.35 HG CYCLE101    ,INCR=02 T=  1.8                    $
    2
TH10101 MCC LINER 1.35 HG CYCLE101    ,INCR=03 T=  2.4                      $
    2
TH10101 MCC LINER 1.35 HG CYCLE101    ,INCR=04 T=  3.4                      $
    2
TH10101 MCC LINER 1.35 HG CYCLE101    ,INCR=05 T=  4.9                      $
    2
TH10101 MCC LINER 1.35 HG CYCLE101    ,INCR=06 T= 20.5                      $
    2
TH10101 MCC LINER 1.35 HG CYCLE101    ,INCR=09 T=395.                       $
    2
TH10101 MCC LINER 1.35 HG CYCLE101    ,INCR=10 T=395.6                      $
    2
TH10101 MCC LINER 1.35 HG CYCLE101    ,INCR=11 T=397.1                      $
    2
TH10101 MCC LINER 1.35 HG CYCLE101    ,INCR=12 T=400.                       $
    2
TH10101 MCC LINER 1.35 HG CYCLE101    ,INCR=13 T=INF.                       $
     1 2   4
           34          35
     1      1      9     9    -1    72     0    64
    2
TH10101 MCC LINER 1.35 HG CYCLE101 +1,INCR=01 T=  1.4                       $
    2
TH10101 MCC LINER 1.35 HG CYCLE101 +1,INCR=02 T=  1.8                       $
    2
TH10101 MCC LINER 1.35 HG CYCLE101 +1,INCR=03 T=  2.4                       $
    2
TH10101 MCC LINER 1.35 HG CYCLE101 +1,INCR=04 T=  3.4                       $
    2
TH10101 MCC LINER 1.35 HG CYCLE101 +1,INCR=05 T=  4.9                       $
    2
TH10101 MCC LINER 1.35 HG CYCLE101 +1,INCR=06 T= 20.5                       $
    2
TH10101 MCC LINER 1.35 HG CYCLE101 +1,INCR=09 T=395.                        $
    2
TH10101 MCC LINER 1.35 HG CYCLE101 +1,INCR=10 T=395.6                       $
    2
TH10101 MCC LINER 1.35 HG CYCLE101 +1,INCR=11 T=397.1                       $
    2
TH10101 MCC LINER 1.35 HG CYCLE101 +1,INCR=12 T=400.                        $
    2
TH10101 MCC LINER 1.35 HG CYCLE101 +1,INCR=13 T=INF.                        $
     1 2   4
           34          35
     1      1      9     9    -1    72     0    64
    2
TH10101 MCC LINER 1.35 HG CYCLE101 +2,INCR=01 T=  1.4                       $
    2
TH10101 MCC LINER 1.35 HG CYCLE101 +2,INCR=02 T=  1.8                       $
    2
TH10101 MCC LINER 1.35 HG CYCLE101 +2,INCR=03 T=  2.4                       $
    2
TH10101 MCC LINER 1.35 HG CYCLE101 +2,INCR=04 T=  3.4                       $
    2
TH10101 MCC LINER 1.35 HG CYCLE101 +2,INCR=05 T=  4.9                       $
    2
TH10101 MCC LINER 1.35 HG CYCLE101 +2,INCR=06 T= 20.5                       $
    2
```

```
TH10101        NER 1.35 HG CYCLE101 +2,INCR=09 T=395.                    $
     2
TH10101        NER 1.35 HG CYCLE101 +2,INCR=10 T=395.6                   $
     2
TH10101 MCC LINER 1.35 HG CYCLE101 +2,INCR=11 T=397.1                    $
     2
TH10101 MCC LINER 1.35 HG CYCLE101 +2,INCR=12 T=400.                     $
     2
TH10101 MCC LINER 1.35 HG CYCLE101 +2,INCR=13 T=INF.                     $
     1 2   4
          34          35
     1     1     9     9    -1    72     0    64
     3     3
     2
TH10101 MCC LINER 1.35 HG CYCLE101 +3,INCR=01 T=  1.4                    $
     2
TH10101 MCC LINER 1.35 HG CYCLE101 +3,INCR=02 T=  1.6                    $
     2
TH10101 MCC LINER 1.35 HG CYCLE101 +3,INCR=03 T=  2.4                    $
     2
TH10101 MCC LINER 1.35 HG CYCLE101 +3,INCR=04 T=  3.4                    $
     2
TH10101 MCC LINER 1.35 HG CYCLE101 +3,INCR=05 T=  4.9                    $
     2
TH10101 MCC LINER 1.35 HG CYCLE101 +3,INCR=06 T= 20.5                    $
     2
TH10101 MCC LINER 1.35 HG CYCLE101 +3,INCR=09 T=395.                     $
     2
TH10101 MCC LINER 1.35 HG CYCLE101 +3,INCR=10 T=395.6                    $
     2
TH10101 MCC LINER 1.35 HG CYCLE101 +3,INCR=11 T=397.1                    $
     2
TH10101 MCC LINER 1.35 HG CYCLE101 +3,INCR=12 T=400.                     $
     2
TH10101 MCC LINER 1.35 HG CYCLE101 +3,INCR=13 T=INF.                     $
     1 2   4
          34          35
     1     1     9     9    -1    72     0    64
     3     4
     2
TH10101 MCC LINER 1.35 HG CYCLE101 +4,INCR=01 T=  1.4                    $
     2
TH10101 MCC LINER 1.35 HG CYCLE101 +4,INCR=02 T=  1.6                    $
     2
TH10101 MCC LINER 1.35 HG CYCLE101 +4,INCR=03 T=  2.4                    $
     2
TH10101 MCC LINER 1.35 HG CYCLE101 +4,INCR=04 T=  3.4                    $
     2
TH10101 MCC LINER 1.35 HG CYCLE101 +4,INCR=05 T=  4.9                    $
     2
TH10101 MCC LINER 1.35 HG CYCLE101 +4,INCR=06 T= 20.5                    $
     2
TH10101 MCC LINER 1.35 HG CYCLE101 +4,INCR=09 T=395.                     $
     2
TH10101 MCC LINER 1.35 HG CYCLE101 +4,INCR=10 T=395.6                    $
     2
TH10101 MCC LINER 1.35 HG CYCLE101 +4,INCR=11 T=397.1                    $
     2
TH10101 MCC LINER 1.35 HG CYCLE101 +4,INCR=12 T=400.                     $
     2
TH10101 MCC LINER 1.35 HG CYCLE101 +4,INCR=13 T=INF.                     $
     1 2   4
```

```
                35
  1        9     9   -1    72     0    64
  1
       34
  1   130     0   227
  1  4  4
       22            1          2          3
  1     1     8     8   -1    56     0    49
 3      1  9.2   5.40  0.0   0.20
    22 -18  9.2   5.40  0.0   0.20
    23 -18  5.2   5.40  0.0   0.20
 81     5
 20          217    10   .00        0.0        1
218          .0000 0     0.0
219          .0000 0     0.0
220          .0000 0     0.0
221          .0000 0     0.0
222          .0000 0     0.0
223          .0000 0     0.0
224          .0000 0     0.0
225          .0000 0     0.0
226          .0000 0     0.0
227          .0000 0     0.0
  1  1  2
       34
  1   130     0   227
  1  2  2
       34          35
  1     1     0    99
 2
 2
```

```
QPLTS,T7,.
USER(Q                )
CHARGE(*)
ACCT(HAVEN     000 4545127*055          )
PURGE,PRD101/NA.
RETURN,PRD101.
DEFINE,PRD101.
GET,PROCPMR/UN=Q0828.
ATTACH,TAPE10=TD10101.
BEGIN,APSAC,PROCPMR,NAPSAC.                              PLOTMCC     1.35HG
REWIND,OUTPUT.
COPYEI,OUTPUT,PRD101.
COPYEI,OUTPUT,PRD101.
```

CARD IMAGES FOR APSAPLOT FOR PLOTS AND OUTPUT SUMMARIES

```
TD10101 MCC LINER 1.35HG  CYCLE101    ,INCR=01 T=  1.4    TMAX=-360        $
    1 5   4
          22              1              2              3              4
     1     1.    8      8     -1     56      0     49
     1 5
          23             11             12             13             14              0
     2                                  END PLOT SET
TD10101 MCC LINER 1.35HG  CYCLE101    ,INCR=02 T=  1.6    TMAX= 488        $
    21
TD10101 MCC LINER 1.35HG  CYCLE101    ,INCR=03 T=  2.4    TMAX= 718        $
    21
TD10101 MCC LINER 1.35HG  CYCLE101    ,INCR=04 T=  3.4    TMAX=1157        $
    21
TD10101 MCC LINER 1.35HG  CYCLE101    ,INCR=05 T=  4.9    TMAX=1465        $
    21
TD10101 MCC LINER 1.35HG  CYCLE101    ,INCR=06 T= 20.5    TMAX=1484        $
    3       1 5.2    5.40  0.0    0.20
    3       1
        1 -18 5.2    5.4   0.0    0.20
        2 -18 5.2    5.4   0.0    0.20
        3 -18 5.2    5.4   0.0    0.20
        4 -18 5.2    5.4   0.0    0.20
       22 -18 5.2    5.4   0.0    0.20
       11 -18 5.2    5.4   0.0    0.20
       12 -18 5.2    5.4   0.0    0.20
       13 -18 5.2    5.4   0.0    0.20
       14 -18 5.2    5.4   0.0    0.20
       23 -18 5.2    5.4   0.0    0.20
       21 -16 5.2    5.4   0.0    0.20
     1401     5.24   5.32  -.02   .06
     1402     5.24   5.32  -.02   .06
     1403     5.24   5.32  -.02   .06
     14 4     5.24   5.32  -.02   .06
     1422     5.24   5.32  -.02   .06
     1411     5.24   5.32  -.02   .06
     1412     5.24   5.32  -.02   .06
     1413     5.24   5.32  -.02   .06
     1414     5.24   5.32  -.02   .06
     1423     5.24   5.32  -.02   .06
     1421     5.24   5.32  -.02   .06
     1 5  16
             1              2              3              4             22
     8       1     0     49      8      2     0     50      8      3     0     51
     8       4     0     52      8      5     0     53      8      6     0     54
     8       7     0     55      8      8     0     56
     1 5
            11             12             13             14             23              0
     1 1    4
           34
     1       1      9      9     -1     72      0     64
     1 1
           35                                                                        0
    21
TD10101 MCC LINER 1.35HG  CYCLE101    ,INCR=09 T=395.     TMAX=1191        $
    21
TD10101 MCC LINER 1.35HG  CYCLE101 +1,INCR=10 T=395.6     TMAX= 858        $
    21
TD10101 MCC LINER 1.35HG  CYCLE101    ,INCR=11 T=397.1    TMAX=-297        $
    21
TD10101 MCC LINER 1.35HG  CYCLE101    ,INCR=12 T 400.     TMAX=-405        $
    1 5  16
             1              2              3              4             22
```

```
 8     1     0    49     8     2     0    50     8     3     0    51
 8     4     0    52     8     5     0    53     8     6     0    54
 8     7     0    55     8     8     0    56
 1 5
          11          12          13          14          23          0
 1 1   4
       34
 1     1     9     9    -1    72     0    64
 1 1
          35                                                          0
 21
TD10101 MCC LINER 1.35HG  CYCLE101    ,INCR=13 AMBIENT  TMAX= 70          $
 3        1 5.2   5.40  0.0   0.20
 3        1
       1 -18 5.2   5.4   0.0   0.20
       2 -18 5.2   5.4   0.0   0.20
       3 -18 5.2   5.4   0.0   0.20
       4 -18 5.2   5.4   0.0   0.20
      22 -18 5.2   5.4   0.0   0.20
      11 -18 5.2   5.4   0.0   0.20
      12 -18 5.2   5.4   0.0   0.20
      13 -18 5.2   5.4   0.0   0.20
      14 -18 5.2   5.4   0.0   0.20
      23 -18 5.2   5.4   0.0   0.20
      21 -18 5.2   5.4   0.0   0.20
    1401     5.24  5.32  -.02  .06
    1402     5.24  5.32  -.02  .06
    1403     5.24  5.32  -.02  .06
    1404     5.24  5.32  -.02  .06
    1422     5.24  5.32  -.02  .06
    1411     5.24  5.32  -.02  .06
    1412     5.24  5.32  -.02  .06
    1413     5.24  5.32  -.02  .06
    1414     5.24  5.32  -.02  .06
    1423     5.24  5.32  -.02  .06
    1421     5.24  5.32  -.02  .06
 1 5  16
          1           2           3           4          22
 8     1     0    49     8     2     0    50     8     3     0    51
 8     4     0    52     8     5     0    53     8     6     0    54
 8     7     0    55     8     8     0    56
 1 5
          11          12          13          14          23          0
 1 1   4
       34
 1     1     9     9    -1    72     0    64
 1 1
          35                                                          0
 21
TD10101 MCC LINER 1.35HG  CYCLE101 +1,INCR=01 T=  1.4   TMAX=-360       $
 2
TD10101 MCC LINER 1.35HG  CYCLE101 +1,INCR=02 T=  1.6   TMAX= 488       $
 2
TD10101 MCC LINER 1.35HG  CYCLE101 +1,INCR=03 T=  2.4   TMAX= 718       $
 2
TD10101 MCC LINER 1.35HG  CYCLE101 +1,INCR=04 T=  3.4   TMAX=1157       $
 2
TD10101 MCC LINER 1.35HG  CYCLE101 +1,INCR=05 T=  4.9   TMAX=1465       $
 2
TD10101 MCC LINER 1.35HG  CYCLE101 +1,INCR=06 T= 20.5   TMAX=1484       $
 2
TD10101 MCC LINER 1.35HG  CYCLE101 +1,INCR=09 T=395.    TMAX=1191       $
```

```
    2
TD10101 MCC LINER 1.35HG  CYCLE101 +1,INCR=10 T=395.6   TMAX= 858      $
    2
TD10101 MCC LINER 1.35HG  CYCLE101 +1,INCR=11 T=397.1   TMAX=-297      $
    2
TD10101 MCC LINER 1.35HG  CYCLE101 +1,INCR=12 T 400.    TMAX=-405      $
    2
TD10101 MCC LINER 1.35HG  CYCLE101 +1,INCR=13 AMBIENT   TMAX= 70       $
    2
TD10101 MCC LINER 1.35HG  CYCLE101 +2,INCR=01 T=  1.4   TMAX=-360      $
    2
TD10101 MCC LINER 1.35HG  CYCLE101 +2,INCR=02 T=  1.6   TMAX= 488      $
    2
TD10101 MCC LINER 1.35HG  CYCLE101 +2,INCR=03 T=  2.4   TMAX= 718      $
    2
TD10101 MCC LINER 1.35HG  CYCLE101 +2,INCR=04 T=  3.4   TMAX=1157      $
    2
TD10101 MCC LINER 1.35HG  CYCLE101 +2,INCR=05 T=  4.9   TMAX=1465      $
    2
TD10101 MCC LINER 1.35HG  CYCLE101 +2,INCR=06 T= 20.5   TMAX=1484      $
    2
TD10101 MCC LINER 1.35HG  CYCLE101 +2,INCR=09 T=395.    TMAX=1191      $
    2
TD10101 MCC LINER 1.35HG  CYCLE101 +2,INCR=10 T=395.6   TMAX= 858      $
    2
TD10101 MCC LINER 1.35HG  CYCLE101 +2,INCR=11 T=397.1   TMAX=-297      $
    2
TD10101 MCC LINER 1.35HG  CYCLE101 +2,INCR=12 T 400.    TMAX=-405      $
    2
TD10101 MCC LINER 1.35HG  CYCLE101 +2,INCR=13 AMBIENT   TMAX= 70       $
   21
TD10101 MCC LINER 1.35HG  CYCLE101 +3,INCR=01 T=  1.4   TMAX=-360      $
   21
TD10101 MCC LINER 1.35HG  CYCLE101 +3,INCR=02 T=  1.6   TMAX= 488      $
   21
TD10101 MCC LINER 1.35HG  CYCLE101 +3,INCR=03 T=  2.4   TMAX= 718      $
   21
TD10101 MCC LINER 1.35HG  CYCLE101 +3,INCR=04 T=  3.4   TMAX=1157      $
   21
TD10101 MCC LINER 1.35HG  CYCLE101 +3,INCR=05 T=  4.9   TMAX=1465      $
   21
TD10101 MCC LINER 1.35HG  CYCLE101 +3,INCR=06 T= 20.5   TMAX=1484      $
   21
TD10101 MCC LINER 1.35HG  CYCLE101 +3,INCR=09 T=395.    TMAX=1191      $
   21
TD10101 MCC LINER 1.35HG  CYCLE101 +3,INCR=10 T=395.6   TMAX= 858      $
   21
TD10101 MCC LINER 1.35HG  CYCLE101 +3,INCR=11 T=397.1   TMAX=-297      $
   21
TD10101 MCC LINER 1.35HG  CYCLE101 +3,INCR=12 T 400.    TMAX=-405      $
   21
TD10101 MCC LINER 1.35HG  CYCLE101 +3,INCR=13 AMBIENT   TMAX= 70       $
    2
TD10101 MCC LINER 1.35HG  CYCLE101 +4,INCR=01 T=  1.4   TMAX=-360      $
   21
TD10101 MCC LINER 1.35HG  CYCLE101 +4,INCR=02 T=  1.6   TMAX= 488      $
    3      1 5.2   5.40  0.0   0.20
      22 -18 5.2   5.40  0.0   0.20
      23 -18 5.2   5.40  0.0   0.20
   21
TD10101 MCC LINER 1.35HG  CYCLE101 +4,INCR=03 T=  2.4   TMAX= 718      $
   21
```

```
TD10101 MCC LINER 1.35HG  CYCLE101 +4,INCR=04 T=  3.4    TMAX=1157       $
   21
TD10101 MCC LINER 1.35HG  CYCLE101 +4,INCR=05 T=  4.9    TMAX=1465       $
   21
TD10101 MCC LINER 1.35HG  CYCLE101 +4,INCR=06 T= 20.5    TMAX=1484       $
   3      1 5.2   5.40  0.0   0.20
   3      1
      1 -18 5.2   5.4   0.0   0.20
      2 -18 5.2   5.4   0.0   0.20
      3 -18 5.2   5.4   0.0   0.20
      4 -18 5.2   5.4   0.0   0.20
     22 -18 5.2   5.4   0.0   0.20
     11 -18 5.2   5.4   0.0   0.20
     12 -18 5.2   5.4   0.0   0.20
     13 -18 5.2   5.4   0.0   0.20
     14 -18 5.2   5.4   0.0   0.20
     23 -18 5.2   5.4   0.0   0.20
     21 -18 5.2   5.4   0.0   0.20
   1401     5.24  5.32  -.02  .06
   1402     5.24  5.32  -.02  .06
   1403     5.24  5.32  -.02  .06
   1404     5.24  5.32  -.02  .06
   1422     5.24  5.32  -.02  .06
   1411     5.24  5.32  -.02  .06
   1412     5.24  5.32  -.02  .06
   1413     5.24  5.32  -.02  .06
   1414     5.24  5.32  -.02  .06
   1423     5.24  5.32  -.02  .06
   1421     5.24  5.32  -.02  .06
    1 5  16
          1          2          3          4         22
    8     1     0    49     8    2     0    50     8    3     0    51
    8     4     0    52     8    5     0    53     8    6     0    54
    8     7     0    55     8    8     0    56
    1 5                                                            0
         11         12         13         14         23
    1 1   4
         34
    1     1     9     9   -1   72     0    64
    1 1                                                            0
         35
   21
TD10101 MCC LINER 1.35HG  CYCLE101 +4,INCR=09 T=395.    TMAX=1191       $
   21
TD10101 MCC LINER 1.35HG  CYCLE101 +4,INCR=10 T=395.6   TMAX= 858       $
   21
TD10101 MCC LINER 1.35HG  CYCLE101 +4,INCR=11 T=397.1   TMAX=-297       $
   21
TD10101 MCC LINER 1.35HG  CYCLE101 +4,INCR=12 T 400.    TMAX=-405       $
   3      1 5.2   5.40  0.0   0.20
   3      1
    1 5  16
          1          2          3          4         22
    8     1     0    49     8    2     0    50     8    3     0    51
    8     4     0    52     8    5     0    53     8    6     0    54
    8     7     0    55     8    8     0    56
    1 5                                                            0
         11         12         13         14         23
    1 1   4
         34
    1     1     9     9   -1   72     0    64
    1 1                                                            0
```

```
          35
    21
TD10101 MCC  LINER  1.35HG   CYCLE101 +4,INCR=13 AMBIENT   TMAX= 70        $
    4 -1
    1.0
    3        1 5.2    5.40   0.0    0.20
    3      . 1
        1 -18 5.2    5.4    0.0    0.20
        2 -18 5.2    5.4    0.0    0.20
        3 -18 5.2    5.4    0.0    0.20
        4 -18 5.2    5.4    0.0    0.20
       22 -18 5.2    5.4    0.0    0.20
       11 -18 5.2    5.4    0.0    0.20
       12 -18 5.2    5.4    0.0    0.20
       13 -18 5.2    5.4    0.0    0.20
       14 -18 5.2    5.4    0.0    0.20
       23 -18 5.2    5.4    0.0    0.20
       21 -18 5.2    5.4    0.0    0.20
    1401      5.24   5.32   -.02   .06
    1402      5.24   5.32   -.02   .06
    1403      5.24   5.32   -.02   .06
    1404      5.24   5.32   -.02   .06
    1422      5.24   5.32   -.02   .06
    1411      5.24   5.32   -.02   .06
    1412      5.24   5.32   -.02   .06
    1413      5.24   5.32   -.02   .06
    1414      5.24   5.32   -.02   .06
    1423      5.24   5.32   -.02   .06
    1421      5.24   5.32   -.02   .06
     1 5  16
            1          2          3          4         22
     8      1    0    49    8     2    0    50    8     3    0    51
     8      4    0    52    8     5    0    53    8     6    0    54
     8      7    0    55    8     8    0    56
     1 5                                                          0
           11         12         13         14         23
     1 1    4
           34
     1      1    9     9   -1    72    0    64
     1 1
                                                                  0
           35
           35
```

```
QPXST,T77.
USER(Q      ,          )
CHARGE(*)
ACCT(HAVEN      000 7545127*055.      )
GET,PROCPMR/UN=QCB28.
ATTACH,TAPE10=TH00101.
DEFINE,TAPE8=EH20X13/CT=PU.          PXSTART
BEGIN,APSAC,PROCPMR,NAPSAC.
```

PXSTART - CARD IMAGES FOR APSAPLOT USED TO EXTRAPOLATE 3RD, 4TH, AND 5TH DUTY-CYCLE RESULTS TO 20TH CYCLE CONFIGURATION

```
TH00101 MCC LINER 1.35 HG CYCLE001    ,INCR=01 T=  1.4                    $
    2
TH00101 MCC LINER 1.35 HG CYCLE001    ,INCR=02 T=  1.6                    $
    2
TH00101 MCC LINER 1.35 HG CYCLE001    ,INCR=03 T=  2.4                    $
    2
TH00101 MCC LINER 1.35 HG CYCLE001    ,INCR=04 T=  3.4                    $
    2
TH00101 MCC LINER 1.35 HG CYCLE001    ,INCR=05 T=  4.9                    $
    2
TH00101 MCC LINER 1.35 HG CYCLE001    ,INCR=06 T= 20.5                    $
    2
TH00101 MCC LINER 1.35 HG CYCLE001    ,INCR=09 T=395.                     $
    2
TH00101 MCC LINER 1.35 HG CYCLE001    ,INCR=10 T=395.6                    $
    2
TH00101 MCC LINER 1.35 HG CYCLE001    ,INCR=11 T=397.1                    $
    2
TH00101 MCC LINER 1.35 HG CYCLE001    ,INCR=12 T=400.                     $
    2
TH00101 MCC LINER 1.35 HG CYCLE001    ,INCR=13 T=INF.                     $
     1 2   4
           34          35
    1      1      9     9     -1    72     0     64
    2
TH00101 MCC LINER 1.35 HG CYCLE001 +1,INCR=01 T=  1.4                     $
    2
TH00101 MCC LINER 1.35 HG CYCLE001 +1,INCR=02 T=  1.6                     $
    2
TH00101 MCC LINER 1.35 HG CYCLE001 +1,INCR=03 T=  2.4                     $
    2
TH00101 MCC LINER 1.35 HG CYCLE001 +1,INCR=04 T=  3.4                     $
    2
TH00101 MCC LINER 1.35 HG CYCLE001 +1,INCR=05 T=  4.9                     $
    2
TH00101 MCC LINER 1.35 HG CYCLE001 +1,INCR=06 T= 20.5                     $
    2
TH00101 MCC LINER 1.35 HG CYCLE001 +1,INCR=09 T=395.                      $
    2
TH00101 MCC LINER 1.35 HG CYCLE001 +1,INCR=10 T=395.6                     $
    2
TH00101 MCC LINER 1.35 HG CYCLE001 +1,INCR=11 T=397.1                     $
    2
TH00101 MCC LINER 1.35 HG CYCLE001 +1,INCR=12 T=400.                      $
    2
TH00101 MCC LINER 1.35 HG CYCLE001 +1,INCR=13 T=INF.                      $
     1 2   4
           34          35
    1      1      9     9     -1    72     0     64
    2
TH00101 MCC LINER 1.35 HG CYCLE001 +2,INCR=01 T=  1.4                     $
    2
TH00101 MCC LINER 1.35 HG CYCLE001 +2,INCR=02 T=  1.6                     $
    2
TH00101 MCC LINER 1.35 HG CYCLE001 +2,INCR=03 T=  2.4                     $
    2
TH00101 MCC LINER 1.35 HG CYCLE001 +2,INCR=04 T=  3.4                     $
    2
TH00101 MCC LINER 1.35 HG CYCLE001 +2,INCR=05 T=  4.9                     $
    2
TH00101 MCC LINER 1.35 HG CYCLE001 +2,INCR=06 T= 20.5                     $
    2
```

```
TH00101 MCC LINER 1.35 HG CYCLE001 +2,INCR=09 T=395.                    $
    2
TH00101 MCC LINER 1.35 HG CYCLE001 +2,INCR=10 T=395.6                   $
    2
TH00101 MCC LINER 1.35 HG CYCLE001 +2,INCR=11 T=397.1                   $
    2
TH00101 MCC LINER 1.35 HG CYCLE001 +2,INCR=12 T=400.                    $
    2
TH00101 MCC LINER 1.35 HG CYCLE001 +2,INCR=13 T=INF.                    $
     1 2  4
          34          35
     1    1    9      9    -1    72     0    64
    5     3
    2
TH00101 MCC LINER 1.35 HG CYCLE001 +3,INCR=01 T=  1.4                   $
    2
TH00101 MCC LINER 1.35 HG CYCLE001 +3,INCR=02 T=  1.6                   $
    2
TH00101 MCC LINER 1.35 HG CYCLE001 +3,INCR=03 T=  2.4                   $
    2
TH00101 MCC LINER 1.35 HG CYCLE001 +3,INCR=04 T=  3.4                   $
    2
TH00101 MCC LINER 1.35 HG CYCLE001 +3,INCR=05 T=  4.9                   $
    2
TH00101 MCC LINER 1.35 HG CYCLE001 +3,INCR=06 T= 20.5                   $
    2
TH00101 MCC LINER 1.35 HG CYCLE001 +3,INCR=09 T=395.                    $
    2
TH00101 MCC LINER 1.35 HG CYCLE001 +3,INCR=10 T=395.6                   $
    2
TH00101 MCC LINER 1.35 HG CYCLE001 +3,INCR=11 T=397.1                   $
    2
TH00101 MCC LINER 1.35 HG CYCLE001 +3,INCR=12 T=400.                    $
    2
TH00101 MCC LINER 1.35 HG CYCLE001 +3,INCR=13 T=INF.                    $
     1 2  4
          34          35
     1    1    9      9    -1    72     0    64
    5     4
    2
TH00101 MCC LINER 1.35 HG CYCLE001 +4,INCR=01 T=  1.4                   $
    2
TH00101 MCC LINER 1.35 HG CYCLE001 +4,INCR=02 T=  1.6                   $
    2
TH00101 MCC LINER 1.35 HG CYCLE001 +4,INCR=03 T=  2.4                   $
    2
TH00101 MCC LINER 1.35 HG CYCLE001 +4,INCR=04 T=  3.4                   $
    2
TH00101 MCC LINER 1.35 HG CYCLE001 +4,INCR=05 T=  4.9                   $
    2
TH00101 MCC LINER 1.35 HG CYCLE001 +4,INCR=06 T= 20.5                   $
    2
TH00101 MCC LINER 1.35 HG CYCLE001 +4,INCR=09 T=395.                    $
    2
TH00101 MCC LINER 1.35 HG CYCLE001 +4,INCR=10 T=395.6                   $
    2
TH00101 MCC LINER 1.35 HG CYCLE001 +4,INCR=11 T=397.1                   $
    2
TH00101 MCC LINER 1.35 HG CYCLE001 +4,INCR=12 T=400.                    $
    2
TH00101 MCC LINER 1.35 HG CYCLE001 +4,INCR=13 T=INF.                    $
     1 2  4
```

```
      34          35
 1     1     9     9    -1    72     0    64
 1 1   2
      34
 1   130     0   227
 1 4   4
      22                1
 1     1     8     8    -1    56     0    49
 3     1  5.2   5.40  0.0   0.20
   22 -18  5.2   5.40  0.0   0.20
   23 -18  5.2   5.40  0.0   0.20
 81    5
 20          217    10  .02          0.0
218        .0200          0.0
219        .0200          0.0
220        .0200          0.0
221        .0200          0.0
222        .0200          0.0
223        .0200          0.0
224        .0200          0.0
225        .0200          0.0
226        .0200          0.0
227        .0200          0.0
 1 1   2
      34
 1   130     0   227
 1 2   2
      34          35
 1     1     0    99
 3     1
 2
 2
```

APPENDIX E

LOCAL HOT SPOT ANALYSIS REFINEMENT STUDY

The primary effort of this study was analysis of the basic SSME MCC liner and evaluation of life-enhancement designs. An additional task was evaluation of increasing the local heating to account for local hot-spot effects. This local heating was accounted for in the modeling by simply increasing the local heat transfer rate, obtaining the resultant temperatures, and analyzing them in the 2D plane strain model. This methodology inherently assumes that the local heating occurs over a significant band of material axially and completely around the hoop direction. For the thermal analysis, this may be an appropriate methodology for obtaining maximum temperatures; but it is only an estimate of the actual stress and strain picture. In reality, and previously noted, the mid-channel cracking predominantly occurs in hot-spot areas. These hot-spots roughly take on the shape of a 3:1 or 4:1 ellipse, with the long axis along the meridian, and the short axis covering from 5- to 10-channel widths.

A pictorial view of a developed liner with a hot spot near the throat throughout a duty cycle is shown in Fig. 112. The liner has two axisymmetric surfaces with axial land members. This results in an orthotropic stiffness path that makes a hot-spot analysis more difficult. During the prechill portion of the duty cycle and up to say 600 or 700 F, the liner wall temperatures and stiffnesses are relatively uniform with little variation from local injector effects. As the temperature rises, the hot-spot markedly affects the stiffnesses and thermal loads. At steady state, the hot-spot is essentially an elliptical hole to the overall liner since its stiffness is much less than the surrounding zone of material. A local hole will result in a distorted shape and load path around this location and strain concentrations at its edges. Within the hot-spot, the hole distortion is additive to the local hot-spot strains. As the engine is throttled back, and goes through the ensuing cutoff conditions, the liner cools and again becomes essentially a stiff membrane that locks in a portion of the strain distortions from the hot-spot. This hot-spot duty cycle has the potential to both add in large local strains in the axial and hoop directions over an axisymmetric model analysis, and add a biased strain to each duty cycle.

A detail model of a total liner to develop this hot-spot duty-cycle strain history is a large study in manhours and computer dollars. A first approximation, though, was made using a 2D plane strain analysis of one-quarter of a hot-spot, with local symmetry assumed. Figure 113 pictorially shows the model and duty cycle.

An approximately 8-inch square model was used. For this first-cut analysis, only the hot wall was modeled, although a refinement of the model would be to add in a variable thickness to simulate added stiffness from the land. The hot-spot was modeled as a stepped variation in x, y dimensions to approximate the hot-spot ellipse. A 4 x 1-inch hot-spot was simulated. Symmetry boundary conditions were applied along x=0 and y=0. Fixed displacements were added to the other boundaries to simulate the hoop and axial displacements.

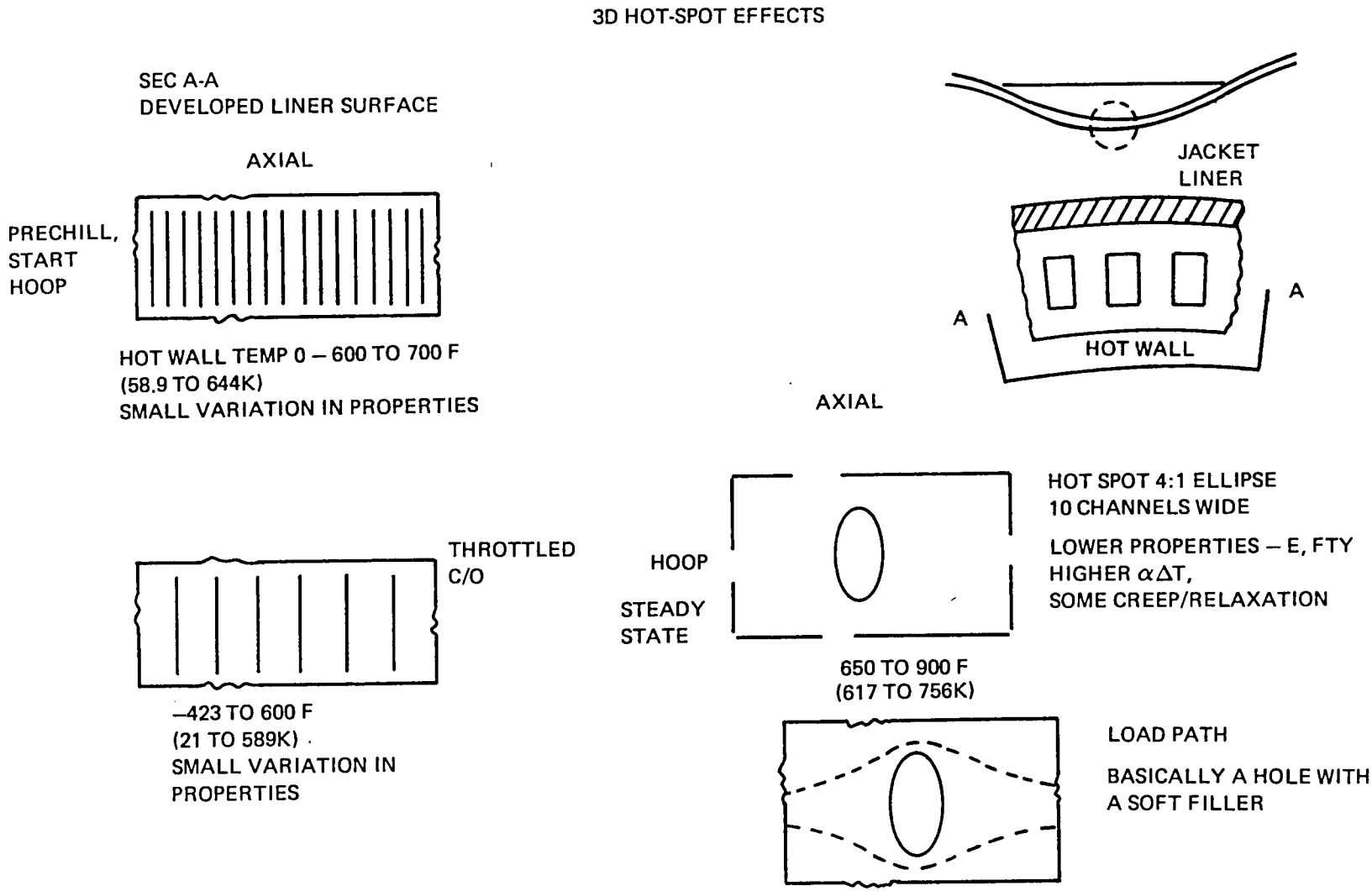

Figure 112. 3D Hot-Spot Effects

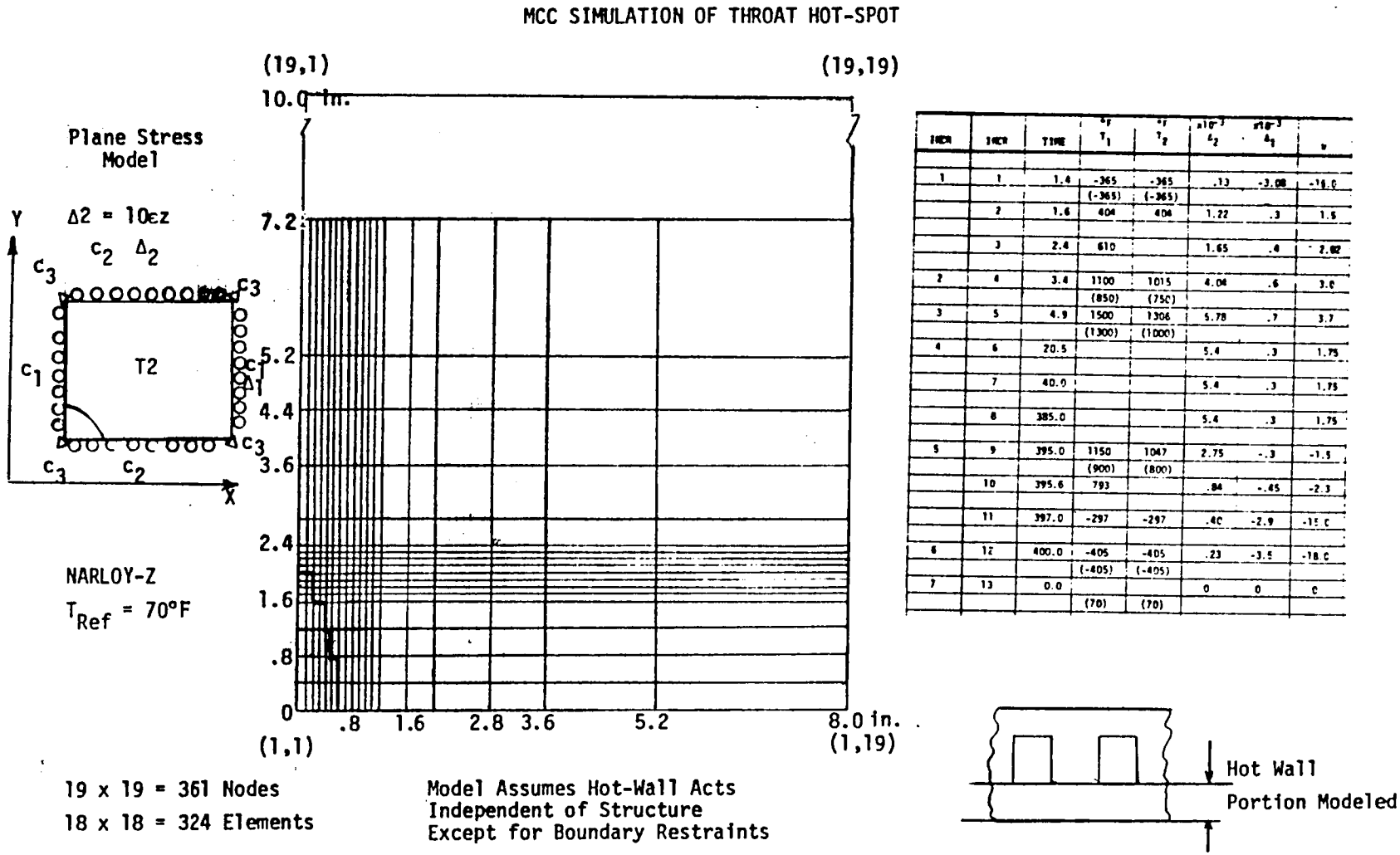

INCR	INCR	TIME	°F T1	°F T2	×10⁻³ Δ2	×10⁻³ Δ1	ψ
1	1	1.4	-365	-365	.13	-3.08	-16.0
			(-365)	(-365)			
	2	1.6	404	404	1.22	.3	1.5
	3	2.4	610		1.65	.4	2.02
2	4	3.4	1100	1015	4.04	.6	3.0
			(850)	(750)			
3	5	4.9	1500	1306	5.78	.7	3.7
			(1300)	(1000)			
4	6	20.5			5.4	.3	1.75
	7	40.0			5.4	.3	1.75
	8	385.0			5.4	.3	1.75
5	9	395.0	1150	1047	2.75	-.3	-1.5
			(900)	(800)			
	10	395.6	793		.84	-.45	-2.3
	11	397.0	-297	-297	.40	-2.9	-15.0
6	12	400.0	-405	-405	.23	-3.5	-18.0
			(-405)	(-405)			
7	13	0.0			0	0	0
			(70)	(70)			

Figure 113. MCC Simulation of Throat Hot-Spot

The duty cycle was reduced to seven load increments, as noted, and constant temperatures applied in two zones--one inside the hot-spot and the remaining area on average liner temperature. Only one duty cycle was run as a test. Figures 114 through 116 are plots of the steady-state condition; and Fig. 117 and 118 shows the residual strains after cooldown at 70 F condition. At both steady state and the cooldown condition, the peak hoop strain in the hot spot zone is about 6 or 7 times the strain level away from the hot spot. The axial strain is about the same throughout the model. From a strain range basis, the peak strain range is 3.4%, which is greater than twice the strain range away from the hot-spot. A bias of almost -3% occurs in the maximum strain condition after cooldown (Table 13).

Some sensitivity studies were made early in the project on adjusting axial strains and hoop effects by using pseudo ΔT effects. These results showed some reduction in life or more rapid thinning, but the results were not consistent with the strain bias or large factors herein shown on hoop strains.

Future efforts on understanding local hot-spot effects should be slanted toward more accurate 3D representations, and possibly more 2D simplified analysis may well explain the difference in actual local hot-spot life in test vs the current axisymmetric (total hot spot) analysis.

TABLE 13. COMPARISON OF HOT-SPOT STRAINS TO NOMINAL CONDITION STRAINS

CONDITION	RATIO PEAK TO AVERAGE ε		PEAK		AVERAGE	
	HOOP, Y	AXIAL, X	HOOP, %	AXIAL, %	HOOP, %	AXIAL, %
STEADY-STATE	6	1.25	-6.2	-1.25	-1	-1
294 K (70 F)	-7	.8	-2.8	0.65	0.4	0.8
DIFFERENCE			-3.4	-1.9	-1.4	-1.8

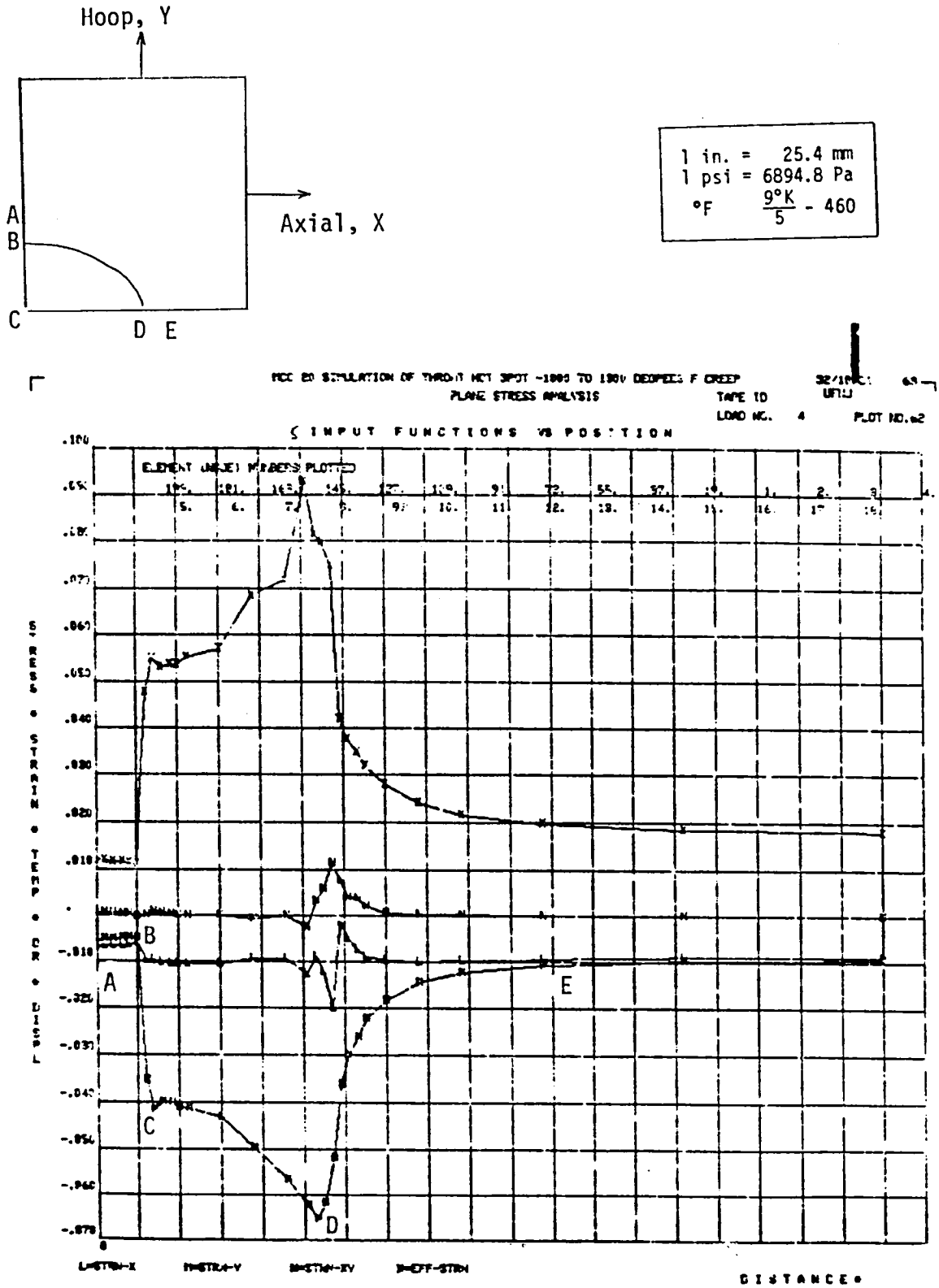

Figure 114. Steady-State Strain Distribution Along Hot-Spot Model Boundary

1 in.	=	25.4 mm
1 psi	=	6894.8 Pa
°F	=	$\frac{9°K}{5}$ - 460

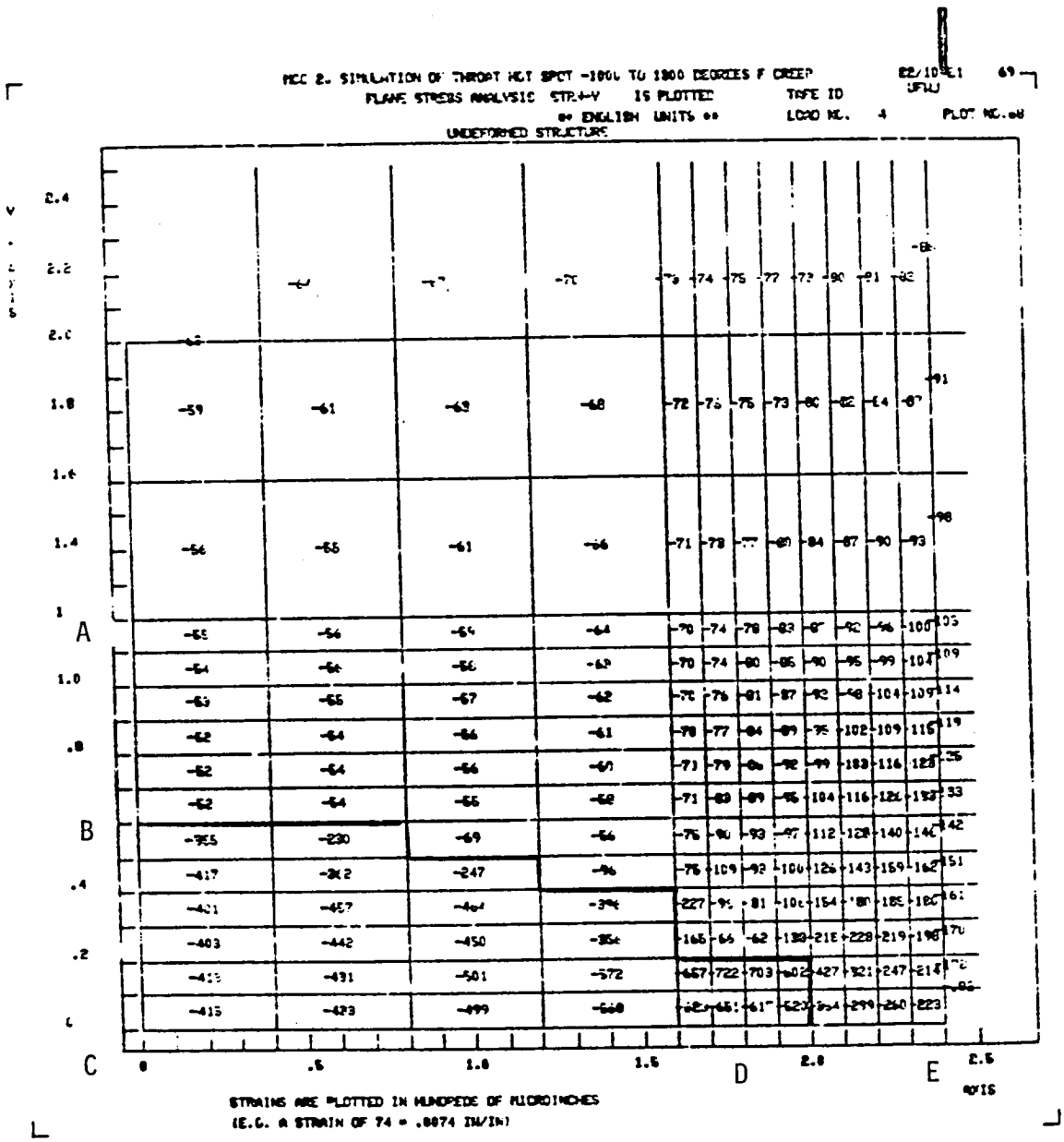

Figure 115. Steady-State Strains in Hot-Spot Model

1 in.	=	25.4 mm
1 psi	=	6894.8 Pa
°F	=	$\frac{9°K}{5}$ - 460

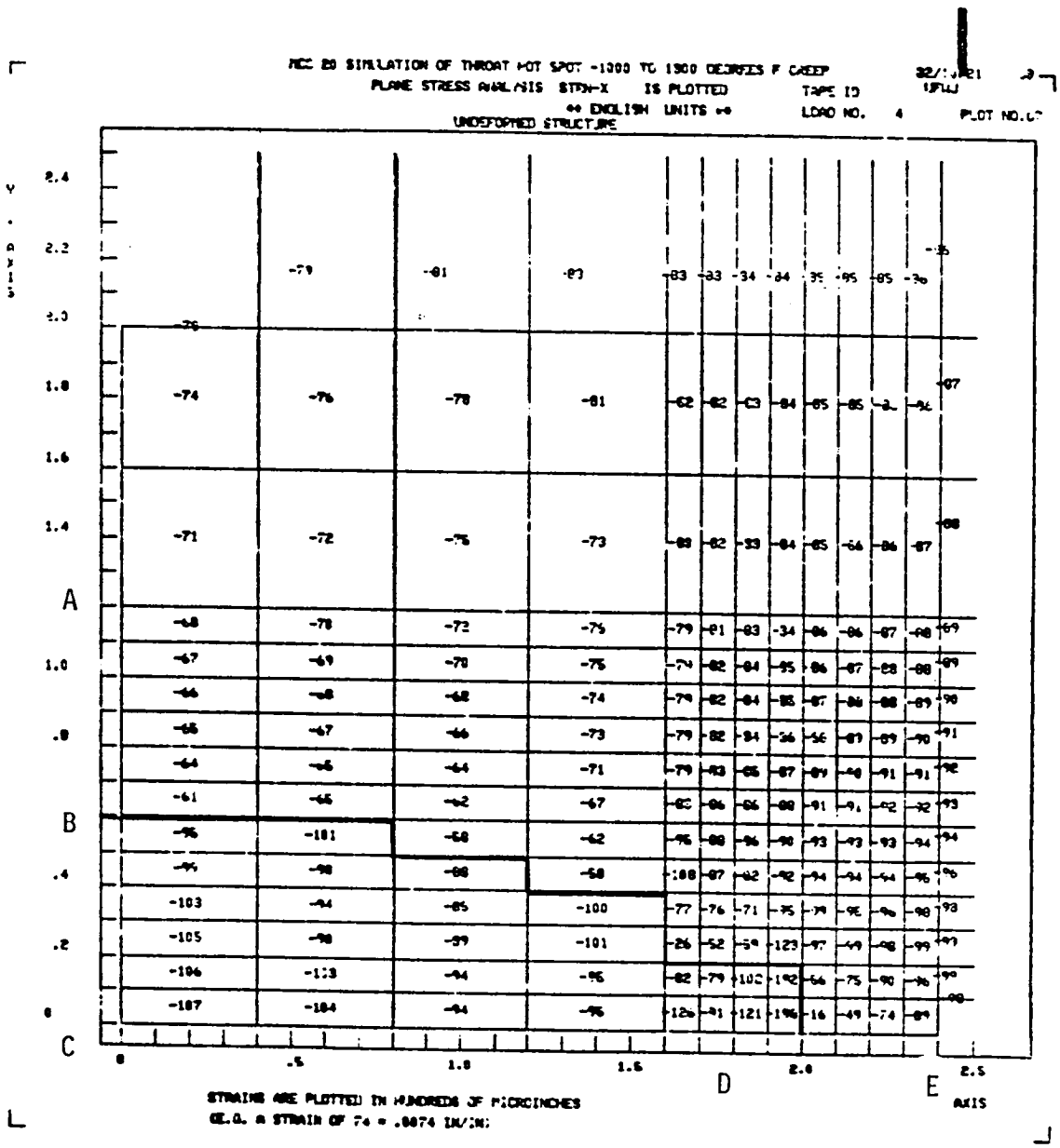

Figure 116. Steady-State Axial Strains in Hot-Spot Model

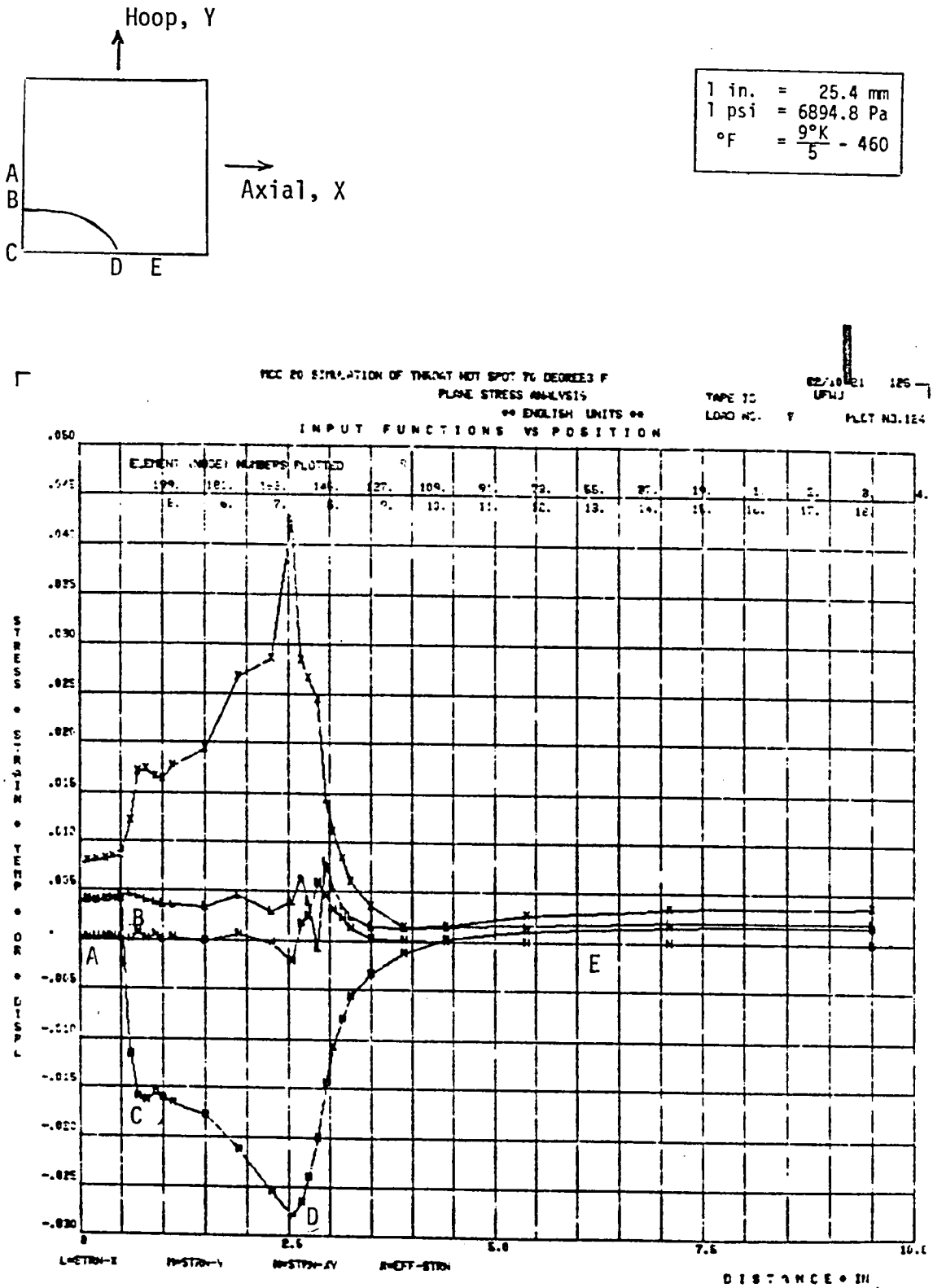

Figure 117. Post-Cutoff Condition, Room Temperature, Strain Distribution Along Hot-Spot Boundary

1 in.	= 25.4 mm
1 psi	= 6894.8 Pa
°F	= $\frac{9°K}{5}$ - 460

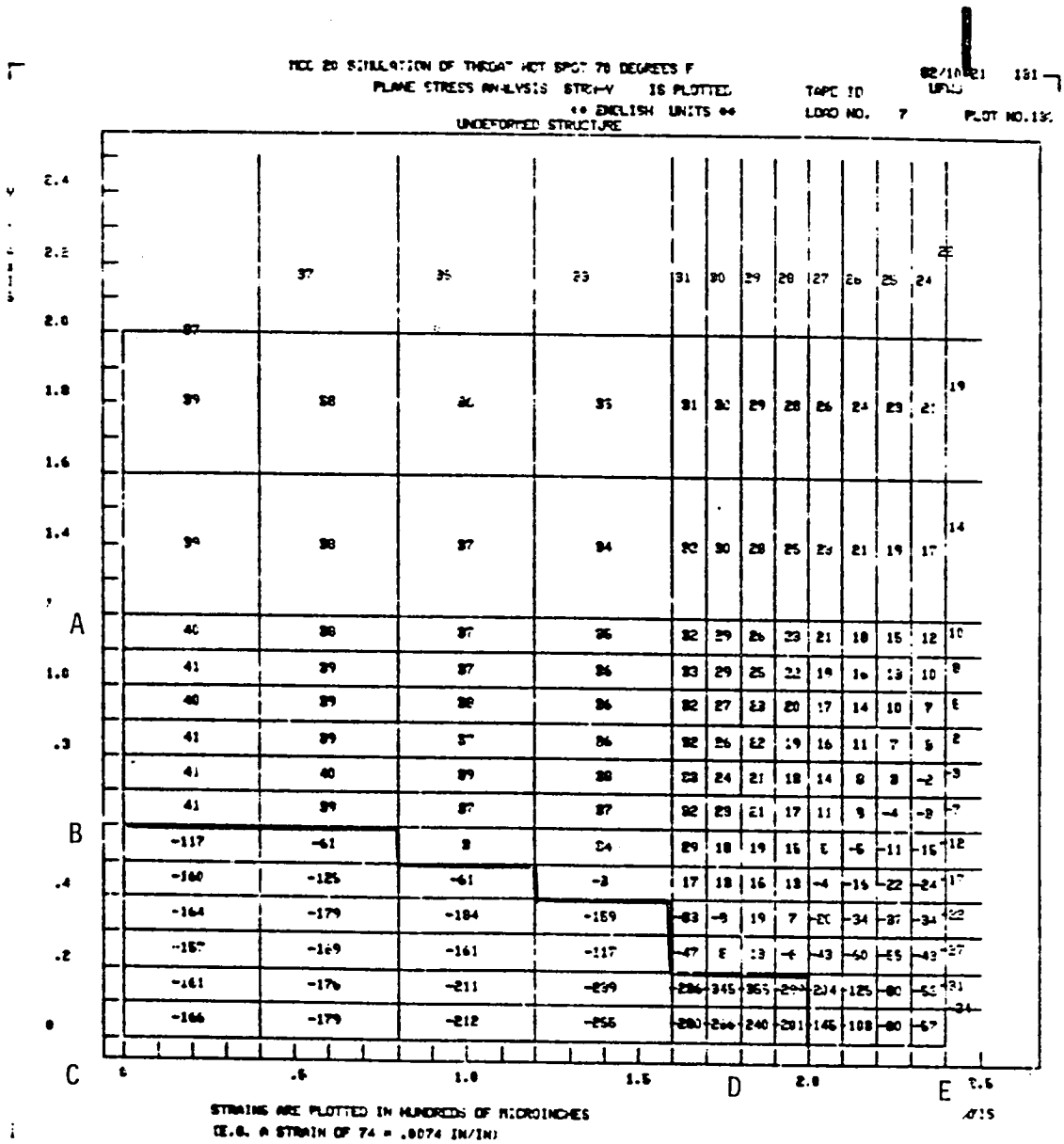

Figure 118. Post-Cutoff Condition, Room Temperature, Hoop Strain Distribution for Hot-Spot Model

APPENDIX F

GEOMETRY OF MCC COOLANT LINER DESIGNS

The MCC coolant liner geometry is presented for each of the designs analyzed as a function of axial length. The hot-gas wall contour is shown by the area-ratio and axial length. The coolant geometry (channel, land, and wall thickness) dimensions are presented as a function of axial location. The contoured-channel enhanced life design is not shown because it is the same as the basic SSME-MCC design, except as previously noted within the text.

TABLE 14. BASELINE SSME MCC COOLING CHANNEL DIMENSIONS (390 CHANNELS) IN SI UNITS

x_j (cm)	E_j	LAND (cm)	WIDTH (cm)	HEIGHT (cm)	WALL (cm)
24.71	5.0	0.3155	0.1575	0.6096	0.0889
20.32	4.052	0.2685	0.1575	0.6096	0.0889
17.78	3.538	0.2405	0.1575	0.6096	0.0889
15.24	3.066	0.2131	0.1575	0.5817	0.0889
12.70	2.608	0.1844	0.1575	0.5476	0.0889
10.16	2.182	0.1554	0.1575	0.5100	0.0889
7.62	1.782	0.1603	0.1227	0.5004	0.0889
5.08	1.426	0.1516	0.1016	0.4953	0.0889
2.54	1.103	0.1209	0.1016	0.4318	0.0711
0.0	1.000	0.1105	0.1016	0.2870	0.0711
-1.27	1.008	0.1113	0.1016	0.2741	0.0711
-2.54	1.038	0.1143	0.1016	0.2609	0.0711
-3.048	1.055	0.1261	0.1016	0.2558	0.0711
-3.81	1.090	0.1196	0.1016	0.2477	0.0711
-5.08	1.169	0.1275	0.1016	0.2352	0.0711
-6.35	1.259	0.1361	0.1016	0.2217	0.0711
-7.62	1.369	0.1463	0.1016	0.2139	0.0711
-8.89	1.481	0.1562	0.1016	0.2337	0.0711
-10.16	1.590	0.1653	0.1016	0.2535	0.0711
-12.70	1.831	0.1847	0.1016	0.2845	0.0711
-15.24	2.085	0.1844	0.1217	0.2619	0.0889
-17.78	2.362	0.1748	0.1509	0.2512	0.0889
-20.32	2.628	0.1857	0.1575	0.2489	0.0889
-22.86	2.812	0.1976	0.1575	0.2489	0.0889
-25.40	2.924	0.2045	0.1575	0.2489	0.0889
-27.94	2.962	0.2068	0.1575	0.2489	0.0889
-30.48	2.962	0.2068	0.1575	0.2489	0.0889
-32.41	2.962	0.2068	0.1575	0.2489	0.0889
-34.29	2.962	0.2068	0.1575	0.5842	0.0889
-35.56	2.962	0.2068	0.1575	0.635	0.0889
NOMENCLATURE:		x_j	= AXIAL DISTANCE FROM THROAT		
		E_j	= CHAMBER AREA RATIO		
		LAND	= LAND WIDTH BETWEEN CHANNELS		
		WIDTH	= CHANNEL WIDTH		
		~~HEIGHT~~	~~= CHANNEL HEIGHT~~		
		WALL	= HOT GAS WALL THICKNESS		

TABLE 14. (Concluded)

BASELINE SSME MCC COOLING CHANNEL DIMENSIONS
(390 CHANNELS) IN ENGLISH UNITS

x_j (in)	E_j	LAND (in)	WIDTH (in)	HEIGHT (in)	WALL (in)
9.73	5.0	0.1242	0.062	0.24	0.035
8.0	4.052	0.1057	0.062	0.24	0.035
7.0	3.538	0.0947	0.062	0.24	0.035
6.0	3.066	0.0839	0.062	0.229	0.035
5.0	2.608	0.0726	0.062	0.2156	0.035
4.0	2.182	0.0612	0.062	0.2007	0.035
3.0	1.782	0.0631	0.0483	0.1970	0.035
2.0	1.426	0.0597	0.04	0.1950	0.035
1.0	1.103	0.0476	0.04	0.17	0.028
0.0	1.000	0.0435	0.04	0.113	0.028
-0.5	1.008	0.0438	0.04	0.1079	0.028
-1.0	1.038	0.0450	0.04	0.1027	0.028
-1.2	1.055	0.0457	0.04	0.1007	0.028
-1.5	1.090	0.0471	0.04	0.0975	0.028
-2.0	1.169	0.0502	0.04	0.0926	0.028
-2.5	1.259	0.0536	0.04	0.0873	0.028
-3.0	1.369	0.0576	0.04	0.0842	0.028
-3.5	1.481	0.0615	0.04	0.0920	0.028
-4.0	1.590	0.0651	0.04	0.0998	0.028
-5.0	1.831	0.0727	0.04	0.1120	0.028
-6.0	2.085	0.0726	0.0479	0.1031	0.035
-7.0	2.362	0.0688	0.0594	0.0989	0.035
-8.0	2.628	0.0731	0.062	0.098	0.035
-9.0	2.812	0.0778	0.062	0.098	0.035
-10.0	2.924	0.0805	0.062	0.098	0.035
-11.0	2.962	0.0814	0.062	0.098	0.035
-12.0	2.962	0.0814	0.062	0.098	0.035
-12.76	2.962	0.0814	0.062	0.098	0.035
-13.50	2.962	0.0814	0.062	0.23	0.035
-14.0	2.962	0.0814	0.062	0.25	0.035

NOMENCLATURE:

x_j = AXIAL DISTANCE FROM THROAT

E_j = CHAMBER AREA RATIO

LAND = LAND WIDTH BETWEEN CHANNELS

WIDTH = CHANNEL WIDTH

HEIGHT = CHANNEL HEIGHT

WALL = HOT GAS WALL THICKNESS

TABLE 15. INCREASED NUMBER OF COOLANT CHANNELS DIMENSIONS (540 CHANNELS) IN SI UNITS

xj (cm)	Ej	LAND (cm)	WIDTH (cm)	HEIGHT (cm)	WALL (cm)
24.71	5.0	0.200	0.142	0.610	0.0813
20.32	4.052	0.165	0.142	0.610	0.0813
17.78	3.538	0.145	0.142	0.610	0.0813
15.24	3.066	0.137	0.130	0.610	0.0813
12.70	2.608	0.129	0.118	0.555	0.0813
10.16	2.182	0.120	0.106	0.500	0.0813
7.62	1.782	0.110	0.094	0.446	0.0813
5.08	1.426	0.101	0.082	0.391	0.0813
2.54	1.103	0.084	0.076	0.337	0.0635
0.0	1.000	0.077	0.076	0.282	0.0635
-1.27	1.008	0.077	0.076	0.269	0.0635
-2.54	1.038	0.080	0.076	0.257	0.0635
-3.048	1.055	0.081	0.076	0.257	0.0635
-3.81	1.090	0.084	0.076	0.257	0.0635
-5.08	1.169	0.089	0.076	0.257	0.0635
-6.35	1.259	0.096	0.076	0.257	0.0635
-7.62	1.369	0.103	0.076	0.257	0.0635
-8.89	1.481	0.110	0.076	0.269	0.0635
-10.16	1.590	0.117	0.076	0.282	0.0635
-12.70	1.831	0.131	0.076	0.307	0.0635
-15.24	2.085	0.126	0.095	0.287	0.0762
-17.78	2.362	0.122	0.113	0.262	0.0762
-20.32	2.628	0.131	0.117	0.257	0.0762
-22.86	2.812	0.139	0.117	0.257	0.0762
-25.40	2.924	0.145	0.117	0.257	0.076
-27.94	2.962	0.146	0.117	0.257	0.0762
-30.45	2.962	0.146	0.117	0.320	0.0762
-32.42	2.962	0.146	0.117	0.369	0.0762
-34.29	2.962	0.146	0.117	0.584	0.0762
-35.56	2.962	0.146	0.117	0.635	0.0762

NOMENCLATURE:

- xj = AXIAL DISTANCE FROM THROAT
- Ej = CHAMBER AREA RATIO
- LAND = LAND WIDTH BETWEEN CHANNELS
- WIDTH = CHANNEL WIDTH
- HEIGHT = CHANNEL HEIGHT
- WALL = HOT GAS WALL THICKNESS

TABLE 15. (Concluded)

INCREASED NUMBER OF COOLANT CHANNELS DIMENSION
(540 CHANNELS) IN ENGLISH UNITS

xj (in)	Ej	LAND (in)	WIDTH (in)	HEIGTH (in)	WALL (in)
9.73	5.0	0.0784	0.056	0,24	0.032
8.0	4.052	0.0651	0.056	0.24	0.032
7.0	3.538	0.0571	0.056	0.24	0.032
6.0	3.066	0.0541	0.0513	0.24	0.032
5.0	2.608	0.0507	0.0465	0.2185	0.032
4.0	2.182	0.0471	0.0418	0.1970	0.032
3.0	1.782	0.0433	0.0371	0.1755	0.032
2.0	1.426	0.0396	0.0324	0.1540	0.032
1.0	1.103	0.0332	0.030	0.1325	0.025
0.0	1.000	0.0302	0.030	0.1110	0.025
-0.5	1.008	0.0305	0.030	0.1060	0.025
-1.0	1.038	0.0314	0.030	0.1010	0.025
-1.2	1.055	0.0319	0.030	0.1010	0.025
-1.5	1.090	0.0329	0.030	0.1010	0.025
-2.0	1.169	0.0351	0.030	0.1010	0.025
-2.5	1.259	0.0376	0.030	0.1010	0.025
-3.0	1.369	0.404	0.030	0.1010	0.025
-3.5	1.481	0.0433	0.030	0.1060	0.025
-4.0	1.590	0.0459	0.030	0.1110	0.025
-5.0	1.831	0.0514	0.030	0.1210	0.025
-6.0	2.085	0.0497	0.0373	0.1130	0.030
-7.0	2.362	0.0480	0.0445	0.103	0.030
-8.0	2.628	0.0515	0.0460	0.1010	0.030
-9.0	2.812	0.0549	0.046	0.1010	0.030
-10.0	2.924	0.0569	0.046	0.1010	0.030
-11.0	2.962	0.0575	0.046	0.101	0.030
-12.0	2.962	0.0575	0.046	0.1260	0.030
-12.76	.2962	0.0575	0.046	0.1451	0.030
-13.50	2.962	0.0575	0.046	0.23	0.030
-14.0	2.962	0.0575	0.046	0.25	0.030

NOMENCLATURE:

xj	= AXIAL DISTANCE FROM THROAT
Ej	= CHAMBER AREA RATIO
LAND	= LAND WIDTH BETWEEN CHANNELS
WIDTH	= CHANNEL WIDTH
HEIGHT	= CHANNEL HEIGHT
WALL	= HOT GAS WALL THICKNESS

TABLE 16. KEEL-RIB CHANNEL DIMENSION (390 CHANNELS) IN SI UNITS

x_j (cm)	E_j	LAND (cm)	WIDTH (cm)	HEIGHT (cm)	WALL (cm)	F.H./C.H. RATIO	FIN BASE (cm)
24.71	5.0	0.3155	0.1575	0.6096	0.0889	N.A.	N.A.
20.32	4.052	0.2685	0.1575	0.6096	0.0889	N.A.	N.A.
17.78	3.538	0.2405	0.1575	0.6096	0.0889	N.A.	N.A.
15.24	3.066	0.2131	0.1575	0.5817	0.0889	N.A.	N.A.
12.70	2.608	0.1844	0.1575	0.5474	0.0889	N.A.	N.A.
10.16	2.182	0.1554	0.1575	0.5093	0.0889	N.A.	N.A.
7.62	1.782	0.1603	0.1227	0.5352	0.0889	N.A.	N.A.
5.08	1.426	0.1516	0.1016	0.4953	0.0889	N.A.	N.A.
2.54	1.103	0.1209	0.1016	0.4318	0.0711	N.A.	N.A.
0.0	1.000	0.1105	0.1016	0.3442	0.0711	0.3	0.0339
-1.27	1.008	0.1143	0.1016	0.3307	0.0711	0.3	0.0339
-2.54	1.038	0.1143	0.1016	0.3147	0.0711	0.3	0.0339
-3.048	1.055	0.1261	0.1016	0.3117	0.0711	0.3	0.0339
-3.81	1.090	0.1196	0.1016	0.2982	0.0711	0.3	0.0339
-5.08	1.169	0.1275	0.1016	0.2977	0.0711	0.3	0.0339
-6.35	1.259	0.1361	0.1016	0.2812	0.0711	0.3	0.0339
-7.62	1.369	0.1463	0.1016	0.2728	0.0711	0.3	0.0339
-8.89	1.481	0.1562	0.1016	0.3987	0.0711	0.3	0.0339
-10.16	1.590	0.1653	0.1016	0.3231	0.0711	0.3	0.0339
-12.70	1.831	0.1847	0.1016	0.4338	0.0711	0.3	0.0339
-15.24	2.085	0.1844	0.1217	0.3792	0.0889	0.3	0.0406
-17.78	2.362	0.1748	0.1509	0.3284	0.0889	0.3	0.0503
-20.32	2.628	0.1857	0.1575	0.3175	0.0889	0.3	0.0525
-22.86	2.812	0.1976	0.1575	0.3175	0.0889	0.3	0.0525
-25.40	2.924	0.2045	0.1575	0.3175	0.0889	0.3	0.0525
-27.94	2.962	0.2068	0.1575	0.3175	0.0889	0.3	0.0525
-30.48	2.962	0.2068	0.1575	0.2489	0.0889	N.A.	N.A.
-32.41	2.962	0.2068	0.1575	0.2489	0.0889	N.A.	N.A.
-34.29	2.962	0.2068	0.1575	0.5842	0.0889	N.A.	N.A.
-35.56	2.962	0.2068	0.1575	0.635	0.0889	N.A.	N.A.
NOMENCLATURE:		X_j = AXIAL DISTANCE FROM THROAT					
		E_j = CHAMBER AREA RATIO					
		LAND = LAND WIDTH BETWEEN CHANNELS					
		WIDTH = CHANNEL WIDTH					
		HEIGTH = CHANNEL HEIGHT					
		WALL = HOT GAS WALL THICKNESS					
		F.H. = FIN HEIGHT					
		C.H. = CHANNEL HEIGHT					
		N.A. = NOT APPLICABLE					

TABLE 16. (Concluded)

KEEL-RIB CHANNEL DIMENSIONS
(390 CHANNELS) IN ENGLISH UNITS

x_j (in)	E_j	LAND (in)	WIDTH (in)	HEIGHT (in)	WALL (in)	F.H./C.H. RATIO	FIN BASE (in)
9.73	5.0	0.1242	0.062	0.24	0.035	N.A.	N.A.
8.0	4.052	0.1057	0.062	0.24	0.035	N.A.	N.A.
7.0	3.538	0.0947	0.062	0.24	0.035	N.A.	N.A.
6.0	3.066	0.0839	0.062	0.229	0.035	N.A.	N.A.
5.0	2.068	0.0726	0.062	0.2155	0.035	N.A.	N.A.
4.0	2.182	0.0612	0.062	0.2005	0.035	N.A.	N.A.
3.0	1.782	0.0631	0.0483	0.2107	0.035	N.A.	N.A.
2.0	1.426	0.0597	0.04	0.1950	0.035	N.A.	N.A.
1.0	1.103	0.0476	0.04	0.1700	0.028	N.A.	N.A.
0.0	1.000	0.0435	0.04	0.1355	0.028	0.3	0.0133
-0.5	1.008	0.0438	0.04	0.1302	0.028	0.3	0.0133
-1.0	1.038	0.0450	0.04	0.1239	0.028	0.3	0.0133
-1.2	1.055	0.0457	0.04	0.1227	0.028	0.3	0.0133
-1.5	1.090	0.0471	0.04	0.1174	0.028	0.3	0.0133
-2.0	1.169	0.0502	0.04	0.1172	0.028	0.3	0.0133
-2.5	1.259	0.0536	0.04	0.1107	0.028	0.3	0.0133
-3.0	1.369	0.0576	0.04	0.1074	0.028	0.3	0.0133
-3.5	1.481	0.0615	0.04	0.1176	0.028	0.3	0.0133
-4.0	1.590	0.0651	0.04	0.1272	0.028	0.3	0.0133
-5.0	1.831	0.0727	0.04	0.1708	0.028	0.3	0.0133
-6.0	2.085	0.0726	0.0479	0.1493	0.035	0.3	0.0160
-7.0	2.362	0.0688	0.0594	0.1293	0.035	0.3	0.0198
-8.0	2.628	0.0731	0.062	0.1250	0.035	0.3	0.0207
-10.0	2.924	0.0805	0.062	0.1250	0.035	0.3	0.0207
-11.0	2.962	0.0814	0.062	0.1250	0.035	0.3	0.0207
-12.0	2.962	0.0814	0.082	0.0980	0.035	N.A.	N.A.
-12.76	2.962	0.0814	0.062	0.0980	0.035	N.A.	N.A.
-13.50	2.962	0.0814	0.062	0.23	0.035	N.A.	N.A.
-14.0	2.962	0.0814	0.062	0.25	0.035	N.A.	N.A.
NOMENCLATURE:		x_j = AXIAL DISTANCE FROM THROAT					
		E_j = CHAMBER AREA RATIO					
		LAND = LAND WIDTH BETWEEN CHANNELS					
		WIDTH = CHANNEL WIDTH					
		~~HEIGHT = CHANNEL HEIGHT~~					
		WALL = HOT GAS WALL THICKNESS					
		F.H. = FIN HEIGHT					
		~~C.H. = CHANNEL HEIGHT~~					
		N.A. = NOT APPLICABLE					

TABLE 17. SLOTTED HOT-GAS WALL COOLANT CHANNEL DIMENSION (460 CHANNELS) IN SI UNITS

xj (cm)	Ej	LAND (cm)	WIDTH (cm)	HEIGHT (cm)	WALL (cm)
24.71	5.0	0.259	0.142	0.610	0.0813
20.32	4.052	0.219	0.142	0.610	0.0813
17.78	3.538	0.195	0.142	0.610	0.0813
15.24	3.066	0.184	0.130	0.610	0.0813
12.70	2.608	0.172	0.118	0.563	0.0813
10.16	2.182	0.159	0.106	0.516	0.0813
7.62	1.782	0.146	0.094	0.470	0.0813
5.08	1.426	0.132	0.082	0.423	0.0813
2.54	1.103	0.112	0.076	0.377	0.0635
0.0	1.000	0.103	0.076	0.330	0.0635
-1.27	1.008	0.104	0.076	0.318	0.0635
-2.54	1.038	0.107	0.076	0.305	0.0635
-3.048	1.055	0.108	0.076	0.300	0.0635
-3.81	1.090	0.111	0.076	0.300	0.0635
-5.08	1.169	0.118	0.076	0.300	0.0635
-6.35	1.259	0.125	0.076	0.300	0.0635
-7.92	1.369	0.134	0.076	0.300	0.0635
-8.89	1.481	0.142	0.076	0.312	0.0635
-10.16	1.590	0.150	0.076	0.325	0.0635
-12.70	1.831	0.167	0.076	0.351	0.0635
-15.24	2.085	0.164	0.095	0.330	0.0762
-17.78	2.362	0.163	0.113	0.305	0.0762
-20.32	2.628	0.174	0.117	0.300	0.0762
-22.86	2.812	0.184	0.117	0.300	0.0762
-25.40	2.924	0.190	0.117	0.300	0.0762
-27.94	2.962	0.192	0.117	0.300	0.0762
-30.45	2.962	0.192	0.117	0.432	0.0762
-32.42	2.962	0.192	0.117	0.510	0.0762
-34.29	2.962	0.192	0.117	0.584	0.0762
-35.56	2.962	0.192	0.117	0.635	0.0762

NOMENCLATURE:

- xj = AXIAL DISTANCE FROM THROAT
- Ej = CHAMBER AREA RATIO
- LAND = LAND WIDTH BETWEEN CHANNELS
- WIDTH = CHANNEL WIDTH
- HEIGHT = CHANNEL HEIGHT
- WALL = HOT GAS WALL THICKNESS

TABLE 17. (Concluded)

SLOTTED HOT-GAS WALL COOLANT CHANNEL DIMENSIONS
(460 CHANNELS) IN ENGLISH UNITS

xj (in)	Ej	LAND (in)	WIDTH (in)	HEIGHT (in)	WALL (in)
9.73	5.0	0.1018	0.056	0.24	0.032
8.0	4.052	0.0861	0.056	0.24	0.032
7.0	3.538	0.0768	0.056	0.24	0.032
6.0	3.066	0.0724	0.0513	0.24	0.032
5.0	2.608	0.0676	0.0465	0.2217	0.032
4.0	2.182	0.0626	0.0418	0.2033	0.032
3.0	1.782	0.0573	0.0371	0.1850	0.032
2.0	1.426	0.0521	0.0324	0.1667	0.032
1.0	1.103	0.0442	0.030	0.1483	0.025
0.0	1.000	0.0407	0.030	0.130	0.025
-0.5	1.008	0.0410	0.030	0.1250	0.025
-1.0	1.038	0.0421	0.030	0.1200	0.025
-1.2	1.055	0.0426	0.030	0.1180	0.025
-1.5	1.090	0.0438	0.030	0.1180	0.025
-2.0	1.169	0.0464	0.030	0.1180	0.025
-2.5	1.259	0.0493	0.030	0.1180	0.025
-3.0	1.369	0.0527	0.030	0.1180	0.025
-3.5	1.481	0.0560	0.030	0.1230	0.025
-4.0	1.590	0.0591	0.030	0.1280	0.025
-5.0	1.831	0.0656	0.030	0.1380	0.025
-6.0	2.085	0.0647	0.0373	0.1300	0.030
-7.0	2.362	0.0641	0.0445	0.1200	0.030
-8.0	2.628	0.0685	0.046	0.1180	0.030
-9.0	2.812	0.0724	0.046	0.1180	0.030
-10.0	2.924	0.0748	0.046	0.1180	0.030
-11.0	2.962	0.0755	0.046	0.1180	0.030
-12.0	2.962	0.0755	0.046	0.1700	0.030
-12.76	2.962	0.0755	0.046	0.2006	0.030
-13.50	2.962	0.0755	0.046	0.23	0.030
-14.0	2.962	0.0755	0.046	0.25	0.030

NOMENCLATURE:

xj = AXIAL DISTANCE FROM THROAT
Ej = CHAMBER AREA RATIO
LAND = LAND WIDTH BETWEEN CHANNELS
WIDTH = CHANNEL WIDTH
HEIGHT = CHANNEL HEIGHT
WALL = HOT GAS WALL THICKNESS

APPENDIX G

MID-CHANNEL WALL THINNING ANALYSIS ADJUSTMENT

The analysis results used to develop the percent of mid-channel thinning vs duty cycles are furnished in this appendix for all configurations. Each curve has the analysis results plotted as a solid line. The dashed line is the adjustment used to eliminate the shakedown conditions that occur during the first one or two cycles of each 5 cycle analysis. Figure 119 depicts the baseline 135% hg analysis results, shows the shakedown condition that occurred in each 5 duty cycles, and the method of adjusting the raw analysis results to acount for the shakedown. Other configurations Fig. 120 through 124 and operating condition analyzed had similar shakedown conditions. For the first 5 duty cycles, adjustment of the residual stress and strain conditions during the load cycling resulted in a realistic shakedown condition. The first shakedown condition also included the gross distortion of the liner as it permanently yields through the 0.51 mm (0.020 inch) tolerance gap and touches the jacket. Thereafter, at the steady-state posttest condition, the liner remains virtually in line-to-line contact with the jacket, so the first shakedown is larger than the remaining ones. The other shakedown condition, where there is a rapid change in thickness fo rhe first 1 or 2 cycles, followed by a much slower change in cycles 3, 4, and 5, occurs because of the approximations made. Each new 5 duty cycles start with a stress-and-strain-free distorted geometry rather than were used directly, a significant error in thinning would be obtained. The final methodology chosen to eliminate the shakedown effect was to assume that the distortions from the first cycles in the 5-cycle analysis were equivalent to a series of thinning cycles at the rate of change used for extrapolation to the restart condition. This is effectively obtained by extending the last 5-20-cycle extrapolation line (e.g., A) until it intersects with a horizontal line drawn from the end of the shakedown condition, B. At this point, the B slope applies until the C slope horizontal line intersects. This technique was used to adjust all the analysis results in this study.

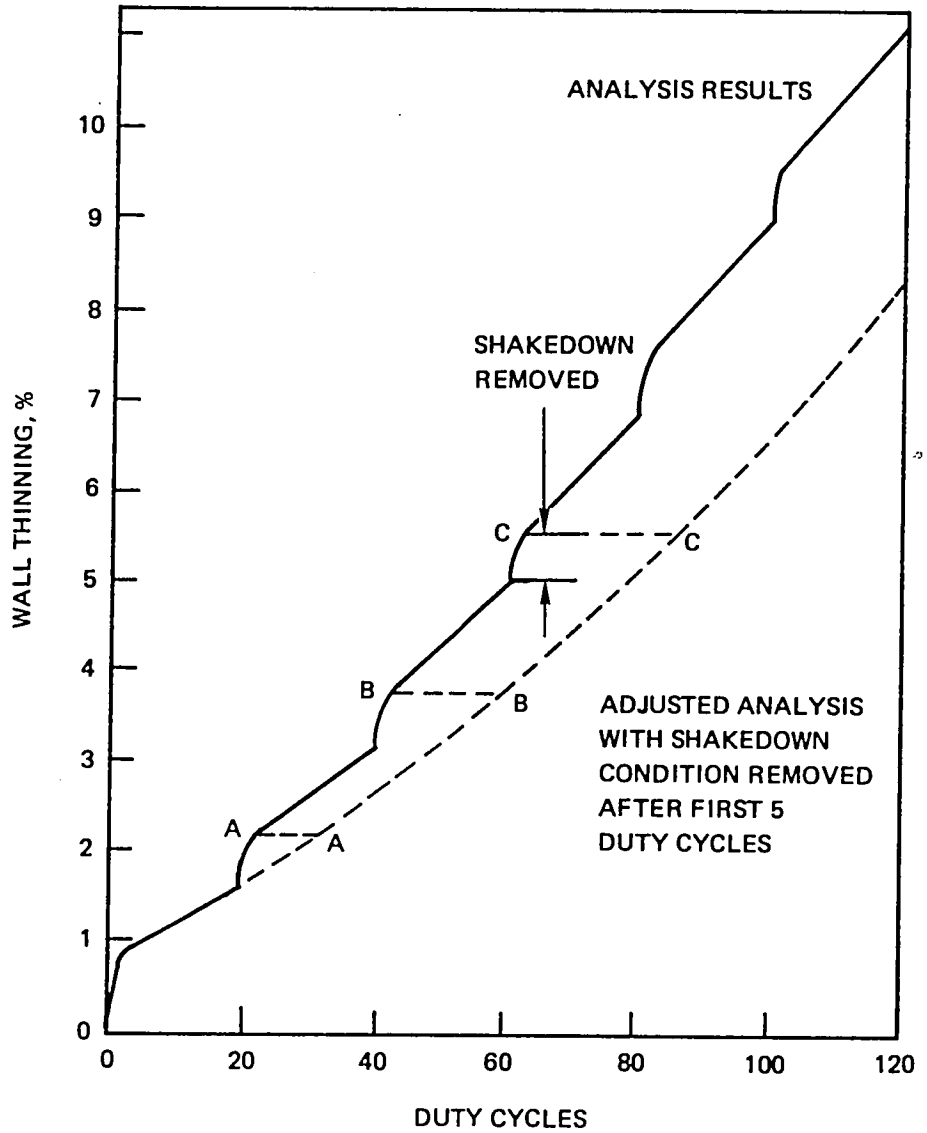

ANALYSIS METHODOLOGY
5 DUTY CYCLE + 15 CYCLE EXTRAPOLATION
RESTART WITH
- DISTORTED GEOMETRY
- VIRGIN MATERIAL(NO RESIDUAL STRAINS)
- MCC LINER IN CONTACT WITH JACKET

INITIAL "SHAKEDOWN" ONLY REALISTIC FOR 1-5 DUTY CYCLES

"SHAKEDOWN" EFFECT SUBTRACTED OUT

Figure 119. SSME MCC Life Prediction, 135% hg Baseline

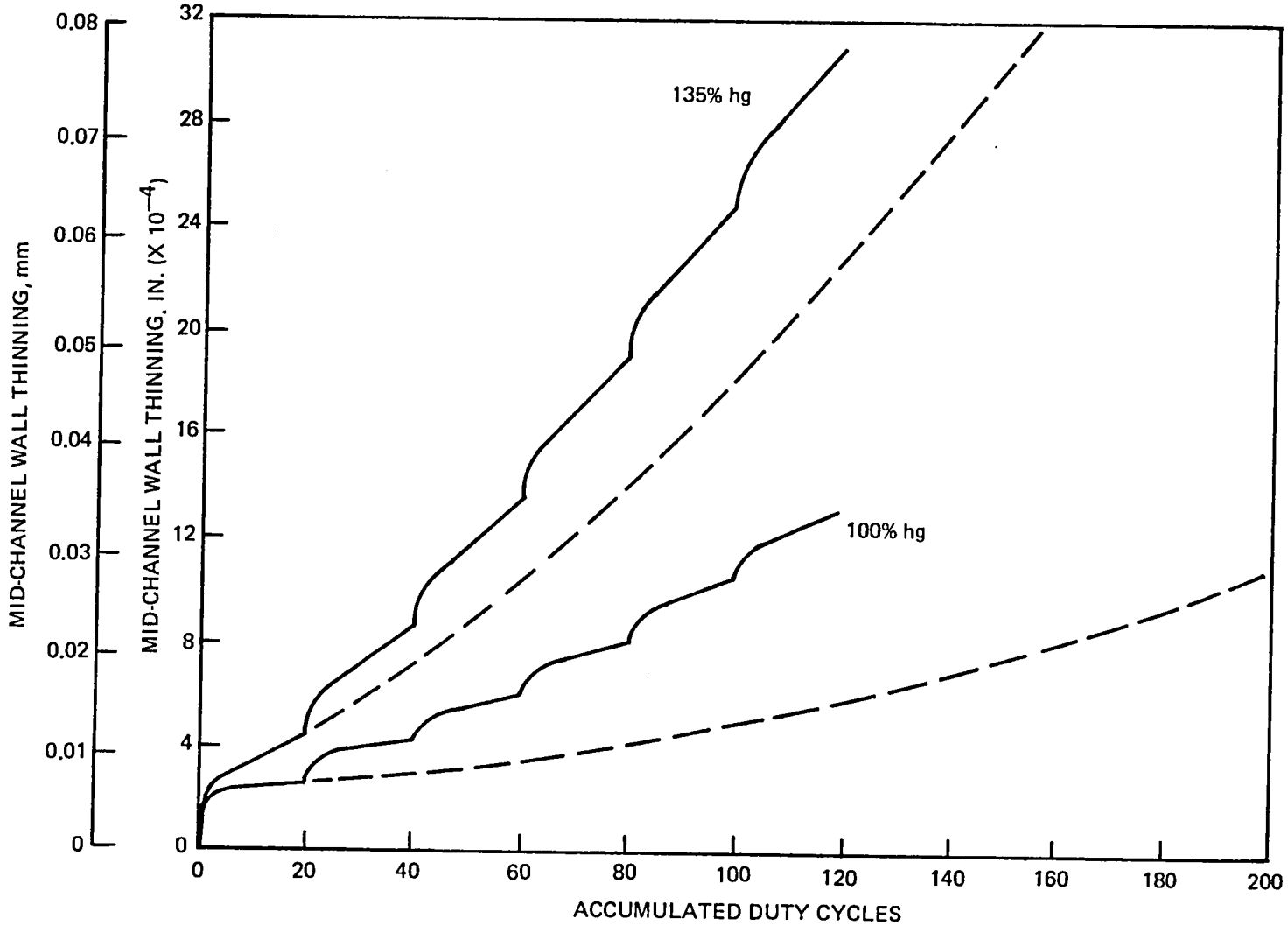

Figure 120. SSME Configuration 135% hg and 100% hg Raw Data Thinning vs Accumulated Duty Cycles

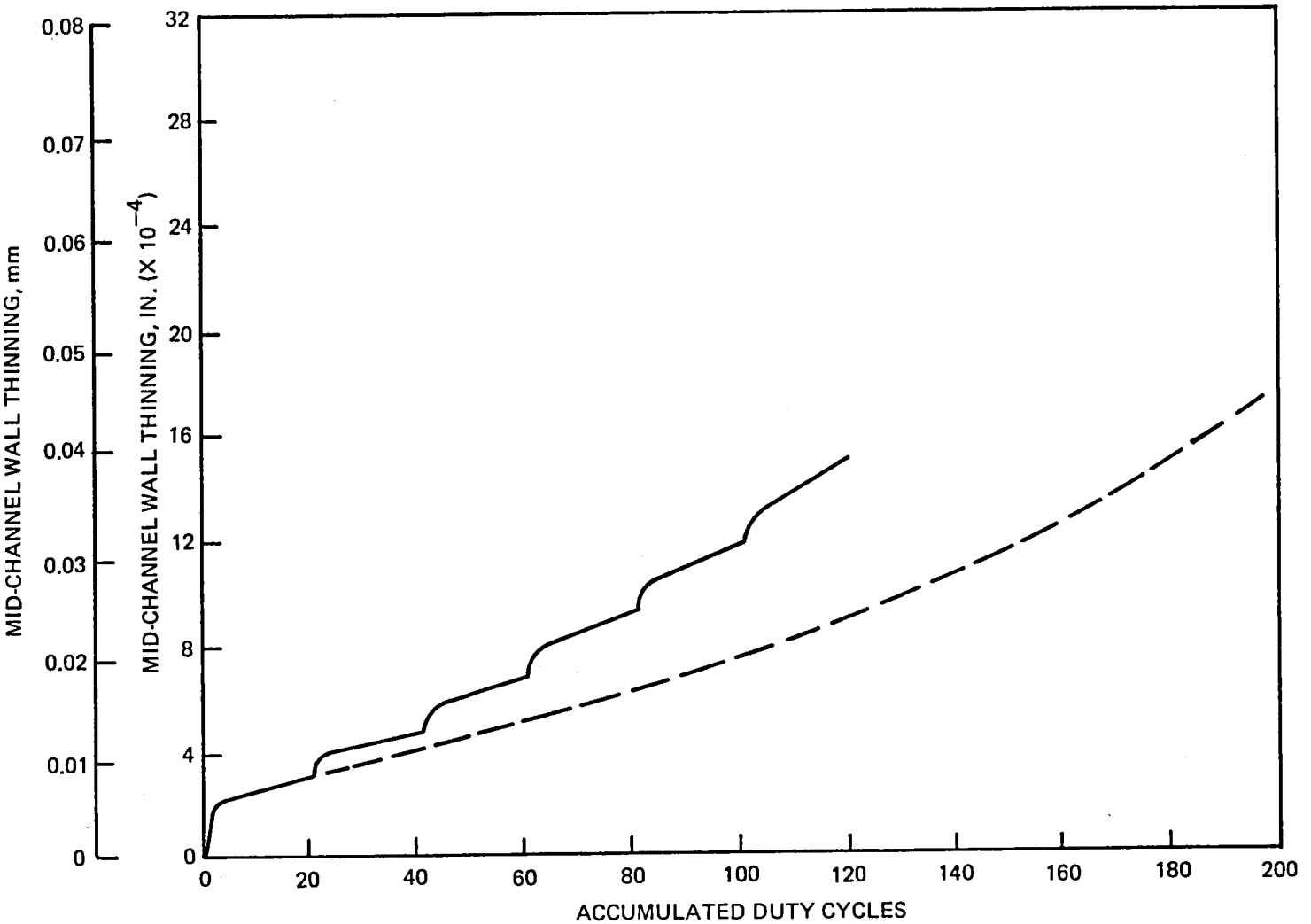

Figure 121. Increased Number of Channels Configuration Raw Data Thinning vs Accumulated Duty Cycles

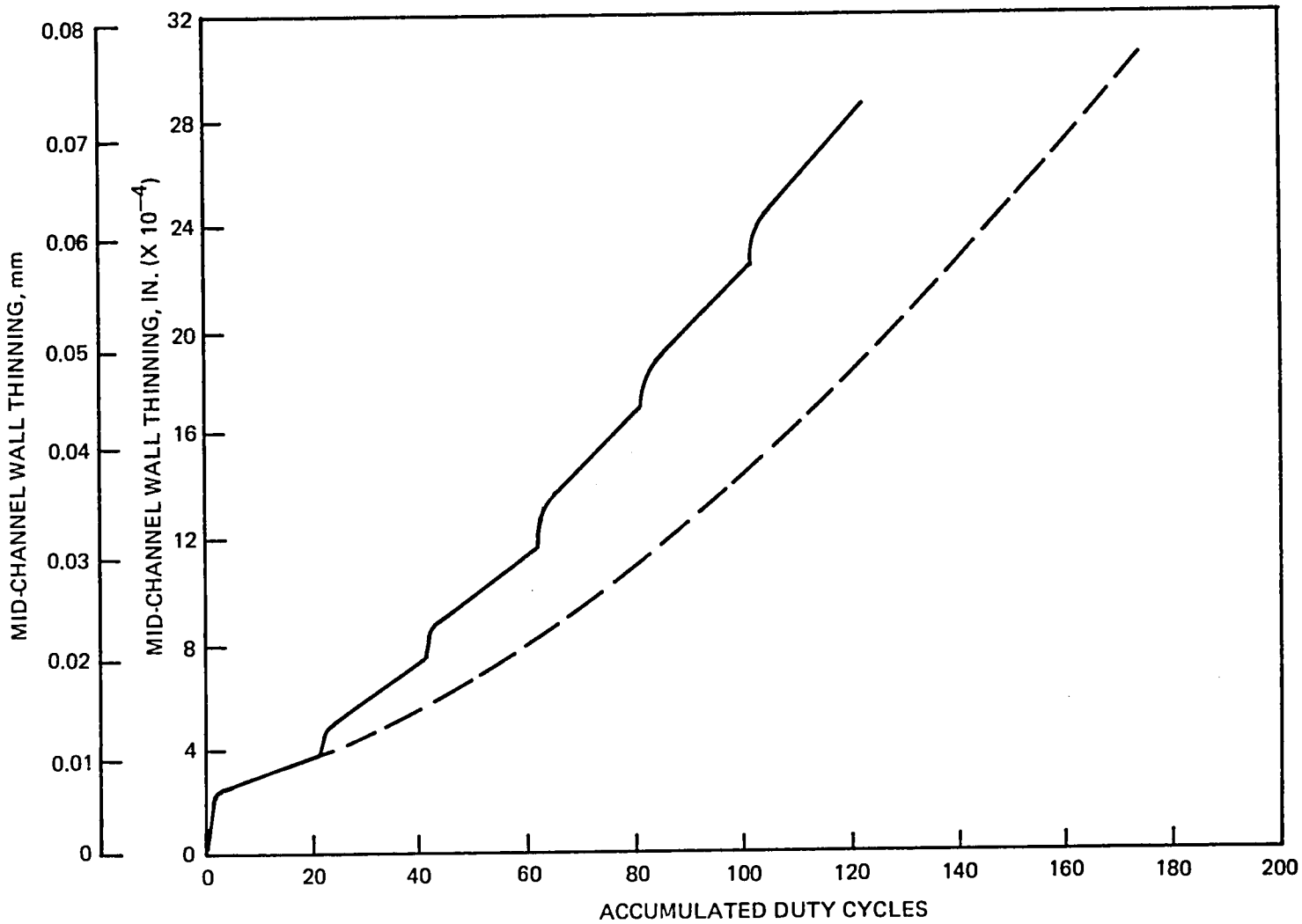

Figure 122. Contoured Wall Configuration Raw Data Thinning vs Accumulated Duty Cycles

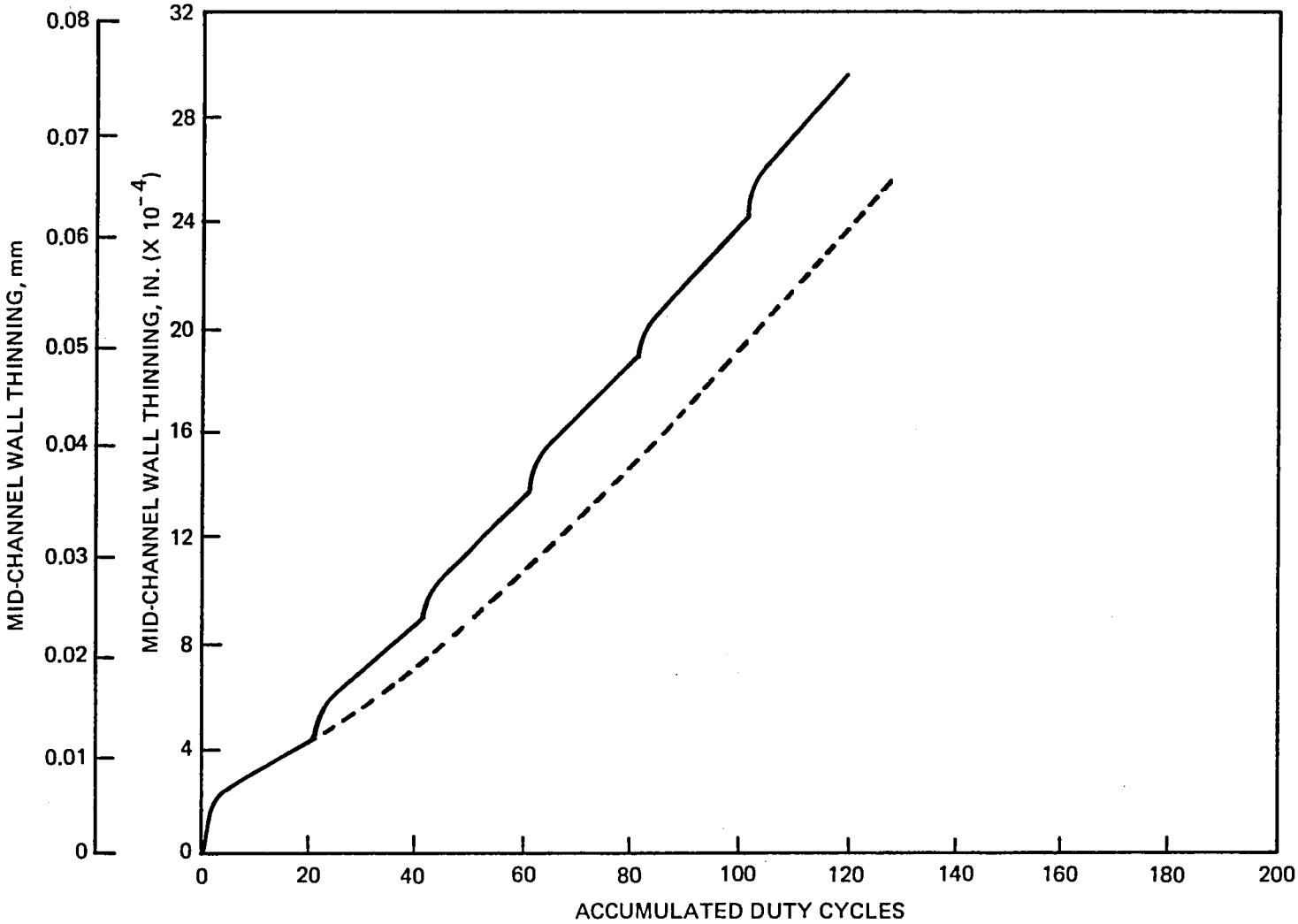

Figure 123. Keel Rib Configuration Thinning vs Accumulated Duty Cycles

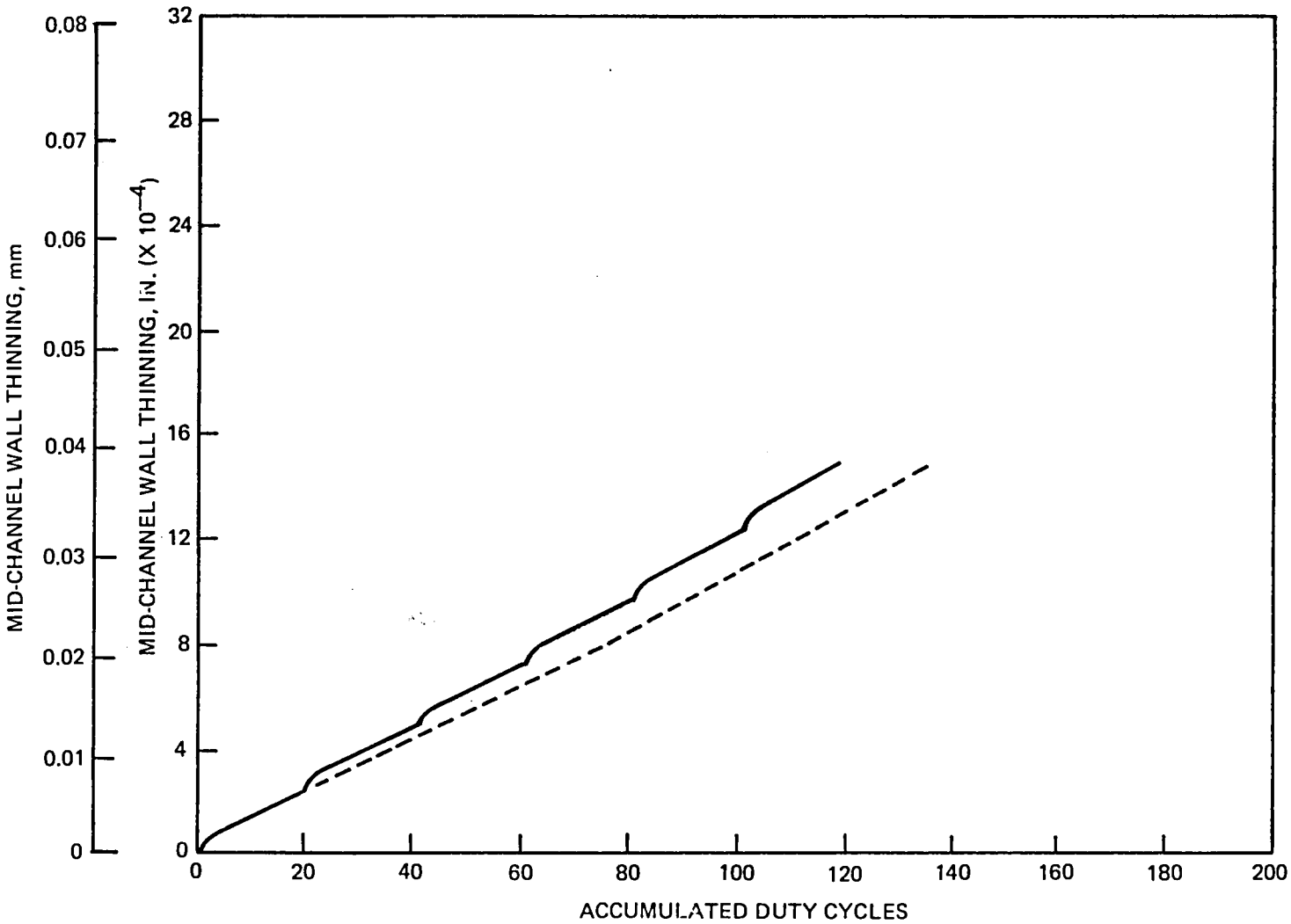

Figure 124. Slotted Configuration Raw Data Thinning vs Accumulated Duty Cycles

APPENDIX H

TYPICAL CONTOUR AND GRAPHICAL DATASET

The enclosed figures and curves are a selected subset of the contour and graphical plots for the baseline SSME MCC configuration. Plots are presented for the first duty cycle, but they are representative of results throughout the analysis. The lod increment and times on the graphs are consistent with the duty cycle analysis presented in the Structural Modeling section of the report. Results are primarily presented for: (1) the steady-state operation condition--increment 6--where maximum compressive strains occur, (2) cut off--increment 10--when the liner is coldest and is at the maximum tension portion of the cycle, and (3) after cutoo off steady-state--increment 11--wqhen the MCC is at 70 F, the condition used as a basis for the extrapolation.

A graphical plot of the stress state around the model hot wall boundary is furnished for increments 7 and 9 during the transient phase of cutoo off. These depict how the stress state changes from comprehension and bending to an average tensile stress while the hot wall f the liner is still hot (600 to 700 F).

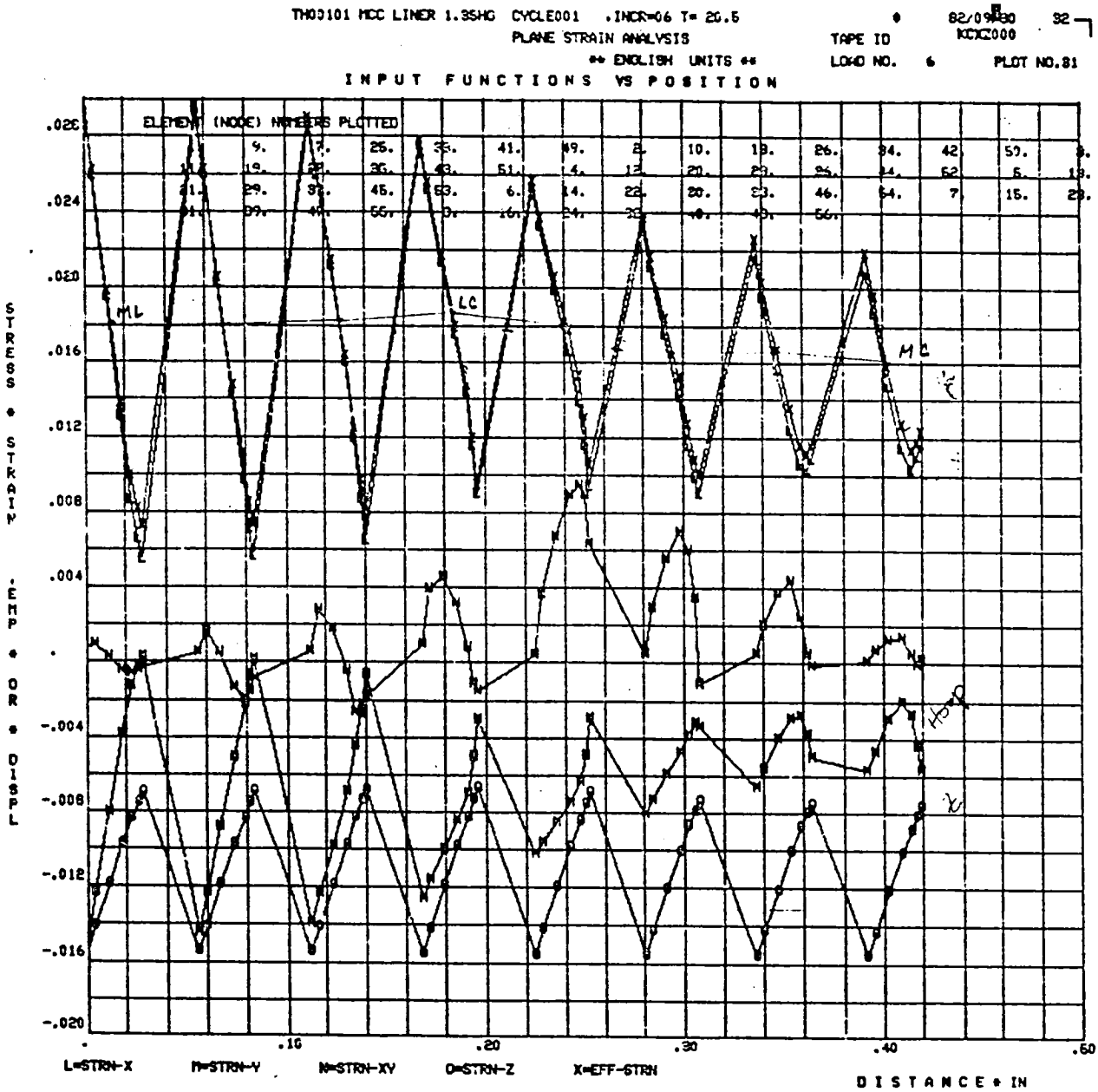

DEFINITION OF PLOT ORDER

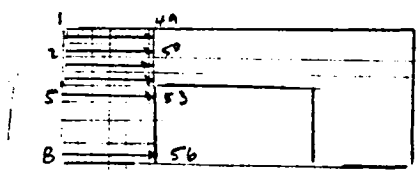

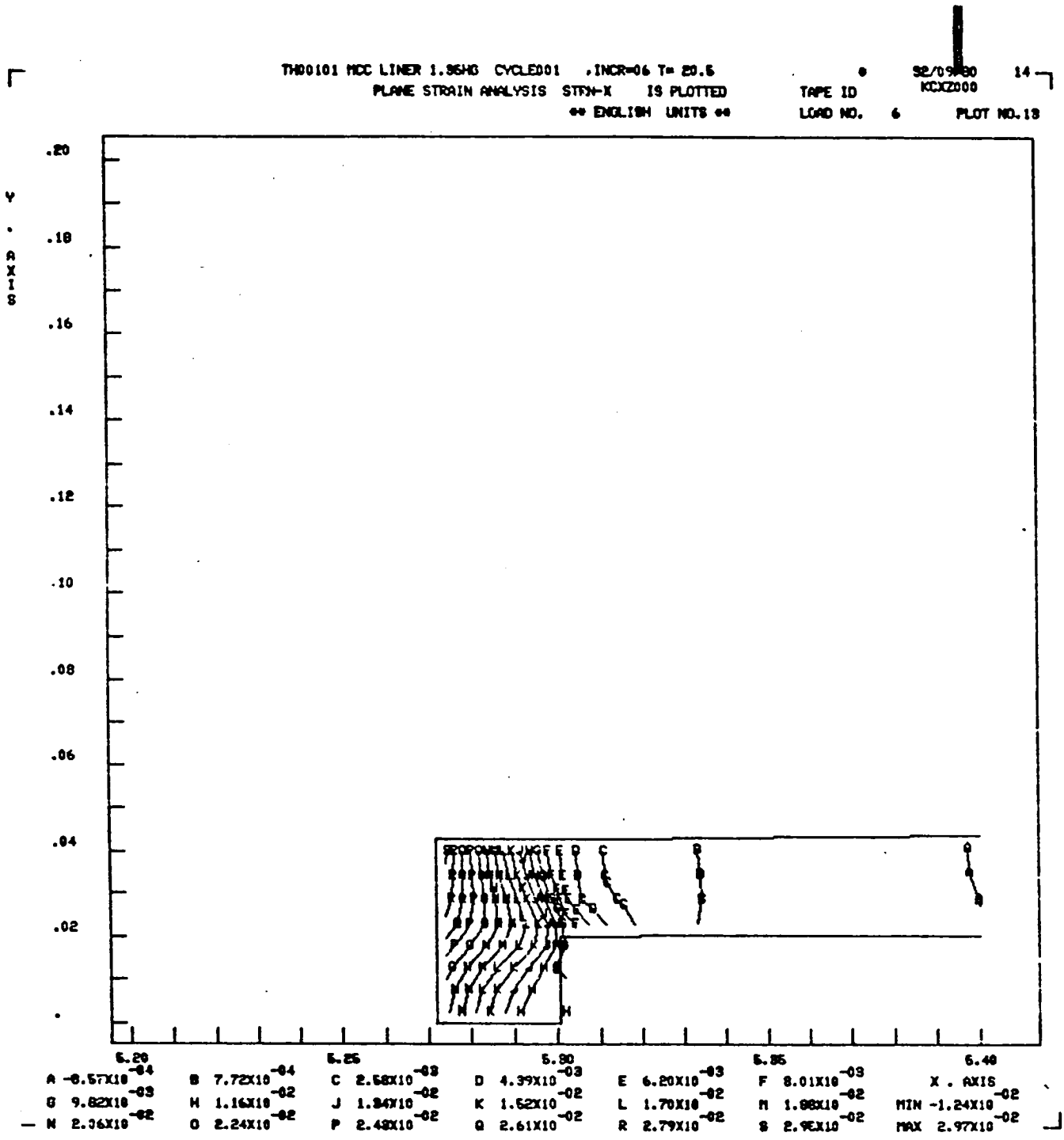
TH00101 MCC LINER 1.96HG CYCLE001 ,INCR=06 T= 20.5
PLANE STRAIN ANALYSIS STRN-X IS PLOTTED
** ENGLISH UNITS **
TAPE ID
LOAD NO. 6
PLOT NO.18
Y . AXIS
.20
.18
.16
.14
.12
.10
.08
.06
.04
.02
5.20
5.25
5.30
5.35
5.40
X . AXIS
A -6.57X10-04
B 7.72X10-04
C 2.58X10-03
D 4.39X10-03
E 6.20X10-03
F 8.01X10-03
G 9.82X10-03
H 1.16X10-02
J 1.34X10-02
K 1.52X10-02
L 1.70X10-02
M 1.88X10-02
N 2.06X10-02
O 2.24X10-02
P 2.42X10-02
Q 2.61X10-02
R 2.79X10-02
S 2.9EX10-02
MIN -1.24X10-02
MAX 2.97X10-02

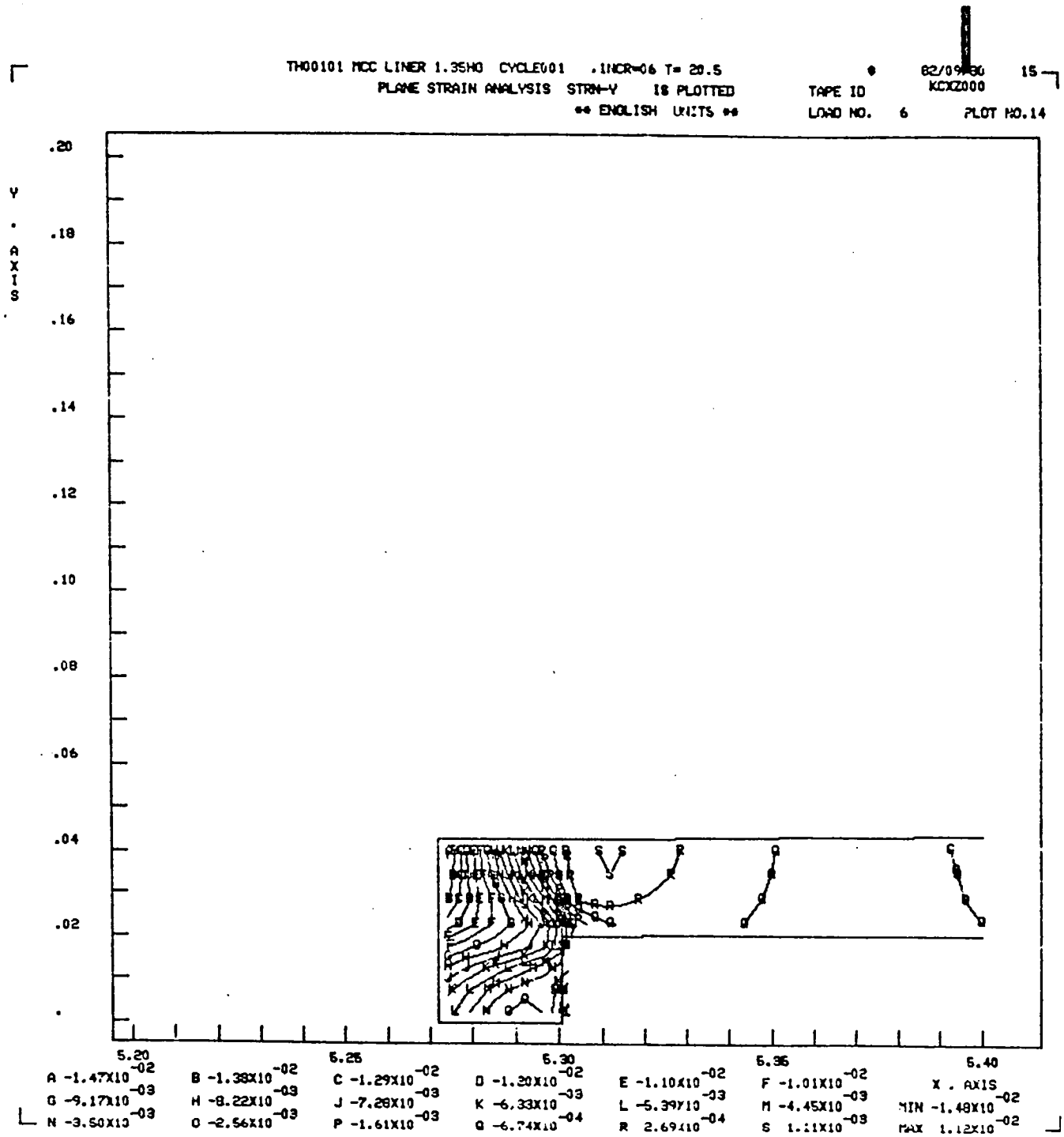
TH00101 MCC LINER 1.3SH0 CYCLE001 .INCR=06 T= 20.5
PLANE STRAIN ANALYSIS STRN-V IS PLOTTED
** ENGLISH UNITS **
TAPE ID KCXZ000
LOAD NO. 6
PLOT NO.14
Y . AXIS
.20
.18
.16
.14
.12
.10
.08
.06
.04
.02
5.20
5.25
5.30
5.35
5.40
X . AXIS
A -1.47X10-02
B -1.38X10-02
C -1.29X10-02
D -1.20X10-02
E -1.10X10-02
F -1.01X10-02
G -9.17X10-03
H -8.22X10-03
J -7.28X10-03
K -6.33X10-03
L -5.39X10-03
M -4.45X10-03
N -3.50X10-03
O -2.56X10-03
P -1.61X10-03
Q -6.74X10-04
R 2.69X10-04
S 1.11X10-03
MIN -1.48X10-02
MAX 1.12X10-02

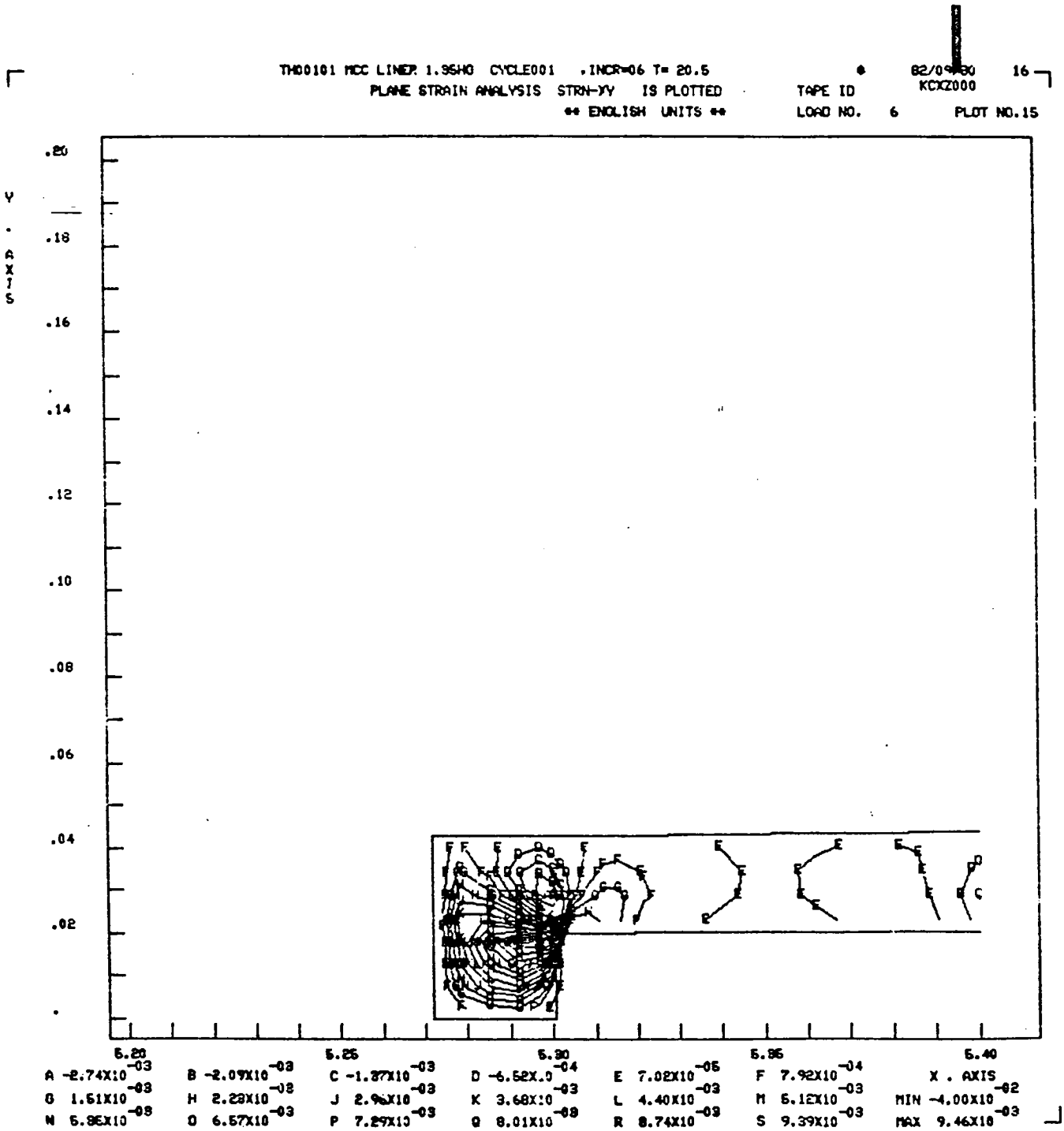
TH00101 MCC LINER 1.95HO CYCLE001 .INCR=06 T= 20.5
PLANE STRAIN ANALYSIS STRN-YY IS PLOTTED
** ENGLISH UNITS **
TAPE ID KCXZ000
LOAD NO. 6
PLOT NO.15
Y . AXIS
.20
.18
.16
.14
.12
.10
.08
.06
.04
.02
5.20
5.25
5.30
5.35
5.40
X . AXIS
A -2.74X10-03
B -2.09X10-03
C -1.87X10-03
D -6.52X.0-04
E 7.02X10-05
F 7.92X10-04
G 1.51X10-03
H 2.23X10-03
J 2.9%X10-03
K 3.68X10-03
L 4.40X10-03
M 5.12X10-03
N 5.86X10-03
O 6.57X10-03
P 7.29X10-03
Q 8.01X10-03
R 8.74X10-03
S 9.39X10-03
MIN -4.00X10-02
MAX 9.46X10-03

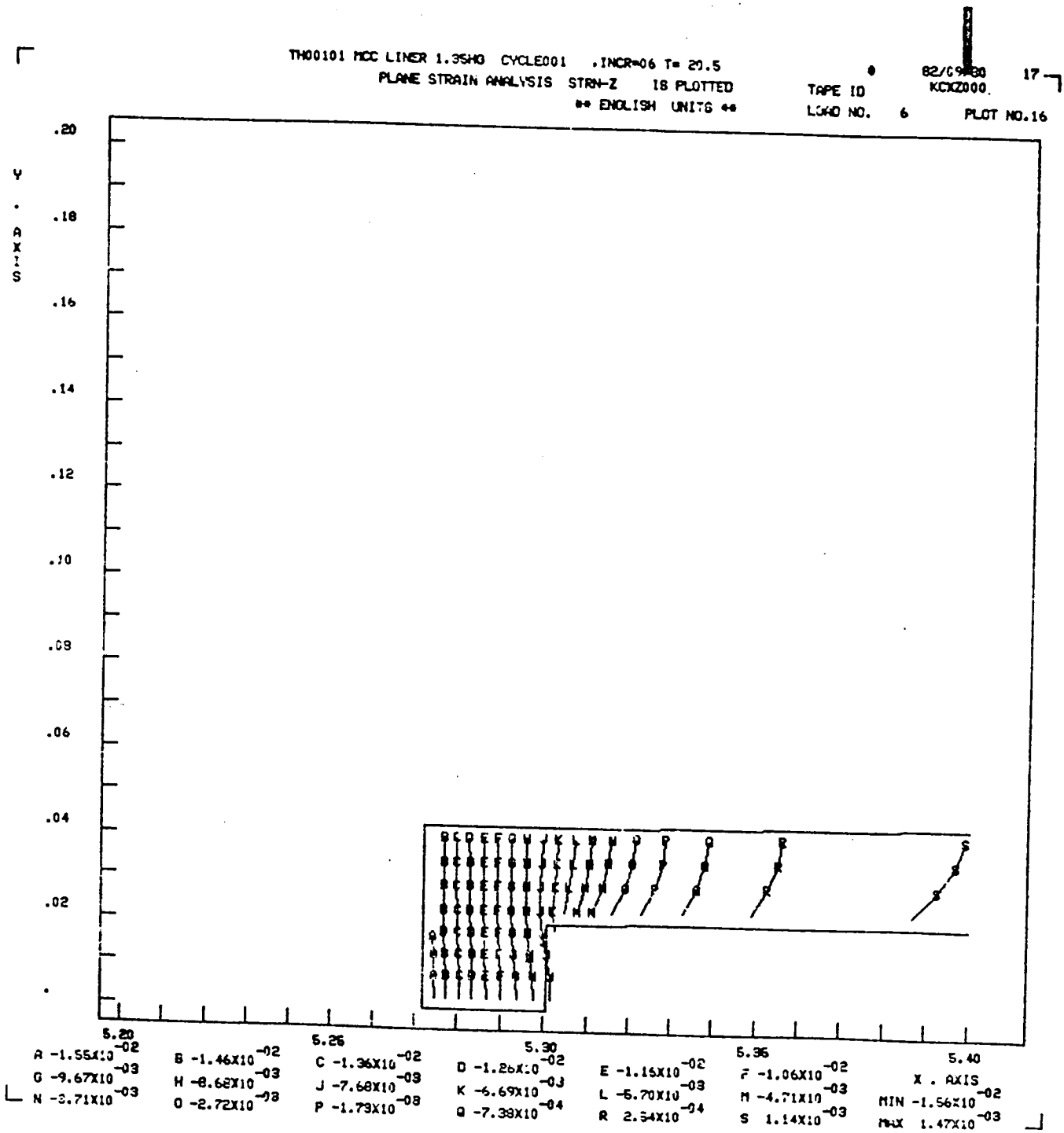
TH00101 MCC LINER 1.3SHO CYCLE001 ,INCR=06 T= 20.5
PLANE STRAIN ANALYSIS STRN-Z 18 PLOTTED
** ENGLISH UNITS **
TAPE ID KCXZ000.
LOAD NO. 6
PLOT NO.16
Y . AXIS
.20
.18
.16
.14
.12
.10
.08
.06
.04
.02
5.20
5.26
5.30
5.36
5.40
X . AXIS
A -1.55X10-02
B -1.46X10-02
C -1.36X10-02
D -1.26X10-02
E -1.16X10-02
F -1.06X10-02
G -9.67X10-03
H -8.68X10-03
J -7.68X10-03
K -6.69X10-03
L -5.70X10-03
M -4.71X10-03
N -3.71X10-03
O -2.72X10-03
P -1.73X10-03
Q -7.39X10-04
R 2.54X10-04
S 1.14X10-03
MIN -1.56X10-02
MAX 1.47X10-03

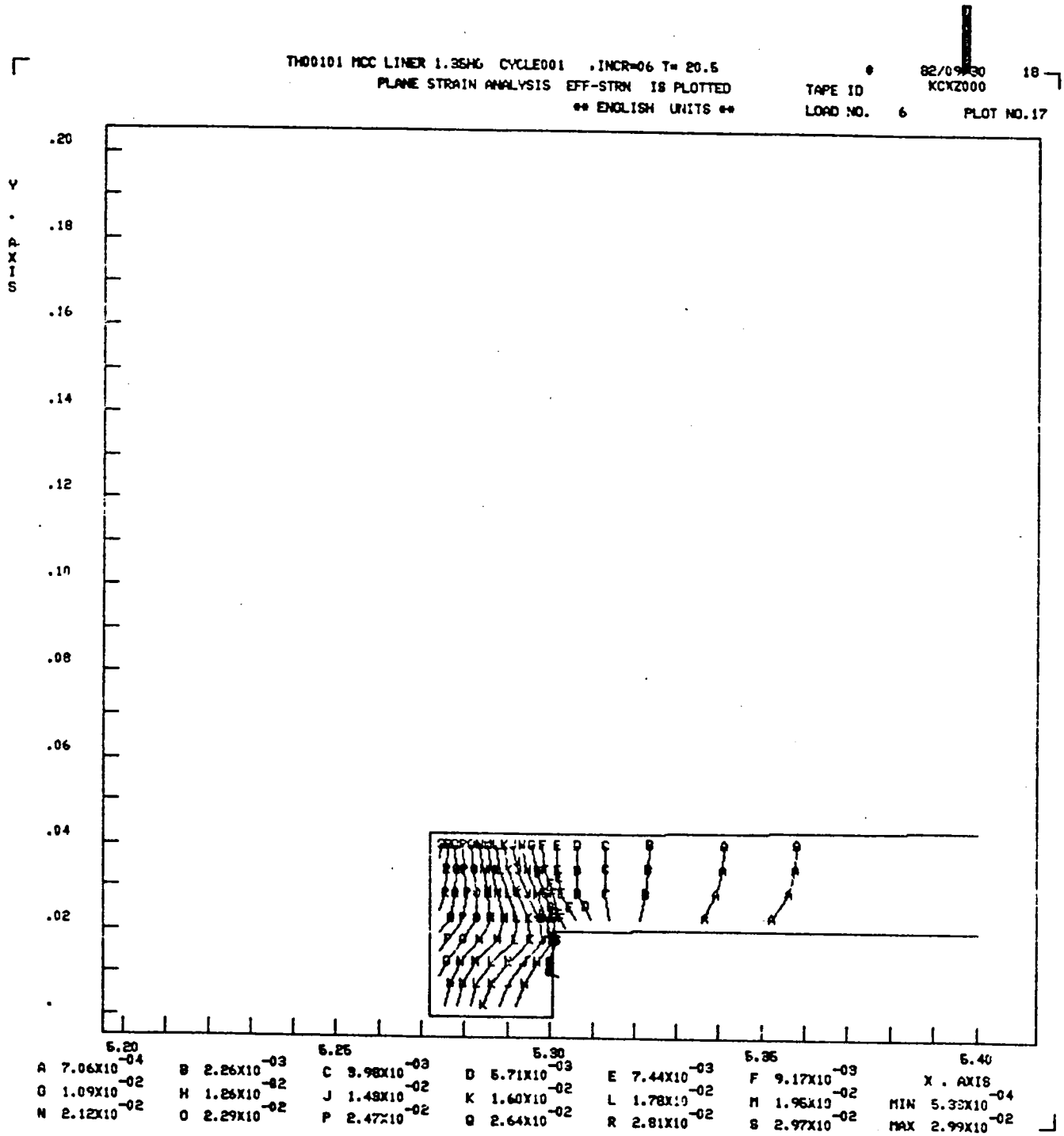
TH00101 MCC LINER 1.3SHG CYCLE001 .INCR=06 T= 20.5
PLANE STRAIN ANALYSIS EFF-STRN IS PLOTTED
** ENGLISH UNITS **
TAPE ID
LOAD NO. 6
PLOT NO.17
Y . AXIS
.20
.18
.16
.14
.12
.10
.08
.06
.04
.02
5.20
5.25
5.30
5.35
5.40
X . AXIS
A 7.06X10-04
B 2.26X10-03
C 3.98X10-03
D 5.71X10-03
E 7.44X10-03
F 9.17X10-03
G 1.09X10-02
H 1.26X10-02
J 1.49X10-02
K 1.60X10-02
L 1.78X10-02
M 1.96X10-02
N 2.12X10-02
O 2.29X10-02
P 2.47X10-02
Q 2.64X10-02
R 2.81X10-02
S 2.97X10-02
MIN 5.33X10-04
MAX 2.99X10-02

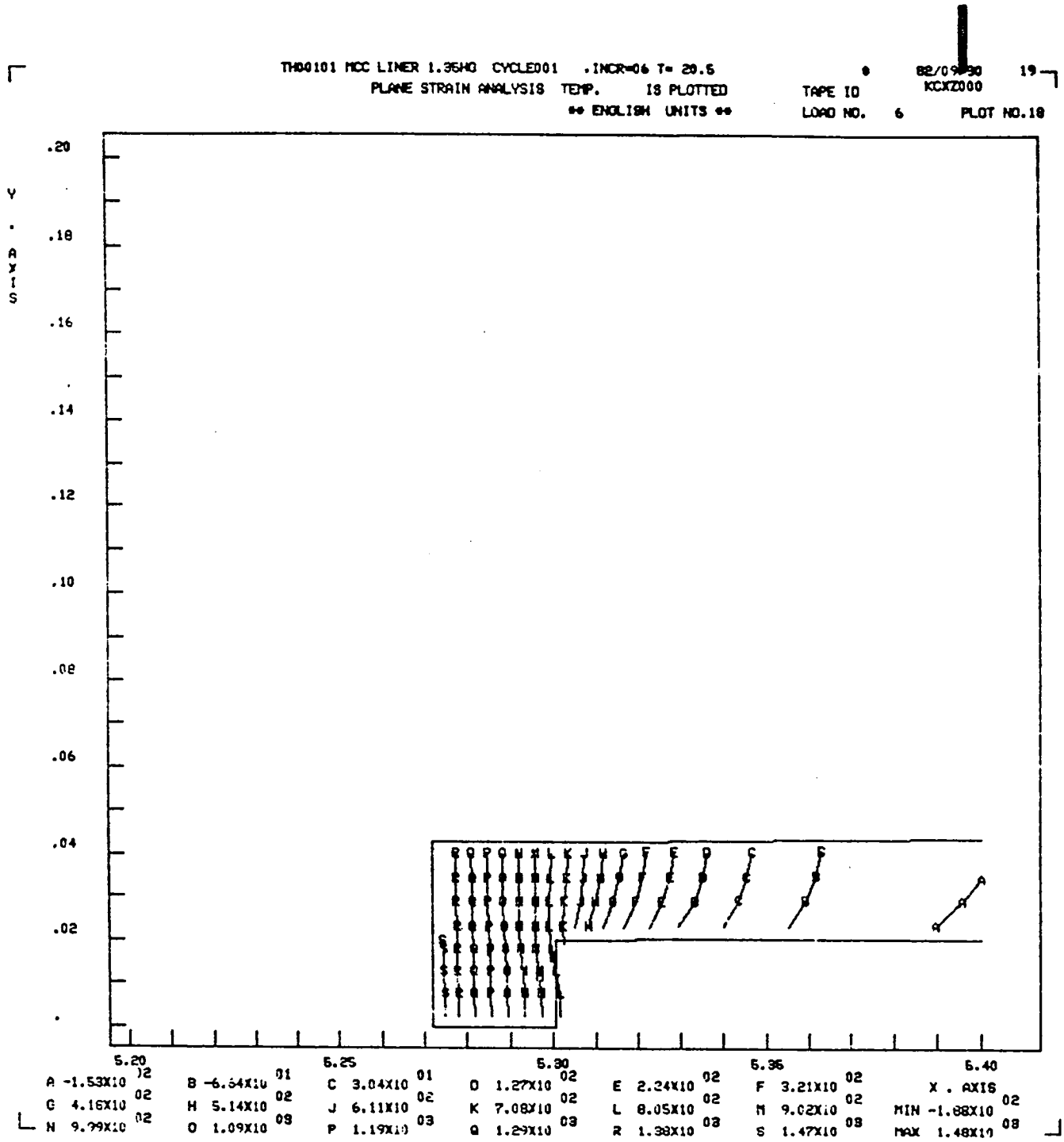
TH00101 MCC LINER 1.36HO CYCLE001 .INCR=06 T= 20.5
PLANE STRAIN ANALYSIS TEMP. IS PLOTTED
** ENGLISH UNITS **
TAPE ID KCXZ000
LOAD NO. 6 PLOT NO.10
Y . AXIS
.20
.18
.16
.14
.12
.10
.08
.06
.04
.02
5.20
5.25
5.30
5.35
5.40
X . AXIS
A -1.53X10 02
B -6.64X10 01
C 3.04X10 01
D 1.27X10 02
E 2.24X10 02
F 3.21X10 02
G 4.16X10 02
H 5.14X10 02
J 6.11X10 02
K 7.08X10 02
L 8.05X10 02
M 9.02X10 02
N 9.99X10 02
O 1.09X10 03
P 1.19X10 03
Q 1.29X10 03
R 1.38X10 03
S 1.47X10 03
MIN -1.88X10 02
MAX 1.48X10 03

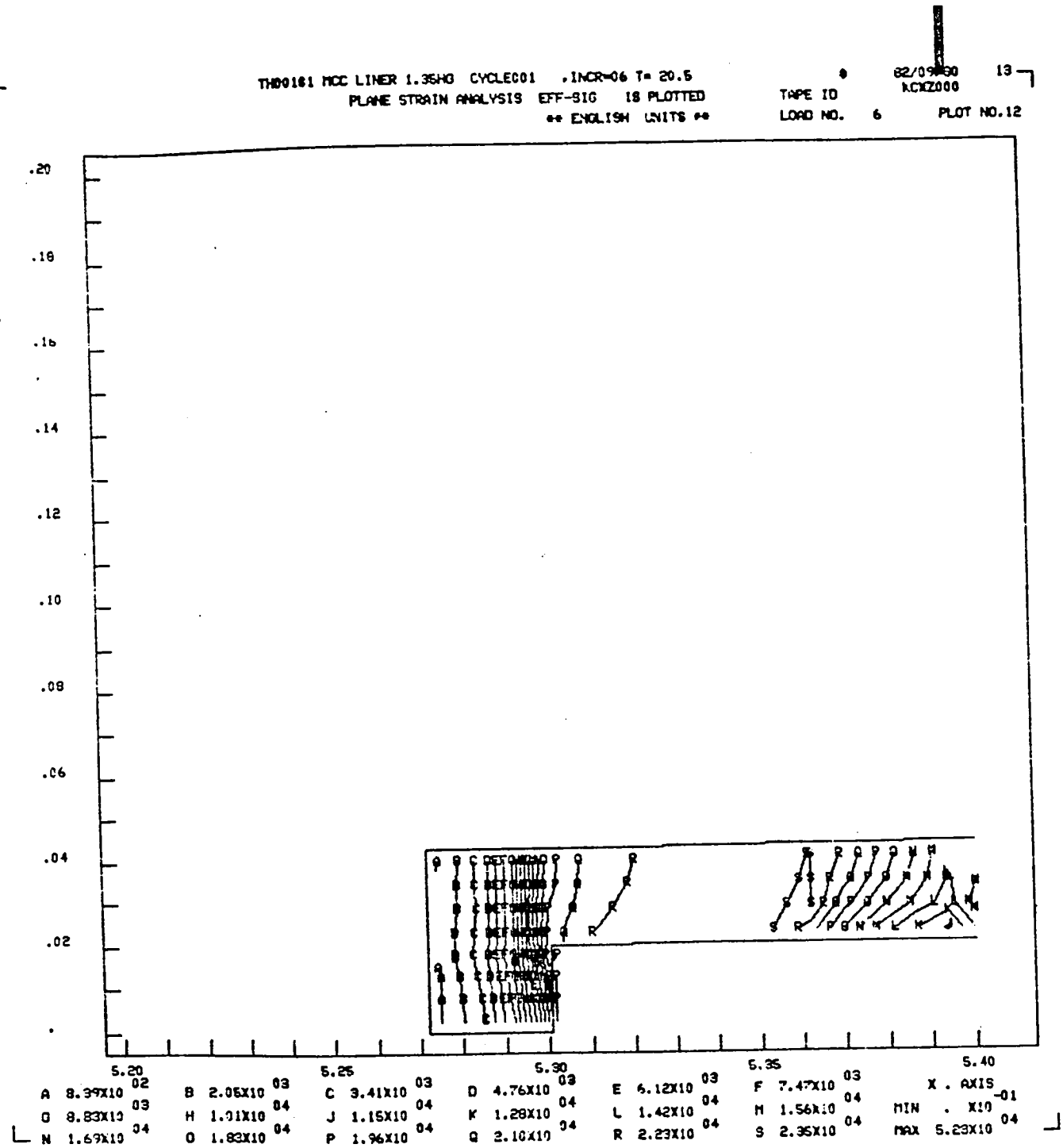
TH00181 MCC LINER 1.35HG CYCLE001 .INCR=06 T= 20.5
PLANE STRAIN ANALYSIS EFF-SIG IS PLOTTED
** ENGLISH UNITS **
TAPE ID
LOAD NO. 6
PLOT NO.12
Y . AXIS
.20
.18
.16
.14
.12
.10
.08
.06
.04
.02
5.20
5.25
5.30
5.35
5.40
X . AXIS
A 8.39X10 02
B 2.06X10 03
C 3.41X10 03
D 4.76X10 03
E 6.12X10 03
F 7.47X10 03
G 8.83X10 03
H 1.91X10 04
J 1.15X10 04
K 1.28X10 04
L 1.42X10 04
M 1.56X10 04
N 1.69X10 04
O 1.83X10 04
P 1.96X10 04
Q 2.10X10 04
R 2.23X10 04
S 2.36X10 04
MIN . X10 -01
MAX 5.23X10 04

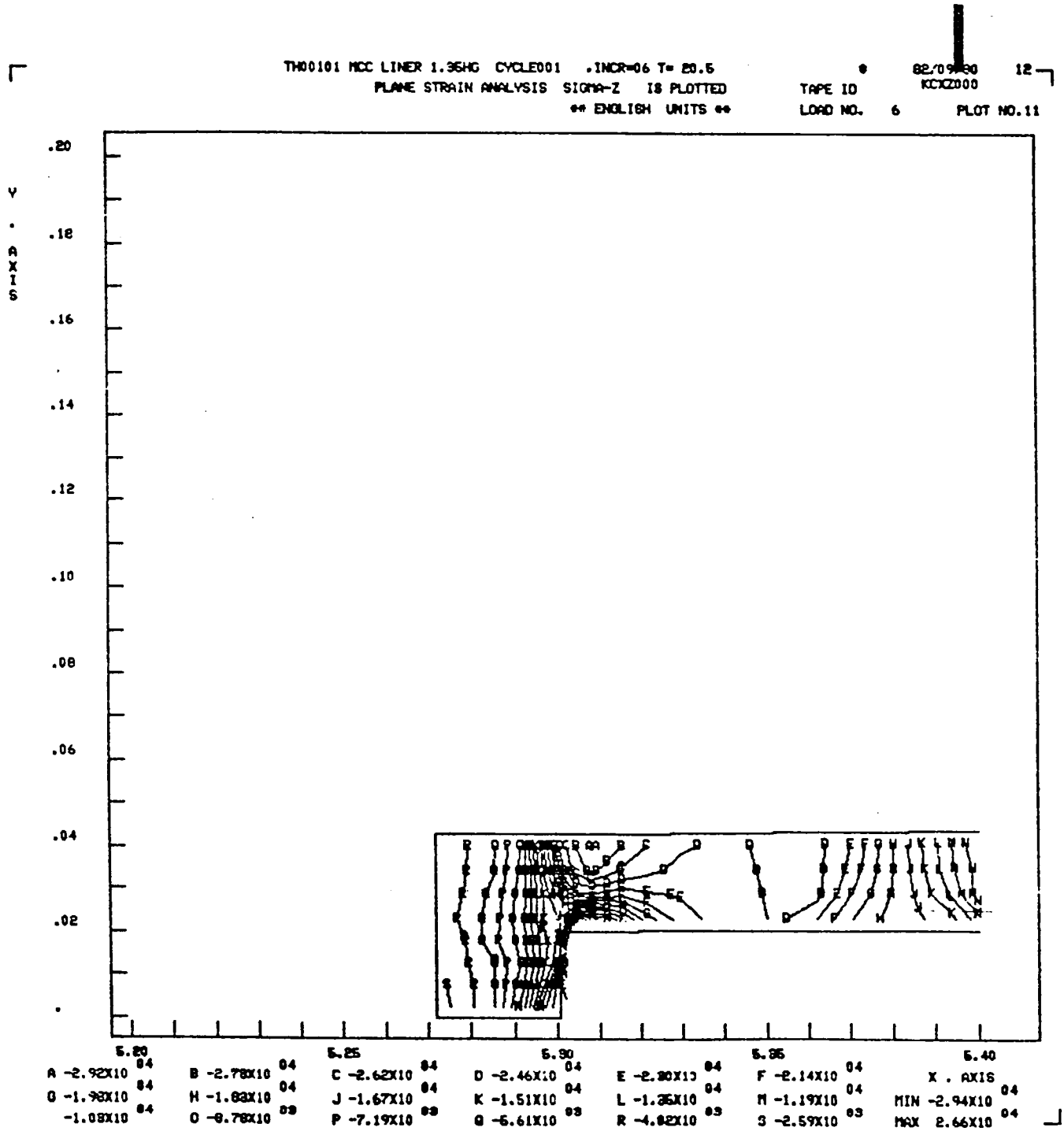
TH00101 MCC LINER 1.36HG CYCLE001 .INCR=06 T= 20.5
PLANE STRAIN ANALYSIS SIGMA-Z IS PLOTTED
** ENGLISH UNITS **
TAPE ID
LOAD NO. 6
PLOT NO.11
Y . AXIS
.20
.18
.16
.14
.12
.10
.08
.06
.04
.02
5.20
5.25
5.30
5.35
5.40
X . AXIS
A -2.92X10 04
B -2.78X10 04
C -2.62X10 04
D -2.46X10 04
E -2.30X10 04
F -2.14X10 04
G -1.98X10 04
H -1.83X10 04
J -1.67X10 04
K -1.51X10 04
L -1.35X10 04
M -1.19X10 04
-1.08X10 04
O -8.78X10 03
P -7.19X10 03
Q -5.61X10 03
R -4.02X10 03
S -2.59X10 03
MIN -2.94X10 04
MAX 2.66X10 04

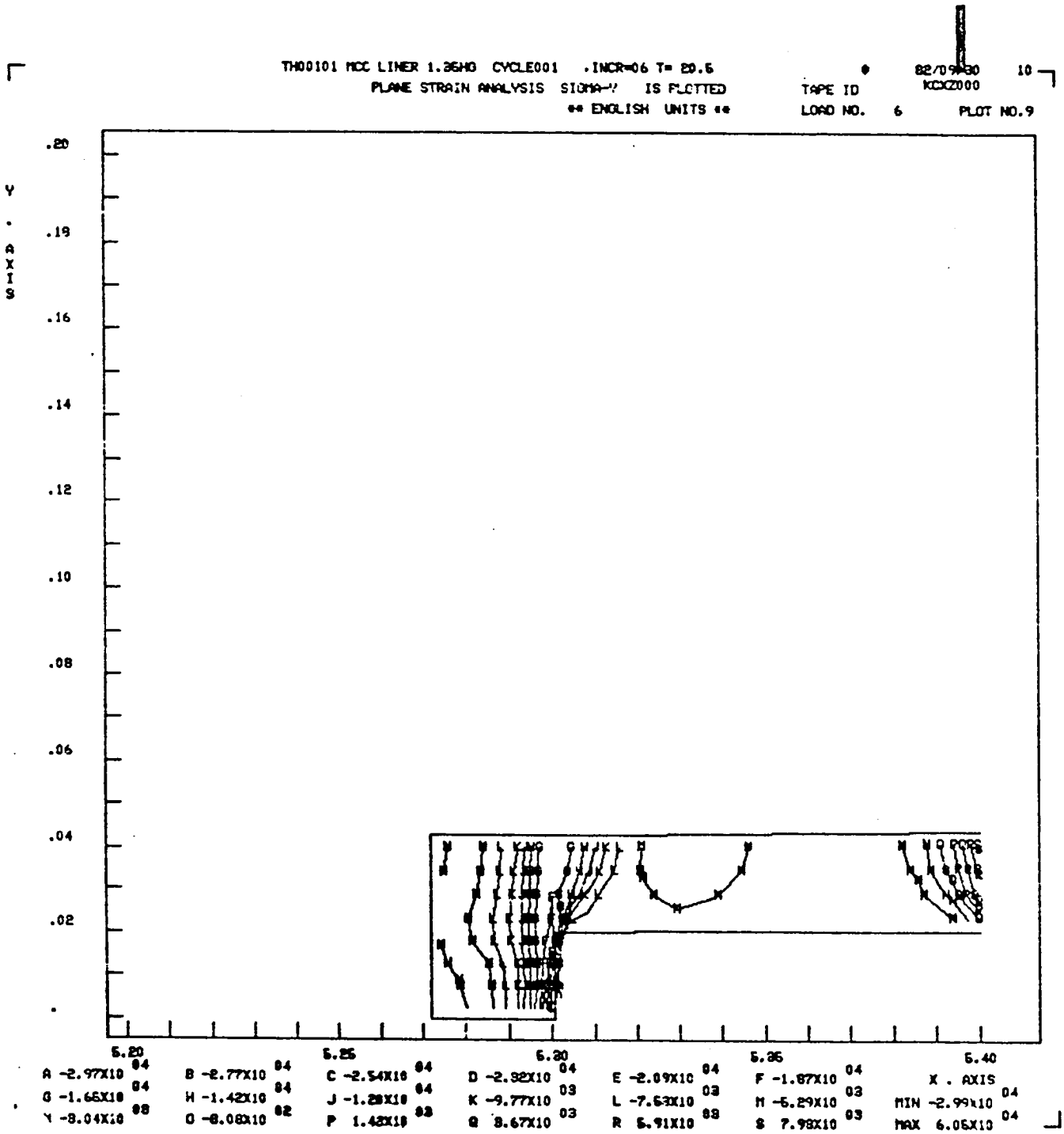
TH00101 MCC LINER 1.36HG CYCLE001 .INCR=06 T= 20.6
PLANE STRAIN ANALYSIS SIGMA-Y IS PLOTTED
** ENGLISH UNITS **
TAPE ID
LOAD NO. 6
PLOT NO.9
Y . AXIS
.20
.18
.16
.14
.12
.10
.08
.06
.04
.02
5.20
5.25
5.30
5.35
5.40
A -2.97X10 04
B -2.77X10 04
C -2.54X10 04
D -2.32X10 04
E -2.09X10 04
F -1.87X10 04
G -1.65X10 04
H -1.42X10 04
J -1.20X10 04
K -9.77X10 03
L -7.53X10 03
M -5.29X10 03
N -8.04X10 03
O -8.08X10 02
P 1.42X10 03
Q 3.67X10 03
R 5.91X10 03
S 7.98X10 03
X . AXIS
MIN -2.99X10 04
MAX 6.05X10 04

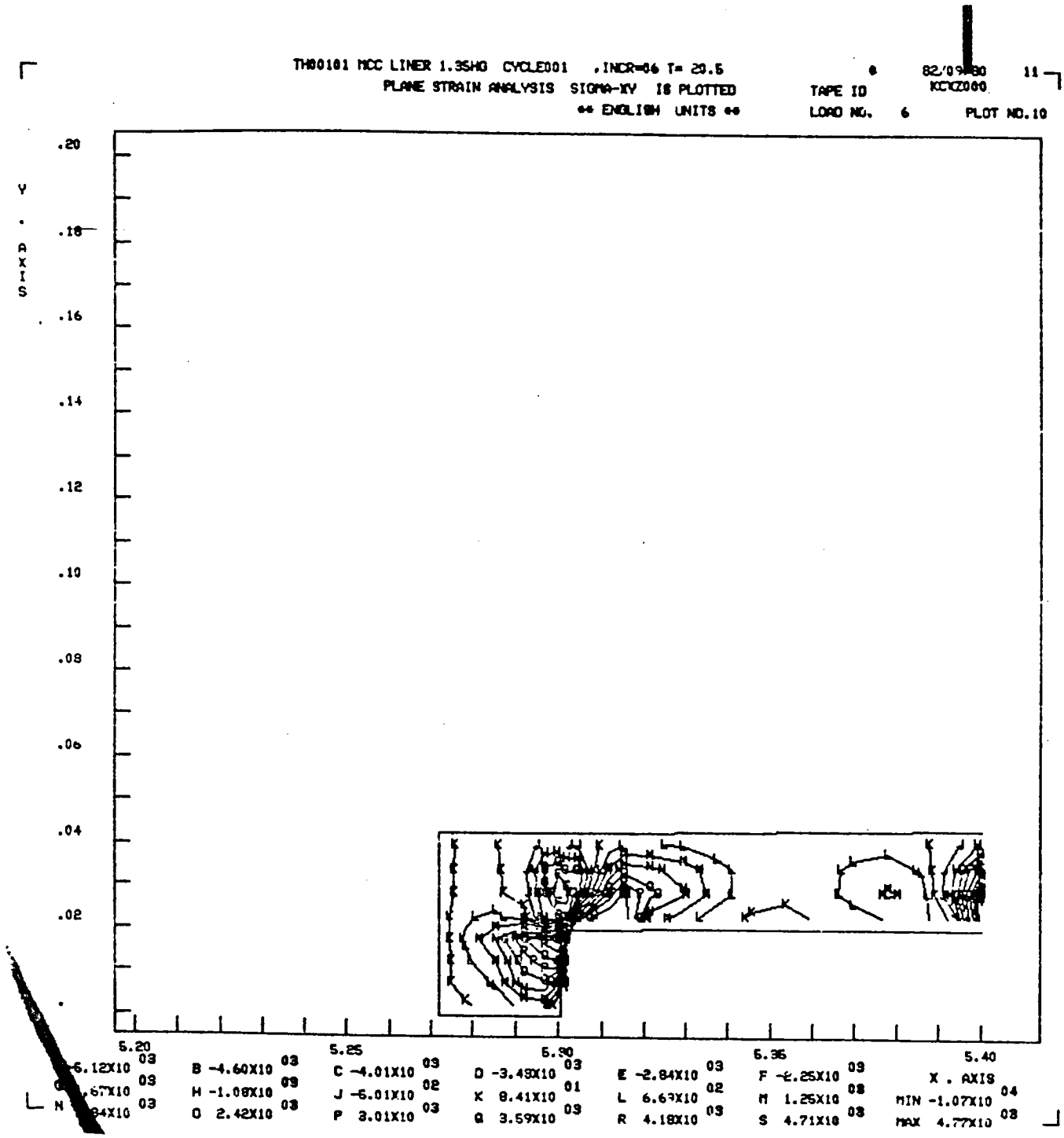
TH00101 MCC LINER 1.35HG CYCLE001 ,INCR=06 T= 20.5
PLANE STRAIN ANALYSIS SIGMA-YY IS PLOTTED
** ENGLISH UNITS **
TAPE ID
LOAD NO. 6
PLOT NO.10
Y . AXIS
.20
.18
.16
.14
.12
.10
.08
.06
.04
.02
5.20
5.25
5.30
5.35
5.40
X . AXIS
B -4.60X10 03
C -4.01X10 03
D -3.48X10 03
E -2.84X10 03
F -2.25X10 03
H -1.09X10 03
J -6.01X10 02
K 8.41X10 01
L 6.69X10 02
M 1.25X10 03
O 2.42X10 03
P 3.01X10 03
Q 3.59X10 03
R 4.18X10 03
S 4.71X10 03
MIN -1.07X10 04
MAX 4.77X10 03

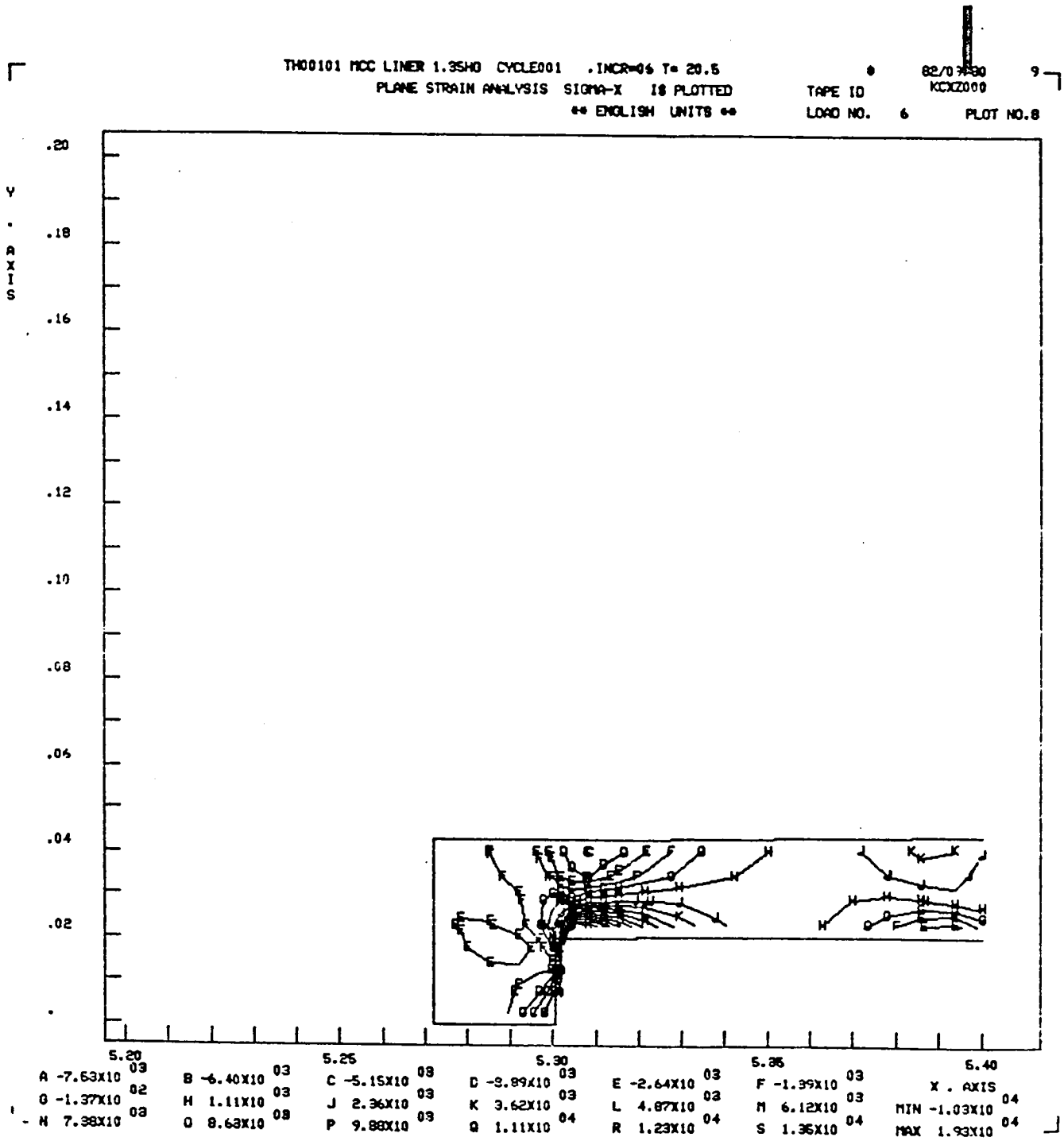
TH00101 MCC LINER 1.3SHO CYCLE001 .INCR=06 T= 20.5
PLANE STRAIN ANALYSIS SIGMA-X IS PLOTTED
** ENGLISH UNITS **
TAPE ID
LOAD NO. 6
PLOT NO.8
Y . AXIS
.20
.18
.16
.14
.12
.10
.08
.06
.04
.02
5.20
5.25
5.30
5.35
5.40
X . AXIS
A -7.63X10 03
B -6.40X10 03
C -5.15X10 03
D -3.89X10 03
E -2.64X10 03
F -1.39X10 03
G -1.37X10 02
H 1.11X10 03
J 2.36X10 03
K 3.62X10 03
L 4.87X10 03
M 6.12X10 03
N 7.38X10 03
O 8.63X10 03
P 9.88X10 03
Q 1.11X10 04
R 1.23X10 04
S 1.36X10 04
MIN -1.03X10 04
MAX 1.93X10 04

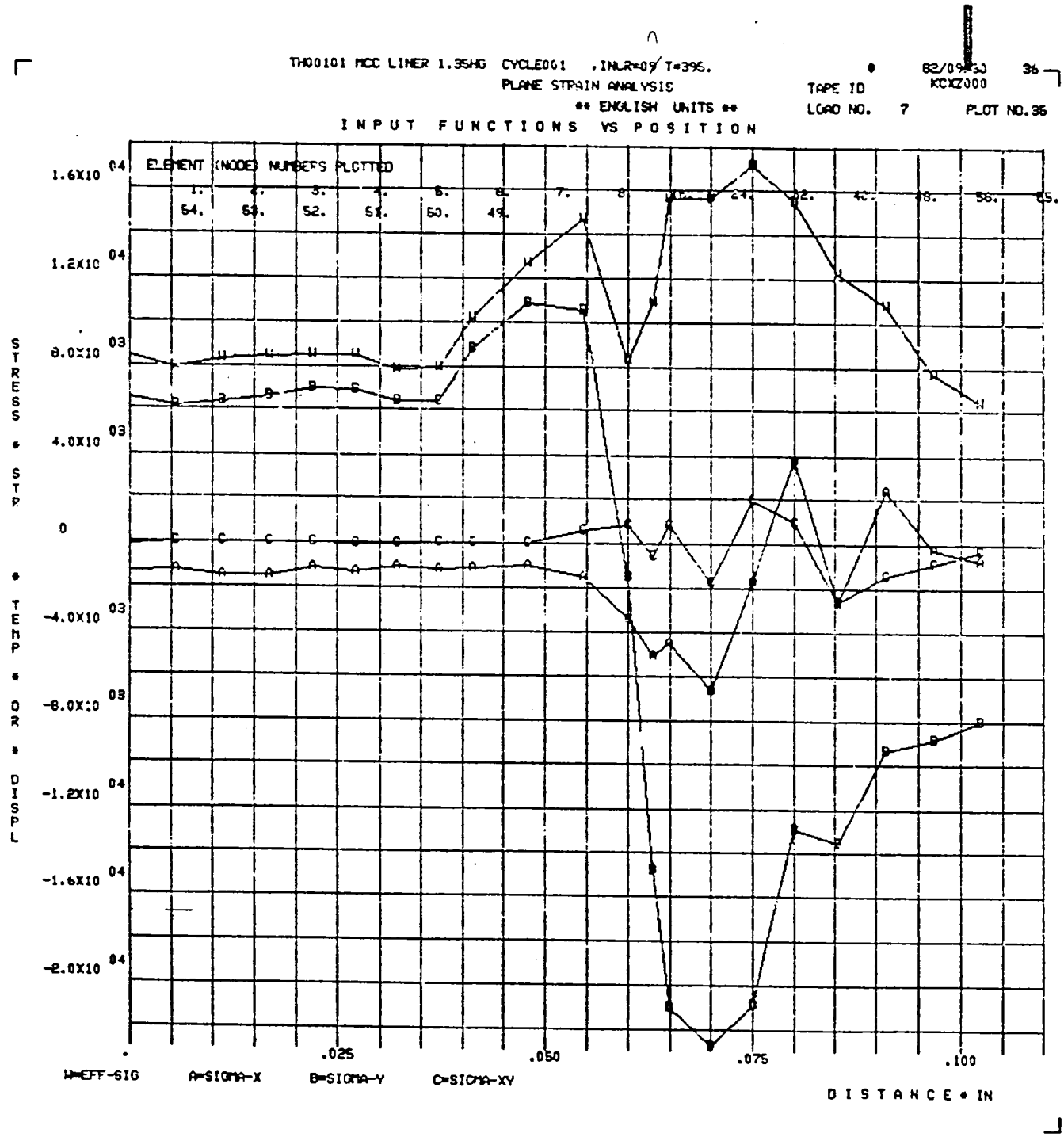
TH00101 MCC LINER 1.35HG CYCLE001 .INLR=05 T=395.
PLANE STRAIN ANALYSIS
** ENGLISH UNITS **
TAPE ID
LOAD NO. 7
PLOT NO.36
INPUT FUNCTIONS VS POSITION
ELEMENT (NODE) NUMBERS PLOTTED
1. 54.
2. 53.
3. 52.
4. 51.
5. 50.
6. 49.
7.
8.
STRESS * STP * TEMP * OR * DISPL
1.6X10 04
1.2X10 04
8.0X10 03
4.0X10 03
0
-4.0X10 03
-8.0X10 03
-1.2X10 04
-1.6X10 04
-2.0X10 04
.025
.050
.075
.100
W=EFF-SIG
A=SIGMA-X
B=SIGMA-Y
C=SIGMA-XY
DISTANCE * IN

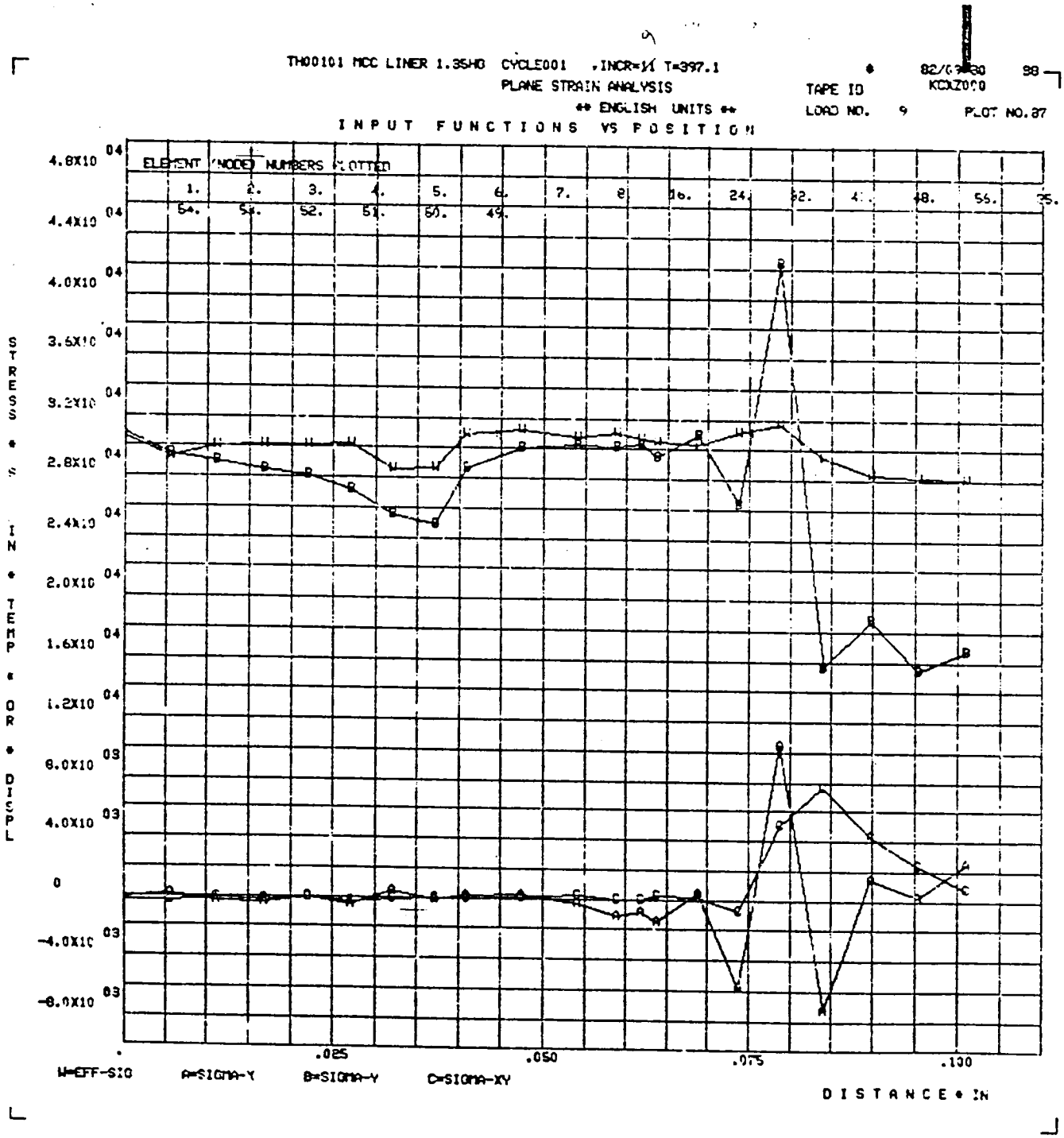
TH00101 MCC LINER 1.35HB CYCLE001 INCR=11 T=397.1
PLANE STRAIN ANALYSIS
** ENGLISH UNITS **
TAPE ID KCXZ000
LOAD NO. 9 PLOT NO.87
INPUT FUNCTIONS VS POSITION
ELEMENT NODED NUMBERS PLOTTED
1. 2. 3. 4. 5. 6. 7. 8. 16. 24. 32. 40. 48. 56. 65.
54. 53. 52. 51. 50. 49.
4.8X10 04
4.4X10 04
4.0X10 04
3.6X10 04
3.2X10 04
2.8X10 04
2.4X10 04
2.0X10 04
1.6X10 04
1.2X10 04
8.0X10 03
4.0X10 03
0
-4.0X10 03
-8.0X10 03
STRESS * IN * TEMP * OR * DISPL
.025
.050
.075
.100
DISTANCE * IN
W=EFF-SIG A=SIGMA-Y B=SIGMA-Y C=SIGMA-XY

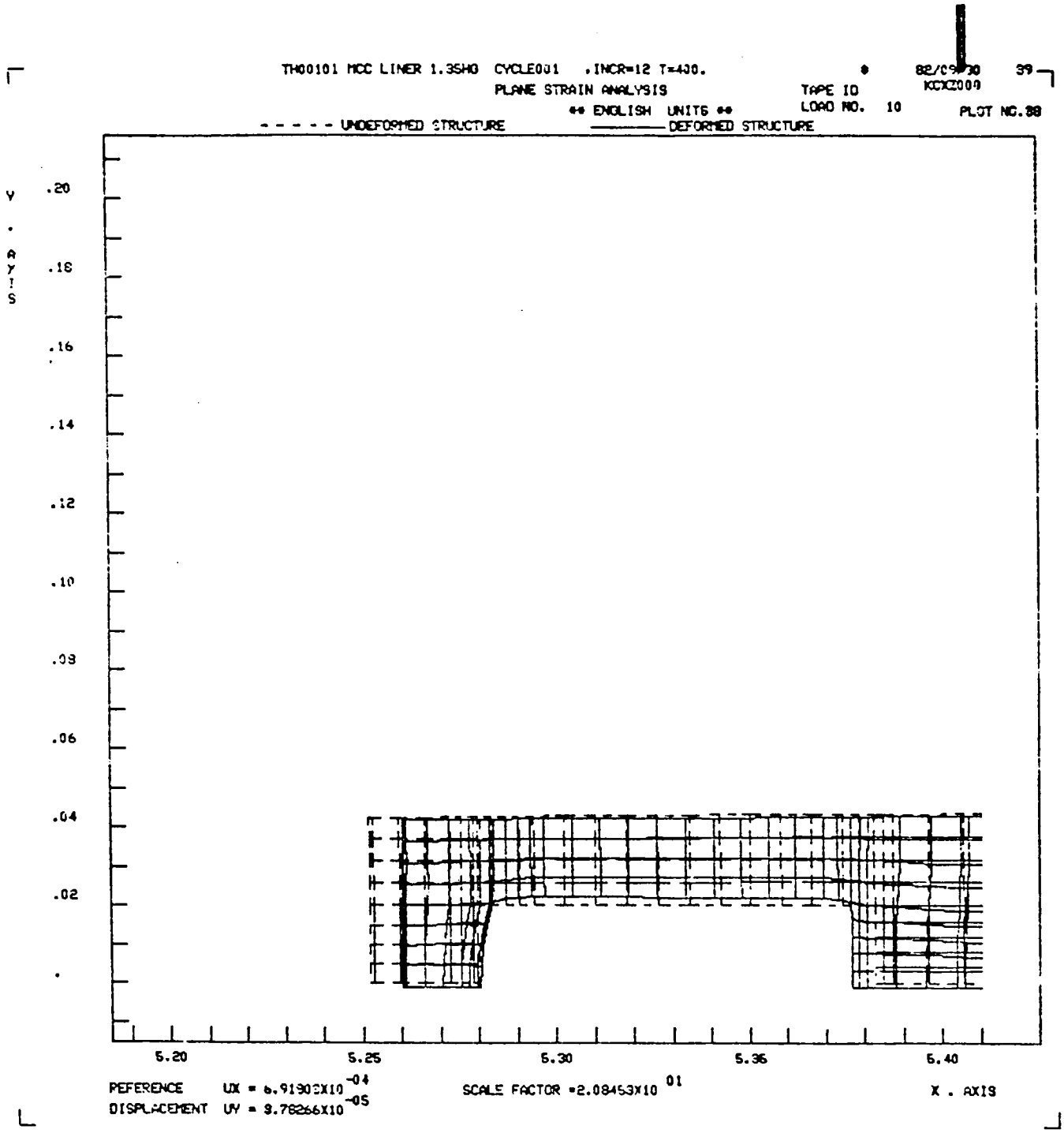
TH00101 MCC LINER 1.3SH0 CYCLE001 ,INCR=12 T=430.
PLANE STRAIN ANALYSIS
** ENGLISH UNITS **
TAPE ID
LOAD NO. 10
PLOT NO.88
- - - - - UNDEFORMED STRUCTURE
——— DEFORMED STRUCTURE
Y . AXIS
.20
.18
.16
.14
.12
.10
.08
.06
.04
.02
5.20
5.25
5.30
5.35
5.40
X . AXIS
REFERENCE UX = 6.91903X10 -04
DISPLACEMENT UY = 9.78266X10 -05
SCALE FACTOR =2.08453X10 01

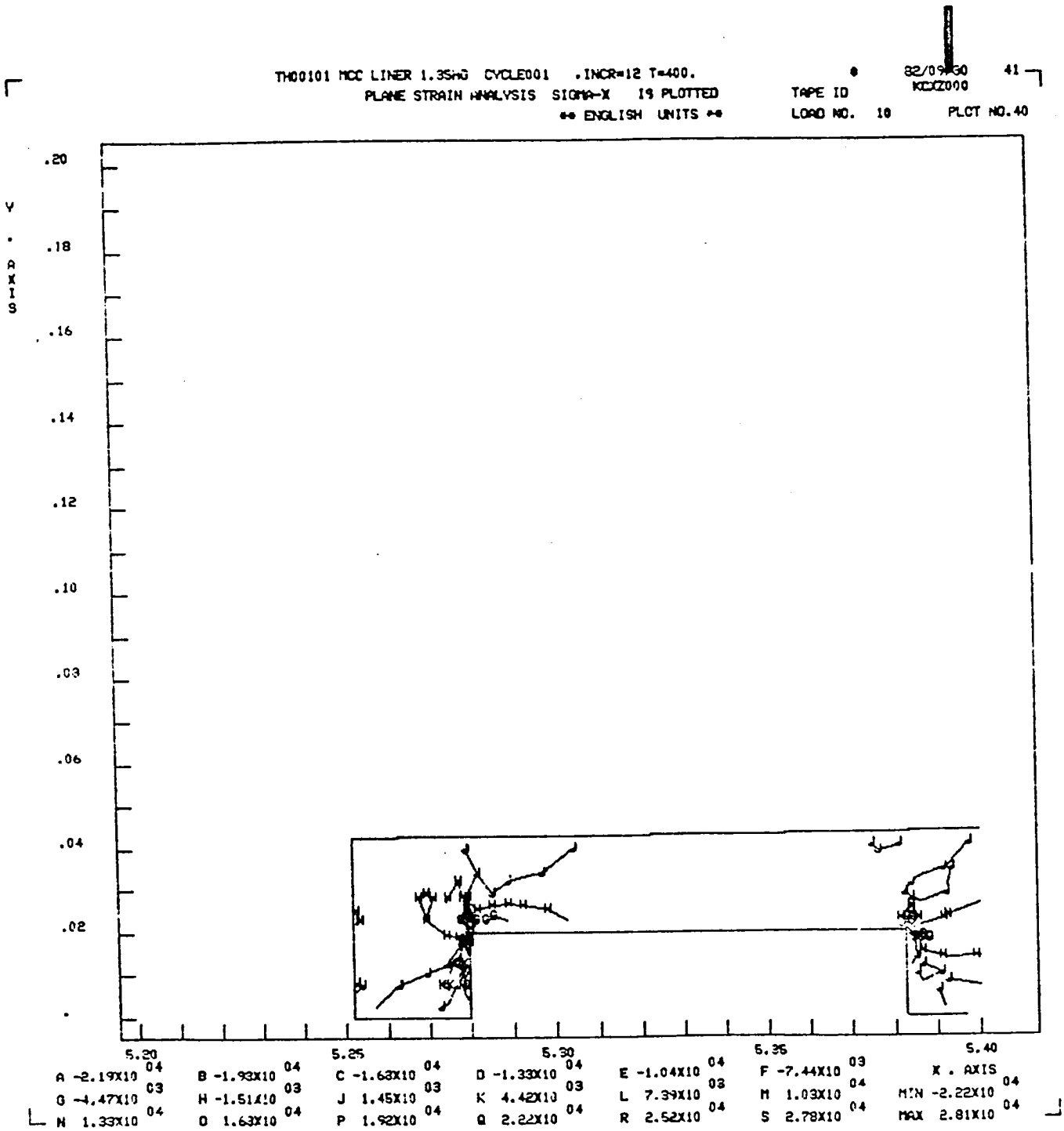
TH00101 MCC LINER 1.3SHJ CYCLE001 .INCR=12 T=400.
PLANE STRAIN ANALYSIS SIGMA-X IS PLOTTED
** ENGLISH UNITS **
TAPE ID
LOAD NO. 10
PLOT NO.40
Y . AXIS
.20
.18
.16
.14
.12
.10
.03
.06
.04
.02
5.20
5.25
5.30
5.35
5.40
A -2.19X10 04
B -1.93X10 04
C -1.68X10 04
D -1.33X10 04
E -1.04X10 04
F -7.44X10 03
X . AXIS
G -4.47X10 03
H -1.51X10 03
J 1.45X10 03
K 4.42X10 03
L 7.39X10 03
M 1.03X10 04
MIN -2.22X10 04
N 1.33X10 04
O 1.63X10 04
P 1.92X10 04
Q 2.22X10 04
R 2.52X10 04
S 2.78X10 04
MAX 2.81X10 04

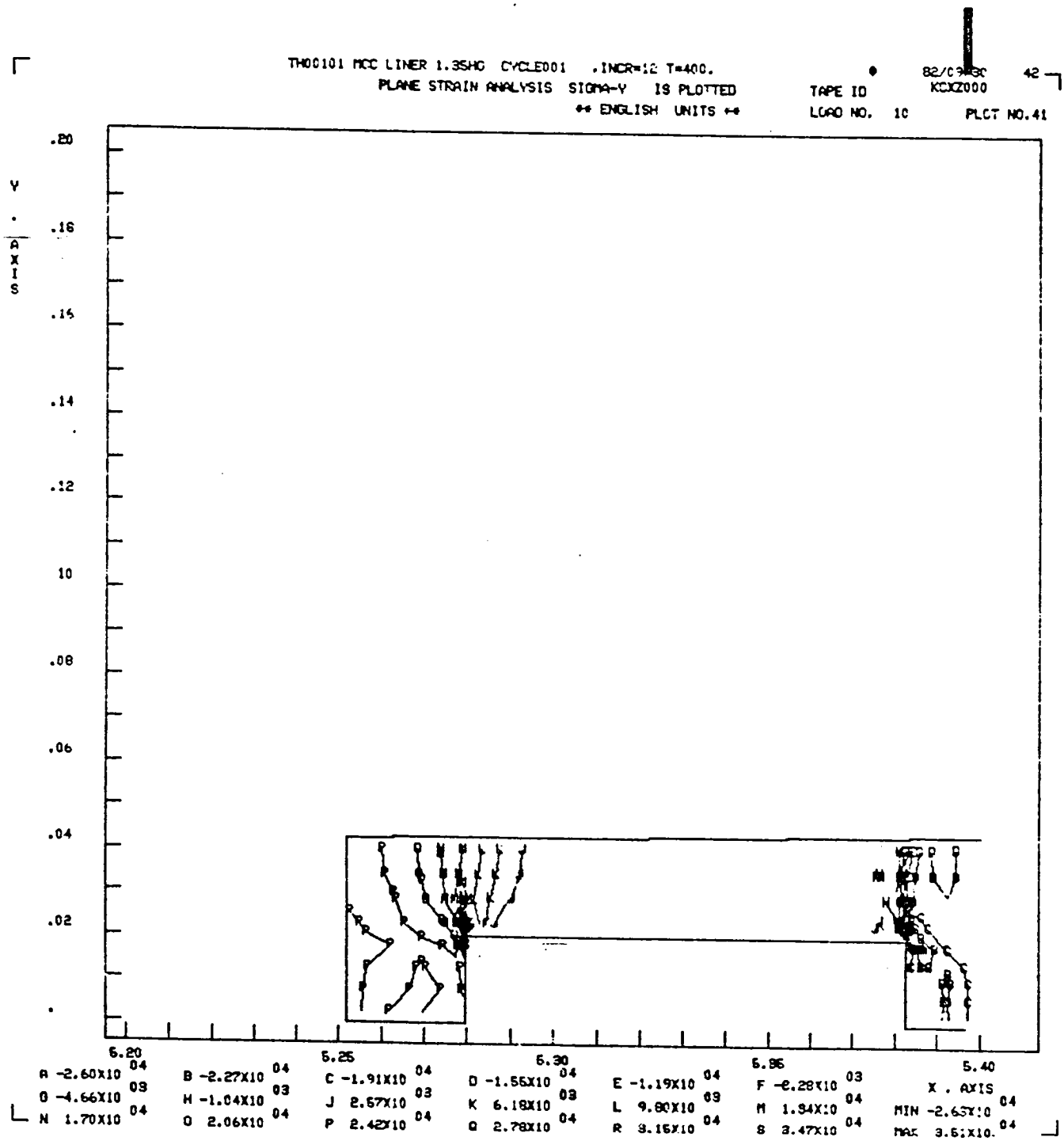
TH00101 MCC LINER 1.3SHO CYCLE001 .INCR=12 T=400.
PLANE STRAIN ANALYSIS SIGMA-Y IS PLOTTED
** ENGLISH UNITS **
TAPE ID KCXZ000
LOAD NO. 10 PLOT NO.41
Y . AXIS
.20
.16
.14
.12
10
.08
.06
.04
.02
5.20
5.25
5.30
5.35
5.40
X . AXIS
A -2.60X10 04
B -2.27X10 04
C -1.91X10 04
D -1.55X10 04
E -1.19X10 04
F -8.28X10 03
G -4.66X10 03
H -1.04X10 04
J 2.57X10 03
K 6.18X10 03
L 9.80X10 03
M 1.34X10 04
N 1.70X10 04
O 2.06X10 04
P 2.42X10 04
Q 2.78X10 04
R 3.16X10 04
S 3.47X10 04
MIN -2.63X10 04
MAX 3.61X10 04

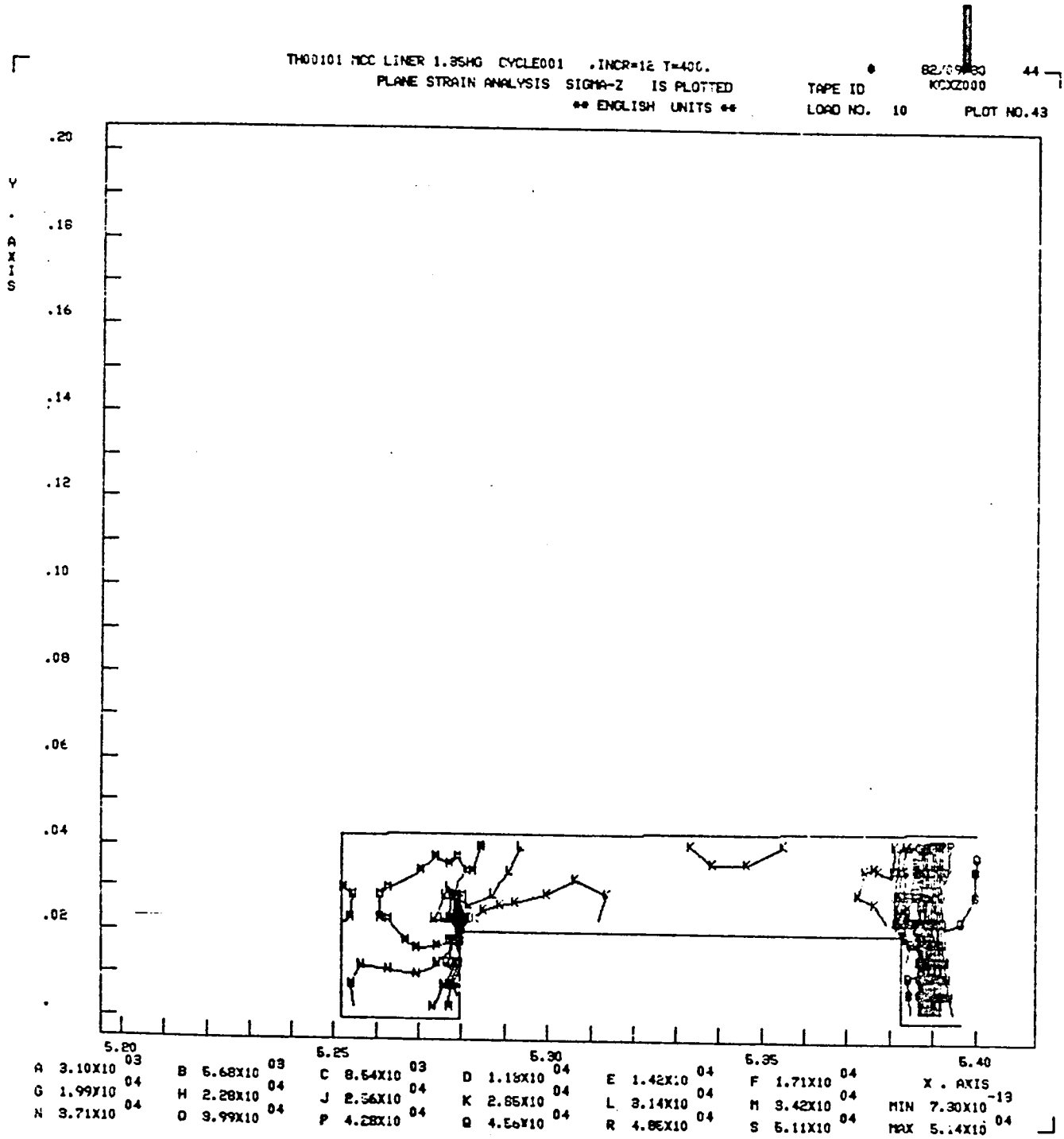
TH00101 MCC LINER 1.85MG CYCLE001 .INCR=12 T=400.
PLANE STRAIN ANALYSIS SIGMA-Z IS PLOTTED
** ENGLISH UNITS **
TAPE ID
LOAD NO. 10
PLOT NO.43
Y . AXIS
.20
.18
.16
.14
.12
.10
.08
.06
.04
.02
5.20
5.25
5.30
5.35
5.40
X . AXIS
A 3.10X10 03
B 6.68X10 03
C 8.64X10 03
D 1.18X10 04
E 1.42X10 04
F 1.71X10 04
G 1.99X10 04
H 2.28X10 04
J 2.56X10 04
K 2.85X10 04
L 3.14X10 04
M 3.42X10 04
N 3.71X10 04
O 3.99X10 04
P 4.28X10 04
Q 4.56X10 04
R 4.86X10 04
S 5.11X10 04
MIN 7.30X10 -13
MAX 5.14X10 04

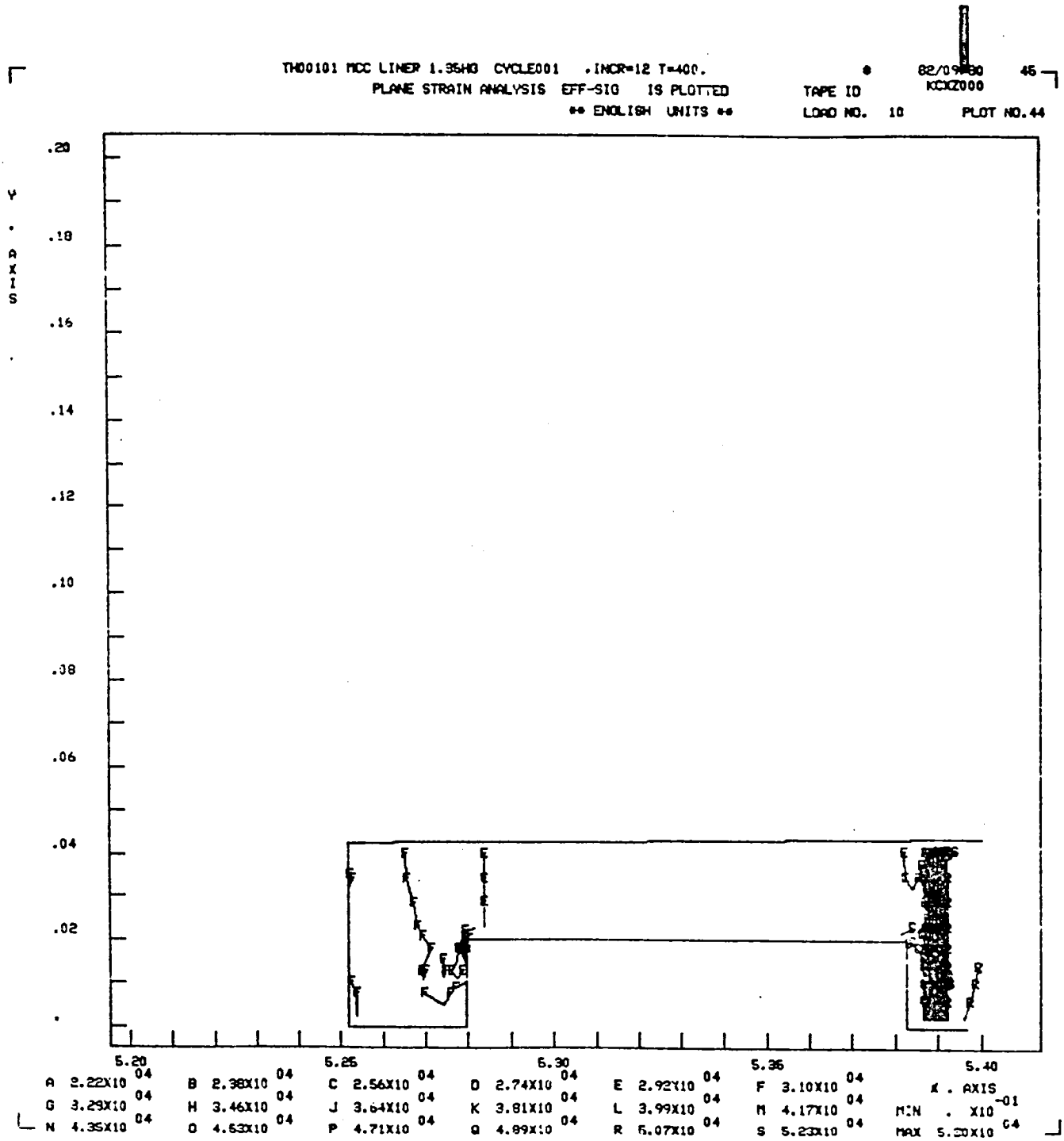
TH00101 MCC LINER 1.35H0 CYCLE001 .INCR=12 T=400.
PLANE STRAIN ANALYSIS EFF-SIG IS PLOTTED
** ENGLISH UNITS **
TAPE ID
LOAD NO. 10
PLOT NO.44
KCXZ000
45
Y . AXIS
.20
.18
.16
.14
.12
.10
.08
.06
.04
.02
5.20
5.25
5.30
5.35
5.40
X . AXIS
MIN . X10 -01
MAX 5.20X10 04
A 2.22X10 04
B 2.38X10 04
C 2.56X10 04
D 2.74X10 04
E 2.92X10 04
F 3.10X10 04
G 3.29X10 04
H 3.46X10 04
J 3.64X10 04
K 3.81X10 04
L 3.99X10 04
M 4.17X10 04
N 4.35X10 04
O 4.53X10 04
P 4.71X10 04
Q 4.89X10 04
R 5.07X10 04
S 5.23X10 04

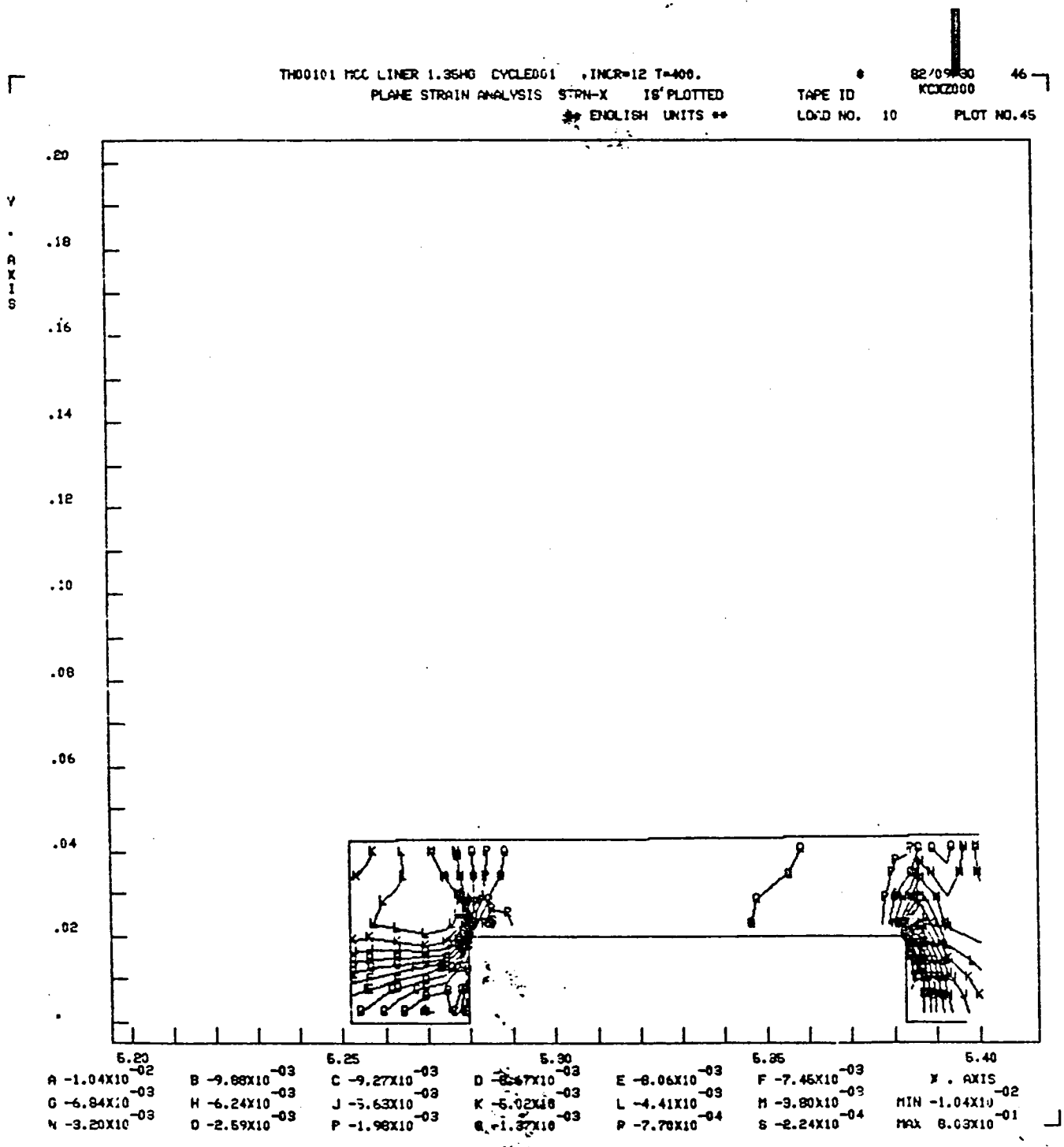
TH00101 HCC LINER 1.35HG CYCLE001 ,INCR=12 T=400.
PLANE STRAIN ANALYSIS STRN-X IS PLOTTED
** ENGLISH UNITS **
TAPE ID
LOAD NO. 10
PLOT NO.45
82/09/30 46
KCXC2000
Y - AXIS
.20
.18
.16
.14
.12
.10
.08
.06
.04
.02
5.20
5.25
5.30
5.35
5.40
A -1.04X10-02
B -9.88X10-03
C -9.27X10-03
D -8.67X10-03
E -8.06X10-03
F -7.46X10-03
G -6.84X10-03
H -6.24X10-03
J -5.63X10-03
K -5.02X10-03
L -4.41X10-03
M -3.80X10-03
N -3.20X10-03
O -2.59X10-03
P -1.98X10-03
Q -1.37X10-03
R -7.70X10-04
S -2.24X10-04
X . AXIS
MIN -1.04X10-02
MAX 8.03X10-01

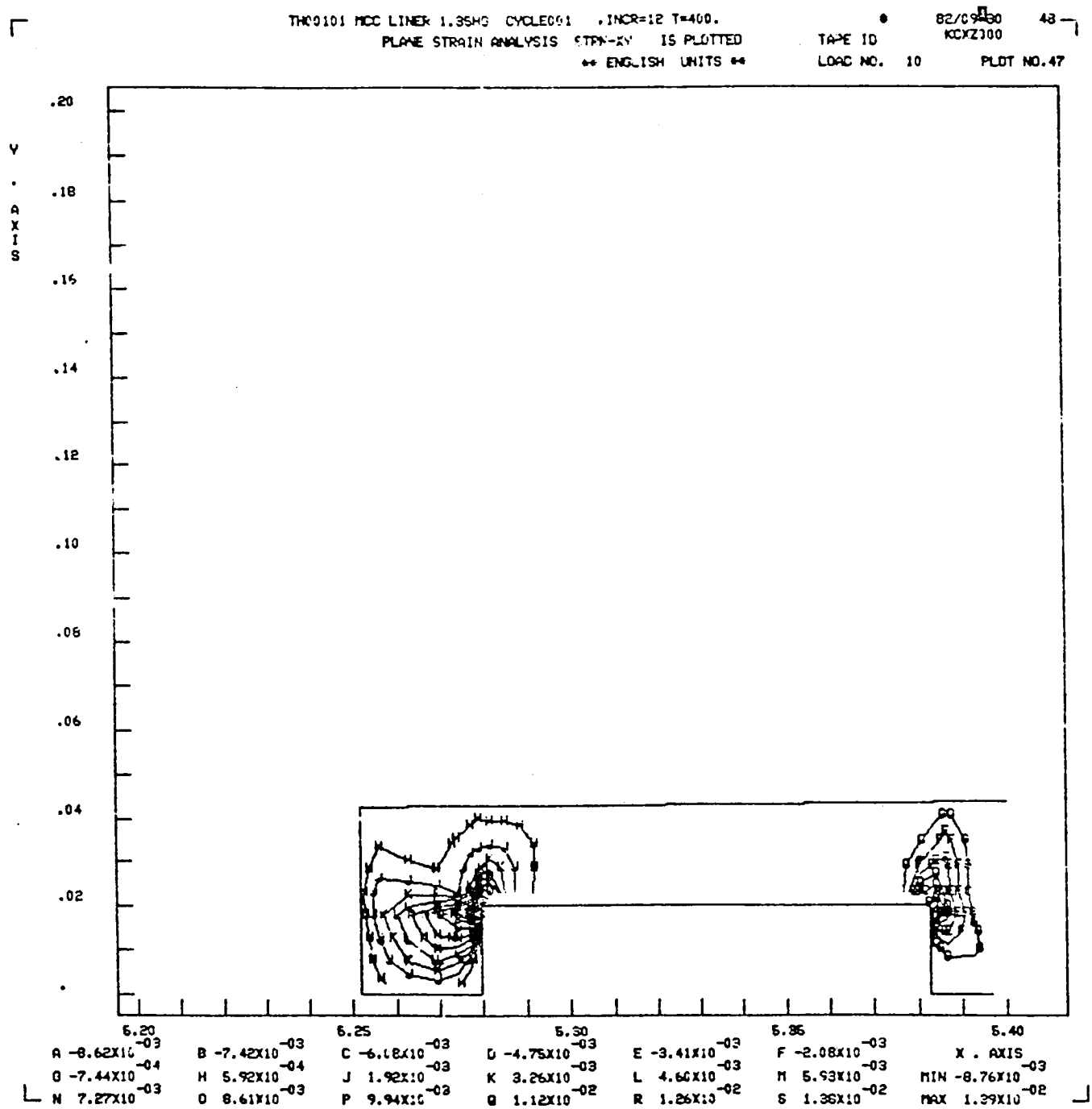
TH09101 MCC LINER 1.3SHG CYCLE091 ,INCR=12 T=400.
PLANE STRAIN ANALYSIS STRN-XY IS PLOTTED
** ENGLISH UNITS **
TAPE ID
LOAD NO. 10
PLOT NO.47
Y . AXIS
.20
.18
.16
.14
.12
.10
.08
.06
.04
.02
.
5.20
5.25
5.30
5.35
5.40
X . AXIS
A -8.62X10-03
B -7.42X10-03
C -6.18X10-03
D -4.75X10-03
E -3.41X10-03
F -2.08X10-03
G -7.44X10-04
H 5.92X10-04
J 1.92X10-03
K 3.26X10-03
L 4.60X10-03
M 5.93X10-03
N 7.27X10-03
O 8.61X10-03
P 9.94X10-03
Q 1.12X10-02
R 1.26X10-02
S 1.39X10-02
MIN -8.76X10-03
MAX 1.39X10-02

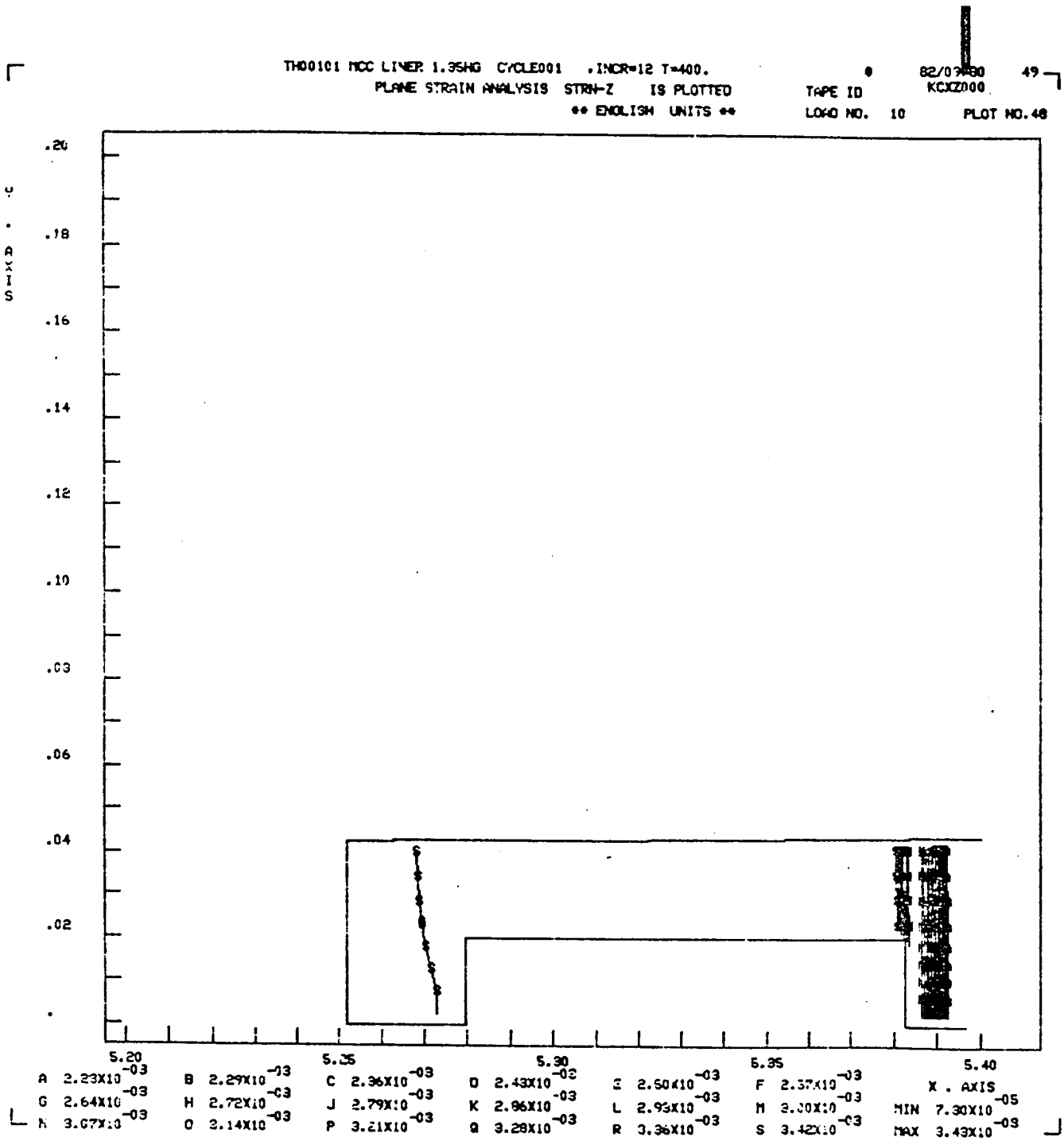
TH00101 MCC LINER 1.35HG CYCLE001 .INCR=12 T=400.
PLANE STRAIN ANALYSIS STRN-Z IS PLOTTED
** ENGLISH UNITS **
TAPE ID KCXZ000
LOAD NO. 10
PLOT NO.48
Y . AXIS
.20
.18
.16
.14
.12
.10
.08
.06
.04
.02
5.20
5.25
5.30
5.35
5.40
A 2.23X10-03
B 2.29X10-03
C 2.36X10-03
D 2.43X10-03
E 2.50X10-03
F 2.57X10-03
G 2.64X10-03
H 2.72X10-03
J 2.79X10-03
K 2.86X10-03
L 2.93X10-03
M 3.00X10-03
N 3.07X10-03
O 3.14X10-03
P 3.21X10-03
Q 3.28X10-03
R 3.36X10-03
S 3.42X10-03
X . AXIS
MIN 7.30X10-05
MAX 3.43X10-03

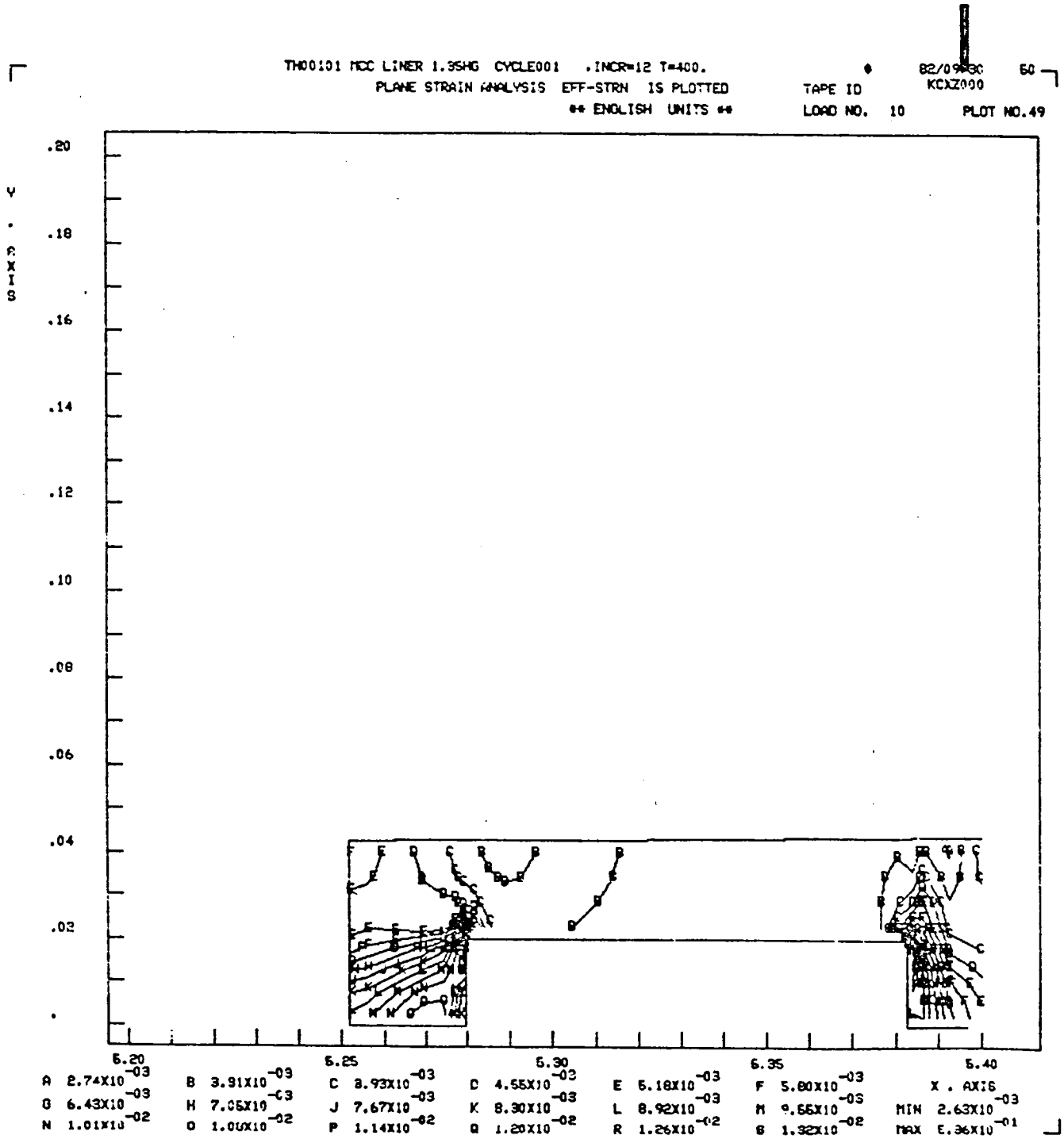
TH00101 MCC LINER 1.3SHG CYCLE001 ,INCR=12 T=400.
PLANE STRAIN ANALYSIS EFF-STRN IS PLOTTED
** ENGLISH UNITS **
TAPE ID
LOAD NO. 10
PLOT NO.49
KCXZ000
Y - AXIS
.20
.18
.16
.14
.12
.10
.08
.06
.04
.02
5.20
5.25
5.30
5.35
5.40
X - AXIS
A 2.74X10-03
B 3.91X10-03
C 8.93X10-03
D 4.55X10-02
E 5.18X10-03
F 5.80X10-03
G 6.43X10-03
H 7.05X10-03
J 7.67X10-03
K 8.30X10-03
L 8.92X10-03
M 9.55X10-03
N 1.01X10-02
O 1.00X10-02
P 1.14X10-02
Q 1.20X10-02
R 1.26X10-02
S 1.32X10-02
MIN 2.63X10-03
MAX 5.36X10-01

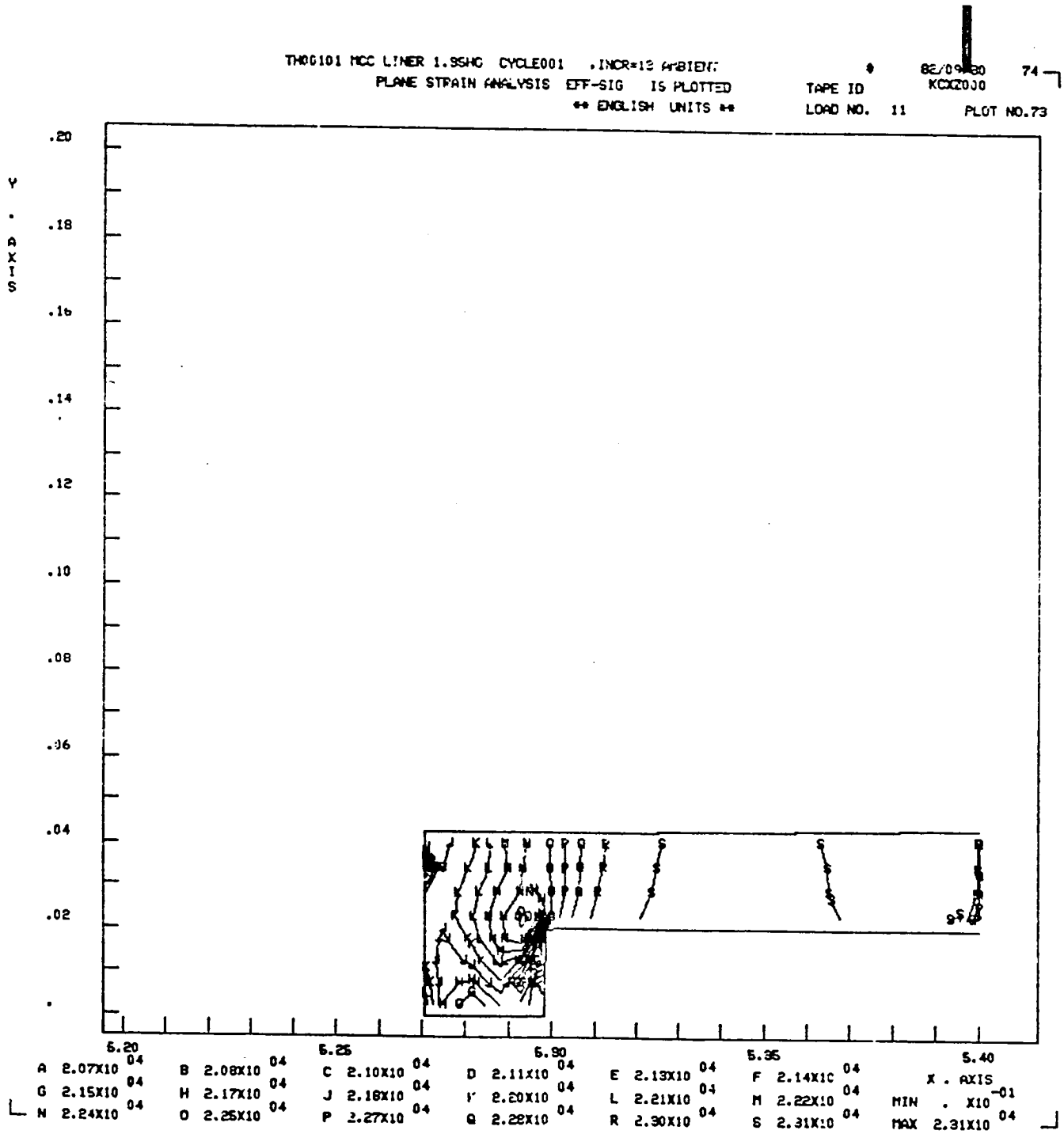
TH0G101 MCC LINER 1.9SHC CYCLE001 *INCR=13 AMBIENT
PLANE STRAIN ANALYSIS EFF-SIG IS PLOTTED
** ENGLISH UNITS **
TAPE ID KCXZ0J0
LOAD NO. 11
PLOT NO.73
Y . AXIS
.20
.18
.16
.14
.12
.10
.08
.06
.04
.02
5.20
5.25
5.30
5.35
5.40
X . AXIS
A 2.07X10 04
B 2.08X10 04
C 2.10X10 04
D 2.11X10 04
E 2.13X10 04
F 2.14X10 04
G 2.15X10 04
H 2.17X10 04
J 2.18X10 04
K 2.20X10 04
L 2.21X10 04
M 2.22X10 04
N 2.24X10 04
O 2.25X10 04
P 2.27X10 04
Q 2.28X10 04
R 2.30X10 04
S 2.31X10 04
MIN . X10 -01
MAX 2.31X10 04

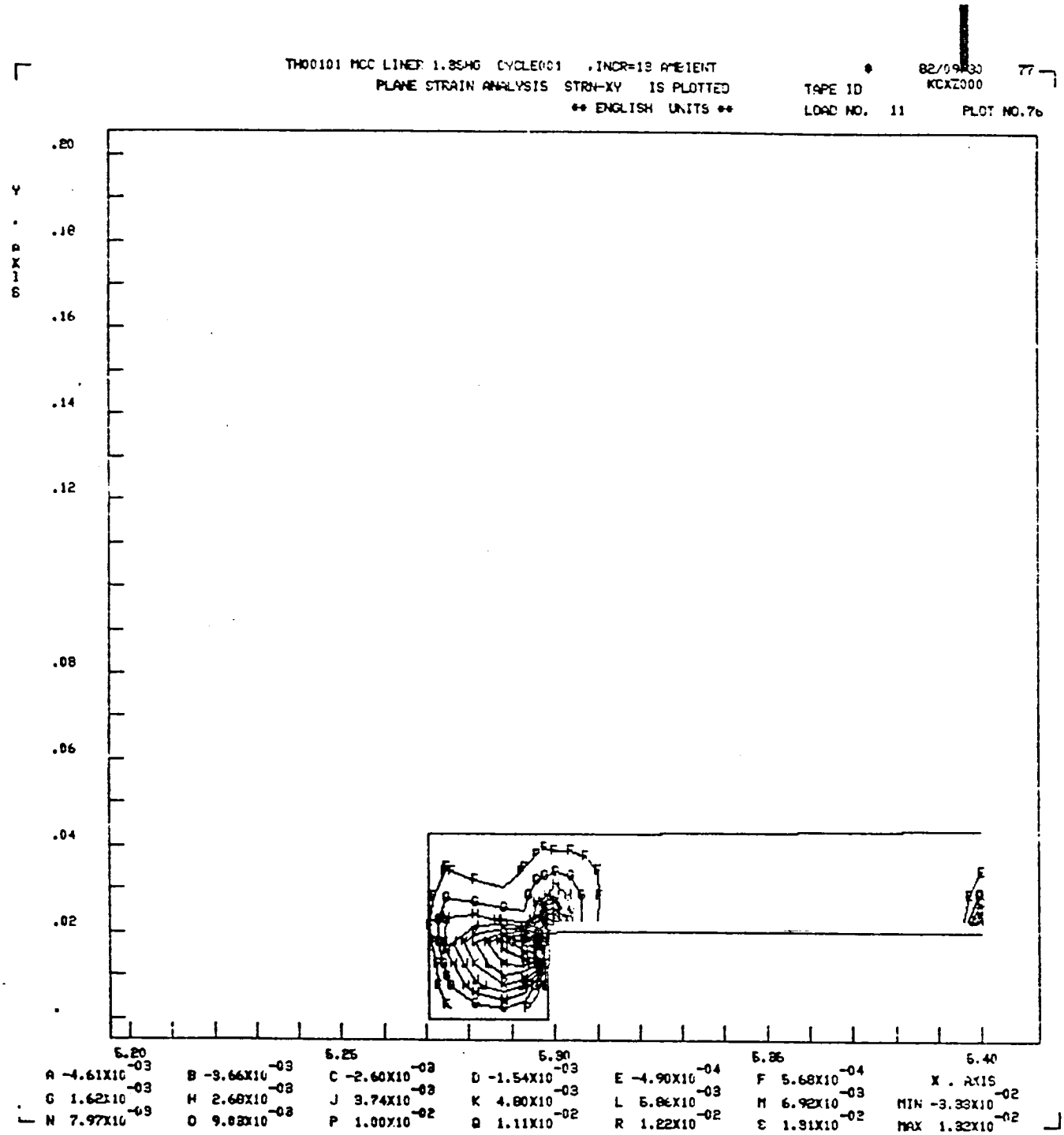
TH00101 MCC LINER 1.35HG CYCLE001 ,INCR=13 AMBIENT
PLANE STRAIN ANALYSIS STRN-XY IS PLOTTED
** ENGLISH UNITS **
TAPE ID KCXZ000
LOAD NO. 11
PLOT NO.76
Y - AXIS
.20
.18
.16
.14
.12
.08
.06
.04
.02
5.20
5.25
5.30
5.35
5.40
A -4.61X10-03
B -3.66X10-03
C -2.60X10-03
D -1.54X10-03
E -4.90X10-04
F 5.68X10-04
G 1.62X10-03
H 2.68X10-03
J 3.74X10-03
K 4.80X10-03
L 5.86X10-03
M 6.92X10-03
N 7.97X10-03
O 9.03X10-03
P 1.00X10-02
Q 1.11X10-02
R 1.22X10-02
S 1.31X10-02
X - AXIS
MIN -3.33X10-02
MAX 1.32X10-02

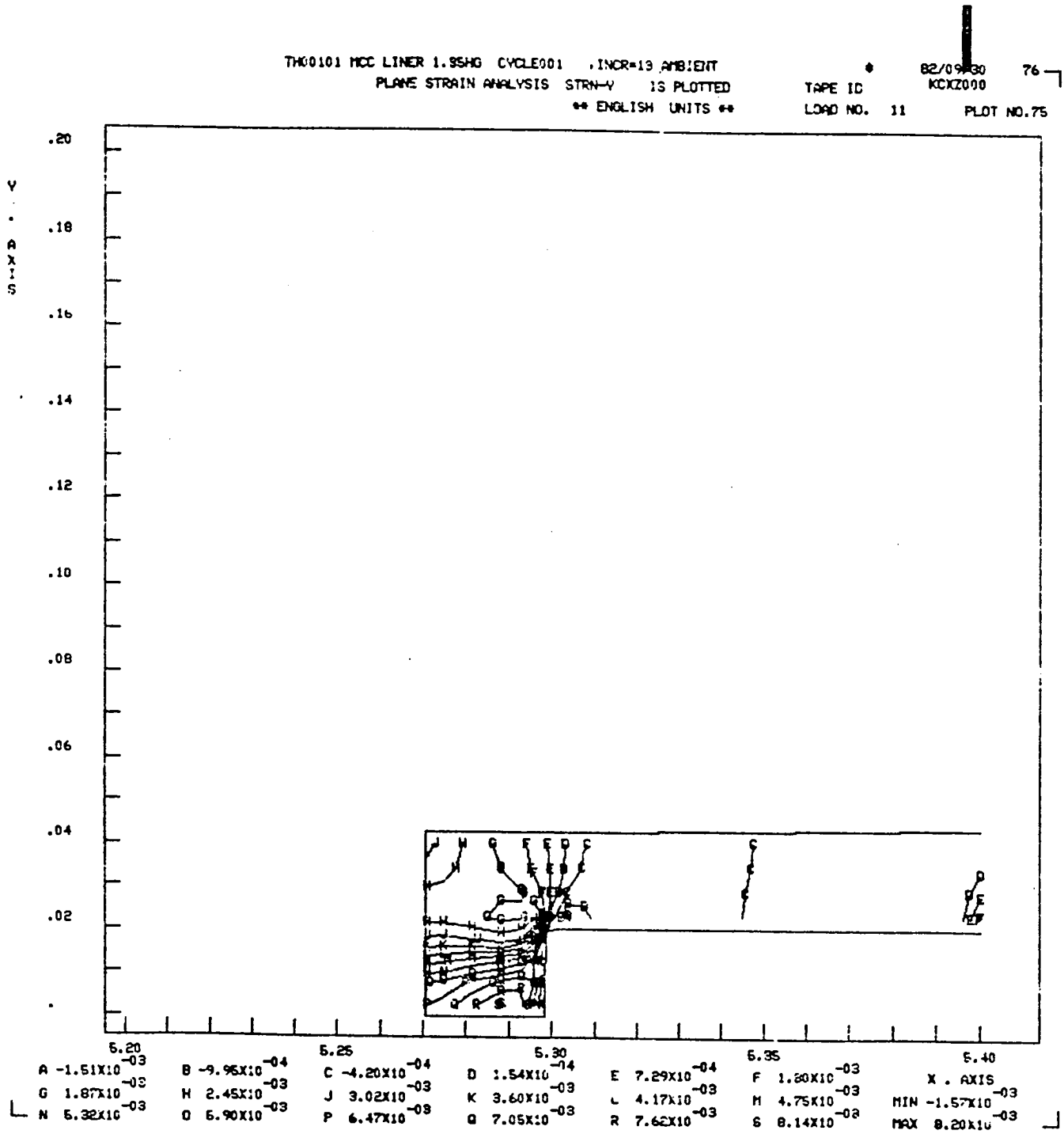
TH00101 MCC LINER 1.95HG CYCLE001 ,INCR=13 AMBIENT
PLANE STRAIN ANALYSIS STRN-Y IS PLOTTED
** ENGLISH UNITS **
TAPE ID
LOAD NO. 11
PLOT NO.75
Y . AXIS
.20
.18
.16
.14
.12
.10
.08
.06
.04
.02
5.20
5.25
5.30
5.35
5.40
X . AXIS
A -1.51X10-03
B -9.96X10-04
C -4.20X10-04
D 1.54X10-04
E 7.29X10-04
F 1.80X10-03
G 1.87X10-03
H 2.45X10-03
J 3.02X10-03
K 3.60X10-03
L 4.17X10-03
M 4.75X10-03
N 5.32X10-03
O 5.90X10-03
P 6.47X10-03
Q 7.05X10-03
R 7.62X10-03
S 8.14X10-03
MIN -1.57X10-03
MAX 8.20X10-03

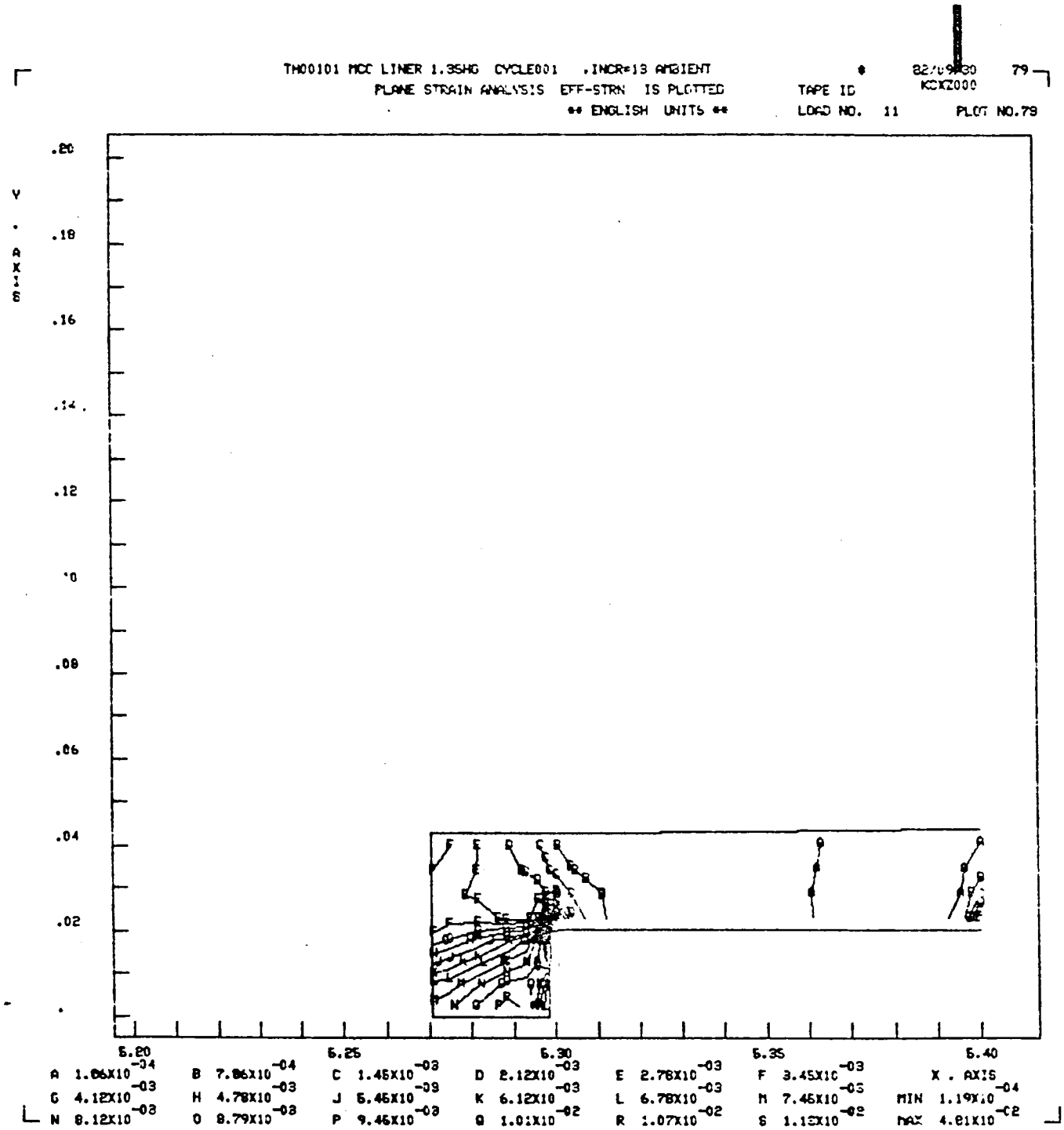
TH00101 MCC LINER 1.35HG CYCLE001 .INCR=13 AMBIENT
PLANE STRAIN ANALYSIS EFF-STRN IS PLOTTED
** ENGLISH UNITS **
TAPE ID
LOAD NO. 11
PLOT NO.79
Y . AXIS
.20
.18
.16
.14
.12
.10
.08
.06
.04
.02
5.20
5.25
5.30
5.35
5.40
A 1.06X10-04
B 7.86X10-04
C 1.45X10-03
D 2.12X10-03
E 2.78X10-03
F 3.45X10-03
G 4.12X10-03
H 4.78X10-03
J 5.45X10-03
K 6.12X10-02
L 6.78X10-02
M 7.45X10-02
N 8.12X10-02
O 8.79X10-02
P 9.46X10-03
Q 1.01X10-02
R 1.07X10-02
S 1.13X10-02
X . AXIS
MIN 1.19X10-04
MAX 4.81X10-02

REFERENCES

1. Posttest Metallurgical Analyses of 40 K Subscale Chamber, HPR 76-2304, Rockwell International, Rocketdyne Division, 6 December 1976.

2. Hannum, N. P., R. J. Quentmeyer, and H. J. Kasper: "Some Effects of Cyclic Induced Deformation in Rocket Thrust Chabmers," NASA Technical Memorandum 79112, Conference on Advanced Technology for Future Space Systems, Hampton, VA, 8 through 11 May 1979.

3. Armstrong, W. H.: "Structural Analysis of Cylindrical Thrust Chambers," LMSC-HREC-TR-D568827-Vol-1, Lockheed Missiles and Space Co.; NASA Contract NAS3-21361), NASA CR -159522, 1979.

4. Armstrong, W. H.: "Structural Analysis of Cylindrical Thrust Chambers," Final Report, Vol. II, NASA CR-165241, Contract NAS3-21953, NASA-Lewis Research Center, Cleveland, OH, March 1981.

5. Newell, J. F. and S. F. Persselin: Finite Element Asymmetric and Planar Structural Analysis," SSME 74-1282, 18 April 1974.

6. Robinson, E. L.: "Effects of Temperature Variation on the Long-Term Rupture Strength of Steels," Transcript ASME, Vol. 74, No. 5, July 1952, pp 777 through 781.

7. Taira, Shuji: "Thermal Fatigue and Its Relation to Creep Rupture and Mechanical Fatigue," Proceedings of the Third Symposium on Naval Structural Mechanics, Pergamon Press, 1964, pp 187 through 213.

8. Manson, S. S. and G. R. Halford: "A Method of Estimating High-Temperature, Low-Cycle Fatigue Behaviour of Materials," Proceedings of the Thermal and High-Strain Fatigue Conference, London, England, 1967, pp 154 through 170.

9. Spera, D. L.: The Calculation of Elevated Temperature Cyclic Life Considering Low-Cycle Fatigue and Creep, NASA TND-5317, April 1969.

10. Manson, S. S.: "Thermal Stress and Low-Cycle Fatigue," McGraw Hill Book Company (1966) p 165.

11. Svenson, N. L.: "The Bursting Pressure of Cylindrical and Spherical Vessels," Journal of Applied Mechanics, March 1958, pp 89 through 96.

12. Porowski, J. S., M. Badlain, B. Kasraie, W. J. O'Donnell, and D. Peterson: "Development of a Simplified Procedure for Thrut Chamber Life Prediction," NASA CR-165585, October 1981.

13. Terry, E. L. and S. W. McClaren: "Biaxial Stress and Strain Date on High-Strength Alloys for Design of Pressurized Components," ASD-TDR-62-401 Chance Vought Corporation, May 1962.

14. SSME Materials Control Report: "Main Combustion Chamber," RSS-8574-7, 8 June 1981.

15. Materials Properties Manual, Rockwell International, Rocketdyne Division, Third Edition, Volumes II and III.

16. Military Standardization Handbook, MIL-HDBK-5C, Vol. II, Chapter 9.

17. Manson, S. S.: "Interfaces Between Fatigue, Creep and Fracture," Proceedings of First International Conference of Fracture, Sendai, Japan, (1966), p 3.

18. Collins, J. A.: "Failure of Materials in Mechanical Design," John Wiley & Sons, New York, NY, 1981, p 241.

19. Plumtree, A. and H. Abdel-Rasuf: Met. Trans. 12A, 1981, p 2049.

20. Manson, S. S., G. R. Halford, M. H. Hirschberg: "Creep-Fatigue Analysis by Strain-Range Partitioning," Symposium on Design for Elevated Temperature Environment, ASME, May 1971, pp 12 through 24.

21. Sherby, O. D.: Acta Met. 10, 1962, p 135.

22. Sherby, O. D. and P. M. Burke: Prog. Mat. Sci. 13, 1968, p 325.

23. Mukherjee, A. K., J. E. Bird, and J. E. Dorn: Trans. ASM 62, 1969, p 155.

24. Lewis, J. R.: "Creep Behavior of NARloy Z," MPTR 70-902, Rockwell International, Rocketdyne Division, 1 July 1970, p. 11.